Distribution Category:
General Energy Research (UC-400)
General, Miscellaneous, and Progress
Reports (Nuclear) (UC-500)

ANL-91/18

ANL--91/18

DE91 014718

ARGONNE NATIONAL LABORATORY
9700 South Cass Avenue
Argonne, IL 60439

CHEMICAL TECHNOLOGY DIVISION
ANNUAL TECHNICAL REPORT
1990

M. J. Steindler — Division Director
P. A. Nelson — Deputy Division Director
J. E. Battles — Associate Division Director
D. W. Green — Associate Division Director

May 1991

Previous reports in this series

ANL-90/11	January-December 1989
ANL-89/15	January-December 1988
ANL-88-19	January-December 1987
ANL-87-19	January-December 1986

TABLE OF CONTENTS

TABLE OF CONTENTS (contd)

TABLE OF CONTENTS (contd)

TABLE OF CONTENTS (contd)

TABLE OF CONTENTS (contd)

CHEMICAL TECHNOLOGY DIVISION
ANNUAL TECHNICAL REPORT
1990

ABSTRACT

Highlights of the Chemical Technology (CMT) Division's activities during 1990 are presented. In this period, CMT conducted research and development in the following areas: (1) electrochemical technology, including advanced batteries and fuel cells; (2) technology for coal-fired magnetohydrodynamics and fluidized-bed combustion; (3) methods for recovery of energy from municipal waste and techniques for treatment of hazardous organic waste; (4) the reaction of nuclear waste glass and spent fuel under conditions expected for a high-level waste repository; (5) processes for separating and recovering transuranic elements from nuclear waste streams, concentrating plutonium solids in pyrochemical residues by aqueous biphase extraction, and treating natural and process waters contaminated by volatile organic compounds; (6) recovery processes for discharged fuel and the uranium blanket in the Integral Fast Reactor (IFR); (7) processes for removal of actinides in spent fuel from commercial water-cooled nuclear reactors and burnup in IFRs; and (8) physical chemistry of selected materials in environments simulating those of fission and fusion energy systems. The Division also has a program in basic chemistry research in the areas of fluid catalysis for converting small molecules to desired products; materials chemistry for superconducting oxides and associated and ordered solutions at high temperatures; interfacial processes of importance to corrosion science, high-temperature superconductivity, and catalysis; and the geochemical processes responsible for trace-element migration within the earth's crust. The Analytical Chemistry Laboratory in CMT provides a broad range of analytical chemistry support services to the scientific and engineering programs at Argonne National Laboratory (ANL).

SUMMARY

Current programs within CMT are briefly summarized below. These programs are discussed in greater detail in the remainder of the report.

1. *Electrochemical Technology*

The CMT Division is engaged in a variety of activities related to the development of advanced batteries and fuel cells for vehicle propulsion, utility load-leveling, and other energy storage applications. These activities include research, performance and lifetime testing, post-test examinations, modeling, technology transfer, and technical management of industrial contracts from the Department of Energy (DOE).

For more than 15 years, CMT has been conducting in-house R&D on lithium/iron sulfide batteries, which have a molten-salt electrolyte and operate at >375°C. In 1990, DOE signed a new industrial R&D contract for SAFT America, Inc., to develop lithium/iron sulfide batteries for electric-vehicle applications. The contract specifies delivery of three full-size Li/FeS batteries in the third year of the contract--one for laboratory evaluation and one for in-vehicle testing. In support of this project, CMT will provide technology transfer to SAFT, technical management for DOE, and R&D on critical technical issues.

Our in-house research program on the lithium/iron sulfide system is concentrated on developing a "bipolar" Li/FeS_2 battery (i.e., cells stacked so that the positive and negative electrodes of adjacent cells have a common current collector). A critical component in the bipolar cell is the hermetic seal formed at the cell periphery. Here, a ceramic ring is sealed to molybdenum on the positive electrode side and steel on the negative electrode side. We have developed sealant materials that are electronic insulators and bond tenaciously to metals and ceramics in the Li/FeS_2 cell environment. This seal has been successfully tested in a stack of four bipolar cells, which operated for >500 cycles with >98% coulombic efficiency. This stack test also demonstrated the capability of the lithium-shuttle mechanism at achieving charge equalization without the need for electronic equipment. Calculations based on measured performance and component weight breakdown indicate that the bipolar configuration should improve specific energy by 30% and the specific power by more than 100% and should increase lifetime beyond the 1000 cycles already demonstrated in cells of conventional design.

In-house research is also being conducted on the sodium/metal chloride battery, which normally operates at 260°C. Recent efforts have focused on improving the performance of the $NiCl_2$ electrode. By fabricating this electrode with larger and more uniform porosity, we obtained significant decreases in the area-specific impedance. In an electrode containing 17 vol % Ni, for example, the area-specific impedance was 0.5 $\Omega\,cm^2$ at 260°C, which is a sizable improvement over that for the positive electrodes in state-of-the-art cells (1.0-1.5 $\Omega\,cm^2$). In studies of electrode chemistry, we found that, during charge, $NiCl_2$ forms a poorly conducting layer on the nickel electrode surface, which produces a marked increase in the area-specific impedance. Upon reaching a certain thickness, the layer hinders further charge of the electrode. Sulfur addition to the $NiCl_2$ electrode was found to improve its charge-discharge characteristics. As an aid to further improvement in the $NiCl_2$ electrode, we have developed an electrochemical model that accurately calculates the area-specific impedance over the course of discharge for a given electrode design.

The Department of Energy placed a contract with Beta Power, Inc., to develop conceptual designs for sodium/metal chloride batteries. The Division provided technical management and support for this effort.

The Analysis and Diagnostic Laboratory (ADL) in CMT includes a test laboratory to conduct battery evaluations under simulated application conditions and a post-test analysis laboratory. In the test laboratory, cells and multicell modules of six battery technologies (Na/S, Zn/Br, Ni/Cd, Ni/Fe, Ni/metal hydride, and lead-acid) fabricated by various industrial firms underwent performance and lifetime testing during 1990. Four battery systems (Na/S, Li/FeS_x, Ni/Fe, and lead-acid) were also subjected to post-test analysis. The information gained from the

performance and lifetime tests and the post-test evaluations provides a measure of the technical progress made by the battery developers and identifies specific areas where changes in design or the materials of construction would improve battery performance.

Two advanced fuel cells are being studied at CMT: the solid oxide fuel cell and the molten carbonate fuel cell. In the solid oxide fuel cell development effort, work is underway to develop a monolithic fuel cell design, which is based on the premise that the thin solid components of oxide cells can be fabricated into compact shapes having power-to-weight ratios that are a factor of 100 higher than those attainable with conventional fuel cells. Since 1988, Allied Signal Aerospace has been conducting development work on the monolithic solid oxide fuel cell with technical support from ANL. In the past year, our support work revealed that the cathode/electrolyte interfacial resistance will increase with operating time, and that sulfur in the coal gas and hydrocarbon fuels will degrade anode performance. In addition, a mathematical model has been developed to simulate the electrochemistry and thermal hydraulics of a monolithic solid oxide fuel cell stack and will be used to assess the effect of various design variables on performance and lifetime.

A project is underway to develop new materials which permit operation of ceramic solid-state fuel cells at lower temperatures (500-800°C vs. 1000°C currently required), which would increase flexibility in cell design and would improve thermodynamic efficiency. Our approach is to start with a search for a new electrolyte. Materials with perovskite and orthophosphate structures have been evaluated. The results indicate that the six evaluated perovskites have the oxygen substoichiometry needed for fuel cell use, but the material conductivity is still too low to be practical. Thus, other perovskites will be evaluated. In the study of orthophosphate structures, lanthanum phosphate was found to have potential for the intended application.

The work on molten carbonate fuel cells is focused on finding improved materials and fabrication techniques for the cathode and anode and testing them in cells. In the anode development effort, we measured the resistivity of undoped and niobium-doped $LiFeO_2$ samples at 140-650°C under anode inlet gas humidified with room-temperature water. The results indicated that niobium doping decreases $LiFeO_2$ resistivity, and that the minimum resistivity would be obtained at a Nb/Fe mole ratio of ~0.06. In cell tests, $LiFeO_2$ is being evaluated as an alternative cathode for the present NiO. We developed a new method for synthesizing the $LiFeO_2$ starting material with higher surface area, which yielded improved performance in cell tests. Cell tests also indicated that the mechanism controlling the reaction rate for $LiFeO_2$ cathodes differs from that of NiO cathodes.

The Division provides technical support to DOE for developing fuel cell and fuel cell/battery systems for transportation applications. In 1990, a study was conducted on fuel reformers for converting alternative fuels (e.g., methanol, ethanol) to a hydrogen-rich gas mixture for powering fuel cells in automotive applications. We found that reformers developed to date lack adequate start-up and dynamic response capability to permit their use in stand-alone systems for automotive applications. A project has been initiated to develop reformer technology which can convert ethanol to hydrogen for use in fuel-cell-powered vehicles. The Division also

provided technical management of contractor efforts to develop a phosphoric acid fuel cell/battery system and a proton exchange membrane fuel cell for transportation applications.

2. *Fossil Fuel Research*

The Chemical Technology Division is the lead division for several projects in the ANL Fossil Fuel Program. These projects involve studies on fluidized-bed combustion (FBC) and heat and seed recovery for coal-fired magnetohydrodynamic (MHD) power generation.

Metal loss from in-bed heat-transfer tubes in FBC is a recurring problem that is impeding commercialization. To address this problem, a cooperative R&D venture was formed with ANL and seven other organizations. Activities undertaken in 1990 included fluidized-bed experiments at Foster Wheeler Development Corp. and the University of Illinois at Urbana-Champaign to determine solids motion around immersed tubes and their erosion in a fluidized bed, analysis of these experiments using ANL-developed computer models of the fluidized-bed hydrodynamics and erosion processes, and development of a three-dimensional hydrodynamics model by Babcock & Wilcox. The overall objective is to translate model predictions and experimental data into simple guidelines for the design and operation of fluidized-bed combustors with minimal metal loss.

Argonne is managing the Atmospheric Fluidized-Bed Cogeneration Air Heater Experiment for DOE. The objective is to assess materials and process performance of in-bed air heaters for cogeneration of electricity and hot air in an atmospheric fluidized-bed combustor (AFBC). Corrosion tests of numerous different alloys at 1150 K for 2000 h in an AFBC unit indicated that the presence of bed material deposit on the alloy surfaces leads to significant, and sometimes catastrophic, corrosion degradation. However, the same alloys exhibit acceptable corrosion when their surfaces are free of bed material deposits.

The presence of vapor-phase alkalis in the exhaust of pressurized fluidized-bed combustors (PFBCs) can lead to unacceptable corrosion of the gas-turbine blade materials. Work is in progress to develop a regenerable activated-bauxite sorber alkali monitor for the *in situ* measurement of alkali vapor in PFBC off-gas. The monitor will use commercial-grade activated bauxite, which contains some clay impurities that can react with alkali vapors. Impregnating the bauxite with either NaCl or LiCl is being investigated as a method to deactivate these impurities. Tests were undertaken to evaluate the alkali-vapor corrosivity of PFBC off-gas generated from burning Illinois coals with high-chlorine, high-sulfur content. The alkali-vapor concentration was more than 2.5 times greater than the current alkali limit of 24 parts per billion for an industrial gas turbine. The results indicate that a method of controlling alkali vapors may be needed if Illinois coals are to be used in PFBC power generation.

A joint project between ANL and Sargent & Lundy was undertaken to evaluate the benefits of cleaning high-sulfur Illinois coal for use in an 80 MW(e) circulating fluidized-bed combustor. Test results in a laboratory-scale PFBC at CMT indicated that burning washed coals reduces SO_2 emissions by more than 50%, NO_x emissions by about 33%, and solid-waste handling burden and run-off pond area by 69%. Use of washed coals also has cost benefits.

Another evaluation is underway to assess two Illinois dolomites and a limestone for their ability to reduce SO_2 and HCl emissions.

In work on the technology for heat and seed recovery in an MHD plant, experiments were performed to determine the corrosion of candidate alloys for an intermediate temperature air heater exposed to MHD conditions (metal temperature, 1035 K; gas temperature, 1255 K) for 500 or 2000 h. Metallographic examination of the alloys is underway to determine the extent of corrosion.

3. *Municipal and Hazardous Waste Research*

The CMT effort on municipal and hazardous waste technologies involves research into the thermochemical conversion of municipal solid waste (MSW) and the development of methods for treating hazardous waste.

A model is being developed to simulate the thermochemical conversion of MSW in a water-wall type mass burner. The model simulates the heatup, pyrolysis, and burnout of the waste as a traveling grate moves it from the inlet of the incinerator to the exit. The model equations are solved to generate the temperature and mass flow profiles along the length of the MSW bed. Calculated results revealed that the grate length necessary for the solids to heat up to pyrolysis temperatures is greater than that necessary to pyrolyze the solids, an increased solids feed rate results in a slowdown of the heating and conversion process, and bed height has a negligible effect on the solids heating rate. In addition, typical simulations indicated that the solids processing rate can be increased by reducing the length of the burnout zone and by distributing the primary air such that it is kept low in the heatup and reaction zones to permit rapid heating and conversion of the solids. Results are given for the effect of primary and secondary air flow rate on the flame and bed temperatures along a 7.6-m bed length.

The research on hazardous waste treatment includes an investigation of a one-step process for converting reactive metal (primarily sodium) to a glass for disposal. Preparations are underway for a pilot-plant demonstration of the process with nonradioactive sodium waste. Work is also underway on determining the technical feasibility of employing a microwave-induced plasma for detoxification of chlorinated hydrocarbons. A 6-kW microwave generator and quartz reactor tube were used to investigate the degradation of 1,1,1-trichloroethane in a water/argon plasma. Destruction removal efficiencies >97% were obtained for a single-pass conversion of 1,1,1-trichloroethane at water/1,1,1-trichloroethane feed ratios of 5.9 to 22.

4. *Nuclear Waste Studies*

The volcanic tuff beds at Yucca Mountain, Nevada, are being studied as a potential site for locating the U.S. high-level nuclear waste repository. For the Yucca Mountain Project, CMT is investigating the reaction of glass and spent reactor fuel under the anticipated repository conditions and evaluating the effects of radiation on the near-field environment. The potential site at Yucca Mountain is unique among sites that have been considered previously in that it lies several hundred meters above the local water table in a hydrologically unsaturated zone. It is anticipated that liquid water will not contact the waste during the approximately 10,000-year

period of regulatory concern about the repository. Since transport of radionuclides via groundwater flow is the primary means of their escape from the repository, the unsaturated environment is viewed as a major advantage of the Yucca Mountain site. Because only water vapor or small volumes of liquid water in the repository horizon are expected to contact the waste forms, traditional test methods used to assess glass durability may not be appropriate for the Yucca Mountain environment. Therefore, we have designed alternative test methods which better represent the expected repository environment and are using them to study the interactions that may occur and to project the long-term behavior of emplaced waste. These tests have resulted in valuable insight into the nature of the interactions, primarily through analyses of reacted solids using sophisticated surface analytical techniques, including analytical electron microscopy.

To date, long-term tests of simulated high-level waste glass and spent fuel have shown that these reacted solids generate secondary phases which can strongly influence subsequent behavior. The reaction conditions can affect the assemblage of secondary phases that are formed and the rapidity with which they appear. Vapor hydration and leach tests are also underway to better model the reaction of simulated waste glasses for long-term projection of their durabilities in the Yucca Mountain site. Present models of glass reaction based on liquid leach tests alone do not accurately describe the reaction under all repository-relevant conditions.

Studies of the influence of radiation in high-moisture, air-like systems indicated that some ammonia will form under the conditions expected for a high-level nuclear waste repository. This is a concern because some copper-based materials under consideration as waste containers are susceptible to ammonia cracking. In other studies, the initial corrosion rate of copper-based materials was found to increase because of the presence of ionizing radiation (1-2 x 10^4 rad/h).

The Defense Waste Processing Facility (DWPF) is scheduled to begin generating borosilicate waste glass in the early 1990s for eventual storage in a high-level waste repository. Several tasks are in progress to assist DOE's Environmental Restoration and Waste Management (EM) Program in demonstrating that the DWPF will produce a consistent product that will perform well in a geologic repository. A detailed technical review of the literature is being undertaken to critically evaluate the available theoretical and experimental results relevant to the long-term stability of waste glass, particularly under conditions relevant to the potential repository at Yucca Mountain. In addition, experiments with simulated waste glasses are being performed to assess the effects of radiation and the amount of water available on the extent and nature of the reaction. Other experiments are using naturally occurring glasses to isolate and study reactions which may occur in borosilicate waste glasses.

In other repository-related work, photoacoustic spectroscopy is being employed to study the solubility and speciation of radionuclides in groundwaters. This work has yielded information concerning complexant and temperature effects on the solubilities of important radionuclide species. Recent emphasis has been on the Pu(VI) hydrolysis in near-neutral aqueous systems.

Experimental effort is also underway to investigate the effect of ionizing radiation on the potential for gas generation in the Waste Isolation Pilot Plant (WIPP) site. In this report

period, experiments were initiated to determine the extent that nonbiodegradable plastics present in the WIPP waste canisters will be radiolytically converted to biodegradable material.

5. *Separation Science and Technology*

The Division's work in separation science and technology is mainly concerned with developing the TRUEX process for removing and concentrating actinides from acidic waste streams contaminated with transuranic (TRU) elements. The objectives of TRUEX processing are to recover valuable TRU elements and to lower disposal costs by generating a nonTRU waste stream containing the bulk of the original waste. The major thrust of the development efforts has been the Generic TRUEX Model (GTM), which has become a useful tool at ANL and elsewhere in designing TRUEX flowsheets and estimating cost and space requirements for installing a process for treating specific waste streams.

Version 2.1 of the GTM was released in 1990 with several enhancements over the first-generation version. These enhancements include greater speed and accuracy of results, compatibility of versions for Macintosh and IBM personal computers, and several new capabilities. The latter includes estimating solvent degradation caused by radiolysis and hydrolysis, performing concentration profile calculations for different contactor types (centrifugal contactor, pulsed column, or mixer settler), and performing speciation calculations for three times more feed components. In addition, new calculational models were developed for the GTM to treat extraction behavior in pulsed columns and the effects of solvent loading.

Data collection for the GTM continues to be an important effort. The data base, generated over the past four years from the literature and our own laboratory experiments, contains information on the extraction behavior of all important feed components over a wide range of possible waste-stream and processing conditions. Our recent experiments have focused on measuring the effects of solvent composition and temperature on the extraction behavior of inorganic species. The backbone of modeling the extraction behavior of many species is the thermodynamic activities of water and hydrogen and nitrate ions. Activities of aqueous solutions of $Al(NO_3)_3$, a major component in many TRU and high-level waste streams, were measured to better calculate thermodynamic activities in the GTM.

Continuous, multistage, countercurrent experiments in centrifugal contactors continue to be an important means of verifying the GTM calculations. The GTM is being used to design a TRUEX flowsheet for treating plutonium-containing waste generated at the New Brunswick Laboratory. Demonstration of this flowsheet will be accomplished with actual plutonium-containing solution, as we recover Pu and Am from this waste for use in the Integral Fast Reactor (IFR) Program and dispose of the bulk of the waste as low-level waste. Development of monitoring and control technology for TRUEX processing has also been initiated.

Another effort in the separation science and technology area involves modifying the centrifugal contactor for specific solvent extraction processes. Accomplishments in this report period include (1) developing a new contactor design that should more than double throughput and (2) establishing the potential of the centrifugal contactor as a concentrating device by

operating it at very high and very low aqueous-to-organic flow ratios with high extraction efficiency. We are also assisting the IFR Program in developing a pyrocontactor for continuous, multistage, molten-salt/molten-metal extraction and the Los Alamos National Laboratory in developing a Kynar contactor for use with highly corrosive acidic chloride solutions.

Two new projects were initiated in 1990 outside the TRUEX program. One involves developing an aqueous biphase process for actinide recovery from solid residues, where materials are finely ground so that different materials can be partitioned between two nonimmiscible aqueous solutions based on the surface properties of the solids. The objective of the second project is to develop a membrane-assisted solvent extraction/membrane-assisted distillation stripping (MASX/MADS) process that removes volatile organic compounds from natural and process waters.

6. *Integral Fast Reactor Pyrochemical Process*

The Integral Fast Reactor (IFR) is an advanced reactor concept proposed by, and under development at, Argonne. One of its distinguishing features is an "integral" fuel cycle in which the discharged reactor core and blanket materials are processed and fabricated into new fuel elements in an on-site facility. The CMT Division has the responsibility for developing the on-site process for recovering plutonium and uranium from the core and blanket, removing fission products, reenriching the core alloy with plutonium bred in the blanket, and immobilizing fission product wastes in suitable media for disposal.

The IFR pyrochemical process flowsheet has the necessary flexibility for providing the desired products (essentially pure uranium and a U-Pu mixture) from all IFR spent fuel compositions while generating a minimum volume of waste that has a very low TRU element content. The major focus of flowsheet refinement is examining the operational and safety issues associated with a planned demonstration of the pyrochemical process in the Fuel Cycle Facility for the Experimental Breeder Reactor II (EBR-II).

As part of supporting chemistry studies, the separation factors for pairs of the rare earth elements up to atomic number 64 (gadolinium) and for neodymium vs. plutonium are being measured. These separation factors are being determined by measuring the distribution of these elements between LiCl-KCl eutectic salt and cadmium phases as a function of electrorefiner operating conditions at 500°C. These studies have provided some unexpected results, e.g., yttrium is more readily oxidized than expected with a separation factor between yttrium and lanthanum of about 30, europium behaves more like an alkaline earth than a rare earth, and only $EuCl_2$ existed in highly oxidizing conditions rather than the expected mixture of $EuCl_2$ and $EuCl_3$.

In process development studies, tests have been conducted to determine the effects of impurities in the argon cover gas (O_2 and H_2O) on the behavior of electrorefiner salt containing U, Pu, and rare earth chlorides. The results showed that the uranium concentration vs. time decreased more rapidly than Pu, Ce, Nd, Sm, or Y concentrations. The rapid decrease in uranium concentration was attributed to interaction of UCl_3 with the MgO crucible used to hold the electrorefiner salt. The rate of decrease in Pu, Nd, Ce, Sm, and Y concentrations depended

on the O_2 and H_2O levels in the argon cover gas. In another study, microscopic examination of our laboratory-scale electrorefiner crucible after four years of operation at ~500°C showed minimal corrosion, confirming that carbon steel is compatible with the cadmium/salt system. Studies are also underway to better define zirconium behavior and to develop a method for removing accumulated zirconium from the electrorefiner.

The key steps in the pyrochemical processing of spent IFR fuel are dissolution and product recovery by electrodeposition using solid cathodes for uranium and liquid cadmium cathodes for U-Pu. Anodic dissolution of chopped, clad U-Zr and U-Zr-fissium alloy pins has been demonstrated at the plant scale (~10 kg batch size) and is now a routine operation. The typical dissolution rate is ~0.5 kg/h. Improved performance has been achieved in the electrotransport of uranium from the cadmium pool anode, as well as directly from an anodic dissolution basket, to a single mandrel cathode. The use of multipin cathodes has been abandoned. Process parameters have been established and transport rates of ~0.35 kg/h and deposits of 10 kg are now reproducible. Tests are continuing to optimize the process parameters for reproducible transport of uranium to a liquid cadmium cathode. Uranium is being used as a stand-in for U-Pu at the engineering-scale level. In one test with a liquid cadmium cathode, about 3 kg uranium was collected in 32 h. Also, prototype equipment being developed for installation in the Fuel Cycle Facility is being tested in an engineering-scale facility.

Processes are being developed to recover TRU elements from the metal and salt wastes in the electrorefiner and to convert the treated materials into disposable high-level waste forms. The metal waste consists of cladding hulls, zirconium, and cadmium, which contains the noble metal fission products. Except for the cladding hulls, these wastes are expected to contain only small amounts of actinides. The salt contains the alkali metal, alkaline earth, rare earth, and halide fission products. It will also contain from 0.5 to 1.0% of the actinides fed to the electrorefiner. Efforts have been concentrated on developing processes for treating and immobilizing the waste salt.

7. *Actinide Recovery*

Spent fuel from commercial water-cooled nuclear reactors (LWRs) contains a considerable quantity of unreacted fissile uranium as well as TRU elements. These actinide elements constitute a valuable energy resource, and the purpose of the current work is to develop processes for their recovery for use as nuclear fuel in IFRs. We expect these processes to be simple and efficient and to provide a cost-effective method for recovery of actinides from LWR spent fuel. Moreover, removal of actinides from the spent fuel could considerably shorten the time required for assured confinement of this waste in a geologic repository.

Two processes for actinide recovery are being considered. In both processes, LWR spent oxide fuel is reduced to an alloy for reaction with calcium metal, and the actinide elements are then separated from the fission products. In one process, molten salt is used to selectively recover the TRU elements, while the other process uses liquid magnesium. Calcium metal is recovered from the CaO in the reduction salt by electrochemical methods and is recycled along with the salt to minimize process wastes. Experiments were initiated to study the salt transport

process, the magnesium extraction process, and electrowinning of calcium from the CaO in reduction salts.

8. *Applied Physical Chemistry*

Liquidus-Solidus Temperatures for Core-Concrete Mixtures. Solidus-liquidus temperatures were determined by differential thermal analysis (DTA) measurements on three calcined concretes (limestone, limestone-sand, and siliceous) and mixtures of each of these concretes with 73 wt % UO_2-ZrO_2. Such mixtures are expected to occur during the molten core-concrete interaction phase of severe reactor accidents in light-water and pressurized-water reactors. The results are to be incorporated into a thermal-hydraulic code (CORCON) that treats core-concrete interactions in hypothetical severe reactor accidents and is an integral part of the Nuclear Regulatory Commission's Source-Term Code Package.

The differences between the solidus and liquidus temperatures for the three core-concrete mixtures were found to be more than 1200°C, while the differences currently employed in CORCON (for 27 wt % concrete) range from 500 to 700°C. Our results are in reasonable agreement with hypothetical liquidus-solidus curves obtained by assuming limited solubilities between the urania-zirconia-calcia phase and the concrete. Additional DTA experiments at 10, 60, and 85 wt % concrete will be required to establish liquidus-solidus curves over the range of core-concrete mixtures that may be encountered in severe reactor accidents.

Support Studies for New Production Reactor. The DOE initiated the New Production Reactor (NPR) Program to plan, design, and construct safe and environmentally acceptable new reactor capacity for an assured supply of tritium. The CMT Division is supporting this program by conducting several studies on an NPR that is a heavy water reactor (HWR-NPR).

One study concerned seal design in the HWR-NPR. Seal design practices that are acceptable in commercial nuclear reactors in the United States will not be acceptable for the HWR-NPR because of the stringent requirements on tritium control. Based on a review of development efforts in seal design and operating experience in commercial reactors, we developed guidelines for designing effective seals to be used for the tritiated water systems in the HWR-NPR.

In another study, we constructed a computer model to simulate the detritiation processes in the event of either chronic or burst releases of tritiated species into the containment structure of the HWR-NPR. The model incorporates the interaction between the vapor phase species and species on the surfaces and the bulk interior of the structural components, such as concrete walls and coatings. Calculated results indicate that, under a wide range of circumstances, the time necessary to reduce the activity level to an acceptable limit after a tritium spill is dominated by the retention capability of the tritiated species in the structural components. This implies that development of optimal barriers against tritium penetration into these components is important.

Computer models are also being developed to predict release of fission products and tritium from Al-U fuel and Al-Li targets in a hypothetical severe accident with the HWR-NPR. The rate of fission product and tritium release will be established for several conditions: initial release during fuel and target melting, long-term release from melts as a function of temperature, and release from molten target during high-temperature oxidation or burning. Two approaches will be used in this investigation: thermodynamic analyses using the SOLGASMIX computer code and experimental measurements using transpiration and high-temperature mass spectrometry.

Thermophysical Properties Studies. Measurements and calculational analyses are being performed to provide needed information on the thermodynamic and transport properties of IFR fuels. In the past year, our efforts focused on gaining a more thorough understanding of the phase relations involved in the U-Pu-Zr fuel and in fuel-cladding systems. Results are presented of an analysis of the Pu-U and the Fe-U systems. Calculations of the Pu-U phase diagram indicated that some of the assignments in the generally accepted diagram are probably incorrect. A revised Pu-U phase diagram is presented. Also, DTA measurements were completed for the Fe-U system, and a revised phase diagram was calculated for that system. Good agreement was found between our DTA measurements and the calculated diagram.

In several IFR fuel cycle concepts under consideration, the recycled fuel could contain concentrations of the so-called minor actinides. We conducted a preliminary analysis of metallic fuel systems containing the minor actinides. It was found that properties of actinide-containing metallic fuel can change markedly depending on the actinides present. Thus, if IFR fuel is to contain significant amounts of minor actinides, particularly Am or Cm, careful study will be needed on its behavior and properties.

Fusion-Related Research. A critical element in the development of the fusion reactor is the blanket for breeding tritium fuel. Several studies are underway with the objective of determining the feasibility of using lithium-containing ceramics as breeder material.

In one such study, temperature programmed desorption (TPD) measurements are in progress to provide data that describe the kinetics of desorption for $H_2O(g)$ and $H_2(g)$ from ceramic tritium breeders. The TPD spectra for H_2O evolution from $LiAlO_2$ pretreated with helium containing 900 ppm $H_2(g)$ at high temperature indicated first-order desorption processes involving three different types of sites on the $LiAlO_2$ surface.

Analysis of results from in-pile tritium release experiments indicated that tritium inventory in a ceramic breeder is determined mainly by a first-order desorption process. The apparent desorption activation energy is dependent on the purge gas composition and also appears to be a function of the surface hydrogen concentration. In addition, results from laboratory experiments with sintered $LiAlO_2$ pellet samples suggested that tritium is retained in the breeder at low temperatures (<550°C). The cause of the retained tritium is under investigation.

Using the diffusion-desorption model developed in CMT, we estimated the tritium inventory and release from lithium zirconate, the breeder of choice for the ARIES conceptual

design (an advanced fusion reactor). The steady-state inventory in the solid breeder was calculated to be extremely low because of the relatively high operating temperatures and the large diffusion coefficient for tritium in the zirconate. However, the intimate mixing of the breeder and the beryllium neutron multiplier and the apparently slow diffusion of tritium in beryllium may give rise to serious inventory problems in the neutron multiplier regions of the breeder blanket.

Preliminary experiments were carried out to determine if structural steel in the breeder blanket of the fusion reactor could be corroded by LiOT (g) and/or LiOH(g) from water reaction with the Li_2O blanket material. It was found that LiOH(g) does corrode structural stainless steel under fusion reactor conditions. In short-time experiments (<6 h), the reaction rate was inversely proportional to the distance between the stainless steel and the Li_2O breeder blanket and directly proportional to the LiOH(g) diffusivity in the helium purge gas. The reaction is driven by a LiOH pressure gradient.

The International Thermonuclear Experimental Reactor (ITER) is an international project whose purpose is to produce a conceptual design of a tokamak reactor which can be used to test components for a prototype fusion reactor. In support of this project, we completed a detailed conceptual design for the tritium processing system needed for the Li_2O/Be breeder blanket in the ITER design.

9. *Basic Chemistry Research*

Fluid Catalysis. This research is designed to determine reaction mechanisms and to explore new catalytic chemistry of small molecules (e.g., CO, H_2, CH_4) that have energy significance. An array of *in situ* kinetic and spectroscopic techniques is used to define or to uncover new reaction processes that occur under forcing conditions of temperature and pressure. The past year's efforts were focused on exploring the unique properties of supercritical fluids which might lead to their use as superior reaction media for several homogeneous and heterogeneous catalytic processes. A new type of high-pressure nuclear magnetic resonance probe developed in CMT was used to measure intermediate and product species in the $Co_2(CO)_8$ catalyzed hydroformylation of propylene in supercritical CO_2 at a gas density of 0.5 g/mL. The several reaction parameters tested indicate that the catalytic reaction behaves normally in CO_2, while use of the supercritical medium could lead to improved rates and selectivities for hydroformylation normally conducted under conditions in which diffusion across the liquid/gas interface controls the rates.

In other research, efforts are in progress to exploit the extremely robust phthalocyanine ligand in attempts to achieve selective functionalization of hydrocarbons through homogeneous catalysis. An alkyl-substituted rhodium phthalocyanine complex that possesses an unusually reactive Rh-Rh bond was synthesized. Equilibrium measurements for reaction of the complex with dihydrogen indicated that the Rh-Rh bond strength is at most 88 kJ/mol. As a result, the complex reacts directly with methane in solution.

Materials Chemistry. This research involves experimental and theoretical studies of high-critical-temperature (T_c) superconducting oxides, associated and ordered solutions at high temperatures, and other materials of interest.

Our electromotive force studies of the $NdBa_2Cu_3O_x$ superconductor did not indicate the presence of an orthorhombic-orthorhombic miscibility gap of the type found in $YBa_2Cu_3O_x$. This finding explains the previously reported difference between these two superconductors with regard to the variation of T_c with composition. The two plateaus observed in the curves for the composition dependence of T_c for the $YBa_2Cu_3O_x$ system seem to be related to a predicted phase separation in the miscibility gap.

Molecular orbital calculations have been performed for the d→s transitions of divalent and monovalent copper in CuO clusters representing chains in $YBa_2Cu_3O_x$ superconductors. These results have permitted us to assign measured spectral lines to this transition. For example, a sharp peak observed at 4.1 eV in optical absorption spectra of $YBa_2Cu_3O_x$ is due to this d→s excitation.

At present, the major failure mode of molten carbonate fuel cells is dissolution of the NiO cathode materials in the molten carbonate electrolyte. From analyses of measurements of NiO solubility in alkali carbonates, it was deduced that NiO dissolves as NiO_2^{2-}, NiO, and Ni^{2+} solution species. From these results, we determined the factor controlling NiO solubility and predicted electrolyte compositions that should improve performance.

We have applied conformal ionic solution theory--a statistical mechanical perturbation theory initially developed for binary molten salts--to aqueous reciprocal salt electrolytes consisting of two cations and two anions, i.e., $(A^+,B^+/X^-,Y^-)$-H_2O mixtures. Equations were derived for the Gibbs energies and enthalpies of mixing for the quaternary solution. The results provide a means for calculating the thermodynamic properties of quaternary solution from those of the lower order binary and ternary solutions.

Measurements of the structures of trivalent metal ion halides revealed a broad range of melting phenomena. For example, both YCl_3 and $AlCl_3$ have the same crystal structure and six coordinated cations. However, they melt at very different temperatures and have very different entropies of melting. Moreover, molten YCl_3 is an ionic liquid, and the local coordination of Y^{3+} is similar in both the liquid and solid. In contrast, molten $AlCl_3$ is composed of Al_2Cl_6 molecules in which the Al^{3+} ions are four coordinated.

A new theoretical procedure, based on *ab initio* molecular orbital theory, was developed for calculating the energetics of molecules of first- and second-row atoms. This new procedure was tested on atomization energies for 125 molecules (average deviation from measurements of 5.06 kJ/mol) and was used to successfully test uncertain data on 79 molecules. We have also developed methods for the study of third-row non-transition metals (Ga through Kr). These methods have broad applications in materials science. For example, we have calculated the increase in binding energy of silicon clusters (Si_n) as a function of addition of the n'th atom. Good agreement was found with previous experimental results for n = 2,3.

Interfacial and Corrosion Science. The research in the area of interfacial and corrosion science continues to focus on the kinetics and mechanisms of aqueous corrosion processes, the catalytic activity and selectivity of novel molecular sieve materials, and methods

for fabricating superconducting films and coatings with high critical temperature and high critical current density.

A major accomplishment in our aqueous corrosion studies was the application of synchrotron radiation (X-rays) to the analysis of metal film corrosion in aqueous media. A novel X-ray/electrochemical cell (XEC) was designed, fabricated, and used in studies of the electrochemical oxidation of copper in borate buffer solution. Parameters describing the copper layer thickness, the oxide film thickness, and the interfacial roughness were derived from the X-ray reflectograms obtained using the XEC. Another accomplishment was the development of a new method for the *in situ* analysis of monolayer amounts of materials on electrode surfaces. The method is based on a Raman difference technique that makes use of a two-dimensional imaging capability of a position-sensitive photomultiplier detector with a resistive anode.

Ab initio molecular orbital theory was employed to investigate the Brønsted acidity of $Si_n(OH)_m$ clusters having molecular sieve-like embodiments. Proton affinities (an important parameter defining Brønsted acidity) were calculated with accuracies in the 5-10% range, making possible a direct correlation of calculated O-H bond strength and observed catalytic activity.

Highly oriented (textured) films of the high-T_c superconductor $YbBa_2Cu_3O_{7-x}$ were fabricated by rapid oxidation of liquid $YbBa_2Cu_3$ layers dip-coated onto single-crystal ceramic substrates. The high-T_c films, nominally 10-μm thick, show strong preference for c-axis orientation perpendicular to the superconductor/substrate interface when $SrTiO_3(100)$ and MgO(100) are used as substrates. Microscopic and microprobe examinations of the best specimens produced to date revealed regions of near-epitaxial ordering of the high-T_c phase.

Geochemistry. The geochemistry research program includes efforts in two general areas: (1) geochemistry and evolution of hydrothermal systems associated with volcanic areas and (2) isotopic and organic geochemistry of carbon in sedimentary basins. The approach being taken is to investigate specific problems through detailed chemical and isotopic analysis of rock, mineral, water, and gas sampled from appropriate field areas. Potential applications of this work are in nuclear waste management; geothermal energy development; and exploration for minerals, oil, and natural gas.

During the past year, high-precision age determinations were made on travertine samples from Yellowstone National Park (Wyoming) by the ^{230}Th-^{234}U method. The ages were determined to be analytically reproducible and consistent with all geologic constraints. The data from this effort will be used to gain an improved understanding of the timing of the last glaciation and the influence of the glaciation on the underlying hydrothermal systems. Geochemical studies are also underway to elucidate organic matter evolution in lacustrine rift basins.

10. *Analytical Chemistry Laboratory*

The Analytical Chemistry Laboratory (ACL) provides analytical chemistry support services to most of the technical divisions and many of the programs at ANL. In addition, the

ACL conducts research in analytical chemistry and provides analytical services for governmental, educational, and industrial organizations.

During the past year, the ACL was involved in a diverse array of activities, including the following: analyses in support of the development of the IFR pyrochemical process, analyses of leachate from activated bauxite beds used in studies of alkalis in the off-gas from pressurized fluidized-bed combustors, analyses of environmental samples (e.g., water, soil, sediment, air, filters) taken from DOE sites, development of a new method for isolating strontium from geologic samples for isotopic analysis, separation of ^{178m}Hf from tantalum target materials for the study of high-spin phenomena in nuclear and atomic physics, measurement of volatiles from microwave decomposition of H_2S, analyses of samples from a study of molten corium-concrete interactions during a degraded-core accident in a nuclear reactor, determination of volatile organic and inorganic compounds in the headspace of storage drums containing radioactive and hazardous waste, preparation of tritium solutions for the National Energy Agency Committee on Reactor Physics Study, analysis of cores from the pressure vessel of the New Experimental Boiling Water Reactor, study of the fouling of heat exchange systems with an organic fluid model, X-ray diffraction measurements on a wide variety of solids (including superconducting ceramics), measurement of radium in waters and soils, development of methods for remote detection of chemical warfare agents and related precursors and degradation products, and measurement of volatile organic compounds for a Lake Michigan environmental study.

11. *R&D Program Coordination Office*

The R&D Coordination Office is assisting DOE in establishing and maintaining a national program of applied R&D in the environmental restoration and waste management area. In April 1990 a request for proposals was announced with the objective of acquiring contractors that will perform the R&D needed to help DOE meet its cleanup goals. Contracts were then offered to 15 organizations (13 private firms, 1 university, and 1 government laboratory). The R&D Program Coordination Office is providing technical and management oversight to assist the contractors in meeting their milestones within budget and on schedule. This Office also provides technical and administrative support to five Hazardous Substance Research Centers co-sponsored by DOE and the Environmental Protection Agency.

12. *Computer Applications*

The Computer Applications Group assists CMT staff in many aspects of computer-related activities, including laboratory data acquisition and control, computer modeling and simulation studies, analysis of experimental results, graphics, information management and data-base development, computer networking, procurement of automatic data processing equipment, and advisory and consulting services. In the past year, the Division's VAX 6220 was upgraded to a Model 6320, providing 35% increased capacity. In providing technical support to CMT staff, the Computer Applications Group has assisted in the effort to develop the Generic TRUEX Model, which can be used to design and optimize flowsheets for processing waste streams by the TRUEX process; developed software and made other improvements to support the testing of advanced battery systems in the Analysis and Diagnostic Laboratory; and implemented a VAX-based chemical inventory system.

I. ELECTROCHEMICAL TECHNOLOGY

The Electrochemical Technology Program in CMT undertakes (1) in-house research, development, testing, post-test analysis, and technical evaluation studies of advanced battery and fuel cell systems and (2) support research, technology transfer, and technical management for industrial R&D contracts to develop these systems. The in-house R&D is focused on two advanced battery technologies, lithium/iron sulfide and sodium/metal chloride. The testing, evaluation, and post-test analysis of a variety of advanced batteries (i.e., lead-acid, nickel/iron, sodium/sulfur) fabricated by industrial firms are performed in CMT's Analysis and Diagnostic Laboratory (ADL). Potential applications of these battery technologies include vehicle propulsion, utility load-leveling, and other energy storage applications. In-house R&D is also being conducted on solid oxide and molten carbonate fuel cells for power plant and transportation applications.

A. *Advanced Battery Research and Development*

This effort is directed toward developing advanced battery systems and transferring the technology to industry. Current work is focused on attaining major improvements in the performance and cycle life of lithium/iron sulfide and sodium/metal chloride systems.

1. Lithium/Iron Sulfide Technology

a. Industrial Contracts

For more than 15 years, CMT has been conducting in-house R&D on lithium/iron sulfide batteries, which have a molten-salt electrolyte and operate at 375-425°C. To date, the Li/FeS technology has been developed to the sub-scale battery level for electric vehicle (EV) applications, while the Li/FeS_2 technology is ready for scaleup to full-size EV cells.

In April 1990, DOE signed a new industrial R&D contract for SAFT America, Inc. (Cockeysville, MD) to develop lithium/iron sulfide batteries for EV applications. In support of this three-year, cost-shared contract, CMT will provide technology transfer to SAFT and technical management of the project for DOE and will conduct R&D on critical technical issues related to this industrial contract.

The DOE/SAFT contract is primarily directed at developing Li/FeS technology into full-size batteries for use in electric vans. It specifies delivery of three full-size batteries in the third year of the contract--one for laboratory testing and two for evaluation in electric vans. The performance and lifetime goals for these batteries are given in Table I-1. In the process of developing full-size EV batteries to meet these goals, SAFT is striving to demonstrate the intermediate performance and life milestones given in Table I-1. The technology transferred from CMT to SAFT during 1990 is now being used to design and build baseline cells and a sub-scale battery. In early 1991 five baseline cells and the sub-scale battery will be delivered for independent evaluation in CMT's ADL. This baseline hardware, and other

intermediate deliverables, will be evaluated at CMT as a means of tracking technical progress toward meeting the contract goals.

Table I-1. Performance and Life Development Milestones for Li/FeS EV Cells and Batteries[a]

Technology	Energy, Wh/kg	Power		Life	
		W/kg	W/L	Cycles	Years
Baseline Cells	90	100	195	300	2
Baseline Sub-Scale Battery	62	80	90	140	1
Improved Cells	100	105	215	600	4
Improved Sub-Scale Battery	80	95	120	370	2
Prototype Cells	125	137	270	800	5
Full-Size Batteries	100	110	150	600	4

[a]All milestones are for simulated driving profiles on the Simplified Federal Urban Driving Schedule (SFUDS). The power is required to 100% depth-of-discharge (DOD), while the cycle-life goal is for operation to 80% DOD.

The DOE/SAFT contract also includes a one-year R&D effort on the Li/FeS_2 technology. For this contract, SAFT will scale up the cell technology, initiate performance/life testing to verify the 1000-cycle performance obtained on small-scale cells fabricated and tested earlier at CMT,[1] conduct an EV battery design/cost trade-off study, and develop a multi-year R&D plan for advancing this technology for EV applications. During 1990, CMT provided significant technology transfer to SAFT, which then designed a full-scale prismatic cell employing 11.7 x 17.3 cm electrodes. This cell design will be used to verify the performance and life achieved in smaller prismatic cells at CMT. Cells of this design are scheduled for evaluation by SAFT in early 1991. A decision to extend industrial R&D on Li/FeS_2 systems will be based on the results of this one-year effort.

In the area of support R&D for SAFT, CMT is conducting compatibility tests on ceramic materials that could be used to form a hermetic seal on the terminal feedthroughs of full-size EV cells. Earlier in the project, CMT personnel developed a test matrix for definitively identifying the life-limiting mechanism for Li/FeS cells; SAFT is utilizing this matrix as the basis for their cell testing in 1991. Our post-test analysis capabilities and expertise will be utilized extensively to help SAFT identify suitable low-cost materials, cell life-limiting mechanisms, factors that control cell life, and methods for predicting cycle life.

b. In-house Research

In our in-house program, we continue to conduct research on high-performance Li/FeS_2 technology. The objective of this research is to develop this technology for

[1]M. J. Steindler et al., *Chemical Technology Division Annual Technical Report, 1988*, Argonne National Laboratory Report ANL-89/15, p. 15 (1989).

high volumetric and gravimetric power and energy in a variety of EV applications. Current efforts are focused on developing sealed bipolar cells that have the potential to achieve a specific power of 500 W/kg and a specific energy of 200 Wh/kg. Emphasis has been on the development of corrosion resistant ceramic materials for peripheral seals in bipolar cells. We also conducted supportive studies on MgO separator technology.

The MgO powder separator, because it is not physically stable under flooded-electrolyte conditions, must be operated in the "electrolyte-starved" condition. The electrical resistivities of 20 electrolyte-starved MgO separator mixtures were measured by an interrupted dc technique developed for paste-like materials.[2] The mechanical properties of these mixtures were also measured. These mixtures were found to exhibit a large variation in resistivities and mechanical properties with salt composition, MgO concentration, and temperature. For example, Fig. I-1 shows the resistivities obtained for pellets of 35 wt % MgO mixed with salt of four different compositions as a function of temperature. The temperature effect is quite pronounced for three salt compositions, but relatively minor for the all-lithium-cation salt composition. The MgO content also influences the resistivity and mechanical properties of these electrolyte-starved separators. The magnitude of the impact differs for each salt composition, most likely due to differences in MgO wetting properties of the different salt mixtures.

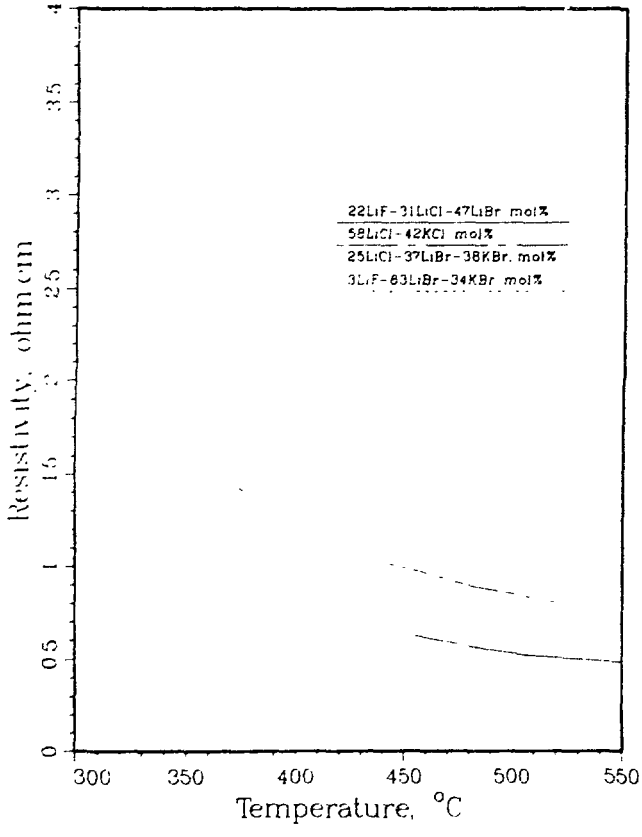

Fig. I-1.

Effect of Temperature on Resistivities of MgO-Salt Mixtures Prepared with 35 wt % MgO

[2]L. Redey and M. McParland, "Resistivity Measurements of High-Temperature Immobilized Electrolytes," Extended Abstracts, Electrochem. Soc. Meeting, Chicago, IL, October 9-14, 1988, Vol. 88-2, p. 1051 (1988).

Our earlier studies[3] indicated that a "bipolar" Li/FeS_2 battery (i.e., cells electronically connected in series so that the positive and negative electrodes of adjacent cells have a common current collector) has the potential for very high performance. In the bipolar cell, a hermetic seal is formed at the periphery prior to cell assembly.[4] Here, a ceramic ring is sealed to molybdenum on one side to form the FeS_2 electrode housing, and a steel assembly is sealed to the other side of the ring to form the lithium-alloy electrode housing. We have developed new sealant materials which are electronic insulators and bond tenaciously to metals and ceramics, even after exposure to molten salt containing lithium alloy or FeS_2 at 400-450°C. To date, we have fabricated over 24 seals and evaluated them in bipolar Li/FeS_2 cells. With emphasis upon ceramics research and seal assembly procedures, we were able to develop a seal with a graded coefficient of thermal expansion (CTE) that approximately matches the CTEs for both steel and molybdenum housings. We then prepared six improved seals for the bipolar cell with similar ceramic compositions and processing methods. One seal was successfully leak-checked at a vacuum of 100 μm--the vacuum limit of our test fixture. Another seal was used to build a sealed bipolar Li/FeS_2 cell (3-cm dia), which operated over 450 cycles and 2000 h and retained >90% of its initial capacity. The area-specific impedance for this small-scale cell was 0.55 $\Omega\,cm^2$, which indicates the potential for high power with this technology. The remaining four seals were used to fabricate sealed bipolar Li/FeS_2 cells for a four-cell stack.

The four-cell stack was operated for >500 cycles (2500 h) with >98% coulombic efficiency, as shown in Fig. I-2. Three of the four cells were employed throughout the tests, while one initially weak cell was replaced at 150 cycles. Bipolar stack capacity (0.45 Ah) was at least 90% that of individual cells. The stack was operated with charge and discharge cutoff voltages of 8.2 and 5.4 V, respectively. As shown in Fig. I-3, the bipolar Li/FeS_2 stack at cycles 100 and 101 was operated at the 4-h charge and 2-h discharge rates. Voltages for the individual cells were well matched during these two cycles without the need for cell-to-cell charge equalization. During stack lifetime, the voltage and capacity of initial cells with repeated recharging were sufficiently well matched that charge equalization was needed only every 20th cycle rather than every cycle. Charge equalization was achieved without electronic equipment by use of an overcharge-tolerance mechanism for molten-salt cells, "the lithium-shuttle mechanism." By cell design, lithium transport near the end of charge safeguards strong cells from overcharging, while weaker cells continue to accept charge capacity.

This bipolar cell stack was assembled from four individual cells stacked with nickel felt pads and voltage leads between the cells. A special Al_2O_3 tube was used to align the cells in the stack and support the voltage taps. Development of a suitable method for integrating cells into a stack is a future task. The average stack discharge voltage, approximately 6.5 V, exceeded the decomposition voltage of the molten-salt electrolyte (3.2 V). Thus, this stack demonstration validated the integrity of the bipolar seal technology. A special cycler--built to

---

[3]M. J. Steindler et al., *Chemical Technology Division Annual Technology Division, 1988*, Argonne National Laboratory Report ANL-89/15, p. 19 (1989).

[4]T. D. Kaun, M. J. Duoba, K. R. Gillie, M. C. Hash, D. R. Simon, and D. R. Vissers, "Development of a Sealed Bipolar Li-Alloy/FeS_2 Battery for Electric Vehicles," Proc. of 25th Intersoc. Energy Conversion Eng. Conf., Reno, Nevada, August 12-17, 1990, Vol. 3, p. 335 (1990).

monitor the individual cells in the stack--was used to establish the efficacy of the overcharge tolerance in achieving cell equalization in this four-cell stack.

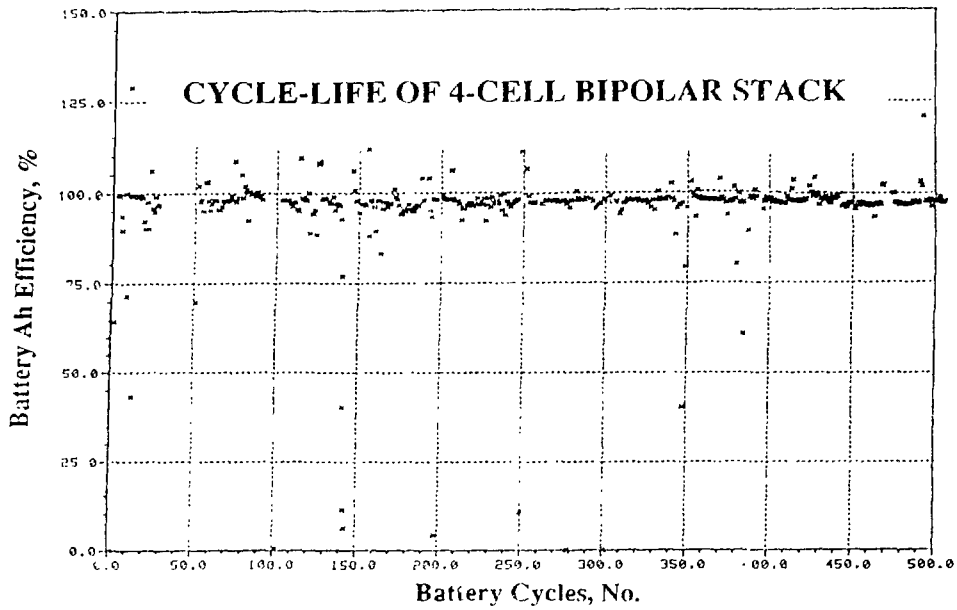

Fig. I-2. Coulombic Efficiency of Four-Cell Bipolar Li/FeS_2 Stack during 500 Cycles of Operation

The high performance of these bipolar cells is indicative of the benefits derived from uniform current distribution across the surface of the electrode and the low internal impedance of this configuration. The observed bipolar cell impedance of 0.55 to 0.65 Ω cm^2 at 400°C is about 50% that observed with "monopolar" cells (i.e., separate current collector for positive and negative electrodes). Further, the weight contribution of hardware to the cell is minimized through the use of the bipolar design. Active material accounts for about 50% of the cell weight for the bipolar cell, compared to about 30% for the monopolar cell. Calculations based on measured performance and component weight breakdown for prototype bipolar cells (capacity of 50 to 75 Ah) indicated that the bipolar configuration should improve specific energy by 30% and specific power by more than 100%. Additionally, we anticipate that the uniform current distribution of the bipolar configuration will help increase cycle life well beyond the 1000 cycles demonstrated with monopolar cells.

We have started a new project, funded jointly by the State of Illinois and DOE, to develop a prototype bipolar Li/FeS_2 battery. The design for this prototype, which includes a vacuum/multifoil insulated case, is shown in Fig. I-4. For this prototype, we will fabricate and test 15-cm-dia bipolar cells with a capacity of 50 to 75 Ah. A stack of 22 such cells would provide a 36-V module, which could be series-connected to other modules in one housing for the full battery voltage of 220 V. An attractive feature of the bipolar Li/FeS_2 battery is its high energy density, about 300 Wh/L. The "monoblock" construction (a single weldment) afforded by the bipolar battery design reduces volume, as well as weight. As shown in Fig. I-4,

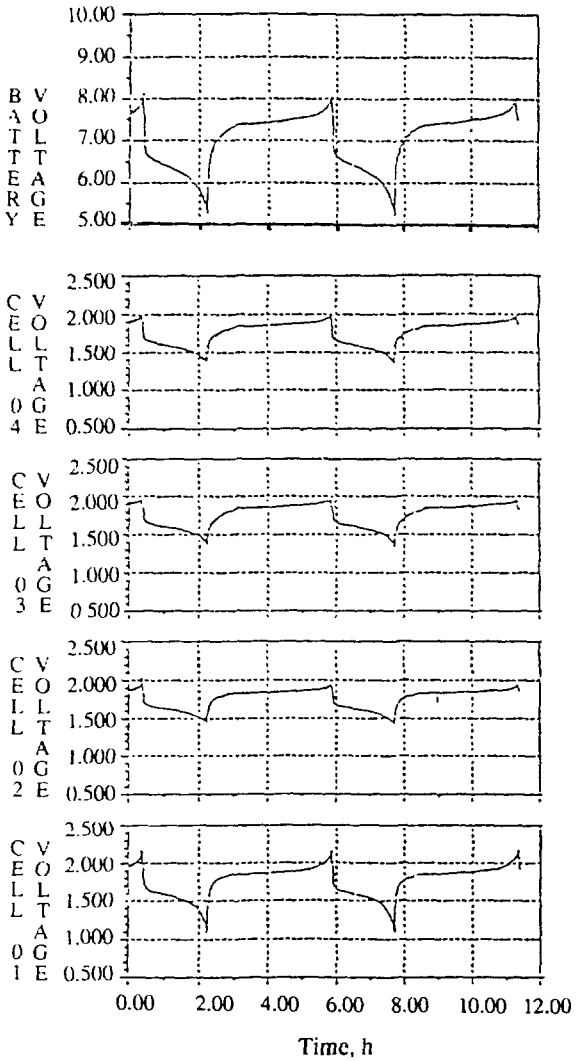

Fig. I-3.

Voltage (in volts) of Bipolar Li/FeS_2 Battery Stack and Individual Cells vs. Time at Cycles 100 and 101

the bipolar Li/FeS_2 battery is designed with almost no free volume internally. The intercell connections, which add excess bulk in monopolar configurations, are eliminated by the bipolar stack configuration.

In a calculational study, we projected the performance of an electric passenger vehicle, the General Motors (GM) Impact, in which a bipolar Li/FeS_2 battery is substituted for its advanced lead-acid batteries. A bipolar Li/FeS_2 battery--possessing about half the weight and volume of the present lead/acid battery for this vehicle--could provide a 250-mi (400-km) range, thereby doubling the range of this vehicle. It would also accelerate the GM Impact at a rate comparable to that for an internal-combustion vehicle, 0 to 60 mph (0 to 96 km/h) in 8 s.

Future research on the Li/FeS_2 bipolar battery will be focused on scaling up the metal/ceramic seal for use in full-size EV cells.

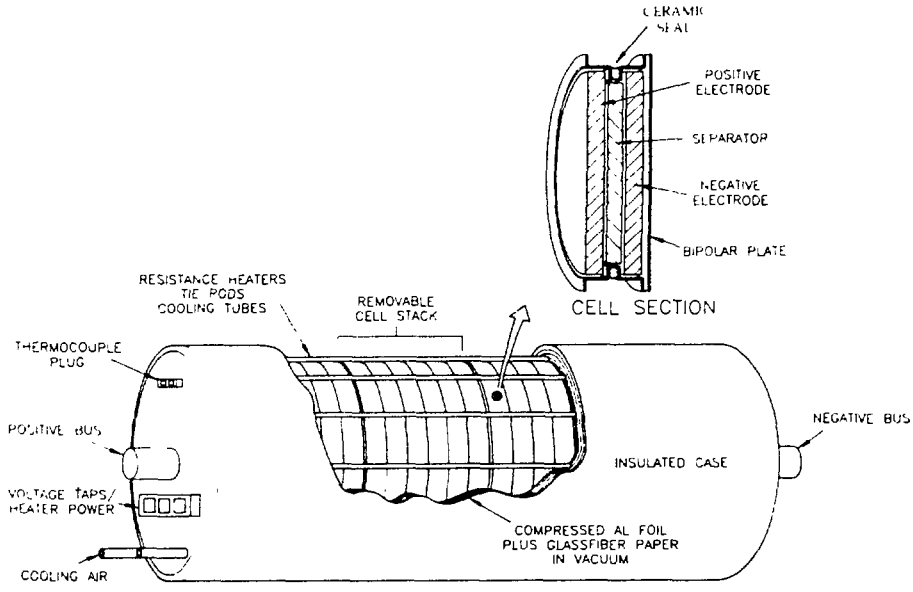

Fig. I-4. Schematic of Li/FeS_2 Bipolar Battery within Vacuum/Multifoil Insulated Housing

2. Sodium/Metal Chloride Technology

The purpose of this CMT research program is to generate the technical information needed to develop advanced sodium/metal chloride (Na/MCl_2) cells with high specific energy (200 Wh/kg at the 3-h rate) and power (>200 W/kg at 80% DOD). The present cell uses a molten sodium negative electrode, a β"-alumina solid electrolyte, and a solid metal chloride such as $NiCl_2$ or $FeCl_2$ for the positive electrode. The metal chloride cathode uses a secondary electrolyte (catholyte) of $NaAlCl_4$. The cell is normally operated at 260°C. Despite the high theoretical specific energy of the $Na/NiCl_2$ cell (790 Wh/kg), the performance of the present β"-alumina single-tube cells is limited (~100 Wh/kg and ~100 W/kg). Our preliminary cell modeling studies suggest that, to develop high-performance Na/MCl_2 cells, it will be necessary to increase the area of the solid β"-alumina electrolyte and operate at low-to-moderate current densities.

Our cathode development studies have focused on increasing the performance of the $NiCl_2$ electrode. In these studies, annular $NiCl_2$ electrodes were operated inside a β"-alumina-tube electrolyte. These electrodes contained between 15 and 20 vol % Ni and possessed a high capacity density, 0.40-0.50 Ah/cm^3. These capacity densities are almost 50% greater than those used in state-of-the-art cells. Last year, we found that an 18 vol % Ni electrode had an area-specific impedance of 1.2 $\Omega\,cm^2$ at 300°C.[5] By fabricating the electrode with larger and more uniform porosity, we obtained significant decreases in the area-specific impedance. A 20 vol % Ni electrode (4-mm dia, 1-cm tall) made by the new fabrication method had an area-specific

[5]I. D. Bloom, S. K. Ong, and D. R. Vissers, "Effect of Some Design Parameters on the Performance of $NiCl_2$ Electrodes," Extended Abstracts, 176th Electrochem. Soc. Meeting, Hollywood, FL, October 15-20, 1989, Vol. 89-2, p. 145 (1989).

impedance of 0.80 Ω cm^2 at 260°C. At lower nickel fractions, similar improvements in area-specific impedance were seen. In an electrode containing 17 vol % Ni, for example, area-specific impedances as low as 0.5 Ω cm^2 were obtained at 260°C. Clearly, these values are lower than those for a nickel electrode in state-of-the-art cells (1.0-1.5 Ω cm^2), and the fabrication method plays an important role in determining the area-specific impedance.

Additional improvements in the performance of these and larger porous electrodes will be realized through changing the morphology and chemistry of the electrode. For this purpose, we are investigating the effects of fabrication parameters on electrode morphology and elucidating the kinetics and mechanisms of the electrochemical processes.

Several structural aspects of the nickel electrode, observable under the microscope, may limit its performance. Among them are nonuniform distributions of Ni and NaCl. Microscopic examination of post-test $NiCl_2$ electrodes revealed an obvious segregation of material, with the NaCl particles clustering together and. in some places, forming strata. This segregation would leave other areas of the electrode deficient in NaCl. If the distribution of NaCl were more uniform, the resulting $NiCl_2$ layer would also be more uniform. As a consequence, the area-specific impedance at deep discharge would be lower. Work is underway to improve the distribution of electrolyte and active material within the electrode and the resulting morphology.

Altering the chemistry of the electrode should also help improve electrode performance. As such, further $NiCl_2$ electrode development will require a thorough understanding of the kinetics and the mechanisms of the electrode processes occurring during cell operation. Three techniques are being used in these investigations: (1) interrupted galvanostatic cycling of nonporous electrodes, (2) cyclic voltammetry of nonporous electrodes, and (3) interrupted galvanostatic cycling of Na/β"-alumina/$NiCl_2$ cells built with porous positive electrodes.

The first two techniques were developed to better understand the electrode processes occurring on a simple nonporous nickel electrode surface (0.15-cm-dia nickel wire) in various NaCl-saturated chloroaluminate electrolytes. Here, the processes occurring on the surface may be clearly observed without the complications due to a porous structure. The cell used in these studies can be depicted schematically by:

(neg.) Al/$NaAlCl_4$, additives/Ni/$NiCl_2$ (pos.)

Use of an aluminum counter electrode has the following advantages: it acts as both a counter and reference electrode because of the well-defined chemistry and fast kinetics, yields results that can indicate the type of soluble nickel species present, and makes cell construction simple. Galvanostatic cycling and cyclic voltammetry with a nonporous electrode are used in a complementary fashion to gain insight into the fine details of electrode kinetics.

The third technique is used to study the performance properties of the porous electrode in the complete Na/$NiCl_2$ cell. The complete cell is designed in such a way that the properties of the three main cell components (sodium electrode, β"-alumina solid electrolyte, and

$NiCl_2$ electrode) can be evaluated to find limiting factors that influence the overall cell performance. The cell containing the porous electrode is operated under a one-dimensional current distribution. From the results of the tests, the important cell parameter, area-specific impedance for a 15-s potential relaxation (ASI_{15s}), can be determined as a function of temperature, cycling regime, and cycle life. These values are indicative of the intrinsic properties of the porous electrode and, therefore, can be used in modeling calculations and cell scaleup.

The most significant information gained from these investigations in 1990 is summarized below. During charge $NiCl_2$ forms a poorly conducting layer on the surface of the nickel electrode, which produces a marked increase in the ASI_{15s} of the electrode (compare curve at 20% active-material utilization with that at 90% in Fig. I-5). Upon reaching a certain thickness, this layer hinders further charge of the electrode. This situation is characterized by a limiting area capacity (units of C/cm^2), which is a strong function of temperature (see Fig. I-5). Cyclic voltammograms and charge-discharge curves of nonporous electrodes indicated that the charge process takes place in two consecutive steps. The reactions associated with these steps are not understood and are being investigated further.

Additives greatly influence the electrode charge-discharge process and, consequently, the limiting area capacity and area-specific impedance. We found that 2 wt % sulfur additive (based on wight of the chloroaluminate salt) in nonporous nickel electrodes increases limiting area capacity by a factor of about five, decreases the ASI_{15s} value by a factor of about two, and improves the coulombic efficiency by up to 100%. The observed improvement in coulombic efficiency of the cell suggests that an insoluble, sulfide-containing nickel species forms on the nickel electrode surface. This sulfur-containing $NiCl_2$ has substantially better performance characteristics than $NiCl_2$ alone.

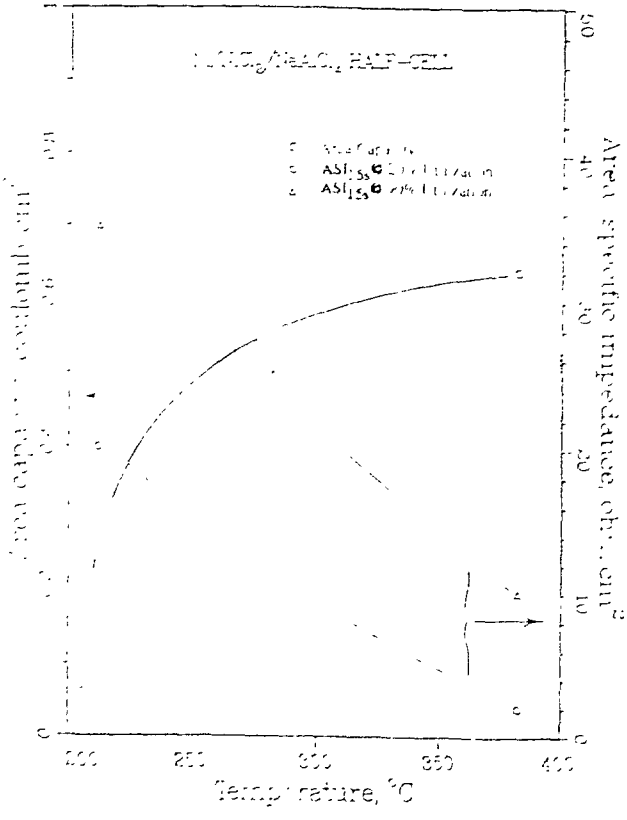

Fig. I-5.

Performance Characteristics of Nonporous Nickel Chloride Electrode Discharged at 1 mA/cm^2 as Function of Temperature

The findings given above suggest ways to modify the chemistry of the porous nickel electrode and thereby improve $Na/NiCl_2$ cell performance. Further investigations are being carried out to determine the chemistry involved in the dissolution of the electrode reaction products and the charge/discharge processes of the nickel electrodes.

As an aid for the further development of the nickel electrode, we have mathematically modeled its electrochemical behavior. The most important factor in modeling Na/MCl_2 cells is determining the impedance of the positive electrode during discharge. Sodium/metal chloride cells have higher impedance than Na/S cells of the same configuration, primarily due to the added resistance associated with the chloroaluminate in the pores of the positive electrode. The $NaAlCl_4$ species is only a moderately good ionic conductor. The transport of sodium ions through the molten $NaAlCl_4$ accounts for a large portion of the total electrode impedance, as reported in the literature for cells having thick electrodes (about 1 cm).[6] The metal matrix contributes little to the impedance of the electrode. The reaction impedance is an important factor if the electrode is thin, the temperature is well below 250°C, or the discharge is nearing completion. All of these conditions are of interest in designing Na/MCl_2 cells for the optimum combination of high specific energy, high specific power, and operability over a wide temperature range.

We developed a finite-element model for cells having positive electrodes inside β''-alumina electrolyte tubes. In this model, the electrode is divided into tubular elements of equal volume. The metal matrix has negligible resistance, and the reaction impedance within an electrode element is inversely proportional to the unreacted $NiCl_2$ capacity in that element. The calculation of the electrode impedance is an iterative process for each one percent of the capacity discharged. Calculations made for 10 and 20 volume elements resulted in the same electrode impedance within 0.5% over the discharge range 0.5% to 94.5%.

Calculations were made for the conditions used in obtaining experimental data from testing a $Na/NiCl_2$ cell with a capacity density of 0.354 Ah/cm^3, an electrode radius of 0.45 cm, and a current collector radius of 0.24 cm. In these calculations, the value of the reaction impedance constant, which we refer to as the "capacity specific resistance" (in units of Ω-Ah), was varied until the calculated impedances were in close agreement with the measured values over the discharge range (Fig. I-6). This indicates that our finite-element model accurately reproduces the true impedance conditions over the course of the discharge.

We extended the finite-element calculations to include 22 cases for a variety of positive-electrode thicknesses, capacity loadings, capacity specific impedances, and configurations (positive electrode either inside or outside the electrolyte tube, and flat-plate bipolar cells). Work is in progress to develop an empirical equation that will duplicate, as nearly as possible, the electrode impedances calculated by the finite-element model. The empirical

---

[6] I. D. Bloom, P. A. Nelson, L. Redey, S. Orth, C. Hammer, D. W. Dees, M. C. Hash, and D. R. Vissers, "Design Considerations for the Development of Advanced Sodium/Metal Chloride Cells," Proc. of 25th Intersoc. Energy Conversion Eng. Conf., Reno, NV, August 12-17, 1990, Vol. 3, pp. 341-347 (1990).

equation is desired because of the many iterations that are required for optimization of cell and battery designs with the finite-element model. Future plans for the modeling effort include adding temperature effects, studying impedance on charging, and determining steady-state chloride distributions within the electrodes.

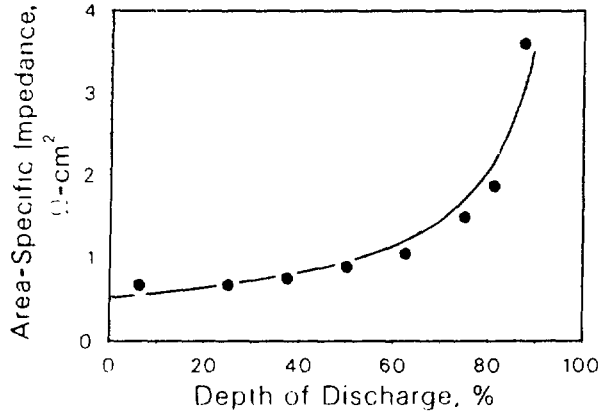

Fig. I-6.

Comparison of Finite-Element Model Prediction (curve) with Experimental Impedance Data (circles)

The Department of Energy placed an industrial contract with Beta Power, Inc., to develop conceptual designs for high-performance Na/MCl_2 batteries. We provided technical management and support for this design effort. In 1990, Beta Power developed two conceptual cell designs for advanced Na/MCl_2 batteries that have the potential of achieving 150 Wh/kg at the 3-h discharge rate and 150 W/kg at 80% DOD. As a result of this successful effort, DOE is preparing to place a new industrial R&D contract to develop advanced Na/MCl_2 batteries for EV applications. We will provide the technical management of this new industrial contract. This multi-year contract is scheduled to be initiated early in 1991. It will be directed toward the development of a full-scale battery for an electric van.

B. *Analysis and Diagnostic Laboratory*

The Analysis and Diagnostic Laboratory (ADL) was established in CMT to study advanced battery systems for EV and utility load-leveling applications. The facilities include a test laboratory to conduct battery experimental evaluations under simulated application conditions and a post-test analysis laboratory to determine, in a protected atmosphere if needed, component compositional changes and failure mechanisms. In 1990, evaluations were performed for the DOE and Electric Power Research Institute (EPRI) to provide insight into those factors that limit the performance and life of six advanced-battery technologies. The results of these evaluations help identify the most-promising R&D approaches for overcoming these limitations and provide battery users, developers, and program managers with a measure of the progress being made in battery R&D programs, a comparison of battery technologies, and basic data for modeling.

1. Performance and Life Evaluations

As shown in Table I-2, performance and life evaluations were conducted on six technologies from eight manufacturers in 1990. These results for each technology are discussed below.

Table I-2. Summary of Test Results from Electric-Vehicle Battery Evaluations in ADL for 1990

Battery Description			Module Weight, kg	Initial Module Capacity,[a] Ah	Specific Energy,[a] Wh/kg	Volumetric Energy Density,[a] Wh/L	Peak Power,[b] W/kg	Battery Eff., %		Battery Life,[c] cycles	Van Range,[d] mi (km)
Technology	Manufacturer	Model						Coulombic	Energy		
Sodium/Sulfur	Powerplex	B-11	253	238	81	83	150	100	91	>200	154 (246)
	CSPL	PB-MK3	29.2	292	79	123	90	100	88	>200	150 (240)
Zinc/Bromine	SEA	ZBB-5/48	81	126	75	56	53	93	75	>300	93 (149)
Nickel/Metal Hydride	Ovonics	C-cell	0.081	3.6	54	186	182	92	80	289	97 (155)
Nickel/Cadmium	SAFT	STM5-200	24.5	217	55	104	191	90	78	>250	102 (163)
Nickel/Iron	Eagle-Picher	NIF220	25	231	56	136	92	74	55	370	76 (122)
		NIF200	25	203	51	118	111	74	58	>200	87 (139)
Lead-Acid	Sonnenschein	6V160	31.5	184	36	92	125	94	84	370	51 (82)
	Chloride	3ET205	32.8	185	33	78	87	87	68	715	47 (75)

[a]Measured at 3-h discharge rate.

[b]Determined from driving profile discharge data at 50% DOD.

[c]Determined for 100% DOD cycles. Ongoing tests are indicated by ">" sign.

[d]Determined for a simplified version of the Federal Urban Driving Schedule with a van having a 695-kg battery.

a. Sodium/Sulfur Technology

Two Na/S systems are undergoing evaluation at ADL. One is a one-half-size (22-kWh) EV battery from Powerplex Technologies, Inc., that has been under test since May 1990. This 90-V battery with thermal and safety management systems was shipped to ANL at operating temperature (310°C). It contains 360 cells (30-Ah rating) configured into three series-connected banks, each containing 8 parallel-connected strings of 15 series-connected cells. The thermal management system satisfactorily maintained the battery within an operating temperature range of 310-340°C for a variety of power discharges. This battery system has exhibited the highest specific energy (and provided the greatest simulated vehicle driving range) of any battery examined to date. After operating for 185 cycles, the battery had to be cooled to ambient temperature to repair an output power terminal. It was subsequently reheated to operating temperature and testing resumed. It has completed >200 cycles in this ongoing test and retains ~98% of its initial 238-Ah capacity.

An 8-V Na/S module from Chloride Silent Power Ltd. (CSPL) has been under test since June 1990. The module contains 120 cells (10-Ah each) configured into 30 parallel-connected strings of 4 series-connected cells. This module is of the same design and assembly as those (24 series-connected modules) in the battery system for the ETX-II vehicle (a light duty van based on the Ford Aerostar). The module has successfully completed >200 cycles in this ongoing test and still retains ~100% of its initial 292-Ah capacity.

b. Zinc/Bromine Technology

The Studiengesellschaft fur Energiespeicher und Antriebssysteme (SEA), Research Group for Energy Storage and Propulsion Systems, in Austria licensed the Zn/Br technology developed by Exxon Corp. under the DOE Electric and Hybrid Vehicle Program and improved the original Exxon design. Evaluation of a 48-V Zn/Br module from SEA was started at ADL in November 1989. The self-discharge capacity loss from the SEA module (~3% in the first hour after charge and, thereafter, continued at a rate of ~0.8%/h) is more than a factor of two improvement over that exhibited by the Exxon technology. The module requires electrochemical maintenance about every six cycles of operation, wherein it is completely discharged to 0 V for ~4 h to strip all the zinc from its electrodes. In between stripping cycles, module capacity declined at the rate of ~1 %/cycle. The SEA module has good specific energy (~75 Wh/kg at 3-h rate), but low power capability (~53 W/kg at 50% DOD). The limited power is due to a high internal module resistance. The module has completed >300 cycles and shows no decline from its initial performance.

c. Nickel/Metal Hydride (C-Cells)

Performance and life tests are being conducted on 3.6-Ah (C-size) nickel/metal hydride cells from Ovonic Battery Co. These cells are viewed as a replacements for commercial Ni/Cd batteries, and Ovonics proposes to scale up to larger cell sizes to fabricate a full-size battery (30 kWh) for EV applications. The ADL tests are designed to determine the suitability of this technology for EV propulsion. These cells exhibited the highest volumetric energy density (186 Wh/L) of any battery system examined to date. An impressive specific

energy of 54 Wh/kg (3-h rate) and peak power of 182 W/kg (50% DOD) were also attained. As with the Na/S battery, the nickel-metal hydride cells provide full capacity with driving profile discharges because of their good power capability. Cell cycle life, however, has been limited. Three cells have been life tested, and the longest life achieved was 289 cycles.

d. Nickel/Cadmium Technology

Performance characterization and life tests are being conducted on two 6-V Ni/Cd modules manufactured by SAFT (Industrial Storage Battery Division), France. These modules are designed for high energy and power density in transportation applications and should provide long cycle life. The modules were delivered to ANL from Idaho National Engineering Laboratory, where they were previously operated for about 35 cycles. Both modules have completed performance characterization tests, and one is undergoing life evaluation using an urban driving profile discharge for the TEVan, an electric van designed by Chrysler Corp. The life-test module has completed >250 cycles and retains all of its initial 217-Ah capacity. Driving profile discharge data show that this technology has the highest peak-power capability (191 W/kg at 50% DOD) of any battery system examined to date. This high power capability allows full capacity discharges and, therefore, maximal vehicle range on several different driving profiles.

e. Nickel/Iron Technology

Two types of advanced Ni/Fe modules (NIF220 and NIF200) from Eagle-Picher Industries, Inc., are being evaluated. Both have sintered-powder nickel electrodes, which have the potential for lower cost than conventional nickel electrodes. The NIF220 design provides a capacity of 220 Ah in the same module package as the 170-Ah module developed for the Dual Shaft Electric Propulsion Program at Eaton Corp. Several NIF220 modules were tested, and all exhibited a rapid capacity loss (~0.1%/cycle) with cycling. The maximum NIF220 life achieved at ADL was 370 cycles. Post-test analyses on a failed cell showed that its capacity was limited by the nickel electrode, but severe deterioration of the iron plates had contaminated the nickel plates. The causes of the iron electrode problem in the NIF220 design were corrected by Eagle-Picher in its later NIF200 design, and good test results have been obtained to date. The NIF200 on life test still retains ~95% of its initial 203-Ah capacity after >200 cycles.

f. Lead-Acid Technology

Performance and life tests were started in 1989 on two valve-regulated lead-acid (VRLA) modules manufactured by Sonnenschein Battery Co. (Germany) with a gelled electrolyte. The maintenance-free cells are equipped with pressure relief valves for venting and use an antimony-free alloy. The 6-V modules are named "dryfit traction blocks" and have a rated 5-h capacity of 160 Ah. One module successfully completed 370 cycles before its simulated driving range declined by 20%. The second module is still on life test and retains 123% of its rated capacity after completing >250 cycles.

2. Post-Test Analyses

Detailed examinations are conducted on selected cells, modules, and batteries that have completed testing either at the ADL or other centers of battery research. The information gained from post-test analyses provides a measure of the technical progress made by the battery developers and identifies specific areas where changes in design or the materials of construction would improve battery performance. Reported below are results from post-test analysis of four battery technologies: Na/S, Li/FeS, Ni/Fe, and lead-acid.

a. Sodium/Sulfur Technology

A joint CSPL-ANL failure analysis was completed on a 19-kWh Na/S battery fabricated by CSPL and tested at ADL for 241 cycles. Radiography identified 51 failed cells in this 960-cell battery. Seventeen failed cells were examined to ascertain the cause of failure. These examinations determined that 75-95% of the failures were due to fracture of the glass seal between the β''-alumina electrolyte and the α-alumina top cap. The fundamental cause of this failure was an improper glazing procedure that resulted in excessive porosity in these seals. Chloride Silent Power has since altered the furnace atmosphere used during glazing to rectify this problem. The defective seals had greater susceptibility to corrosion by sodium and reduced resistance to crack propagation. Factors that accelerated this failure included higher cell temperatures, a low position in the four-tiered array of cells within the battery, and the failure of adjacent cells.

Our examinations also revealed that the use of sodium safety cans greatly alleviated, but did not eliminate, the potential for cell failure propagation due to loss of the sodium seal. The integrity of a cell case was also threatened by accelerated corrosion once a cell failed and remained at operating temperature. Examination of four unfailed cells from this battery confirmed that recent design improvements were effective in reducing calcium contamination of the electrolyte and controlling corrosion of the cell components under normal operating conditions.

b. Lithium/Iron Sulfide Technology

Failed cells from a 36-V Li/FeS electric-van module were examined to determine the cause(s) of failure. This module had been fabricated by the Westinghouse Naval Systems Division and life tested at ADL for 141 cycles. The cause of short circuiting was electrochemical deposition of metallic iron in the separators. This mode of failure has been well documented for this electrochemical couple when LiCl-KCl salt is used as the electrolyte. Problems with thermal management of the module exacerbated iron deposition and led to the failure of 12 of 27 cells. Most failed cells were situated in the central core of the module. At times, these cells experienced temperatures >500°C and were consistently 20°C hotter than the outer cells. Operation above the desired temperature of 450°C accelerated the deposition reaction and led to premature failures.

Thermal Li/FeS_2 cells from Sandia National Laboratories were examined to determine how variations in the active materials affect Li_2S deposition within the separators of

these primary cells, a mode of cell failure. The standard thermal cell consists of an FeS_2 cathode, MgO powder separator, Li-Si anode, and LiCl-KCl eutectic electrolyte. Cells representing 20 variations in cathode, anode, and electrolyte materials were studied. All of the cells were held at 500°C on open circuit for up to an hour, a condition found to accelerate deposition in the separators. Microscopy studies identified that Li_2S deposition was affected by virtually all changes in overall cell composition. Lithiation of the cathode enhanced Li_2S formation. Deposition of Li_2S was lower when (1) cathodes were prepared from intermediate discharge phases ($Li_3Fe_2S_4$ rather than FeS_2), (2) cathodes had higher concentrations of iron-bearing impurities, and (3) ternary salts were used instead of the standard LiCl-KCl electrolyte. With respect to anode variations, electrodes with higher lithium activities had increased Li_2S deposition. Also, the location of the Li_2S deposits was affected by changes in cell materials. Any variation from the standard cathode composition moved the deposition minima closer to the anode. In the anode-variation samples, higher lithium activities shifted the deposition maxima closer to the cathode. There appeared to be no clear trend, however, in the electrolyte-variation samples with respect to deposition location. Undoubtedly, the quantity and location of deposited Li_2S are governed by the type of soluble species originating in both electrodes and their solubility in the different electrolytes. Fundamental studies are required to address these issues.

c. Nickel/Iron Technology

We examined a Ni/Fe module (NIF-270) removed from a battery pack built by Eagle-Picher for in-vehicle testing that began in 1983. At the time of removal from testing, the module had accumulated over 66,000 actual and equivalent miles (106,000 km).* The capacity decline in this module was totally attributable to the voltage reversal of one cell. The primary cause of this reversal was degradation of the iron plates, including excessive active-material loss and the loss of adhesion between the active material and the grid. Overdischarge, as evidenced by Fe_3O_4 formation, promoted the degradation of these electrodes. Two factors contributed to the tendency to overdischarge the iron electrodes: (1) the cell capacities were limited by the iron electrodes rather than the nickel electrodes, and (2) the KOH concentration of the electrolyte was well below the nominal composition. Our analysis did not definitively identify the reason for the precipitous failure of this cell. The iron electrodes in four adjacent cells were subjected to similar conditions, yet they maintained capacities near their rated value. Presumably, variations in cell fabrication and/or operation, such as temperature, led to the accelerated failure of this cell.

d. Lead-Acid Technology

A flooded-electrolyte lead-acid module from Chloride EV Systems Ltd. was life tested in ADL under driving profile discharges to 100% DOD to evaluate a worst-case condition. The module successfully completed 715 cycles before its simulated driving range declined by 20%. Post-test analysis indicated that the declining performance was caused by the presence of high levels of antimony and the poor adhesion between the grids and the active materials. The unusually high antimony concentration in the negative active materials indicated

*The battery pack was removed from the vehicle and tested in the laboratory. Hence, the reference to "equivalent" miles.

that the antimony generated by corrosion of the positive grids had plated onto the negative electrodes during operation. Antimony "poisoning" of the negative active materials reduced charging efficiency and decreased the effective capacity of the electrodes. Meanwhile, loss of adhesion between the grids and the active material caused an increased resistance and a reduction in the charging efficiency of the negative electrodes.

Two VRLA technologies for utility cycling applications were tested: (1) gelled-electrolyte modules from Johnson Controls, Inc., and (2) absorbed-electrolyte modules from GNB Industrial Battery Co. The study used a matrix of operating temperature and DOD conditions designed to vary the stress of known mechanisms that cause battery end-of-life. The cycle life of the Johnson Controls modules was less than expected due to a manufacturing defect that caused accelerated corrosion of the cast-on strap for the positive plate lugs. The lugs were not properly fused to the strap during the casting process. The corrosion rate of the straps was a function of module operating temperature and DOD. The strap problem is correctable through better quality control procedures.

The GNB modules had about twice the life of the Johnson Controls modules, and corrosion also varied with temperature and DOD. Preliminary post-test findings are that corrosion of the positive-electrode grids limited the life of the GNB cells. A study was also conducted to measure the quantity of potentially toxic stibine emissions from these GNB modules. Stibine was found to be present in only trace quantities under operating conditions that caused venting of internally generated gases. Early in life, when emissions were highest, the rate of stibine emission was quite low (<25 μg/min), requiring only minor ventilation. With time, the quantity of electrolyte gas diminished, due to improved oxygen recombination efficiency, and the potential toxicity problem was further reduced.

C. *Fuel Cell Research and Development*

We are developing two types of high-temperature fuel cell: one with a solid oxide electrolyte, and the other with a molten carbonate electrolyte.

1. Monolithic Solid Oxide Fuel Cell

The solid oxide fuel cell has an oxide-ion conducting electrolyte material, yttria-stabilized zirconia (YSZ). The electrode materials are strontium-doped lanthanum manganite (LM) on the air side (cathode) and nickel-YSZ on the fuel side (anode). The material that connects the individual cells in electrical series (bipolar plate) is strontium-doped lanthanum chromite. These components are all oxide-ceramic materials. On the fuel side, at the nickel-electrolyte-gas (electrochemically active) interfacial area, hydrogen and carbon monoxide in the fuel gas react with oxide ions from the electrolyte to form water and carbon dioxide, giving up electrons to the external circuit. Similarly on the air side, at the LM-electrolyte-gas interfacial area, oxygen in the air accepts electrons from the external circuit to form oxide ions, which are conducted through the electrolyte to the anode interface. These cells operate at temperatures of 800 to 1000°C.

The Chemical Technology and Materials and Components Technology Divisions have developed a monolithic solid oxide fuel cell (MSOFC). The cell design is based on the premise that the thin solid components of oxide cells can be fabricated into compact shapes having power-to-weight ratios that are a factor of 100 higher than those of conventional fuel cells. The principal building blocks of the MSOFC structure are two multilayer composites: the anode/electrolyte/cathode (A/E/C) and the cathode/interconnect/anode (C/I/A). Good performance of the monolithic fuel cell requires the layers in these composites to be well bonded and free from cracks or other gas-transmitting defects. The characteristics of the electrode/electrolyte interfaces, such as electrode porosity and microstructure, are also important to achieving good fuel cell performance.

In 1988, Allied Signal Aerospace/AiResearch began development work on the MSOFC with technical support from ANL. In the past year, our support work has focused on the problems with long-term performance of the cathode, the effect of sulfur on the anode, and multicell stack performance.

The effect of long-term operation (40,000 h) on the MSOFC cathode performance is a concern because densification, manganese migration, and other physical and chemical changes in the cathode may be a problem. An accelerated test of the long-term cathode performance was conducted by operating a series of cathode/electrolyte/cathode composites at elevated temperatures (1000-1200°C) in air for 1000 h. The cathode interfacial electrochemical performance was monitored during the test by an established ac impedance technique. Selected results from this test are given in Fig. I-7. The results indicate that the cathode interfacial resistance increases with time at both temperatures. This effect is more pronounced at 1200°C. Theoretical calculations based on the accelerated test indicated that the cathode interfacial resistance in an actual MSOFC will increase by 0.13 Ω cm^2 in 40,000 h of operation at 1000°C. This increase is not expected to be a problem for the MSOFC development effort.

Since the MSOFC would operate on coal gas and hydrocarbon fuels, which contain sulfur at low part-per-million (ppm) concentrations, we evaluated the effect of sulfur on the anode performance. Symmetric anode/electrolyte/anode composites were operated in a reducing environment at 1000°C and subjected to various levels of H_2S (1-100 ppm). During the test, the anode performance was monitored by an ac impedance technique. Figure I-8 illustrates the detrimental effect that sulfur can have on the anode performance. Work is underway on determining the sulfur degradation mechanism.

We have developed a mathematical model that simulates the electrochemistry and thermal hydraulics of an MSOFC stack with cross-flow design (i.e., corrugated layers of anode and cathode materials are placed between flat A/E/C and C/I/A layers, with the electrode corrugations oriented at right angles to each other). Dividing a single cell into a number of nodes, the model sets up the steady-state heat and mass transfer equations for each node in a cell layer. The model calculations yield the temperature distribution and fuel and oxidant compositions for the entire cell. The simulation also provides related performance parameters for the fuel cell stack, such as energy efficiency, fuel utilization, and power density. The model can be used to simulate operation with different fuel gases, such as hydrogen, coal gas, and methanol. The mathematical model is being used to assess the effect of various design variables

on performance and lifetime and to evaluate the effectiveness of laboratory efforts in hardware development.

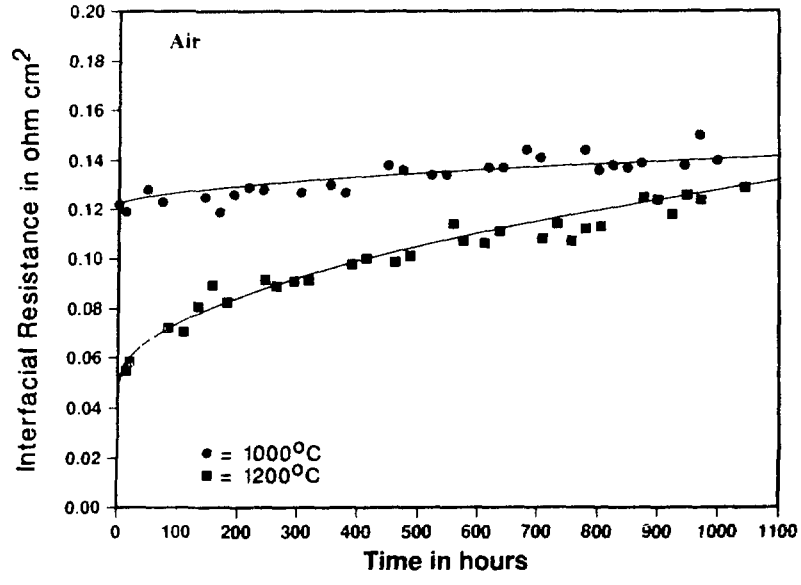

Fig. I-7. Interfacial Area-Specific Resistance of Cathode/ Electrolyte/Cathode Composites at High Temperatures in Accelerated Aging Test

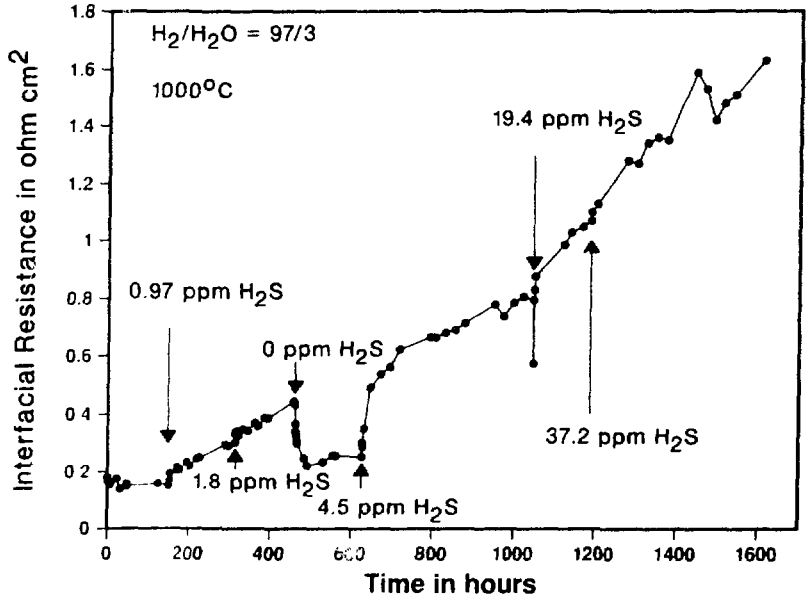

Fig. I-8. Interfacial Area-Specific Resistance of Anode/ Electrolyte/Anode Composite at the Indicated H_2S Level (H_2/H_2O ratio = 32)

Besides continuing the work on determining detrimental electrode effects and mathematical modeling, future efforts will include improving MSOFC electrochemical performance and developing ancillary materials (manifolds, current collectors, and cements).

2. Advanced Materials for Solid Oxide Fuel Cells

The objective of this work is to develop materials which permit the operation of a ceramic, solid-state fuel cell at temperatures of 500-800°C instead of the 1000°C now used. Lowering temperature would increase the flexibility in cell design, allowing metal components to be used as bipolar plates between cells and as gaskets. In turn, this would make fabrication of the cell stack easier. As an added bonus, the thermodynamic efficiency of the fuel cell would be improved. Our approach is to develop new electrolyte materials first. Once highly conductive candidate materials have been found, compatible electrode and interconnect materials will be developed.

The new electrolyte materials must be chemically stable toward oxygen and hydrogen and should have a conductivity close to the target value of 0.05 Ω^{-1} cm^{-1}. The approach to finding candidate materials is to identify and test materials which are known to have oxygen substoichiometry or crystallographic features which might facilitate ionic transport. The search included materials with perovskite and orthophosphate structures.

In the perovskite class of materials, two hypotheses about the factors which affect conductivity are being tested: maximum conductivity is achieved by having (1) a large amount of free volume in the lattice through which the oxide ion can diffuse or (2) a moderate metal-oxygen interaction. The second hypothesis is based on the following reasoning. If the metal-oxygen interaction is very strong, the mobility of the oxide ion is expected to be low. On the other hand, if the metal-oxygen interaction is very weak, oxide ion mobility is expected to be very high. However, for thermodynamic stability in a hydrogen/oxygen atmosphere, very weak metal-oxygen bonds will be readily reducible. Hence, there has to be a compromise between thermodynamic stability and conductivity.

We determined the conductivity and ionic transference number (i.e., fraction of the total conductivity due to ionic transport) at 600°C for several different perovskites. Results are given in Table I-3.

Table I-3.Conductivity and Ionic Transference Number for Selected Perovskites at 600°C

Material	Conductivity, $\Omega^{-1}cm^{-1}$	Ionic Transference Number	Ionic Conductivity, $\Omega^{-1}cm^{-1}$
$SrZrO_3$	7.35×10^{-7}	0.89	6.54×10^{-7}
$SrZrO_3$[a]	2.20×10^{-5}	0.77	1.69×10^{-5}
$SrSnO_3$	1.63×10^{-5}	0.15	2.45×10^{-6}
$SrSn_{0.9}Zr_{0.1}O_3$	1.96×10^{-4}	0.15	2.94×10^{-5}
$SrZr_{0.5}Sn_{0.5}O_3$	2.54×10^{-5}	0.69	1.75×10^{-5}
$SrZr_{0.5}Sn_{0.5}O_3$[a]	4.40×10^{-5}	0.50	2.20×10^{-5}

[a]Doped with 10 at. %Y.

The perovskite initially chosen for study, $SrZrO_3$, had a fair amount of free volume, and based on the thermodynamics of its constituent oxides, we expected it to be stable under fuel cell conditions. However, the $SrZrO_3$ conductivity was found to be low. Doping the perovskite with 10 at. % Y^{3+} increased the vacancy population and, hence, the conductivity. As a result, the conductivity of $SrZrO_3$ was increased 30-fold with a small loss in ionic transference. A method to further improve the conductivity of $SrZrO_3$ is to combine it in a solid solution with another perovskite that has a weaker metal-oxygen bond. Based on lattice parameters and metal-ion sizes, $SrSnO_3$ was chosen to test the hypothesis. As shown in Table I-3 its conductivity is better than that of $SrZrO_3$, but still not good enough for practical use. As compared with $SrSnO_3$, the solid-solution $SrSn_{0.9}Zr_{0.1}O_3$ has a 10-fold increase in the conductivity and no net change in ionic transference. It also has nearly a 100-fold increase in ionic conductivity compared with $SrZrO_3$.

More zirconium was then added to $SrSnO_3$ in order to increase the transference number of the stannate. Comparing the data for the solid-solution $SrZr_{0.5}Sn_{0.5}O_3$ to those from $SrZrO_3$ and $SrZr_{0.9}Y_{0.1}O_{2.95}$, we found a 25- and a 1.25-fold increase in ionic conductivity, respectively, as well as a 5- and 3-fold decrease in activation energy. Clearly, formation of a solid solution in the Sr-Zr-Sn-O system improved the ionic conductivity over that observed in the undoped and unmixed perovskites ($SrSnO_3$ and $SrZrO_3$). The improvement was better than that obtained by substituting lower-valent elements on the zirconium site. Doping $SrZr_{0.5}Sn_{0.5}O_3$ with 10 at. % Y^{3+} produced an approximately 2-fold increase in total conductivity and a decrease in ionic transference. The net ionic conductivity of the yttrium-doped material is slightly larger than that observed for $SrZr_{0.5}Sn_{0.5}O_3$, indicating that the additional vacancies do not significantly improve the conductivity. The metal-oxygen interaction strength appears to be the dominant factor improving the conductivity of the material.

The other class of materials that has been investigated, the orthophosphates, represents a radical departure from the anionic mechanism observed in vacancy conductors. The proposed transport mechanism in these materials is based on cationic transport. That is, the lattice contains fixed, charged sites which are balanced by mobile counter ions. These ceramics tend to have some structural feature which can facilitate ionic transport. The counter ions can migrate from one fixed charge site to the next when an electric field is applied. This type of transport can be more effective than the lattice-vacancy mechanism. The exact nature of the mobile ion depends on how the material is made; theoretically, the mobile ion could be a proton, oxide, or hydroxide. The transport of the mobile ion in, for example, a tunnel may produce the necessary increase in conductivity that we are seeking. To our knowledge, no one has proposed this sort of mechanism for the transport of oxide ions through a ceramic.

Lanthanum phosphate ($LaPO_4$) was selected for study because it has a channel parallel to the crystallographic c-axis that may be large enough to accommodate a proton or vacancy, although this channel is too small for optimal conductivity. Our characterization of doped versions of this material showed that it is conductive. With lower-valent dopants, the maximum conductivity was found in a 10%-Sr-doped material. At 600°C, the conductivity of the material was about $1.5 \times 10^{-4}\ \Omega^{-1}cm^{-1}$ with a transference number of 0.42. The conductivity increased to $1 \times 10^{-3}\ \Omega^{-1}cm^{-1}$ with a transference number of 0.48 at 800°C. These low conductivity values may be due to a large metal-oxygen interaction or the crowding caused by

the small channel. Just as in the perovskite case, we can modify the metal-oxygen interactions by replacing some of the La^{3+} with Bi^{3+}. The total conductivity of $La_{0.9}Bi_{0.1}PO_4$ did not change significantly from that of $La_{0.9}Sr_{0.1}PO_4$. However, the transference number increased to a value close to 1.

In summary, the above results indicate that the perovskites have the oxygen substoichiometry needed for fuel cell use. However, the conductivity of the materials studied is still too low for practical use. For this reason, other perovskite materials are being evaluated. The conductivity observed in $LaPO_4$, with less-than-optimal channel diameter, indicates that this class of material has much potential for the intended application. Other materials in this class will be included in the search for new electrolyte materials.

3. Molten Carbonate Fuel Cell

The present molten carbonate fuel cell (MCFC) consists of a porous nickel anode, a porous nickel oxide cathode, a liquid electrolyte of lithium and potassium carbonates contained by a $LiAlO_2$ matrix, and appropriate metal separator sheets. The cell operating temperature is 650°C. The objective of our research on this fuel cell is to develop electronically conductive ceramic materials that are chemically and polymorphically stable in MCFC environments and to test these materials as MCFC components, i.e., electrodes and separator sheets. Our work is focused on developing alternative cathode and anode materials, developing fabrication techniques, and testing electrode structures in cells.

a. Anode Material Studies

We had previously reported that $LiFeO_2$ and MnO are stable in the anode environment and, at 650°C, have bulk resistivities of 0.2 and 20 Ω cm, respectively,[7,8] which are in the range that might be applicable for fuel cell use. Our recent work on these materials examined the effect of gas composition and doping on their electronic behavior.

The electronic resistivity of two undoped $LiFeO_2$ samples and two niobium-doped $LiFeO_2$ samples was measured under anode inlet gas humidified with room-temperature water. These data are shown in Fig. I-9 for the temperature range 140-650°C. The data show a significant difference in resistivity between the two undoped $LiFeO_2$ samples, which were prepared by different methods. While the reason for the difference has not been quantitatively defined, a qualitative assessment is possible.

In separate studies, we determined that $LiFeO_2$ is reduced to iron metal when heated to 800-900°C in a dry reducing environment (i.e., 6% H_2 balance He or Ar). In environments containing H_2, CO_2, and water vapor, however, the oxygen partial pressure is high

---

[7]M. J. Steindler et al., *Chemical Technology Division Annual Technical Report, 1988*, Argonne National Laboratory Report ANL-89/15, pp. 36-40 (1988).

[8]M. J. Steindler et al., *Chemical Technology Division Annual Technical Report, 1989*, Argonne National Laboratory Report ANL-90/11, pp. 37-40 (1989).

enough (~1 x 10^{-18}Pa) to keep iron in an oxidized state. For the data presented in Fig. I-9, one undoped sample was synthesized at 700°C in an environment that represents an extreme in fuel inlet conditions: 35% H_2, 51% CO, 9.5% CO_2, 3% H_2O, balance N_2. With this low-humidity gas, the oxygen partial pressure is about 9 x 10^{-19}Pa. The other undoped sample was prepared at 700°C under the typical fuel inlet conditions of 80% H_2-20% CO_2 humidified with 60°C water. The oxygen partial pressure is about a factor of five higher than for the first sample. Thus, the starting materials for the undoped samples are expected to have different Fe^{2+}/Fe^{3+} ratios and, therefore, different resistivities. The data in Fig. I-9 demonstrate the importance of the cover gas composition for the material synthesis and resistivity measurement.

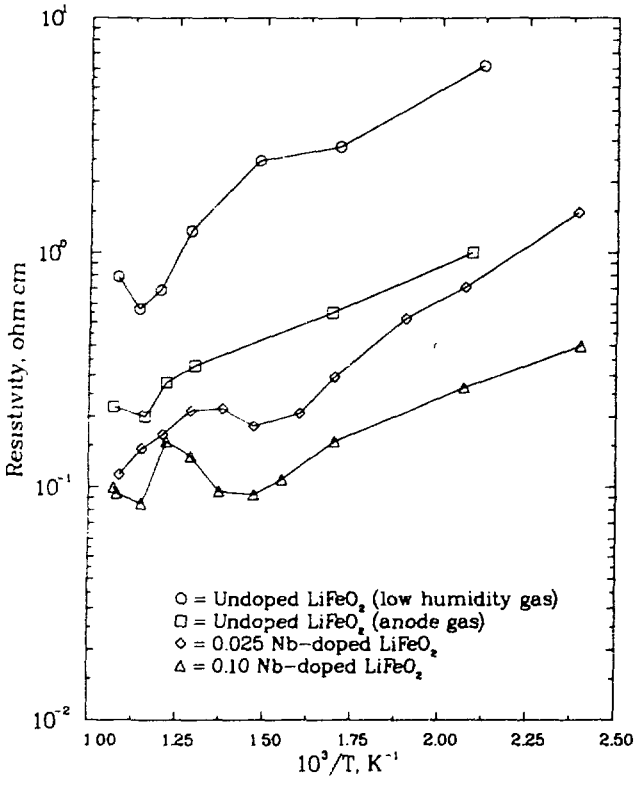

Fig. I-9.

Resistivity of Undoped and Niobium-Doped $LiFeO_2$ Samples Measured under Anode Inlet Gas Humidified with Room-Temperature Water

The effect of niobium doping on anode-prepared $LiFeO_2$ samples is also shown Fig. I-9. The synthesis gas composition was 80% H_2-20% CO_2 humidified with 60°C water. The data show that niobium doping results in a decrease in resistivity for $LiFeO_2$. However, the data show little difference between the Nb-doped material prepared with Nb/Fe ratios of 0.025 and 0.10. While a greater difference might be expected, the nature of the anode-prepared material probably precludes this. Undoped, anode-prepared $LiFeO_2$ contains about 35 mol % Fe^{2+} (Fe^{3+}/Fe^{2+} ~1.8). In the simplest case, the maximum conductivity (caused by electron hopping from Fe^{2+} to Fe^{3+}) would occur when the Fe^{3+}/Fe^{2+} ratio is 1. Assuming complete dopant incorporation, the Fe^{3+}/Fe^{2+} ratio is about 1.4 for the 0.025 Nb-doped material and about 0.6 for the 0.10 Nb-doped material. Thus, it is likely that, at the higher dopant level, a barrier to electron hopping comes from excess Fe^{2+} and Nb sites. From this simple model, it appears that doping with an Nb/Fe ratio of ~0.06 would give maximum conductivity.

The resistivities of two specimens of anode-prepared MnO were measured over the temperature range 375 to 650°C in anode gas humidified with room-temperature water vapor. The data show an average bulk resistivity at 650°C of 18 Ω cm. Stoichiometric MnO is green in color, while the anode-prepared material is black, suggesting *in situ* lithium doping analogous to that of NiO. Crevecoeur and DeWit[9] in their study of Li-doped MnO, prepared in both CO/CO_2 and H_2/N_2 mixtures, report a resistivity of about 20 Ω cm at 650°C when the lithium concentration is about 0.1 at. %. From our resistivity data, we calculated that the activation energy of conduction is 0.41 eV. This value is in good agreement with that calculated from the data of Crevecoeur and DeWit,[9] where the activation energy for Li-doped MnO is 0.45 eV for the temperature range 25 to 725°C. The effect of other dopants on the resistivity of MnO is also under study.

b. Cell Testing

We are testing both 25 cm^2 full-size cells and smaller diagnostic cathode half-cells to gain a better understanding of cathode performance. The effect of varying microstructures and material resistivities on relative performance is under study to provide insight into cathode reaction mechanisms. The current work focuses on the performance and reaction kinetics of $LiFeO_2$, a material which we had previously found to have promise as a thermodynamically stable replacement for NiO as the cathode material.[10] The NiO cathode has dissolution/precipitation problems that limit lifetime in the MCFC environment.

Previously, we reported that the $LiFeO_2$ cathodes are limited in performance by slow electrode reaction kinetics, while NiO is limited by reactant diffusion.[8] We reasoned that increasing the active surface area of the $LiFeO_2$ cathodes would yield better cathode performance. As a result, we developed a new method for synthesizing the $LiFeO_2$ starting material that produces smaller, more even-sized particles (and hence, higher surface area) than the previously used commercial material. Photomicrographs of Co-doped $LiFeO_2$ produced by the standard Pechini process and our modified process are given in Fig. I-10.

With this new starting material, we found some improvement in cathode performance, but not a very significant one. To understand more fully the relative importance of surface area and cathode pore structure, we tested a series of $LiFeO_2$ and $LiCoO_2$ cathodes in half-cells. The focus was on increasing the total surface area in the cathode, with less attention being given to its pore structure (which controls reactant gas access to the bulk of the electrode). The IR-free overpotential ($\eta_{IR\text{-}free}$) of these cathodes versus total surface area is plotted in Fig. I-11. This figure shows that performance can be improved (i.e., $\eta_{IR\text{-}free}$ decreases) by increasing the surface area, but that this improvement is probably limited by gas access to the bulk of the cathode. Figure I-11 also shows the performance of several cathodes fabricated with fibrous agglomerates obtained by our fiber-making process,[7] where the pore structure is more controlled. Again, the indication is that higher surface area yields better performance, although

---

[9]C. Crevecoeur and H. J. DeWit, J. Phys. Chem. Solids **31**, 783 (1970).

[10]M. J. Steindler et al., *Chemical Technology Division Annual Technical Report, 1986*, Argonne National Laboratory Report ANL-87-19, p. 37 (1987).

the correlation is less precise. A better correlation would probably result if we could identify the active rather than just the total surface areas. In Fig. I-11, the better performing half-cell cathodes are $LiCoO_2$, which suffers from the same metal dissolution/precipitation problems as NiO. These cathodes are being used as models to help improve the performance of the $LiFeO_2$ cathodes.

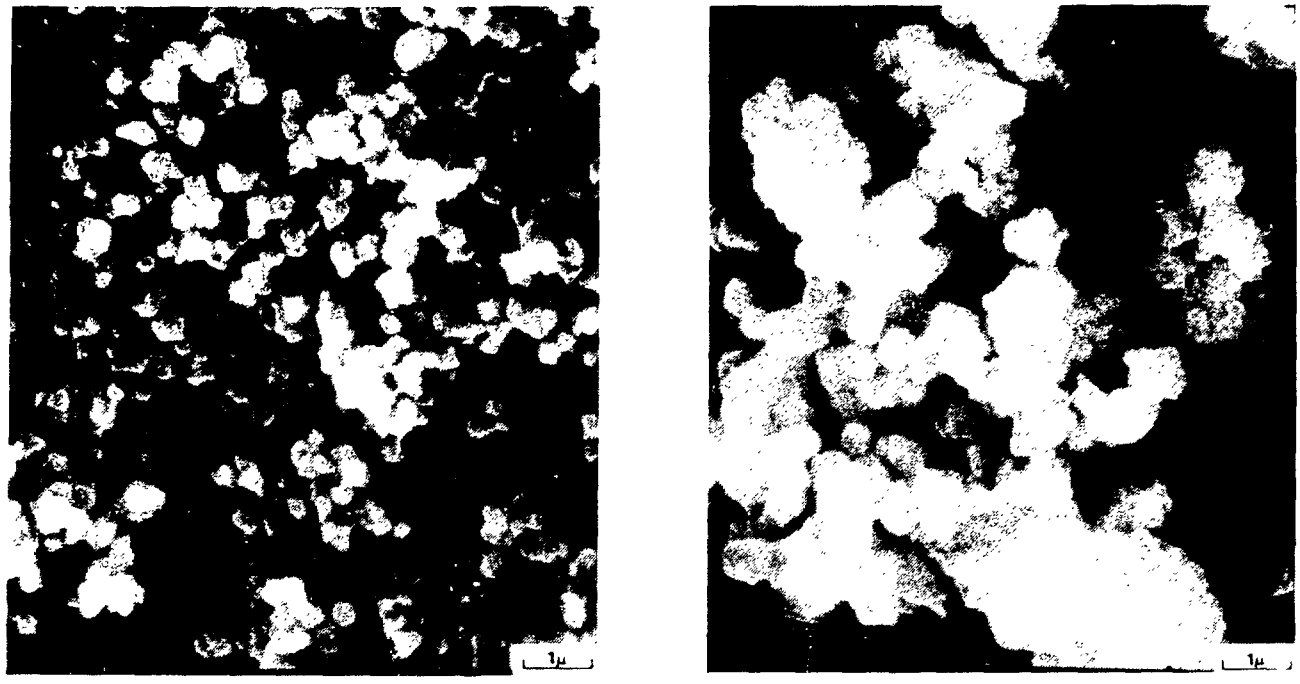

(a) (b)

Fig. I-10. Photomicrographs of Co-doped $LiFeO_2$ Obtained by Lithiation of Co-Fe_2O_3 Produced by (a) Standard Pechini Process and (b) ANL Modified Pechini Process

In our full-cell tests, the best-performing $LiFeO_2$ cathode was cobalt doped and had the high-surface-area (poor gas access) configuration mentioned above. Voltage vs. current density curves for this cell at 650 and 700°C are shown in Fig. I-12, along with one for the conventional NiO cathode. With increasing temperature, the performance of the $LiFeO_2$ cathodes comes closer to that of the NiO cathode. However, the magnitude of this improvement is larger than predicted from the behavior of NiO cathodes. This suggests that with the $LiFeO_2$ a different mechanism controls the reaction rate. This conclusion is supported by what we found previously by studying the reaction-rate gas dependencies in the half-cell.[8] Future work will include a more detailed investigation of the effect of temperature on $LiFeO_2$ and NiO cathode performance. We also will continue studying the effects on cathode performance of pore structure, material conductivity, and active surface area.

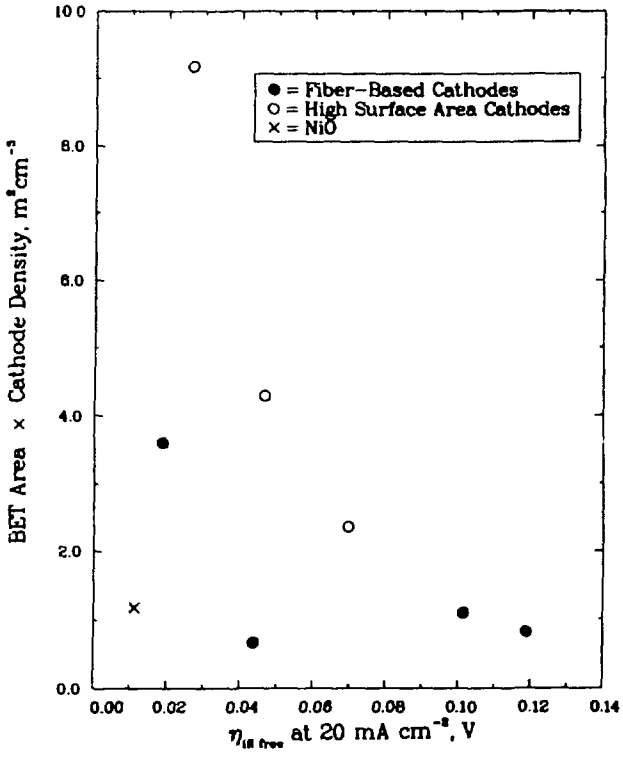

Fig. I-11.

Cathode IR-Free Overpotential as a Function of Total Surface Area (current density of 20 mA/cm^2)

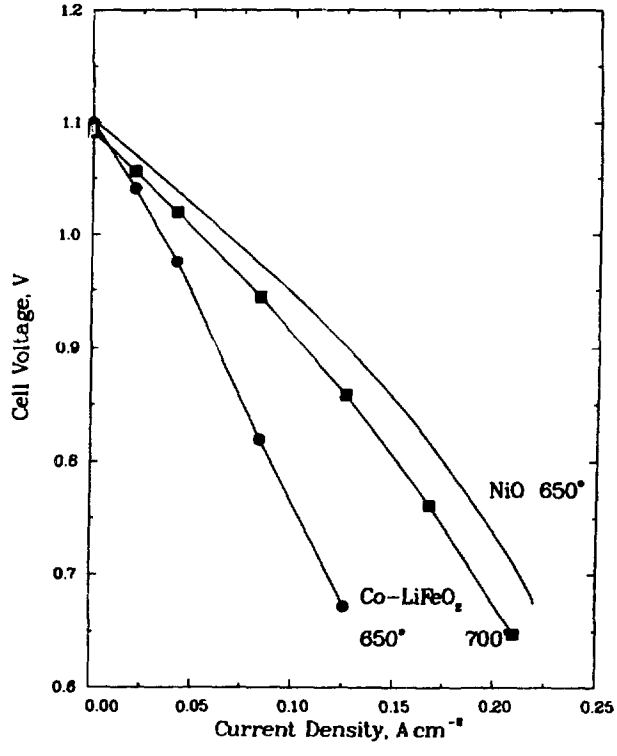

Fig. I-12.

Effect of Operating Temperature on Performance for Cell Containing a Co-Doped $LiFeO_2$ Cathode

c. Separator Studies

The separator (bipolar sheet) in the MCFC stack must be electronically conductive in both oxidizing and reducing environments and also corrosion resistant. These separators are usually thin stainless steel sheets coated on the anode side with a nickel layer. We are examining the feasibility of replacing the metal sheet with a corrosion-resistant ceramic separator.

We designed and fabricated an apparatus to provide a means to evaluate the relative rates of conversion of a dense body from oxidizing-to-reducing and reducing-to-oxidizing conditions. The initial test, conducted at 650°C under reducing conditions, examined the change in resistance of a specimen (>94% dense) prepared in oxidizing conditions. The test, which ran for 550 h, demonstrated the suitability of the apparatus for determining the diffusion (depth of penetration) of hydrogen or oxygen in a dense body. The initial characterizations will emphasize iron- and manganese-based materials in their undoped and doped states.

D. *Technical Support for Development of Fuel Cell/Battery Systems*

The CMT Division provides technical support to DOE for the development of fuel cell/battery systems for transportation applications. This support includes technical assessments, system analyses, assistance in program planning, preparation of work statements for developmental contracts, and technical management of several major DOE contracts with industrial developers.

Fuel cells, operating on nonpetroleum fuels, can potentially provide an alternative propulsion system for transportation needs with nearly twice the fuel efficiency and greatly reduced emissions and noise compared with those of the internal combustion engine. The objective of the DOE Fuel Cells for Transportation Program is to advance fuel cell technologies from the R&D phase, through optimization and scaleup, to demonstration in cars, vans, and buses. These technologies would provide energy savings, fuel flexibility, and air quality improvements.

1. Fuel Cell System Analyses and Modeling

During 1990, we conducted a study on fuel reformers to assess the present state of technology for converting alternative fuels (methanol, ethanol, and compressed and liquefied natural gas) to a hydrogen-rich gas mixture for powering fuel cells in automotive applications. The objective of this study was to identify the R&D needs for developing reformers that achieve the thermal, chemical, and hydrodynamic performance required to supply the anode gas for fuel-cell-powered vehicles.

This study included a literature search to identify the different types of fuel reformers that have been or are being developed, an analysis of the available data on these reformers to evaluate their expected performance in automotive applications, investigation of the potential for reformer/fuel cell systems integration, and recommendations for further research and development. Specifically, we found that the reformers developed to date lack adequate

start-up and dynamic response capability to permit their use in stand-alone fuel-cell power systems for automotive applications. Based on the heat transfer characteristics and the desired small size and low weight, we recommend that a catalytic partial oxidation reformer be developed. The desirable features for such a reformer would include a small catalyst bed for a quick-starting, light, and compact reformer; multiple catalysts for optimum operation of the different reforming steps; partial oxidation by direct heat transfer for rapid response to fluctuating loads; and a fuel processing scheme thermally independent of the rest of the fuel cell system.

In a related project, the State of Illinois and DOE have agreed to co-sponsor a program at ANL to develop reformer technology which can convert ethanol to hydrogen for use in fuel-cell-powered vehicles. Besides being a renewable energy resource, ethanol has 30% more energy than an equal volume of methanol, and the energy required to steam reform ethanol is less than half that required to steam reform methanol. Little research, however, has been done to date on reforming ethanol. The limited data available on ethanol reforming suggest that, in addition to higher reformer temperatures, soot formation and excess water requirements are concerns that must be addressed. In 1991, we will determine the optimum reaction conditions (temperature, pressure, water injection, etc.) required to carry out the conversion of ethanol to a hydrogen-rich gas mixture. Commercially available catalyst materials will be evaluated for this purpose. In the second year of this project, a prototype ethanol reformer will be designed, built, and tested.

2. Fuel Cell/Battery Powered Bus System

The CMT Division provides technical management for the DOE Fuel Cell/Battery Powered Bus System Program. This program is also co-sponsored by the U. S. Department of Transportation (DOT) and the California South Coast Air Quality Management District (SCAQMD). The objective of this program is to demonstrate an urban bus powered by a phosphoric acid fuel cell (methanol-fueled) combined with a battery. An urban bus was selected as the initial test vehicle for fuel-cell propulsion because the large size of a bus can readily accommodate the volume requirements of a first-generation fuel-cell propulsion system, and because the present-day acquisition of fuel-cell systems can be amortized over a longer service life in a bus than in passenger cars. The use of a battery in parallel with the fuel cell minimizes the size of fuel cell required; the fuel cell provides the average power required, and the battery, which is recharged by the fuel cell during bus idle periods, provides the supplemental power needed during vehicle acceleration. For maximum energy efficiency, the energy released during vehicle braking can also be used to charge the battery.

In Phase I of this program, DOE awarded cost-shared contracts to two industrial teams for this work (one led by Energy Research Corp., the other by Booz-Allen & Hamilton, Inc.), and CMT provided overall technical management. During 1990, the Energy Research team completed a 29-month contract to develop an air-cooled phosphoric acid fuel cell/battery system, and the Booz-Allen & Hamilton team completed a 29-month contract to develop a liquid-cooled phosphoric acid fuel cell/battery system. Both teams completed evaluation of a laboratory propulsion system that is one-half the size needed for the bus. Based on the successful results of Phase I, all sponsors (DOE, DOT, and SCAQMD) agreed to proceed to Phase II, which is directed at installing full-size fuel cell/battery propulsion systems into three test-bed buses

(8-9 m long). A system design and integration contractor for the 30-month Phase II effort is being sought through a competitive procurement. The work will also include the design of a full-size urban transit bus (12-m long).

3. Advanced Fuel Cells for Transportation Applications

The proton exchange membrane (PEM) fuel cell, when fully developed, could offer significant advantages over the phosphoric acid fuel cell for transportation applications. These include reduced size and weight, faster start-up, better transient response, increased reliability, and potentially lower cost. Accordingly, a four-phase development program managed by CMT was established. Phase I (feasibility evaluation) will lead to the demonstration of a 10-kW PEM system. Phase II (proof-of-feasibility) will be directed at proving feasibility by means of a 25-kW system. Phase III (system scale-up) will result in the laboratory evaluation of a full-scale 50-kW propulsion system. In Phase IV (proof-of-concept), this full-scale system will be installed and evaluated in a test-bed vehicle.

During 1990, Phase I of the PEM Fuel Cell R&D Program was initiated when DOE awarded a two-year, cost-shared contract to Allison Gas Turbine Division of General Motors Corp. Allison plans to use Los Alamos National Laboratory, Dow Chemical Co., Ballard Power Systems, and General Motors Research Laboratories as subcontractors. The work includes the conceptual design of a PEM-based propulsion system, R&D on limiting components to advance the technology to meet transportation needs, and integration and testing of a complete 10-kW PEM fuel cell system.

In another small project managed by CMT, the Delco Remy and Hughes Aircraft Divisions of General Motors completed the first year of a feasibility study on the development of a novel thermo-electrochemical (TECH) power source under a cost-shared contract with DOE. The TECH system converts heat into electricity by the reaction of an acid and a base across a cation exchange membrane in an electrochemical cell, with thermal regeneration of the resulting salt into the initial reactants to form a closed-loop system. The TECH system can use almost any fuel as the heat source and provides power for electric propulsion with much lower emissions than internal combustion engines because the external combustion of fuel is much cleaner.

During 1990, Hughes completed a conceptual design for a TECH-based propulsion system and conducted component design and development studies which quadrupled the cell operating current density. In the second year of this two-year feasibility effort, Hughes will scale up the cell size and fabricate and test a laboratory-scale TECH demonstration system. This unit is expected to supply the information needed for an engineering assessment of overall system efficiency. A major emphasis in this development effort is on demonstrating high overall efficiency at low system cost.

The monolithic solid oxide fuel cell (Sec. I.C.1) may offer the best long-term prospects for transportation because it operates with internal fuel reforming and does not require a separate reformer or peaking power source, but it is at the earliest stage of development of any fuel cell system. A feasibility study to evaluate the applicability of the MSOFC for transportation applications is planned for 1991.

II. FOSSIL FUEL RESEARCH

The Chemical Technology Division is the lead division for several projects in the ANL Fossil Fuel Program. These projects involve studies on fluidized-bed combustion (FBC) and heat and seed recovery for open-cycle, coal-fired magnetohydrodynamic (MHD) power generation.

A. *Fluidized-Bed Combustion Studies*

Fluidized-bed combustion involves a process in which coal is burned under atmospheric or pressurized conditions in a fluidized bed of limestone or dolomite, which reacts with most of the SO_2 released during combustion. The fluidized-bed combustion projects at CMT include investigations into (1) metal wastage on FBC heat exchanger surfaces, (2) materials performance in an atmospheric fluidized-bed cogeneration air heater, (3) alkali vapor emissions in the off-gas from pressurized fluidized-bed combustion (PFBC), (4) the combustion of cleaned coals in FBCs, and (5) the use of Illinois limestones for reducing SO_2 and HCl emissions during the PFBC of an Illinois coal with high S and Cl content.

1. Metal Wastage in Fluidized-Bed Combustors

Metal loss from in-bed heat-transfer tubes in FBCs is a recurring problem that is impeding the commercialization of this technology. To address this problem, a cooperative research and development venture was formed with the following organizations: DOE, Electric Power Research Institute (EPRI), Center for Research on Sulfur in Coal (CRSC), Tennessee Valley Authority (TVA), ASEA Babcock PFBC, Foster Wheeler Development Corp. (FWDC), and ABB Combustion Engineering Systems (ABB/CE). The overall objectives are to (1) develop models and computer codes that will predict hydrodynamics and metal wastage of tubes in fluidized beds and (2) translate model predictions and experimental data into simple guidelines for the design and operation of FBCs with minimal metal loss. The ANL divisions involved in this project are CMT, Energy Systems (ES), and Materials and Components Technology (MCT).

Activities undertaken in 1990 include (1) fluidized-bed experiments at FWDC and the University of Illinois at Urbana-Champaign (UI-UC) to determine solids motion around immersed tubes and their erosion at ambient conditions, (2) analysis of these experiments using ANL-developed mechanistic computer models of the fluidized-bed hydrodynamics and erosion processes, and (3) development of a three-dimensional hydrodynamics model at Babcock and Wilcox (B&W). As reported previously,[1,2] the ANL computer models predict hydrodynamics of the solids and bubble motion and the erosion of tubes resulting from the impaction and abrasion

---

[1]M. J. Steindler et al., *Chemical Technology Division Annual Technical Report, 1988*, Argonne National Laboratory Report ANL-89/15, p. 49 (1989).

[2]R. W. Lyczkowski, J. X. Bouillard, D. Gidaspow, and G. F. Berry, *Computer Modeling of Erosion in Fluidized Beds*, Argonne National Laboratory Report ANL/ESD/TM-1 (January 1990).

of particles. The hydrodynamics model is capable of two-dimensional, time-dependent solutions of mass, energy, and momentum conservation equations for multiphase nonequilibrium systems.

In 1990, FWDC continued testing in a "cold-model" fluidized bed (room temperature, no combustion) in which a movable vertical partition plate is used to control the length of tubes exposed (bed thickness) in each test. By adjustment of the partition plate between tests, data were obtained to compare erosion and hydrodynamic behavior in thin and full-size fluidized beds. Nine tubes, nominally 51-mm OD and 3.75-mm wall thickness, were included in each test, which ran for 200 or 400 h. The tube material was either aluminum, carbon steel, or polyvinyl chloride. Wall thickness and tube specimen OD were measured before and after each test to evaluate erosion behavior.

General observations during testing and from review of the data indicated that (1) material-loss patterns developed during the 400-h tests closely resembled those observed in operating FBC units, and (2) while variations up to 0.5 mm occurred along the 1.65-m length of polyvinyl chloride tubes in high-wastage locations, average wastage rates and material-loss patterns were similar in the thin and full-size beds.

Both pressure and differential-pressure measurements were recorded during the FWDC tests to obtain hydrodynamic information for correlation with ANL computer model calculations. The data were analyzed at ANL to deduce bubble behavior and its effect on erosion patterns. On a qualitative basis, videotapes of bubble patterns taken through the front of the fluidized bed during testing were very similar to computer-generated graphical representations of hydrodynamic model calculations.

The experiments at UI-UC investigated particle velocity in a two-dimensional fluidized bed similar to that at FWDC. The static-bed height was 40 6 cm, and the superficial fluidizing velocity (U_o) was 39.0 cm/s ($U_o/U_{mf} = 1.91$, where U_{mf} is the minimum fluidizing velocity). Data were obtained by a particle tracking technique,[3] which involved the continuous tracking of a radioactive tracer particle (polyurethane-coated scandium) dynamically similar to the particle species under study. The tracer's position was tracked at 5-ms intervals for 40 h. The individual tubes were arranged in a five-tube array, as shown in Fig. II-1. For each rod, the various surface locations analyzed are identified by numerals, shown in the upper right-hand corner of Fig. II-1.

An analysis was completed of the directional and velocity distributions for particles hitting the indicated surfaces on the rods. Our earlier studies of tube erosion indicated that there is a critical particle velocity below which erosion is insignificant ($U_c=0.8\ U_{mf}$). Thus, data from the UI-UC experiments were used to generate directional-distribution plots for particles hitting surfaces 4, 5, and 6 of rod 1 at all velocities and at velocities > U_c. The plots indicated significant redistribution of the relative proportion of particles hitting these surfaces when velocities are > U_c.

---

[3] J. S. Lin, M. M. Chen, and B. T. Chao, AIChE J. **31**(3), 465 (1985).

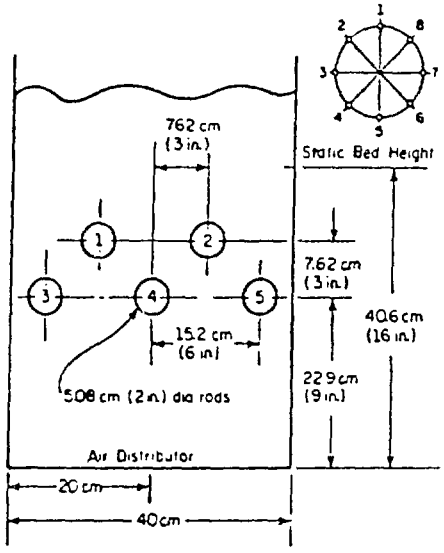

Fig. II-1.

Key Dimensions and Location of Simulated Tube Bank in Two-Dimensional Air Fluidized Bed. (Numerical designations of various surfaces of the rod are given in the upper right-hand corner.)

The velocity-distribution plots of particles hitting surface 4 of Rod 1 along six directions are given in Fig. II-2. As shown in this figure, the speeds of particles hitting surface 4 are generally higher along directions (1,2) and (9,10) than along directions (5,6). The impinging angle corresponding to directions (1,10) is 9°, and that corresponding to directions (2,9) is 27°. The information provided by the directional-distribution and velocity-distribution plots suggests that particles hitting surfaces 4, 5, and 6 in the directions (1,2) would cause the maximum damage, those in directions (9,10) would be next in severity, and those in directions (5,6) would be the least harmful. Qualitatively, the observations for the three surfaces of rod 1 also hold for the other four rods.

Pressure fluctuation measurements were made at numerous locations in the two-dimensional and a three-dimensional fluidized bed at UI-UC. These data and those from FWDC were used in validating the ANL hydrodynamic and erosion models. The computed solids flow patterns, except for a few locations, agreed with the experimental data, and the computed solids velocities were, in general, only a factor of two higher than indicated by the experimental data. The major frequencies of the computed pressure fluctuations agreed quite closely with the experimental data, even though some of the flow patterns were incorrect.

Bubble velocities in the fluidized bed were computed for comparison with those derived from differential-pressure measurements in the FWDC experiment. Both the experimental and computed bubble velocities increased monotonically with elevation in the bed. Spectral analysis of the computed pressure fluctuations agreed closely with spectral analysis of the pressure-signal data. Major frequencies for pressure fluctuations were found to lie in a narrow range of slightly below 2 Hz to about 3 Hz.

Babcock & Wilcox completed development of a three-dimensional hydrodynamics model. This computer model was validated by comparing its output with that from the ANL

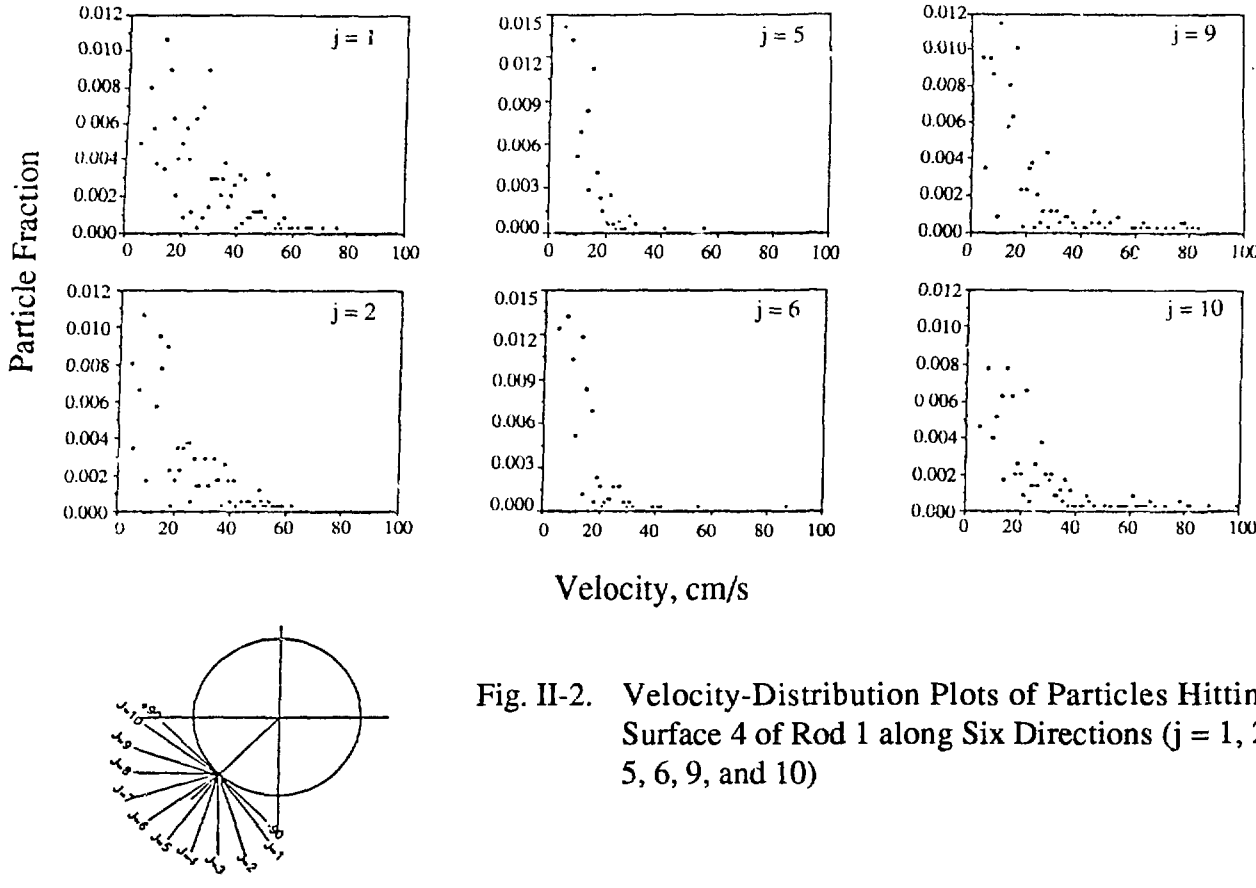

Fig. II-2. Velocity-Distribution Plots of Particles Hitting Surface 4 of Rod 1 along Six Directions (j = 1, 2, 5, 6, 9, and 10)

two-dimensional model when both models ran the "standard" ANL-developed problem of a fluidized bed containing a centrally located obstacle.

The FWDC and UI-UC experiments will be continued to provide hydrodynamics and erosion data over a wider range of design and operating conditions. These data will then be analyzed with the ANL computer models.

2. Atmospheric Fluidized-Bed Cogeneration Air Heater Experiment

Argonne is managing the Atmospheric Fluidized-Bed Cogeneration Air Heater Experiment for DOE. The objective of this project is to assess materials and process performance of in-bed air heaters for cogeneration of electricity and hot air in an atmospheric fluidized-bed combustor (AFBC). The ANL divisions involved in this effort are CMT and MCT.

Rockwell International was subcontracted for the experimental testing of heat-exchanger tube bundles in the DOE-owned AFBC unit (1.8 x 1.8-m cross section) located at a Rockwell site in El Segundo, CA. Test articles made from a wide variety of metal alloys were supplied by ANL, B&W, FWDC, and ABB/CE (the latter three, under subcontract to Westinghouse Electric Corp.). The test articles are intended to provide material wastage information that will enable projections of service life in an AFBC environment. Several types

of articles were tested: platen specimens assembled into in-bed tube bundles, cylindrical specimens inserted into internally cooled probes, specimens of various geometries attached to uncooled probes, and tube clamps made from a candidate alloy. The duration and bed temperatures of the test were about 2000 h and 1150 K, respectively. Argonne and the three subcontractors are performing data analysis and an assessment of the heat-exchanger performance, which will be completed in 1991. Results of oxygen partial pressure measurements and corrosion analysis are discussed below.

a. Oxygen Probe Measurements

During testing, the oxygen partial pressure, $p(O_2)$, in the AFBC was measured with Y_2O_3-stabilized ZrO_2 solid electrolyte cells.[4] Extensive corrosion information, developed in laboratory tests under simulated FBC environments, indicates that high chromium alloys exhibit acceptable corrosion rates when the $p(O_2)$ in the environment is 10^{-3} Pa or higher.[5,6] The corresponding sulfur partial pressures in such environments is less than 10^{-15} Pa (in the temperature range of 1073-1173 K), and the intergranular penetration of sulfur in the substrate alloy is also minimal. As a result, the $p(O_2)$ data were compiled on the basis of 10^{-3} Pa as the value separating oxidation and oxidation/sulfidation regions for the high chromium alloys undergoing corrosion testing.

The oxygen-concentration data were obtained from the east wall of the combustor at three different insertion depths (8-30 cm, 33-61 cm, and 63-84 cm) and were plotted as a percent of the total time that the local environment had $p(O_2)$ exceeding 10^{-3} Pa. The data show a substantial variation both with exposure time and distance from the wall. Between ~300 and 500 h, the $p(O_2)$ values were above 10^{-3} Pa at all locations for only 25-50% of the time. Further, the bed essentially operated under reducing conditions for the second 500 h of testing. The flue-gas sample line developed a leak during the second 500 h, which was interpreted as an insufficient coal feed rate. During this period, the coal feed rate was increased to reduce the flue-gas oxygen concentration. This step, in effect, decreased the in-bed oxygen concentration, leading to operation under reducing conditions. It should be noted, however, that the combustor was operated under reducing conditions for considerably less than half of the total test duration of 2000 h.

b. Corrosion Test Results

In this experiment, uncooled alloy specimens were exposed on probes supplied by ANL, B&W, FWDC, and ABB/CE. Several specimens from selected probes were analyzed at ANL using a scanning electron microscope (SEM) equipped with an energy dispersive X-ray (EDX) analyzer and an electron microprobe to (1) identify the morphological

---

[4]J. Campbell, *Phase II - Primary Heater Module, Final Report for the Period February 1980 - November 1983*, DOE/ET/15020-1634 (Vol. 2), pp. 4-142 to 4-170 (1983).

[5]K. Natesan, S. A. Miller, and W. F. Podolski, *An Assessment of the Performance of Heat Exchanger Materials in Fluidized-Bed Combustors*, Argonne National Laboratory Report ANL-86-42 (1986).

[6]K. Natesan, High Temp. Tech. 4(4), 193 (1986).

features of corrosion product phases in the scale layers and (2) establish the thickness of scales and depths of intergranular penetration, if any, of the substrate material.

The corrosion data for 11 alloys exposed in B&W probes for 1980 h indicated that the penetration was considerably less on the outer surfaces of the alloy specimens compared with that on the inside surfaces, which had been exposed to deposits of bed material during testing. The penetration on the outer surfaces for these alloys was only ~100 μm after 1980 h (compared with ~500-3000 μm on the inside surfaces for eight alloys). The corrosion penetration in alloys exposed for 1980 h in an ANL probe was similar on both the inside and outside surfaces of the specimens, which had no deposit accumulation during exposure. The corrosion penetration for the ANL probe specimens was similar to the low values obtained for the outer surfaces of the specimens exposed in the B&W probes. The SEM/EDX analysis of the corrosion products from the ANL probe indicated predominantly oxide phases with some isolated sulfide particles in the grain boundary regions of the specimens. The penetration data for specimens exposed in an FWDC probe for 1980 h, including data for chromized and aluminized specimens, were comparable to the low values for the ANL probe specimens. Figure II-3 shows corrosion data for the outer surfaces of specimens from probes exposed for 1980 h by the three organizations. If parabolic kinetics is assumed, penetration rates for the alloys would range between 50 and 500 μm/yr, which is acceptable for FBC applications.

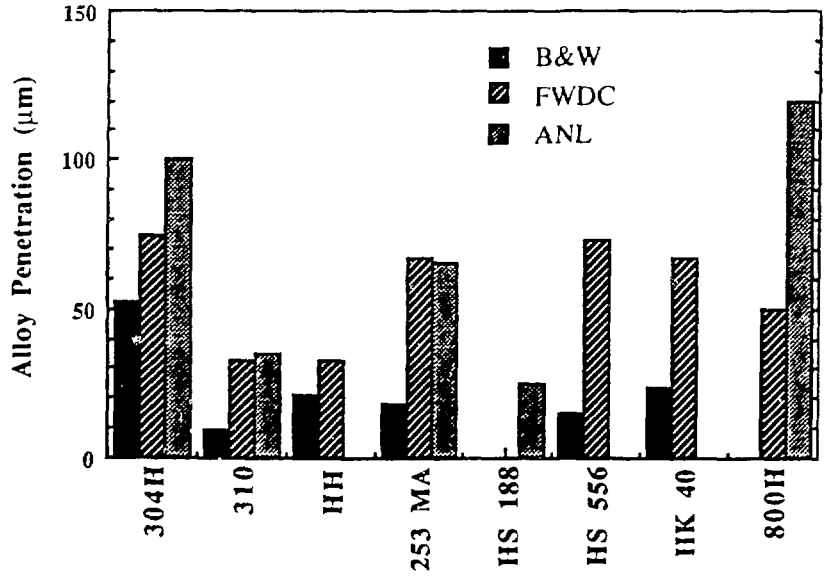

Fig. II-3. Corrosion Penetration for Outside Surfaces of Alloys on ANL, B&W, and FWDC Probes Tested for 1980 h

In conclusion, the results indicate that the presence of bed material deposit on the specimen surfaces leads to significant, and sometimes catastrophic, corrosion degradation of materials. On the other hand, the same alloys exhibit acceptable corrosion rates when the surfaces are free of bed material deposits. The acceptable performance of even alloy 800H (an

alloy that has been shown to undergo substantial corrosion in exposures in other FBC facilities) indicates that the combustion atmosphere in the present test was much more benign than other systems, and that the operating conditions/procedures, if duplicated in a commercial system, can result in enhanced reliability.

3. Development of Regenerable Activated-Bauxite Sorbent Alkali Monitor

The presence of vapor-phase alkalis in the exhaust of pressurized fluidized-bed combustion (PFBC) of coal can lead to unacceptable corrosion of the turbine blade materials. Our past experience has shown that a time-averaged alkali-vapor concentration in PFBC exhaust can be reliably obtained using an analytical activated-bauxite sorber bed.[7] For this measurement, the alkali vapors in PFBC off-gas are captured by the adsorbent through physical adsorption, the adsorbed alkalis are recovered by simple water leaching, and the resulting solution is analyzed for alkalis by atomic absorption spectrometry. The objective of this work is to develop a regenerable activated-bauxite sorber alkali monitor (RABSAM) for the *in situ* measurement of alkali vapor in PFBC off-gas. The RABSAM will use commercial-grade activated bauxite, which contains some clay impurities that can react with alkali vapors; therefore, these clay impurities need to be either removed or deactivated. Impregnating the bauxite with either NaCl or LiCl solution has been studied as a method to deactivate these impurities.

a. NaCl-Solution Impregnation

The deactivation of clay impurities has been achieved by impregnating fresh activated bauxite with NaCl solution and then heat-treating the activated bauxite in a ceramic crucible at a controlled temperature (about 1000 K), followed by water leaching, acid leaching, and Soxhlet extraction with deionized water. The sodium in the activated bauxite produced by the NaCl-solution impregnation method is present as residual NaCl and non-chloride compounds, such as silicates. The water leaching step effectively removes the residual NaCl, while the subsequent acid leaching removes the non-chloride sodium compounds. Soxhlet extraction serves as a final cleanup step for both residual NaCl and non-chloride sodium compounds.

The stability of the water- and acid-insoluble sodium compounds that remain in the activated bauxite when it is exposed to actual PFBC exhaust remains a concern. Heat treating the activated bauxite in a simulated PFBC off-gas at 1173 K showed that the residual sodium compounds can be subsequently released in water-soluble forms, indicating the necessity for completely removing the residual sodium compounds in the activated bauxite. This has been achieved by a cyclic treatment: preconditioning the activated bauxite in a simulated PFBC exhaust followed by acid leaching with 2 N H_2SO_4 or Soxhlet extraction with deionized water. Further improvement in the rate of sodium removal from activated bauxite is still needed, however.

---

[7] M. J. Steindler et al., *Chemical Technology Division Annual Technical Report, 1988*, Argonne National Laboratory Report ANL-89/15, pp. 44-46 (1988).

b. LiCl-Solution Impregnation

Lithium chloride has chemical properties that are similar to, but more reactive than, those of NaCl; therefore, we are investigating replacement of NaCl with LiCl for the deactivation of clay impurities in fresh activated bauxite. One immediate advantage for using LiCl is that the amount of non-chloride sodium compounds, products of the deactivation of clay impurities, would be significantly reduced. Also, the presence of lithium compounds, whether they are water soluble or water insoluble, is not expected to affect the adsorption property of the activated bauxite for sodium and potassium vapors and their subsequent analyses in water leachate by atomic absorption spectrometry.

We conducted a preliminary study to prepare a batch of activated bauxite by LiCl-solution impregnation. The residual sodium and potassium compounds in the activated bauxite were essentially extracted by water leaching, followed by acid leaching with 2 N H_2SO_4 and one cycle of preconditioning the activated bauxite in a simulated PFBC off-gas followed by Soxhlet extraction with deionized water. When NaCl was used as the deactivation agent, complete removal of the residual sodium compounds required, in addition to the water and acid leachings, more than six cycles of the PFBC preconditioning/Soxhlet extraction treatment.

Studies will be continued with an ultra-pure LiCl (+99.99% purity) to reduce the sodium and potassium impurities during LiCl-solution impregnation and a platinum crucible for heat treatment to eliminate possible contamination of the activated bauxite by sodium and potassium compounds present in ceramic crucibles. The activated bauxite will then be tested for its capability for alkali-vapor sorption and water-leaching regeneration.

4. Alkali-Vapor Measurement in PFBC of Illinois Coals

The Illinois Center for Research on Sulfur in Coal (CRSC) sponsors research to promote the utilization of Illinois high-sulfur coals. The objective of this effort was to evaluate the alkali-vapor corrosivity of PFBC off-gas generated from burning Illinois coals with high-chlorine, high-sulfur content.

Two Illinois No. 6 coals and an Illinois No. 5 coal were combusted in the ANL laboratory-scale (15.4-cm dia) FBC facility at a bed temperature of 1173-1223 K, system pressure of 0.9 MPa (9.2 atm) absolute, and fluidizing velocity of 0.91 m/s. Our analytical activated-bauxite sorber bed technique (see Sec. II.A.3) was used to measure the alkali-vapor emissions during combustion. The test results showed that (1) the alkali-vapor emissions increased linearly with both the Na and Cl contents in the coals, (2) sodium was the major alkali-vapor species present in the PFBC off-gas, and (3) the time-averaged alkali-vapor concentrations were more than 2.5 times greater than the current alkali limit of 24 ppb for an industrial gas turbine. The results suggest that a way of controlling these alkali vapors may be needed to utilize Illinois coals in PFBC power generation.

Further work is needed to (1) develop a technique that will control alkali vapors for protecting gas turbines from hot corrosion and (2) evaluate the effectiveness of coal washing (to remove volatile sodium compounds, such as NaCl) in reducing the emission of alkali vapors.

5. Evaluation of the Combustion of Cleaned Coals in FBCs

Fluidized-bed combustors are able to burn a wide range of coals and comply with current environmental regulations. Coal quality has a significant impact on costs, emissions, and the amount of solid-waste products. A joint project between ANL and Sargent & Lundy was initiated with CRSC funding to evaluate differences between an 80 MW(e) circulating fluidized-bed combustor (CFBC) burning an Illinois No. 6 coal (5 wt % H_2O, 39 wt % ash, and 3.7 wt % S) and the same coal after physical cleaning (6 wt % H_2O, 8 wt % ash, and 2.6 wt % S). These coals were burned in the ANL laboratory-scale FBC facility at atmospheric pressure to determine differences in performance between them. The ash from the test burns was also analyzed for eight metals currently listed by the Environmental Protection Agency as toxic.

Sargent & Lundy evaluated the installation and operating costs for use of an 80 MW(e) CFBC in electrical generating stations designed for the two grades of coal. The plant designs were based on input obtained from the test burns of the untreated and washed coals in the ANL test facility and from CFBC vendor-supplied information. The effects on generating station size, equipment design, material storage requirements, and site run-off collection and treatment were included in the economic evaluation.

Test results indicated that burning washed coal will result in more than 50% reduction in SO_2 emissions on an equivalent heat input and sulfur removal basis, and that 95% sulfur removal with a limestone sorbent was possible for both coals. Emissions of nitrogen oxides (NO_x) from the washed coal were about 33% lower when compared with untreated coal on an equivalent heat input basis; nevertheless, NO_x emissions from both coals were below the current standard of 260 ng/J (0.6 lb/10^6 Btu). Burning washed coal would result in a 69% reduction in the solid-waste handling burden and run-off pond area needed. Laboratory analysis of the solid wastes indicated that waste disposal will not result in excessive toxic metal concentrations in the storage area run-off or leachate. Nevertheless, the plant designs evaluated by Sargent & Lundy are based on collection and treatment of the run-off and leachate.

The capital and operating cost savings (in 1991 dollars) associated with designing a plant to burn a washed coal are equivalent to a \$0.59/10^6 kJ (\$0.62/10^6 Btu) increase in the cost of the washed coal over that of the untreated coal.[8] A cost differential for washed coals over untreated coals that is less than this amount would give a life-cycle cost advantage to a plant designed for washed coal. The cost differential would be even more in favor of the washed-coal unit if emission allowances, maintenance, and water-supply systems were included in the life-cycle cost evaluation.

---

[8]M. K. Clemens and W. F. Podolski, "Comparison of Costs, Emissions, and Waste Products for an 80-MW CFBC Burning Mine-Run and Washed Coals," presented at Eleventh Int. Conf. on Fluidized-Bed Comb., Montreal, Quebec, Canada, April 21-24, 1991.

6. Evaluation of Illinois Limestones for Reducing SO_2 and HCl Emissions

In this study for the CRSC, two Illinois dolomites and a limestone are being evaluated for reducing the emissions of SO_2 and HCl from the ANL 15.2-cm dia FBC. This past year, the tests were conducted under excess air conditions typical of a single-stage, bubbling-bed PFBC. The objectives of the tests are to (1) assess the selected sorbents with respect to their ability to reduce SO_2 and HCl emissions, (2) compare the reductions in SO_2 and HCl emissions obtained in these tests with results obtained by the Illinois State Geological Survey (ISGS) in laboratory-scale tests with the same sorbents, and (3) provide data that could be used in the development and/or assessment of models for applying laboratory data on sorbent reactivity and physical characteristics to the design of larger scale FBCs.

The sorbents tested were a Fredonia limestone, a Racine/Sugar Run dolomite, and a Racine dolomite from Illinois quarries. The combustion tests were conducted in the ANL laboratory-scale FBC unit with a Herron No. 6 coal (2.6 wt% S) at the following nominal conditions: pressure, 0.8 MPa (8 atm) absolute; O_2 in the flue gas, 3.5%; and bed height, 0.9 m. Parameters varied during the tests included the Ca/S mole ratio (0.75-4.6) and bed temperature (1080-1180 K).

Measured sulfur retentions ranged from 67.4% with the Fredonia limestone at a Ca/S ratio of 1.3 to a high of 98.0% with this same limestone at a Ca/S ratio of 4.6. As expected, sulfur retention was strongly influenced by Ca/S ratio and, to a much lesser extent, by bed temperature. These effects are illustrated by the sulfur retention data for the Racine dolomite shown in Fig. II-4. The percent sulfur retention obtained with the three sorbents decreased in the order Racine/Sugar Run dolomite, Racine dolomite, and Fredonia limestone at all Ca/S ratios

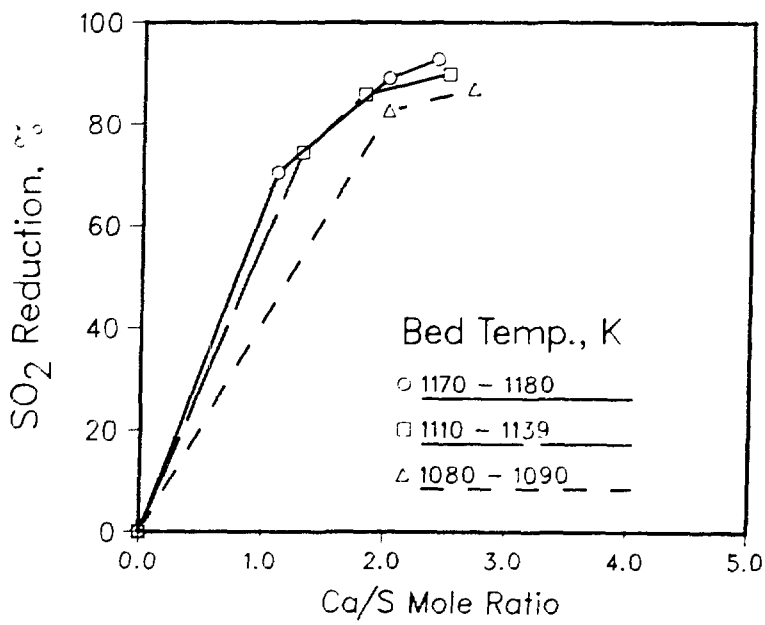

Fig. II-4. Effect of Ca/S Ratio and Bed Temperature on SO_2 Reduction with Racine Dolomite Sorbent

(see Fig. II-5). These results are in qualitative agreement with those reported by the ISGS for the same sorbents based on laboratory-scale reactivity tests. Additional tests are planned in which combustion will be under fuel-rich conditions typical of the first stage in staged PFBC concepts.

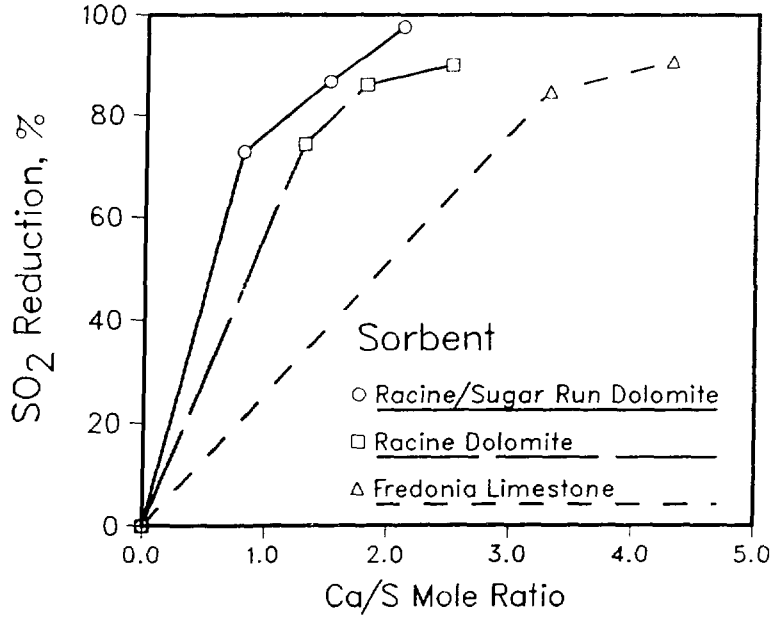

Fig. II-5. Effect of Sorbent Type and Ca/S Ratio on SO_2 Removal with Bed Temperatures in the Range 1110-1140 K

B. *Magnetohydrodynamic Heat and Seed Recovery Studies*

Open-cycle MHD is a developing technology with the potential to improve substantially the electrical efficiency of coal-fired power plants and to reduce their environmental impact. In the coal-fired concept of MHD, an easily ionized seed material (usually a potassium salt) is injected into a high-temperature, slag-rejecting coal combustor. The resulting electrically conductive combustion gas then flows through a high-velocity channel in the presence of a strong magnetic field. An electrical potential develops across electrodes in contact with the gas stream in the channel walls and produces an electrical current. The fuel-rich combustion gas leaves the MHD topping cycle at approximately 2300 K and enters a bottoming cycle that is similar in function to the steam bottoming cycle of a conventional coal-fired power plant. However, the MHD steam plant must not only extract heat from the combustion gas to produce high-pressure steam, but also separate the seed from the ash, recover the seed material for reuse, preheat the primary combustion air to at least 1000 K, lower nitrous oxide emissions to acceptable levels, and inject secondary air to complete combustion of the fuel. The Chemical Technology Division is the lead ANL division in a multidivisional project that is directed toward developing the technology required for the heat and seed recovery in an MHD plant.

Combustion gases containing sulfur and alkalis have been a concern with regard to the corrosion of heat-exchanger tube materials in conventional coal boilers. Such corrosion is also a

problem for bottoming-cycle components, the intermediate temperature air heater (ITAH) and steam superheater (SSH), exposed to MHD combustion gases, especially because of their higher alkali content.

We are undertaking laboratory autoclave tests to study the corrosion of candidate SSH and ITAH alloys exposed to simulated MHD conditions of gas temperature and composition, deposit chemistry, and metal temperatures. In earlier laboratory autoclave tests,[9] austenitic steels exposed at SSH conditions exhibited negligible corrosion. Moreover, the low- to medium-chromium steels and all of the austenitic alloys (except 310 steel) tested at ITAH conditions exhibited unacceptably high corrosion rates (greater than 0.5 mm/yr). As a result, we began a second round of tests at high-temperature ITAH conditions (metal and gas temperatures of 1035 and 1255 K, respectively). The following alloys were selected for testing: 253MA, RA85H, CR35A, CR30A, HR-160, HR-120, 556, 310, and chromized 304 and 300. Half of each specimen was coated with a typical tube deposit material (containing approximately 85 wt % K_2SO_4) from the superheater test sections of the Coal-Fired Flow Facility (CFFF) at the University of Tennessee Space Institute. The other half of each specimen was coated with the same deposit material mixed with 25 wt% iron oxide to evaluate the possible influence of iron oxide injection in the MHD topping cycle on the corrosion of downstream bottoming-cycle components. Exposure tests of 500- and 2000-h duration have been completed in the autoclave materials test facility. The metallographic examination of the specimens is in progress to determine the extent of corrosion. The results will be summarized in the next report in this series.

We are also providing materials evaluation support for the MHD topping cycle. A piece of a cooling panel (SA 387, a low chromium-molybdenum steel) tested for 250 h in the combustor section of the CFFF was examined for TRW. The panel material was used during the combustion of Illinois No. 6 coal and was subjected to peak metal temperatures of 478 and 355 K on the gas and water sides of the panel, respectively. Scanning electron microscopy of the panel specimen detected no sulfur in the gas-side scale or substrate alloy, even though the coal being burned contained 3.6 wt % sulfur. Isolated locations on the water side exhibited what looked like pitting corrosion of the alloy accompanied by nodules protruding from the surface.

Eleven candidate alloys for cooling circuits in the MHD channel were also tested for corrosion in water at simulated MHD conditions. Exposure was for approximately 200 h at a nominal water temperature of 395 K and pressure of 3 MPa (500 psi). Based on the normalized weight-loss data, W-Cu alloys exhibited the least corrosion of the eleven alloys tested (see Fig. II-6).

Finally, work was completed on the detailed design of a small-scale, one-dimensional flow reactor. The system will be used to (1) obtain experimental data on NO_x decomposition for

---

[9] M. J. Steindler et al., *Chemical Technology Division Annual Technical Report, 1989*, Argonne National Laboratory Report ANL-90/11, pp. 50-51 (1990).

validation of the ANL NO_x kinetic code[10,11] and (2) study the chemistry of fouling deposits under MHD conditions. Fabrication of the reactor and testing are scheduled for 1991.

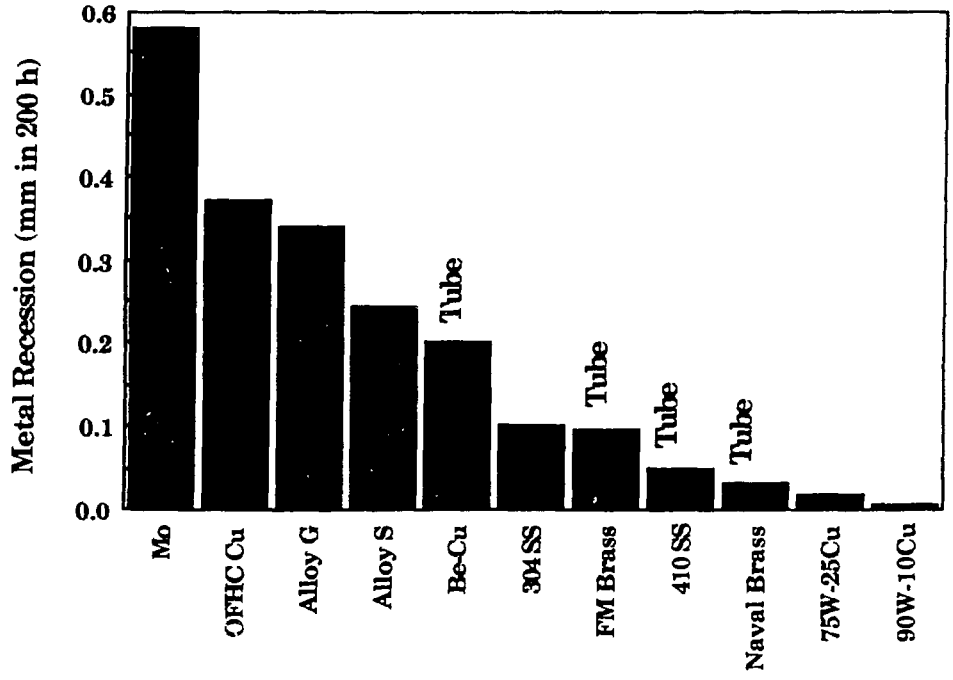

Fig. II-6. Calculated Recession of Metals and Alloys in 200-h Water Corrosion Tests at 395 K and 3 MPa

[10]A.-I. Sistino, *Analytical Studies of NO_x Decomposition in the Radiant Boiler of an Open-Cycle MHD Power Train*, Argonne National Laboratory Report ANL/MHD-79-7 (1979).

[11]A.-J. Sistino, *Comparison of Analytical and Experimental Studies of NO_x Kinetics in MHD Systems*, Argonne National Laboratory Report ANL/MHD-80-17 (1981).

III. MUNICIPAL AND HAZARDOUS WASTE RESEARCH

This CMT effort involves research into the thermochemical conversion of municipal solid waste (MSW) and the development of methods for the treatment/disposal of reactive metals and microwave-assisted detoxification of hazardous waste containing halocarbons.

A. *Mathematical Modeling Studies of Municipal Solid Waste Incineration*

Past attempts at producing an economical fuel from MSW have not been successful because the basic mechanisms of thermally degrading MSW have not been well understood. We have developed the first version of a mathematical model for thermochemical conversion of MSW in a water-wall type mass burner. Based on published kinetic data, the model simulates the heatup, pyrolysis, and burnout of the waste as a traveling grate moves it from the inlet of the incinerator to the exit. Primary air, supplied below the grate, carries the pyrolysis gases from the MSW bed upwards into a flame zone where they burn in contact with secondary air. The flue gases leave the incinerator at the top and are taken for further heat recovery and cleanup. The char and ash are discharged into a quench tank.

For this two-dimensional model, we assumed that MSW is composed of pseudocomponents, such as cellulose, plastics, etc., which pyrolyze through numerous parallel pathways to yield fuel gases, ash, and char. The model incorporates the kinetics of pyrolysis of the solids and simulates heat and mass transfer within the bed. All heat generation is by combustion of the fuel gases in the flame zone above the bed. It is assumed that (1) the bed is well mixed in the vertical direction, owing to the tumbling action caused by the movement of the grate, and (2) the flame zone, the only source of heat for the bed, is homogeneous and at one temperature across the entire bed.

We are simulating MSW pyrolysis with this model to examine the effects of variables (such as the MSW composition and feed rate, the combustion air flow rate and its distribution between primary air and secondary air, and the grate travel rate) on incinerator performance. Calculations employed in the simulations can determine key operating parameters, including the flame temperature and the lengths of the grate required for the various stages in the MSW conversion process. Such studies can benefit both the design and operation of an incinerator by, for example, identifying means to increase the solids processing rate for a given incinerator facility.

The model equations are solved to generate temperature and mass flow profiles along the length of a given MSW combustor bed. These profiles indicate (1) the extent of conversion, (2) the length of grate necessary for the drying, heating, and volatilization of the solids, (3) the sensible heat lost with the exiting solids, and (4) the equilibrium flame temperature that would result from combustion of the pyrolyzed gases.

The temperature profiles generated by this model have shown that the grate length necessary for the solids to heat up to pyrolysis temperatures is greater than that necessary to actually pyrolyze the solids. Parametric studies with the model indicated that an increased solids

feed rate results in a slowdown of the heating and conversion process, and that bed height has a negligible effect on the solids heating rate. In addition, typical simulations indicated that the solids processing rate can be increased by reducing the length of the burnout zone (i.e., no more solids pyrolysis) and by distributing the primary air such that it is kept low in the heatup and reaction zones to permit rapid heating and conversion of the solids.

Figure III-1 shows the sensitivity of the flame and bed temperatures to variations in the primary air flow rate along a 7.6-m bed length. Since a constant flow rate of the secondary air is maintained, the total air fed to the mass burner changes. With increasing primary air, the total air fed into the mass burner increases, lowering the flame temperature. The lower flame temperature, in turn, results in lower radiant heat input to the bed. Also, with increasing primary air, the additional air flow through the bed keeps the bed temperatures down and the temperature profiles flatter. Increasing the primary air flow rate beyond approximately 67% slows down heating so much that total conversion within the 7.6-m bed is not attained, fuel gas generation is inhibited, and the process cools down.

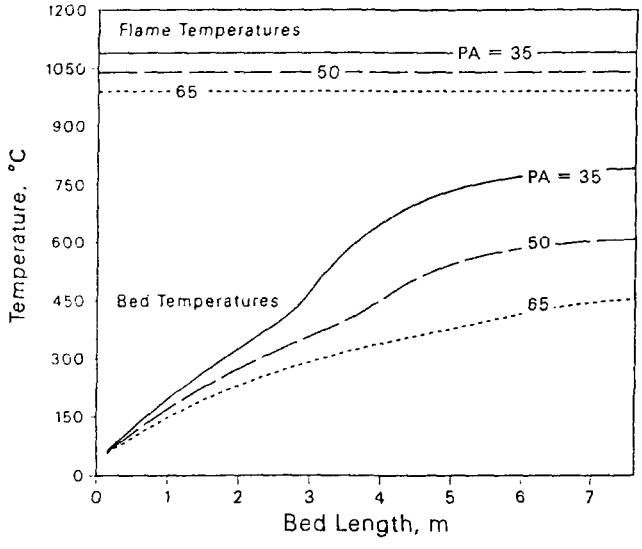

Fig. III-1.

Effect of Primary Air Flow Rate on the Flame and Bed Temperature Profiles. The primary air flow rate, PA, is given as percent of stoichiometric air. The secondary air flow rate is maintained constant at 100% of stoichiometric air.

The effect of varying the secondary air flow rate while the primary air flow rate is maintained at 50% of the stoichiometric air is shown in Fig. III-2. With increasing secondary air flow rate, the flame temperature decreases and the bed temperature profile flattens out. The average bed temperature drops because the radiant heat transfer to the bed decreases.

The two-dimensional model is a good beginning for the simulation of the physical and chemical phenomena occurring simultaneously in a mass burner. To proceed to the next level will require more data on the chemical decomposition (pyrolysis and combustion) of MSW components, such as plastics, hemicellulose, etc. Determination of synergistic effects of these reactions is also needed for the input data base. Mechanisms describing the char combustion reactions should also be incorporated.

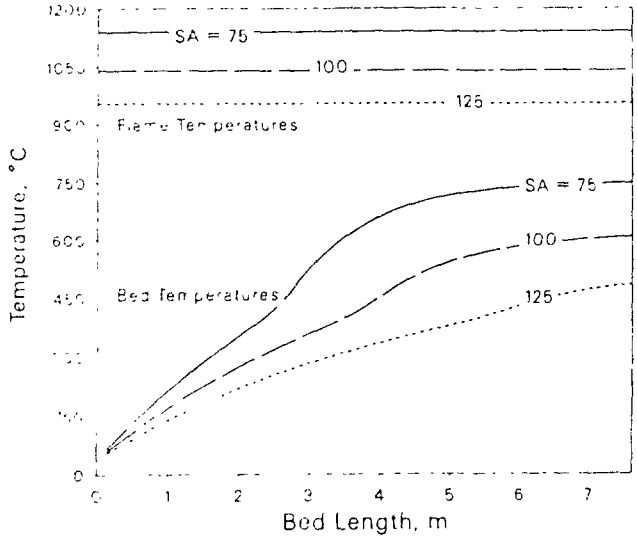

Fig. III-2.

Effect of Secondary Air Flow Rate on the Flame and Bed Temperature Profiles. The secondary air flow rate, SA, is given as percent of stoichiometric air. Primary air held constant at 50% of stoichiometric air.

B. *Treatment/Disposal of Reactive Metals*

The objective of this effort is to design and analyze a process for the conversion of waste sodium, including sodium contaminated with small amounts of radionuclides, to a glass form and to provide technical assistance in the commercial demonstration of the process on a pilot scale of 50 to 100 kg/h. In earlier work, a one-step integrated process was developed for the conversion of waste sodium to a glass form for ultimate disposal.[1] At the heart of the process is a low-g and low-pressure drop cyclonic reactor designed to withstand high operating temperatures. The solid reactants, such as silica and lime, are introduced into the reactor pneumatically. Liquid sodium is injected into the reactor with nitrogen as an aspirator and atomizer. The oxidation of the sodium and the formation of the glass both occur primarily at the walls of the cyclonic reactor, and the product glass is withdrawn from the reactor bottom.

Our earlier experimental work[2] had identified different glasses as suitable waste forms for use with sodium containing no radioactive contaminants, short-lived radionuclides, or long-lived radionuclides. During this past year, work was directed toward preparation for a pilot-plant demonstration of the process with nonradioactive sodium. The objective of the demonstration includes testing and verification of the reactor design, feed systems, and product removal equipment. Under the demonstration program, an industrial subcontractor will be selected; the appropriate permits will be acquired; the process will be designed in detail; the necessary

---

[1]M. J. Steindler et al., *Chemical Technology Division Annual Technical Report, 1986*, Argonne National Laboratory Report ANL-87-19, p. 77 (1987).

[2]M. J. Steindler et al., *Chemical Technology Division Annual Technical Report, 1988*, Argonne National Laboratory Report ANL-89/15, pp. 62-63 (1989).

equipment will be procured, assembled, and tested; and finally, technology demonstration tests will be conducted with nonradioactive sodium.

In 1990, we sent out a request for proposals to carry out process demonstration. Vortec Corp. and Westinghouse Electric Corp. were the two respondents who had submitted technical proposals evaluated to be fully responsive to the needs of the program. Based on the technical and cost proposals, we recommended that the ANL Procurement Office should initiate contract negotiations with Vortec, which was the low bidder. Planning is also underway to perform some of the preliminary demonstration work (e.g., cold-flow modeling and reactor design) at ANL.

C. *Microwave-Assisted Detoxification*

Chlorinated hydrocarbons, particularly 1,1,1-trichloroethane and trichloroethylene, constitute a major hazardous waste problem at many DOE Defense Program sites. Owing to the toxicological and carcinogenic properties of chlorinated hydrocarbons, safe and effective methods for disposing them have attracted considerable research effort. The objective of this program is to investigate the technical and economical advantages of microwave-assisted technologies for detoxifying halogenated hydrocarbons (i.e., converting them to safe and more easily disposable compounds, such as CO_2, CO, HCl, H_2O, and H_2).

In earlier work involving a microwave-induced plasma reactor,[3] we used a microwave generator (6 kW, 2.45 GHz) with a single-mode-resonance quartz reactor (2.1-cm dia) to investigate the oxidative degradation of 1,1,1-trichloroethane and trichloroethylene in an oxygen/argon plasma (20.13% oxygen) at atmospheric pressures. We demonstrated that an oxygen/argon plasma can be maintained at atmospheric pressures in the presence of a chlorinated hydrocarbon vapor stream, and that destruction removal efficiencies of 95.9-98.3% can be achieved in a single pass of the stream through the reactor. Analysis of the degradation products for 1,1,1-trichloroethane, indicated nearly complete conversion to CO_2, H_2O, and HCl; however, for trichloroethylene, a significant portion of the chlorine was converted to nonparent chlorinated hydrocarbons (60 to 70%) due to insufficient hydrogen.

During 1990, we used the 6-kW microwave generator and quartz reactor tube to investigate the degradation of 1,1,1-trichloroethane in an H_2O/argon plasma. The use of H_2O vapor provides hydrogen for removing chlorine as HCl and oxygen for removing carbon as carbon oxides (CO or CO_2), e.g.,

$$C_2H_3Cl_3 + 4H_2O \rightleftharpoons 2CO_2 + 4H_2 + 3HCl \qquad (1)$$

The reactants were generated in the vapor phase by passing separate streams of argon through gas washing bottles containing liquid reservoirs of the desired chlorinated hydrocarbon and H_2O. The two reactant feed streams were mixed with a third stream of argon before entry into the reactor. Flow controllers were used to control the flow rate of each argon stream and,

---

[3]M. J. Steindler et al., *Chemical Technology Division Annual Technical Report, 1989*, Argonne National Laboratory Report ANL-90/11, pp. 58-59 (1990).

consequently, the partial pressure of the reactants. Gas chromatography was used to analyze the reactor effluent.

While investigating factors affecting H_2O/argon plasma stability, we found that including a silica frit in the quartz reactor tube was not necessary for plasma stability and/or improved gas flow distribution, as previously thought.[3] However, the presence of H_2O vapor enhanced the devitrification of the quartz reactor under reaction conditions, causing mechanical failure. Insertion of a quartz liner retarded devitrification and helped maintain the mechanical integrity of the reactor tube.

In these tests, we obtained destruction removal efficiencies of >97% for a single-pass conversion of 1,1,1-trichloroethane with feed rates of 0.0038 to 0.0118 g/min and an H_2O/1,1,1-trichloroethane mole fraction of 5.9 to 22. Primary products were H_2O, CO, CO_2, HCl, and unreacted 1,1,1-trichloroethane. As shown in Table III-1, at the lower H_2O/1,1,1-trichloroethane ratio, CO is the primary carbon oxide in the effluent stream, whereas, at the higher H_2O/1,1,1-trichloroethane ratio, CO and CO_2 are produced in near equal amounts. It is not known whether the CO results from incomplete oxidation of carbon to CO_2 or from the following water-gas shift reaction:

$$CO + H_2O \rightleftharpoons CO_2 + H_2 \qquad (2)$$

Preliminary calculations based upon an estimation of the gas-phase temperature suggested that the water-gas shift reaction may be near equilibrium.

Table III-1. Product Distribution for Reaction of 1,1,1-Trichloroethane (TCE) and H_2O in Argon Plasma[a]

	Conc., mol fraction	
	5.9[b]	22[b]
Inlet Feed		
H_2O	0.0289	0.0286
TCE	0.0049	0.0013
Products[c]		
H_2	0.013	0.0055
CO_2	0.0022	0.0017
CO	0.0074	0.0010
TCE	$<10^{-6}$	$\sim10^{-5}$

[a]Conditions: flow rate, 560 mL/min; microwave power, 0.6 kW.
[b]H_2O/TCE feed ratio.
[c]Determined by gas chromatography.

Experimental work in 1991 will continue to examine the kinetics of chlorinated hydrocarbon degradation in H_2O/argon and H_2O/air plasmas. Correlations relating plasma stability and destruction removal efficiencies to operating parameters, such as feed rate and concentration, microwave power input, and reactor geometry, will be developed.

IV. NUCLEAR WASTE STUDIES

The volcanic tuff beds at Yucca Mountain, Nevada, are being studied as a potential site for locating the U.S. high-level nuclear waste repository. The Yucca Mountain Project (YMP) is characterizing the potential site to assess its suitability for long-term isolation of high-level waste. Both the YMP participants and waste producers are conducting experimental programs to characterize the waste packages to be emplaced in the repository. The ultimate goal is to be able to (1) project the durability of the waste over long time periods in the anticipated repository environment and (2) detect possible waste/environmental interactions which may affect the waste durability. In support of this effort, we are undertaking several experimental programs in which borosilicate waste glass analogs are being reacted in vapor, static liquid solutions, and an unsaturated, dripped-water environment. Work is also being done to investigate the radiolytic effects of emplaced waste on the host environment, the waste packaging materials, and the waste itself. These experiments monitor the behavior of glass waste under the various environmental conditions which may occur over the 10,000-yr service life of the YMP repository. Another experimental effort involves determining the effects of radiation on the salt caverns at the Waste Isolation Pilot Plant.

A. *Yucca Mountain Project*

For the YMP, we are investigating the reaction of glass and irradiated reactor fuel under anticipated repository conditions at the Yucca Mountain site and evaluating the effect of radiation on the near-field environment and on the corrosion of proposed container materials. In this work, we have developed new experimental techniques for simulating and monitoring materials interactions in systems with small amounts of water and have focused on obtaining data that will be used directly in licensing the proposed site. Our experimental work also yields data that support both the development and validation of a YMP computer simulation to project the durability of waste glass and spent fuel over the service life of the repository.

1. Glass Studies

Simulated waste glasses are being studied by long-term unsaturated, vapor hydration, and static leach tests at high temperatures.

a. Unsaturated Testing

Because the potential nuclear waste repository lies in the hydrologically unsaturated vadose zone, it is anticipated that only very small amounts of liquid water will be available to interact with the waste glass and the stainless steel waste package components throughout the service life of the repository. The YMP Unsaturated Test was designed to study glass/steel/fluid interactions under these conditions. In this test, groundwater from the Yucca Mountain site is dripped onto a model waste package composed of a cylinder of waste glass sandwiched between two perforated stainless steel disks at 90°C. The nature and degree of reaction are assessed from solution analysis and inspection of the waste package surface using various analytical techniques, including scanning electron microscopy (SEM) with an energy

dispersive X-ray fluorescence spectrometer (EDS), secondary ion mass spectrometry (SIMS), X-ray diffraction (XRD), and transmission electron microscopy (TEM).

Because the precise conditions in the repository over long times are not known, it is important to understand the effects that different parameters have on the glass reaction rate and subsequent release of radionuclides from the glass. A series of parametric experiments has been ongoing for over four years to investigate the influence of various parameters on glass reaction. All the experiments are performed at 90°C with a simulated waste glass (SRL 165) and groundwater pre-equilibrated with tuff at 90°C (designated EJ-13). Experimental conditions for the standard test and five variations are summarized in Table IV-1.

Table IV-1. Experimental Conditions Used in Parametric Unsaturated Test Series

Experiment No.	*Experimental Parameter(s)*
Standard Test	Glass surface area of 13.5 cm^2, drop volume of 0.075 mL, drop interval every 3.5 days, glass in contact with sensitized 304L stainless steel.
P-II	Exclusion of metal contact with glass, standard conditions.
P-III	Cast glass area reduced 65%, standard conditions.
P-IV	Cast glass area reduced 65%, drop volume reduced 50%.
P-V	Drop interval rate increased from 3.5 to 14 days.
P-VIII	Varying degrees of metal sensitization, standard conditions.

The reaction progress as measured by elemental release from the glass samples to solution has continued as previously described,[1] with tests P-III and P-IV showing a markedly greater release compared with the other parametric tests. Exfoliation of the surface layer on the glass samples occurred to varying degrees and had an important role in the observed extent of glass reaction. To investigate the reason for this effect, the reacted glass samples from previously terminated tests were examined by TEM. The advantage to TEM is that it provides high-resolution detail of the structure of the reacted glass, which helps define the mechanism by which the glass reacts.

A section of a reacted layer from a bottom glass surface is presented in Fig. IV-1. The layer consists of a series of alternating dark bands sandwiched between less dense fibrous regions. The dark bands are iron rich and are amorphous, while the fibrous bands are a poorly crystalline clay. No glass is apparent in the section, which indicates that the layer had become separate from the glass. Because of this, the layer may be carried away from the glass during the water transport process, and increased elemental release is measured.

The initial stage of formation of an unattached layer is shown in Fig. IV-2. This figure shows a section of the side surface of a glass which has undergone less reaction than

[1]M. J. Steindler et al., *Chemical Technology Division Annual Technical Report, 1989*, Argonne National Laboratory Report ANL-90/11, pp. 79-80 (1990).

the bottom because of lesser water contact. Here we observe that the layer forms loosely attached to the glass. As the glass continues to react, the banded structure shown in Fig. IV-1 forms while solids precipitate from solution. As the glass reacts by dissolution (the open gaps in the glass structure), the layer eventually becomes separate from the glass.

Fig. IV-1.

Transmission Electron Micrograph of Layer from the Bottom of Glass in Test P-VIII

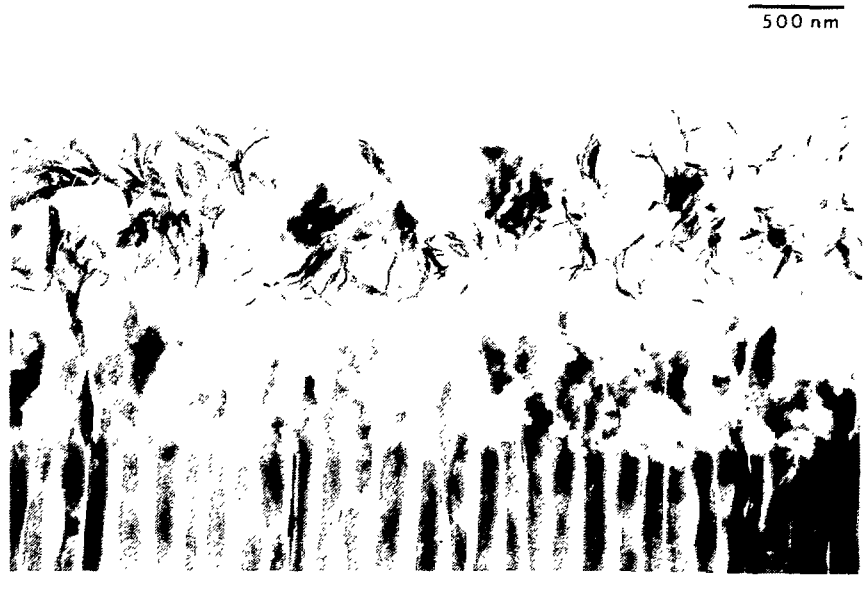

Fig. IV-2. Transmission Electron Micrograph of Side of Glass in Test P-III

The separation of a layer from the reacted glass and the subsequent release of the layer into solution have important ramifications in assessing the performance of glass in a repository environment. If the long-lived actinide elements are associated with the layer, and the layer is released as particulate material to the groundwater, then the release of actinides may not be strictly solubility controlled, as is now assumed in many performance assessment codes, but may be controlled by the formation and transport of these colloidal materials. The nature of the colloids in solution is being further investigated.

b. Vapor Hydration/Leach Experiments

We are performing experiments in which samples of simulated waste glass are reacted in a saturated steam environment at elevated temperatures (up to 240°C) to assess the nature of the reaction at a very high ratio for the glass surface area to leachant volume (SA/V). In this environment the liquid phase is restricted to a thin layer of water which sorbs/condenses on the glass. Reaction generates a highly concentrated solution after short reaction times, and secondary minerals precipitate from solution after only a few days. The reaction rate accelerates upon formation of these secondary minerals. This is consistent with the model of glass dissolution used in YMP computer simulations.[2] The assemblages of secondary phases generated by reaction in steam can be compared to those predicted to form in computer simulations so that we can identify phases which need to be added to the data base for the simulation.

In work this year, we determined the structure and composition of a reaction layer produced on a simulated waste glass (SRL 202) in both liquid and vapor environments to verify that the reaction process is similar in both environments. The layer is generated by selective depletion of alkali metals and boron and includes microcrystalline clays thought to precipitate within the layer.[3] Samples of the SRL 202 glass, which is the current reference composition of glass to be produced by Westinghouse Savannah River Co. (WSRC), were reacted in liquid solution (EJ-13) at 90°C and in vapor at 200°C and then taken for SEM and TEM analysis before and after secondary mineral formation.

The analyses revealed that clay minerals with identical structures form within the layers of samples reacted in liquid at 90°C and vapor at 200°C. Crystallites were abundant in the layers of samples reacted in vapor which had and had not formed secondary minerals. As anticipated, compositional analysis showed layers on all samples to be depleted in alkali metals and boron relative to the unreacted glass. Compared with the vapor-reacted sample on which no minerals formed, the layer on the liquid-reacted sample was enriched in alkaline earths and low solubility elements such as aluminum, while the layer on the vapor-reacted sample that did form secondary minerals was depleted in some elements having low solubilities. These differences are

---

[2]W. L. Bourcier, *Geochemical Modeling of Radioactive Waste Glass Dissolution using EQ3/6: Preliminary Results and Data Needs*, Lawrence Livermore National Laboratory Report UCID-21862 (1990).

[3]T. A. Abrajano, Jr., J. K. Bates, and J. P. Bradley, Ceram. Trans. **9**, 211 (1990).

due to (1) etching of the glass in liquid and (2) the incorporation of elements having low solubility into secondary minerals.

Our analyses show that both high temperature and high SA/V ratio can be used to accelerate the glass reaction. The glass reacts by a similar reaction path to produce similar reaction products at 90 and 200°C and at low and high SA/V ratios. The generation of secondary minerals in the vapor environment is controlled by nucleation events, which are influenced by the degree of solution supersaturation and the availability of nucleating sites. Although reaction in a vapor environment eventually leads to a highly concentrated solution on all samples, nucleation of secondary minerals and the coincident acceleration of the reaction may not be observed in all experiments. Work is in progress to determine experimental conditions that will more consistently generate secondary minerals. These "vapor-hydrated" samples may then be used in subsequent leaching tests at lower temperatures to simulate repository conditions of long exposure times to water vapor, followed by possible intrusion of liquid water many hundreds of years after emplacement.

2. Radiation Studies

The objective of this effort is to evaluate the effect of ionizing radiation on the performance of the waste package in the potential Yucca Mountain site. The placement of high-level waste containers in the underground facility will perturb the pre-emplacement environment by raising the ambient temperature and exposing the environment to gamma radiation levels which initially may be greater than 0.1 Mrad/h. Determining the effects of both of these perturbations on the gaseous/aqueous environment of the waste package is important to characterizing the performance of the high-level waste package during the containment period. In 1990, we conducted experiments to determine (1) the yield of ammonia in high-moisture, air-like systems and (2) the atmospheric corrosion of copper-based materials in irradiated moist air systems. Ammonia formation is a concern because some copper-based materials under consideration as containers are susceptible to ammonia cracking.

In the first series of experiments, we determined ammonia/NO_x yields in an irradiated environment (0.14-0.36 Mrad/h) at 28-150°C with the following initial gas compositions: (1) 0.1% oxygen in nitrogen saturated with water vapor and (2) 0.1% oxygen, 20% hydrogen in nitrogen. Results from these experiments revealed that the presence of oxygen was not sufficient to preclude ammonia formation. Oxygen, however, significantly decreased the rate of ammonia production.

In the 0.1% oxygen-20% hydrogen system, the presence of oxygen lowered the yield of ammonia until the oxygen and nitrogen oxides initially generated from the oxygen present were depleted. Subsequently, ammonia production proceeded with a yield of 1.0 molecules per 100 eV, which is in agreement with published values for comparable hydrogen-nitrogen systems.[4]

---

[4]C. H. Cheek and V. F. Linnenbom, J. Phys. Chem. **62**, 1475 (1958)

In the water vapor-nitrogen-oxygen system, the role of oxygen is more complex. Here, the reducing agent is water vapor and its associated radiolytic products rather than hydrogen. In this system, the ammonia concentration increased and then decreased as oxygen was depleted. This was attributed to (1) an increase in the ammonia oxidation rate and (2) the buildup of NO_x as oxygen was depleted from the system. Direct reaction of atomic nitrogen with water vapor was proposed as a possible mechanism for ammonia formation, but further verification of this conclusion is needed. Initial yields for ammonia formation were low (approximately 0.001 mol %/Mrad), and the buildup of ammonia was not linear with absorbed dose. However, ammonia is usually detected as a product even when systems with high oxygen concentrations (i.e., high-humidity air systems) are irradiated.

The second series of experiments was performed with three copper-based materials: oxygen-free copper, 70/30 copper nickel, and 7% aluminum bronze. These are the candidate copper-based materials currently under investigation by the YMP for use in waste containers. Experiments were performed at a dose rate of 1-2 x 10^4 rad/h, temperatures of 90 and 150°C, durations of 30 and 75 days, and dry and moist (40% relative humidity at 90°C) air environments. Changes in the bulk composition of the gas phase were tracked, and the specimens were analyzed to identify the corrosion products formed and to determine weight changes incurred as a result of corrosion.

Under the experimental conditions, only oxides of copper (cuprite and tenorite) were identified as corrosion products. No evidence of localized corrosion (e.g., pit formation) was found. General corrosion rates observed were between 0.1 and 3 mg/cm^2/yr and increased with temperature. At 150°C, the corrosion rate increased by 50% due to the presence of the ionizing radiation. Comparisons between analytical results from the dry and moist air experiments indicated that radiolytic products of water are more effective oxidants than those of molecular oxygen (i.e., ozone and atomic oxygen).

From the above work, we reached two overall conclusions with respect to the YMP effort. First, some ammonia will be formed under the conditions expected in the high-level nuclear waste repository. The possibility that the ammonia generated will crack copper-based materials, therefore, needs to be factored into the YMP material selection process. Second, the initial corrosion rate of copper-based materials in irradiated systems is increased by the presence of ionizing radiation. The long-term effects of this increase need to be determined. Furthermore, the conditions under which pit formation may occur is a complex function of temperature, dose rate, and relative humidity. Additional work is needed to more completely address this concern.

3. Spent Fuel Studies

We exposed two sets of Zircaloy-clad UO_2 pellets to dripping EJ-13 water under conditions that simulate reactions expected for spent reactor fuel in an unsaturated repository environment. These experiments examine reactions of UO_2 samples at 90°C and variable SA/V ratios in the presence of stainless steel and Teflon support plates and have been underway for periods of 1.25 yr (stainless steel plate) and 5.5 yr (Teflon plate). Goals for these experiments are to develop procedures for studies conducted with actual spent fuel, identify secondary

alteration phases, and describe parameters that control the uranium release from the waste package assembly.

Results from the long-term tests can be summarized as follows. The UO_2 matrix readily reacts under liquid water/oxidizing conditions. Reactions are characterized by a large pulsed release of uranium and the formation of several uranyl oxide hydrate (UOH) mineral phases on the sample surface after one to two years of testing (Table IV-2). After two years, the reactions are characterized by reduced rates of uranium release, dissolution of the earlier formed UOH phases, the formation of a diverse population of uranyl silicate phases (Table IV-2), and the depletion of alkali, alkaline earth, and silicon concentrations from solutions contacting the samples. The top surfaces of these samples exhibit complex mineral zonations that develop in response to differential precipitation rates and restricted liquid flow patterns across the sample surface.

Table IV-2. Secondary Uranyl Phases Identified on Reacted UO_2 Surfaces

Uranyl Oxide Hydrates (UOH)	Uranyl Silicates
Schoepite $UO_3 \cdot 2H_2O$	Uranophane $Ca(UO_2)O_2(SiO_3)_2(OH)_2 \cdot 5H_2O$
Dehydrated Schoepite $UO_2 \cdot 0.8H_2O$	Boltwoodite $K(H_3O)UO_2(SiO_4) \cdot nH_2O$
Compreignacite $K_2U_6O_{19} \cdot 11H_2O$	Sklodowskite $Mg(UO_2)_2(SiO_3)_2(OH)_2 \cdot 5H_2O$
Becquerelite $CaU_6O_{19} \cdot 10H_2O$	Soddyite $U_5Si_2O_{19} \cdot 6H_2O$

Detailed SEM examinations of the granular UO_{2+x} surface showed evidence of grain boundary dissolution during the initial one- to two-year period. Rapid corrosion of intergrain boundaries and spallation of fine particulate UO_{2+x} granules appear to be responsible for much of the uranium released during this period (Fig. IV-3). After this rapid release period, uranium

Fig. IV-3.

Surface of UO_2 Samples after 1.5 Years of Reaction Showing Evidence for Granular and Intergranular Corrosion and Spallation of Micron-Sized Particles from the Sample Surface

release rates decrease, and a more stable assemblage of uranyl silicate phases form by incorporating cations from the groundwater leachate. These phases appear to represent the final solubility-limiting phases that form during UO_2 alteration tests. The observed experimental paragenetic sequence (from uraninite, to UOH, to uranyl silicates) is identical to mineralogic sequences that form in weathered zones of natural uraninite occurrences. These experiments are being continued to observe whether additional phases form as the reaction progresses and to assess the possible interaction of dissolved Teflon with uranium mobility and secondary phase formation.

B. *Environmental Restoration and Waste Management Program*

The Defense Waste Processing Facility (DWPF) at WSRC is scheduled to begin production of radioactive glass early in the 1990s. Prior to startup, the glass producers must demonstrate that they can produce a product of consistent durability, and DOE must demonstrate that the glass will meet performance criteria after being emplaced in the YMP storage environment. We have identified several environmental parameters that may affect the performance of emplaced waste glass and have undertaken several tasks to better characterize the influence of these parameters on glass reaction. The tasks include the following: (1) a detailed technical review of literature regarding the parameters that may affect glass reaction in an unsaturated environment, (2) long-term leach testing of fully radioactive glasses similar to those to be produced by DWPF, (3) tests with simulated waste glass to determine the effect of radiation on glass reaction at large SA/V ratios, (4) tests with simulated waste glass to relate high SA/V experiments to the MCC-1 leach test,[5] and (5) tests with naturally occurring rhyolitic glass to assist in understanding the more complicated reactions for waste glass.

1. Critical Review

The predicted repository environment at Yucca Mountain has been described by the YMP as hydrologically unsaturated with possible air exchange with the neighboring biosphere. We have identified several environmental conditions that may affect the durability of waste emplaced in such an environment over repository-relevant time periods and have reviewed the existing literature to evaluate the state of knowledge regarding the influence of these conditions on the glass reaction. Commonly used experimental methods were also critically analyzed to determine if the data produced were useful in characterizing the waste stability in an unsaturated repository.

The first factor subjected to in-depth review was the effect of temperature on waste glass/water interactions. The objective was to assess whether temperature can be used as an accelerating parameter in durability testing of glasses, particularly nuclear waste glasses. Temperature is an important parameter to consider because it affects glass reaction mechanisms and rates in laboratory glass durability tests, as it will within the repository itself.

---

[5]D. M. Strachan, B. O. Barnes, and R. P. Turcotte, "Standard Leach Tests for Nuclear Waste Materials," in *Scientific Basis for Nuclear Waste Management*, Vol. 3, ed., T. G. Moore, Plenum Press, New York, pp. 347-354 (1988).

Our review indicated that the overall glass/water reaction is a cumulative result of the constituent reactions: molecular water diffusion, ion exchange, silicate network dissolution, and secondary mineral precipitation. These reactions often operate simultaneously and are poorly understood at present.

We examined studies relevant to the temperature dependence of the above individual reactions; however, these studies are generally for other chemical systems (i.e., the reactions are usually unable to be isolated for glass/water systems). The constituent reaction mechanisms of glass reactions usually have a temperature dependence that can be quantitatively expressed by an Arrhenius equation. The temperature dependence is often described by the activation energy, i.e., the threshold energy above which a chemical reaction is likely to occur. The basis for Arrhenius-type formulations can be related to physical chemistry principles, although the connection has not been rigorously defined. Researchers have used the Arrhenius equation to describe the temperature dependence of glass dissolution based on several kinetic measurements, including the cation release rate to solution and the growth rate of alteration layers and secondary minerals. In general, we found that temperature can be used as an accelerating parameter when the chemical reaction is identified and understood.

Often, experimental results indicate that the rate-controlling mechanisms in glass/water reactions vary as a function of temperature. Because glass reaction is the result of a complex interaction of several reaction mechanisms, changes in experimental temperatures often result in a change in the dominance or control of a particular reaction mechanism on the overall reaction. Consequently, the effect of temperature as an accelerating parameter on the overall glass/water reaction is poorly understood.

Based on the results of our review, we concluded that several key aspects of glass/water reactions must be investigated to gain an understanding of the reaction at any temperature. These include changes in solution concentrations over time and the alteration phases formed. The most effective technique for studying alteration phases is analytical electron microscopy (AEM), a powerful tool that allows high-resolution investigations of alteration phases and provides mechanistic insight (see Sec. IV.B.6). This type of information, considered in conjunction with more routinely collected measurements such as solution concentrations, can allow researchers to elucidate reaction mechanisms more easily. After the key aspects of glass/water reactions are known, the final step is to develop a kinetic model of the glass/water reaction process. This step will synthesize an understanding of the overall reaction into a description that can be used in a predictive manner. With calculations provided by such a model, temperature can then be used to accelerate glass/water reactions in a meaningful way.

Future work will include reviewing the literature to assess the effects of parameters other than temperature (glass compositions, radiation, SA/V ratio, vapor and dripping water, and composition of reacted layers) on waste glass durability.

2. Long-Term Testing of Fully Radioactive Glass

Because of the long time frames (>10,000 yr) involved in disposing of high-level nuclear waste, performance of the DWPF glass must be determined from predictions with

mechanistic models. The models require information describing the glass reaction mechanisms, the initial and final reaction rates, the affinity of the glass to react, and the dependence of the glass reactions on the interactions with other components of the waste package. The models must be validated to demonstrate their predictive capability. This validation will involve long-term tests that closely simulate the expected conditions for waste storage, including parameters related to the glass and the repository. We are conducting such long-term tests not only to validate glass reaction models but also to demonstrate an understanding of the glass reaction processes that will occur in an unsaturated environment. In addition, these tests will indicate if the reaction of fully radioactive glass differs from that of a nonradioactive glass with the same nominal composition.

To determine the long-term performance of glass under repository conditions, we are conducting tests such that "final" reaction conditions (steady state) are achieved. This will be accomplished by carrying out long-term static tests (for up to eight years) with glass monoliths at an SA/V ratio of 340 m^{-1} and powdered glass having an SA/V ratio of 2000 m^{-1}. The tests will be performed with three different glass compositions (designated 131/11, 165/42, and 200R). The 131/11 glass is lowest in silicon and is in the lower portion of the stability range of waste glasses. The 165/42 glass is higher in silicon and is expected to be near the best range for durability. The 200R glass is poorer in silicon than the 165/42 glass, and a glass with this composition could be produced in the DWPF.

The tests are carried out in duplicate, except for those with the 131/11 glass because insufficient glass is available. The test temperature is 90°C, which is at the high range applicable to the YMP repository and is the temperature commonly used in evaluating glass performance. The leachant is J-13 well water equilibrated with tuff rock (EJ-13), representative of the YMP site. While the tests will continue over an eight-year period, solution samples are being taken periodically for analysis. To date, the 165/42 and 131/11 glass tests have been completed through 91 and 140 days. The 200R glass has been received from WSRC, and preparation of the appropriate samples is in progress.

At selected intervals, the solutions have been analyzed for pH, anions, cations, and organic and total carbon in tests with both nonradioactive and radioactive glasses, as well as fission products and transuranic elements in tests with radioactive glasses. Since blank runs have not yet been completed, the reported results will have to be corrected as the blank run data become available. While the results are preliminary, several interesting trends related to pH and cation release (Table IV-3) are apparent.

The pH of the starting groundwater is approximately 8.1. As shown in Table IV-3, the test solutions for the 165/42 monolith glasses undergo a small increase in pH, all of which appears after 28 days. For the 131/11 monolith glass, pH after 28 days shows a rise similar to that of the 165/42 glass. But after 91 days, pH drops to 8.0. For the 131/11 and 165/42 powder glasses, pH increases significantly with time. This finding indicates increased reaction for the powders.

Lithium and boron are the cations usually used to assess the extent of glass reaction. We used these elements for this purpose because of their low concentration in EJ-13 water. For

Table IV-3. Selected Results for the Reaction of 165/42 and 131/11 Glasses with EJ-13 Water at 90°C

Glass Type[a]	SA/V, m^{-1}	Test Duration, days	pH	Normalized Elemental Release,[b] g/m^2		
				Li	B	Pu
165/42	340	28	8.54	0.64	0.06	0.06
monolith		91	8.37	0.86	0.05	0.07
165/42S	340	28	8.60	0.64	0.13	--
monolith		91	8.64	1.01	0.17	--
165/42	2000	30	9.38	0.34	0.06	0.04
powder		70	9.60	0.45	0.11	0.06
		140	9.77	0.52	0.15	0.09
165/42S	2000	30	9.30	0.32	0.04	--
powder		70	9.34	0.41	0.05	--
		140	9.47	0.48	0.07	--
131/11	340	28	8.69	0.66	0.15	--
monolith		91	7.99	1.10	0.83	--
131/11	2000	30	10.06	0.35	0.16	0.005
powder		70	10.30	0.47	0.24	0.05
		140	10.70	0.51	0.29	--

[a]Simulated nonradioactive glasses are identified by "S" after glass designation, e.g., 165/42S. No "S" indicates radioactive glass.
[b]Normalized to the initial surface area and elemental composition of the glass.

the 165/42 powder glass, the lithium release is greater than the boron release for both radioactive and nonradioactive glasses; the lithium release is essentially the same for both radioactive and nonradioactive glasses; and the boron release from the nonradioactive glass is about half that from the radioactive glass. The lithium release is essentially the same from both 165/42 and 131/11 powder glass, but the boron release from the 131/11 powder glass is about twice as great as that from the 165/42 powder glass. The data for the 165/42 glasses indicate significantly higher lithium release from monoliths compared with that of the powders, but less so for boron release. For the 131/11 glass, the boron release from the monolith is significantly greater than that from the powder.

As shown in Table IV-3, the plutonium release from the 165/42 monolith glass is about the same as the boron release, but the plutonium release from the 131/11 powder glass is much less than the boron release.

It is too soon to assess whether the glasses are reacting similarly, but the differences in the lithium and boron releases for the radioactive and nonradioactive 165/42 glasses should be noted. Reasons for these differences may be revealed in physical examination of the reacted samples.

3. Tests of Radiation Effects

Leaching experiments in an irradiated, water-saturated environment have shown minor accumulations of radiolytic products, such as nitric and carboxylic acids, in leachate solutions (deionized water and groundwater). These products have little effect on glass performance for two reasons: the diluting effects of the relatively large water volumes used in the experiments and the buffering capacity of bicarbonate in the leachant solution. However, a buildup of radiolytic products may be expected in an unsaturated repository environment, where only small volumes of liquid water are expected to contact the samples as thin films of condensate. Thus, in an unsaturated environment, the limited amounts of bicarbonate present in the leachate may be quickly overwhelmed by nitric acid produced in radiolysis reactions. In this situation, the nitric acid that forms may react with the glass, significantly accelerating its degradation. Our present radiation experiments are thus designed to examine the effects of radiolysis and radiolytic-product formation on the performance of glass in an unsaturated repository environment, i.e., high ratios of air to liquid volume (G/L) and glass surface area to liquid volume (SA/V).

To determine the effect of radiolysis, experiments were carried out in pressure vessels containing deionized water (G/L ratio = 100) at room temperature under alpha and gamma radiation fields. Results indicate that NO_3^-, organic carbon, and inorganic carbon are readily produced in both gamma and alpha fields, and that NO_3^- production varies linearly with respect to time and dose rate. The results also suggest that the radiolytic products are concentrated in thin films of water that condense on the test vessel walls and/or radioactive source materials. Experiments are in progress to measure rates of nitric acid formation under a gamma field at 90 and 200°C and a G/L ratio of 10.

To determine the cumulative effects of these radiolytic products, glasses of identical compositions were reacted in unsaturated conditions (SA/V = 340 cm^{-1}) under radiation (3.7 x 10^3 R/h) and nonradiation fields at 150 and 200°C. Our results indicate that glass reaction rates in the radiation field exceed those in the nonradiation field by a factor of 50 to 200. In fact, the thin films of water in contact with the glass were so corrosive that the irradiated samples had reacted completely through their 2-mm thicknesses in as little as 35 to 56 days (Fig. IV-4).

The radiation field also appears to have influenced the development of secondary mineral phases on the glass surfaces. Samples reacted in the radiation field developed thick precipitate layers that contain analcime ($NaAlSi_2O_8 \cdot H_2O$), weeksite ($K_2(UO_2)_2(Si_2O_5)_3 \cdot 4H_2O$), and an acicular calcium silicate phase (possibly tobermorite, $Ca_5(OH)_2Si_6O_{16} \cdot 4H_2O$). By contrast, samples reacted without radiation developed a thin and discontinuous precipitate layer that contains analcime, relatively minor weeksite, a bladed rosette-shaped calcium silicate phase (possibly gyrolite, $Ca_4(Si_6O_{16})(OH)_2 \cdot 3H_2O$), unidentified potassium-aluminum silicate buttons, and an unidentified sodium silicate phase radiating fibrous masses.

4. Tests of Surface Area-to-Volume Ratio Effects

Glasses incorporating high-level nuclear waste must be shown to meet performance criteria prior to emplacement in a waste repository. Glass producers utilize simple leach tests

such as MCC-1[5] to assure product consistency. The large volume of test results available from MCC-1 and similar tests may be helpful in projecting glass performance in the YMP repository environment. While most tests of glass durability are performed under dilute conditions at low SA/V ratios, the unsaturated environment typical of what is expected for the potential Yucca Mountain site will limit the amount of water that may contact the waste to small volumes, and very high SA/V ratios are anticipated. Before durability tests such as the MCC-1 test can be used as an indication of glass durability in the repository, the durability of a glass measured under dilute testing conditions must be demonstrated to be representative of its durability under the expected repository conditions. We must therefore understand the changes that may occur in the glass reaction rate or reaction pathway as the SA/V is increased.

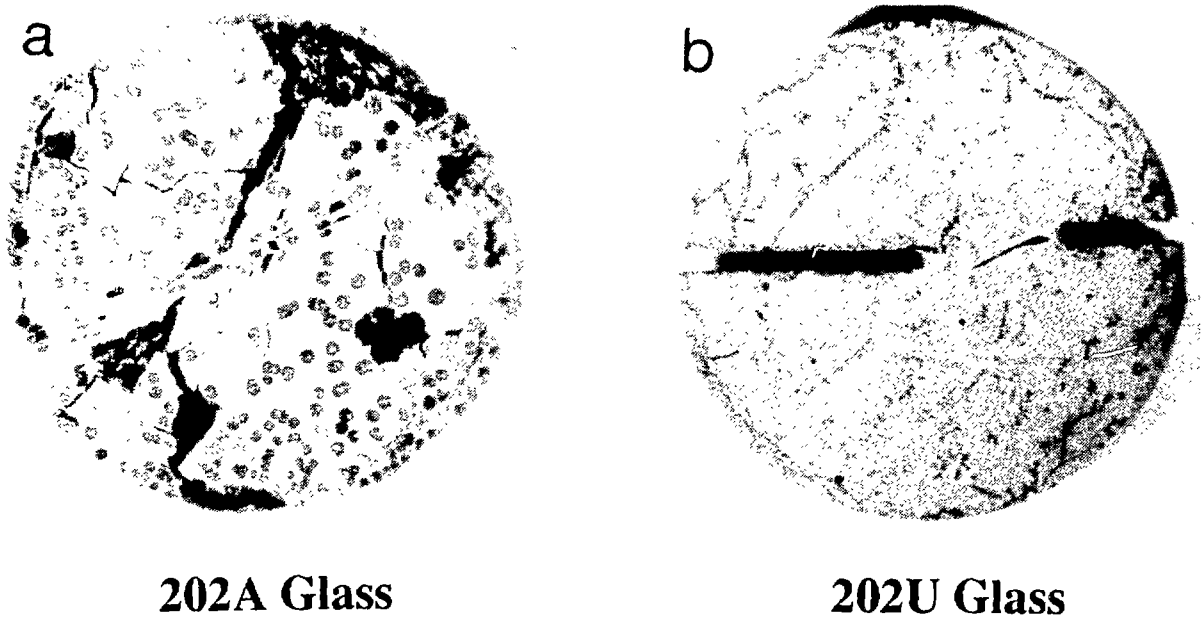

Fig. IV-4. Reflected Light Photomicrographs of Actinide- and Uranium-Doped Glasses Exposed to (a) Irradiated and (b) Nonirradiated Environments. Both glasses were exposed to a vapor-saturated environment at 200°C for 35 days. The 202A glass was also exposed to 5000 rad/h.

We have initiated a large series of tests to compare the extent and nature of glass reaction at different SA/V ratios (10, 2000, and 20,000 m^{-1}) using two glass compositions: SRL 202 and SRL 131. The SRL 202 represents the current reference composition for glass to be produced by the DWPF, while SRL 131 represents the least durable glass that will be produced for disposal in the repository. The glasses are doped with Tc, U, Np, Pu, and Am to track the fate of radionuclides during the glass reaction and are referred to as SRL 202A and SRL 131A. Monolith samples with an approximate area of 1.7 cm^2 are used in tests at 10 m^{-1}, and powder glasses with particle size fractions between 74 μm and 149 μm (-100 +200 mesh) are used for tests at 2000 and 20,000 m^{-1}. Reactions are carried out in stainless-steel Parr vessels at 90°C

with groundwater from well J-13. Tests are performed for reaction times of a few days to a few years to assess the reaction rates at the different SA/V ratios. Analyses of both the leachate and the reacted solids are performed to characterize the reaction.

The reaction times (t) were selected to (1) monitor the temporal changes and thereby track the reaction rate and (2) provide overlapping values of SA/V•t among the three SA/V ratios. Pederson et al.[6] observed that the solution chemistry scales as SA/V•t early in the reaction process but deviates at very high SA/V•t. Our tests will provide results that may be used to describe the source of the deviation observed at large values of SA/V•t and the usefulness of SA/V•t scaling in general.

We have completed short-term tests of 30 days or less and are analyzing the leachate and reaction products. Figure IV-5 shows the leachate pH values for tests with SRL 202A and SRL 131A glass at the three SA/V ratios. The pH is consistently higher in tests at the larger SA/V ratios for both glass types. This is a result of the greater dilution at lower SA/V ratios. The pH clearly does not scale as SA/V•t, even at short reaction times for these glasses. Also, the pH values for both glass types are significantly different after 30 days at 2000 m^{-1} compared with 3 days at 20,000 m^{-1}, where both have SA/V•t values of 60,000 days/m. After about 30 days, the pH values appear to be approaching a limiting value unique to each SA/V ratio and glass composition.

The results in Fig. IV-5 also show that, as expected, the SRL 131A glass is more reactive than the SRL 202A glass. The release of alkali metals through ion exchange with protons is the major source of hydroxide and the pH rise. Although the release of other species may alter the pH slightly, the pH increase primarily reflects the extent of alkali release. The SRL 131A has about 1.2 times more alkali than SRL 202A, while the pH difference is about 1 unit after 28 days at 20,000 m^{-1}. This pH difference is greater than can be attributed to glass composition differences.

The uranium concentrations of the leachate analyzed to date are shown in Fig. IV-6. Both SRL 202A and 131A glasses show a similar trend at each SA/V ratio. At 20,000 m^{-1}, the uranium concentration significantly increases within the first 14 days, then decreases after 28 days. The pH results suggest that the glasses have reacted to a similar extent after 14 and 28 days; thus, the drop in uranium concentration beyond 14 days may indicate the formation of a uranium-containing secondary phase. While SRL 131A had higher final pH values than SRL 202A, the amount of uranium in solution in the 20,000 m^{-1} tests was higher in tests with SRL 202A glass reacted more than 3 days. Since SRL 131A glass has about 1.4 times more uranium than SRL 202A glass, the results suggest that uranium-containing secondary phases may be more abundant in tests with SRL 131A glass at high SA/V. The reacted solids of tests run for 14 and 28 days will be analyzed to identify secondary phases that formed. The concentrations of other elements in solution will also be determined and compared with the uranium results. Too few data are currently available to speculate on any release trends. As more tests are completed

---

[6]L. R. Pederson, C. Q. Buckwalter, G. L. McVay, and B. L. Riddle, Nucl. Technol. **62**, 151 (1983).

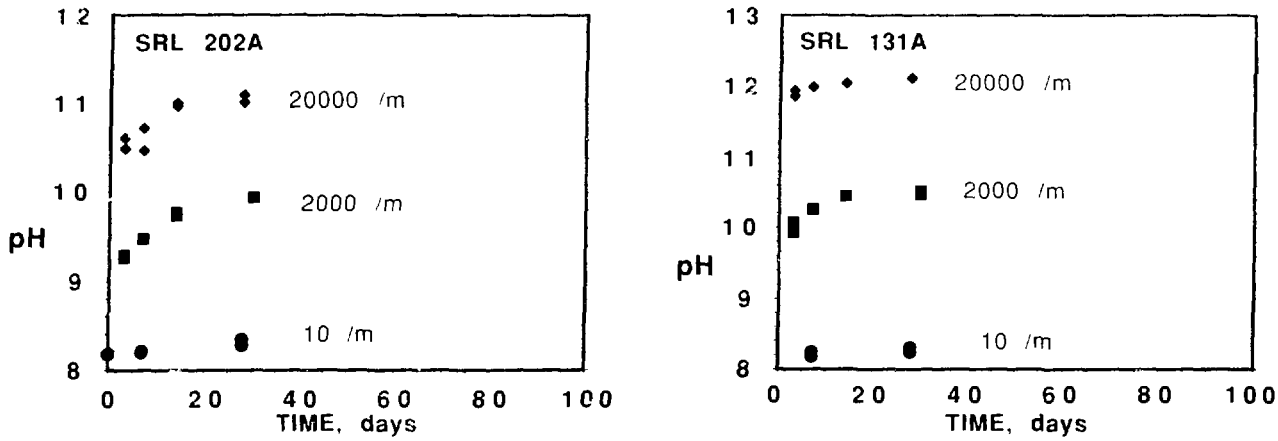

Fig. IV-5. Leachate pH Values vs. Reaction Time for Tests at 20,000, 2000, and 10 m^{-1} for SRL 202A and SRL 131A Glass

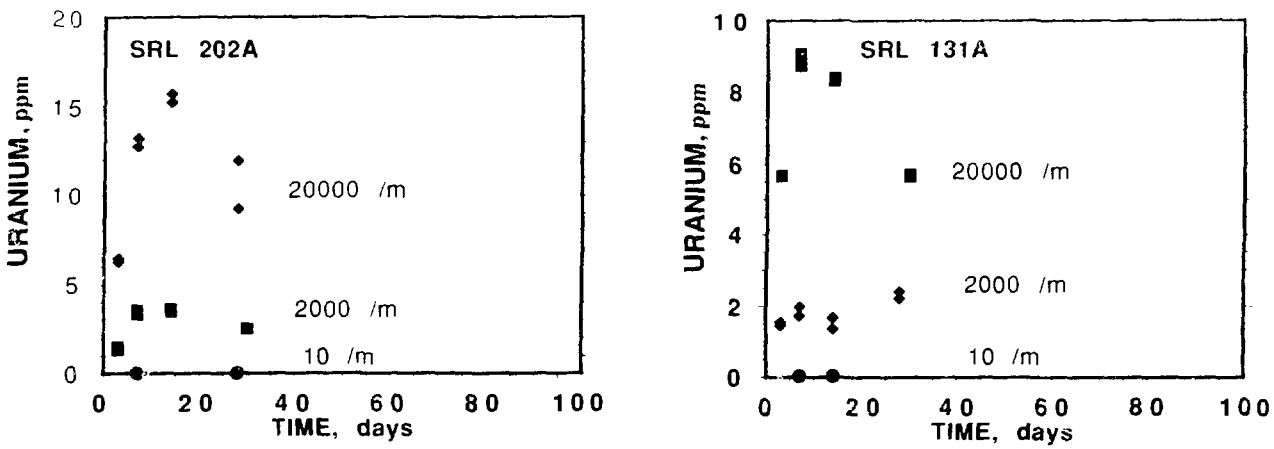

Fig. IV-6. Uranium Concentration in Leachates vs. Reaction Time of Tests at 20,000, 2000, and 10 m^{-1} for SRL 202A and SRL 131A Glass

in the upcoming year, we will be able to obtain a more detailed comparison of the reaction of the two glass types at the various SA/V ratios.

5. Natural Analog Tests

The reaction of naturally occurring rhyolitic glass (obsidian) with water under conditions where the SA/V ratio is large (i.e., reaction in water vapor) has been identified as a

system with a relatively simple reaction mechanism, molecular water diffusion.[7-9] We have initiated a detailed study of this reaction process to assist in understanding more complicated reaction mechanisms for nuclear waste glasses. Although obsidians are enriched in silica and depleted in alkalis and boron relative to nuclear waste glasses, their survival in nature for extensive periods of time (up to millions of years) can offer insights into the long-term corrosion of glass in a geologic setting.

For this effort, we hydrated different obsidians in vapor between 110 and 180°C for up to 64 days at relative humidities of 60, 90, 95, or 100%. Reaction progress was monitored by the growth rate of the birefringent hydration layer, thought to be caused by a strained glass network forming as molecular water diffuses into the glass.[9] In all cases, the growth rate was proportional to the square root of time, a dependence consistent with a diffusion process. We found that the hydration rate for obsidian is significantly affected by relative humidity, an effect previously believed to be negligible.[9] The relative humidity dependence could be correlated to the amount of water sorbed onto the glass surface: this suggests that the diffusion process is driven by chemical potential differences between the glass and the sorbed water. We also found that the isothermal hydration rate of obsidian strongly depends on the obsidian composition, specifically the intrinsic water content. Our correlation between intrinsic water content and hydration rate (correlation coefficient of 0.97) is superior to that obtained with previously proposed models (e.g., see Refs. 10 and 11). Our plot of the temperature effect on obsidian hydration rates conformed to an Arrhenius equation in which the activation energy strongly depends on the intrinsic water content.

As a test of our correlation, we also considered the experimental hydration of tektite. Tektite is a natural glass somewhat similar in composition to obsidian, but containing a very small (~0.01 wt %) amount of water. The tektite data are consistent with intrinsic water content controlling the diffusion process, whereas the other compositional models could not successfully account for these tektite values.

Our results suggest that obsidian hydration dating,[9,12] a chronometric tool used extensively by archaeologists, has the potential to be accurately calibrated. The technique currently relies on experimental determinations of the activation energy of hydration for each obsidian under study. Our results will allow practitioners of obsidian hydration dating to estimate the ages of obsidian artifacts or features from the intrinsic water content. Furthermore, better age estimates will also result when the effects of relative humidity are taken into account.

---

[7]J. K. Bates, T. A. Abrajano, Jr., W. L. Ebert, J. J. Mazer, and T. Gerding, "Experimental Hydration Studies of Natural and Synthetic Glasses," in *Materials Issues in Art and Archaeology*, eds., E. Sayre et al., Mat. Res. Soc. Symp. Proc., Vol. 123, p. 237 (1988).

[8]R. R. Lee, D. A. Leich, T. A. Tombrello, and I. Friedman, Nature **250**, 44 (1974).

[9]I. Friedman and R. L. Smith, Am. Antiq. **25**(4), 476 (1960).

[10]I. Friedman and W. Long, Science **191**, 347 (1976).

[11]J. E. Ericson, J. D. Mackenzie, and R. Berger, "Physics and Chemistry of the Hydration Process in Obsidians. I: Theoretical Implications," in *Advances in Obsidian Glass Studies*, ed., R. E. Taylor, Noyes Press, Park Ridge, New Jersey (1976).

[12]I. Friedman and F. W. Trembour, Am. Sci. **66**, 44 (1978).

We are currently trying to quantify the effect of intrinsic water content on obsidian hydration in a way that will allow archaeologists and geologists to account for molecular water diffusion where obsidians are encountered.

6. Analytical Support

Analytical electron microscopy (AEM) involves a combination of transmission electron microscopy (TEM), energy dispersive X-ray spectroscopy (EDS), electron energy loss spectroscopy (EELS), and electron diffraction (ED). Point-to-point resolution for images obtained with the TEM approaches 3 Å, and the smallest region that can be investigated using EDS, EEL, and ED is about 200 Å. The AEM is a very powerful tool for investigating inhomogeneous samples with very small inclusions, thin layers, and intercalated materials. We have used AEM to examine the structure of reacted glass and obtained accurate information as to the reaction process.

For AEM identification of secondary phases to be successful, one must have extremely thin samples, 500 Å or thinner. Since reaction layers are usually much thicker, frequently ≥50 μm, transverse cross sections must be prepared. The layers of the glass reaction product are extremely fragile, and the cross sections must be prepared in a way which minimizes damage to these delicate structures and still provides an electron transparent region that extends over all the reaction layers.

Ultramicrotomy, i.e., thin sectioning with a specially designed diamond knife, has proven successful in preparing ultrathin sections of a large variety of reacted glasses. Competing techniques for preparing the thin samples needed for TEM have serious limitations, including differential thinning rates, radiation damage, implantation damage, restricted lateral extent of the thinned regions, and difficulty in controlling the exact position of the thinned region. We have successfully employed ultramicrotomy to prepare TEM specimens of glasses with no reaction layer and with reaction layers up to 100-μm thick. Ultramicrotomy preparation artifacts do not interfere with the analyses required, and the layer structure of the reaction products is preserved.

Using these AEM techniques, we have analyzed sections of three identically prepared glass samples from a matrix designed to determine whether SA/V•t satisfies the scaling assumption that, given the same SA/V•t, the reaction progress is identical (Sec. IV.B.4). Figure IV-7 shows photomicrographs from the three glass samples, which are reacted to the same SA/V•t value, 1000 days/m, but for different times (10, 20, 100 days). Closely corresponding, but not identical, secondary phases were identified in each of these samples. A similarly reacted sample was previously reported.[13] Secondary phases observed in that case also correspond closely with those observed here.

---

[13]T. A. Abrajano, Jr., J. K. Bates, A. B. Woodland, J. P. Bradley, and W. L. Bourcier, Clays and Clay Miner. **38**, 537 (1990).

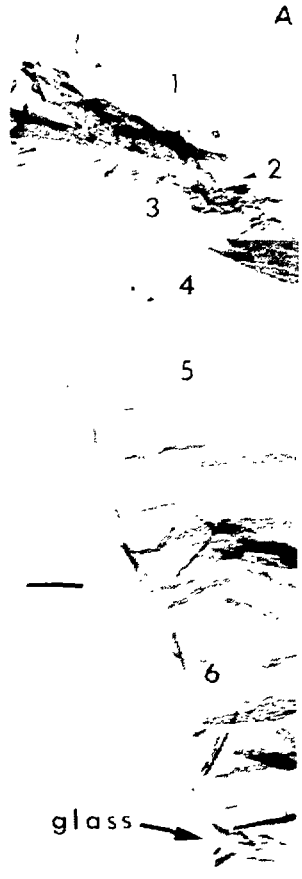

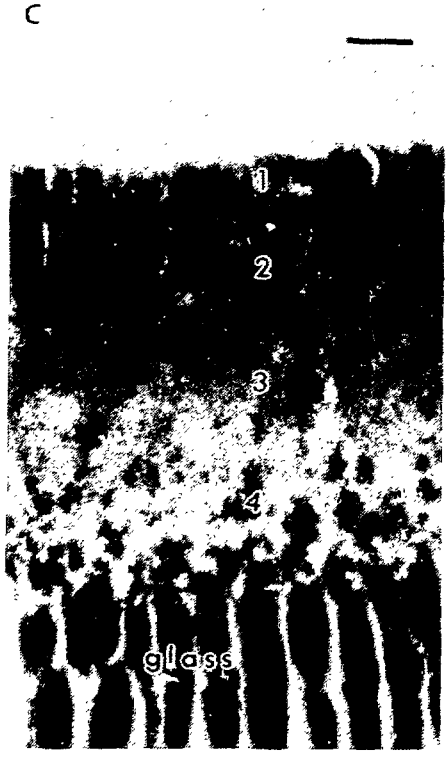

Fig. IV-7.

Photomicrographs of Three Identically Prepared Glass Samples Reacted to the Same SA/V•t Value but Different Reaction Times: (a) 100 days, (b), 20 days, (c) 10 days. Bars in these figures represent 2, 0.5, and 1 μm, respectively.

Despite the similarities, obvious differences suggest that there are processes for which the kinetics are independent of SA/V•t. We found changes in gross features such as layer thickness, the number of layers, and the morphology of layers. For example, reaction layers on the 100-day sample were about 25 times thicker than those on the 10-day sample. At higher magnification, we could make finer distinctions. In a high-resolution image of the 100-day sample, we observed nanometer-sized crystallites as regions of lattice fringes that have the spacing of crystalline lattice planes. Similar regions are present in the other samples; however, the density and size of the crystallites are greater in samples that have been reacted the longest.

The AEM technique will continue to be applied to samples generated in our ongoing test programs.

C. *Radionuclide Speciation Studies*

Studies are underway to investigate radionuclide speciation in groundwater systems. For this work, we are using high-sensitivity, laser-based techniques, primarily laser photoacoustic spectroscopy (LPAS), and ultraviolet-visible (UV-VIS) absorption techniques to directly measure the formation constants for important inorganic and organic complexants under groundwater-relevant conditions. Our recent emphasis has been on the Pu(VI) hydrolysis in near-neutral systems.

There has been recent interest in the environmental chemistry of plutonium species because of their importance in waste management-related concerns. The role of Pu(VI) in the migration of plutonium in natural systems is, however, uncertain. Its high solubility in natural systems relative to Pu(IV), combined with the high mobility of U(VI) in natural systems, suggests that greater importance needs to be placed on determining its role. The chemistry of Pu(VI) is expected to be most important to modeling the release of plutonium at its source and in environments, such as near-surface groundwaters, where oxidizing conditions may exist.

The hydrolysis of plutonium species is of importance to natural systems since many of them are at a pH that is near neutral or mildly alkaline. Hydrolysis data for plutonium species were reviewed by Baes and Messmer.[14] An unresolved complexity in the initial hydrolysis of Pu(VI) is the competition between the formation of PuO_2OH^+ (1:1 complex) and its dimerization [i.e., formation of $(PuO_2OH)_2^{2+}$]. For this reason, the 1:1 hydrolysis constant has not been firmly established.

To more clearly resolve the initial hydrolytic behavior of plutonium species, we are investigating the hydrolysis of Pu(VI) in 0.1M sodium perchlorate medium as a function of pH, total Pu(VI) concentration, and temperature.

The following observations were made from analysis of LPAS spectra. In noncomplexing media, Pu(VI) remains as the aquo ion below a pH of 3. Increasing pH leads to the gradual disappearance of the Pu(VI) aquo-ion absorption band at 622 nm, with a corresponding

---

[14]C. F. Baes and R. E. Messmer, *The Hydrolysis of Cations*, John Wiley and Sons, New York (1976).

appearance of new absorption bands as hydrolysis products of Pu(VI) are formed. In the wavelength range investigated (600-700 nm), four spectroscopically distinct Pu(VI) species were identified in the pH range of 3 to 7. Determining these species is the subject of future efforts.

The initial hydrolysis of Pu(VI) was more extensively investigated by UV-VIS and LPAS techniques. Absorption spectra of the initial hydrolysis products of Pu(VI) were obtained over a broad range of Pu(VI) concentration (10^{-2}-10^{-4} M). Our data indicate that the extent of hydrolysis is greater and the contribution of polynuclear hydrolysis products is much more important than previously thought. The accurate determination of the formation constant and its speciation for the initial hydrolysis product of Pu(VI) is in progress.

We also determined the influence of temperature (10-45°C) on the formation of the initial hydrolysis product of Pu(VI). The temperature variable studies led to the first experimental determination of the free energy of formation for the hydrolytic products. Our results indicate that the effect of temperature is much lower than estimates published in the literature.[15]

D. *Waste Isolation Pilot Plant Project*

The effect of ionizing radiation on the performance of the Waste Isolation Pilot Plant (WIPP) repository is being investigated as part of an overall effort, coordinated through Sandia National Laboratories, to evaluate the suitability of WIPP for disposing of TRU-containing waste. Ionizing radiation will be present in the WIPP primarily as alpha particles due to the radioactive decay of the TRU elements. The objective of our effort is to evaluate the effect of the interaction of these alpha particles, with both the WIPP waste and the anticipated environment, on factors important in assessing the long-term performance of the WIPP site.

Three technical concerns, related to the presence of ionizing radiation, were identified by researchers for the WIPP Project: (1) radiolytically induced conversion of non-biodegradable plastics to those that are biodegradable, (2) gas generation due to the interaction of alpha particles with WIPP waste and brine, and (3) the general effect of radiolysis on the redox conditions in the site, with particular emphasis on the speciation of dissolved transuranics.

The first concern was the focus of our work in 1990. In this effort, polyethylene and polyvinyl chloride, supplied from Rocky Flats Plant, were irradiated for approximately three months with alpha particles in three environments identified as relevant to the anticipated WIPP environment: (1) a gas phase of 90 vol % nitrogen and 10 vol % carbon dioxide, (2) a gas phase of 90 vol % nitrogen, 6.25 vol % carbon dioxide, 2.5 vol % hydrogen, and 1.25 vol % oxygen, and (3) WIPP brine. Irradiations were performed with ^{210}Po and ^{241}Am alpha foils. The dose rates corresponding to the alpha activity of these foils were measured with an ethylene gas dosimeter. Gas phase composition was tracked as a function of time, and changes in the weight and general appearance of the plastic were noted. The irradiated materials were sent to Stanford University, where bioassays will be performed by Dr. Grbic-Galic. Results will be given in next year's report.

---

[15]R. J. Lemire and P. R. Tremaine, J. Chem. Eng. Data **25**, 361 (1980).

In addition to the plastic irradiation studies, we completed some support experiments concerning the effect of ionizing radiation on the WIPP performance. In these experiments, we determined the effects of gamma and alpha radiation on the two gas compositions used in the plastic irradiations. The two-component gas mixture was stable to radiolytic decomposition, with only minor amounts of oxygen and carbon monoxide generated from the carbon dioxide at absorbed doses greater than 40 Mrad. In the four-component gas mixture, nitrous oxide, carbon monoxide, ammonia, and NO_x were generated. No significant linear energy transfer effects were noted.

We also performed stability studies of Pu(VI) in WIPP brine. We successfully stabilized concentrations of plutonium [as Pu(VI) and Pu(V)] in excess of 0.001 M for over two months as dissolved species in actual WIPP groundwater. This indicated that the plutonium was sufficiently stable as a dissolved species to proceed with the planned work on gas generation due to dissolved actinides in WIPP brine.

V. SEPARATION SCIENCE AND TECHNOLOGY

The Division's work in separation science and technology consists of four projects. The first is concerned with removing and concentrating actinides from waste streams contaminated by transuranic (TRU) elements. The objective is to recover valuable TRU elements and lower disposal costs of nuclear waste. The major project in this area involves development of a generic data base and modeling capability for the TRUEX (TRansUranic EXtraction) solvent extraction process. This capability will allow users to design flowsheets for specific waste streams and estimate the cost and space requirements for implementing a site- and feed-specific TRUEX process. It will also be useful as a tool for plant operators to vary, monitor, and control the process once it is in place. The second project is the development of the ANL-designed centrifugal contactor for nuclear waste processing. The greatest part of this effort has been done in support of the first project, where centrifugal contactors have been developed for specific TRUEX applications. Support of work on waste treatment processes for the Integral Fast Reactor (Sec. VI.D) continues in the development of a pyrocontactor for use at high temperature with molten salt and molten metal. The third project is concerned with examining the feasibility of concentrating plutonium solids in pyrochemical residues by aqueous biphase extraction. The fourth project involves the development of a membrane-assisted solvent extraction method for treating natural and process waters contaminated by volatile organic compounds.

A. *TRUEX Technology-Base Development*

The TRUEX process extracts, separates, and recovers TRU elements from solutions containing a wide range of nitric acid and nitrate salt concentrations. The extractant found most satisfactory for the TRUEX process is octyl(phenyl)-N,N-diisobutylcarbamoylmethylphosphine oxide, which is abbreviated CMPO. This extractant is combined with tributyl phosphate (TBP) and a diluent to formulate the TRUEX process solvent. The diluent is typically a normal paraffinic hydrocarbon (NPH) or a nonflammable chlorocarbon, tetrachloroethylene (TCE). The TRUEX flowsheet includes a multistage extraction/scrub section that recovers and purifies the TRU elements from the waste stream, and multistage strip sections that separate TRU elements from each other and the solvent. Our current work is focused on facilitating the implementation of TRUEX processing of defense TRU-containing waste and high-level waste (HLW), where such processing offers financial and operational advantage to the DOE community.

1. The Generic TRUEX Model

The Generic TRUEX Model is a computer program that we developed to (1) act as a tool in designing TRUEX process flowsheets for specific waste stream compositions, process constraints, and process goals, (2) estimate the space and cost requirements for installing a TRUEX process, and (3) act as a guide to process monitoring and control. In 1989, the first version of the Generic TRUEX Model, GTM 1.1, was released for the Macintosh and IBM-compatible personal computers. Since that time new features have been added and improvements have been made to existing code. The updated version, GTM 2.1, was released for the Macintosh computer this year.

a. Improvements

The GTM calculates a TRUEX solvent extraction flowsheet based on input of a specific feed and a set of process goals and constraints. The output of this model is (1) the compositions of all effluent streams and the compositions of the organic and aqueous phases in each stage of the contactor at steady state and (2) estimates of the space and cost requirements for installing this flowsheet in a plant situation. This is accomplished through the execution of four sections of code: SASSE, SASPE, SPACE, and INPUT/OUTPUT. The interactions of these sections are schematically represented in Fig. V-1.

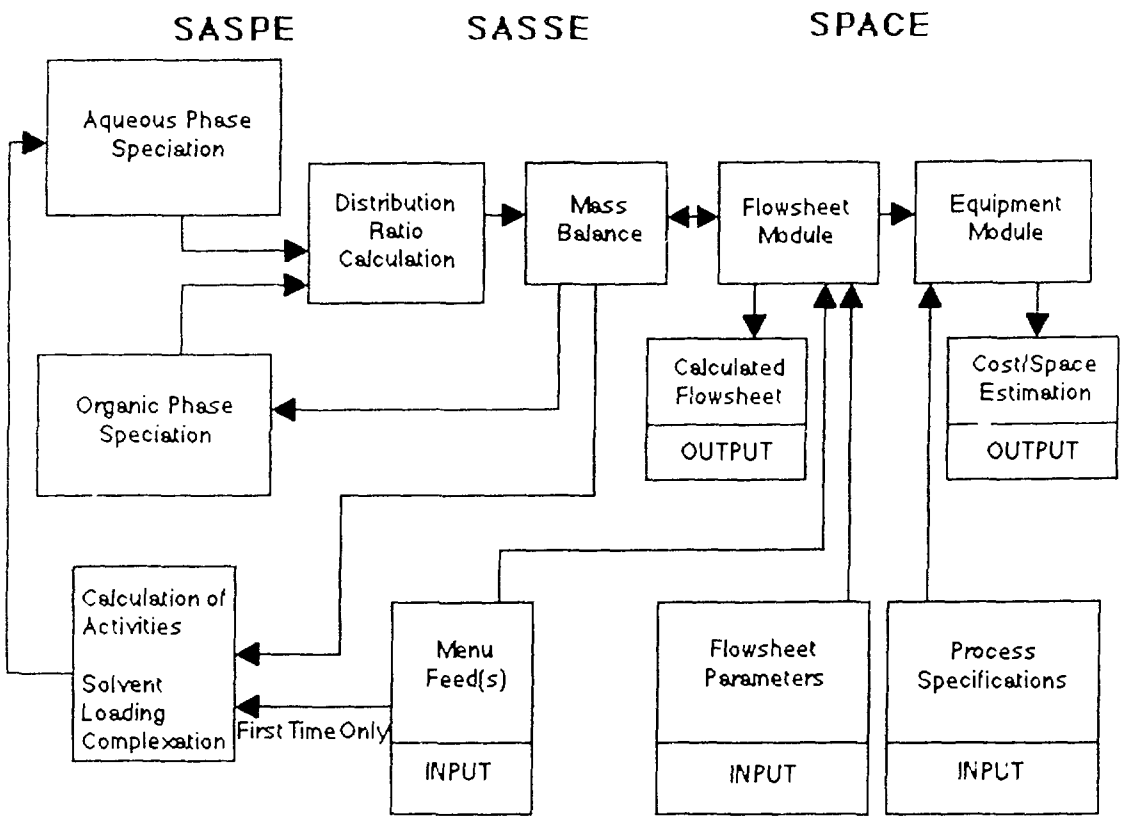

Fig. V-1. Interactions among Computer Program Modules of the Generic TRUEX Model for Flowsheet Calculations

The SASSE (Spreadsheet Algorithm for Stagewise Solvent Extraction) section was developed to allow the design and detailed evaluation of proposed flowsheets in conjunction with distribution ratios generated in the SASPE (Spreadsheet Algorithms for Speciation and Partitioning Equilibria) section. In addition to (1) establishing that each feed component will be able to reach its design composition in the extraction raffinate and product streams and (2) providing the compositions of the organic and aqueous solutions in each stage of the flowsheet at steady state, SASSE can be used to identify key points for process monitoring and control.

The SASPE section calculates distribution ratio (D) values for each aqueous-phase composition from user-specified feeds (feed menu) and from stage compositions generated in SASSE during SASPE/SASSE iterations. Many routines in the SASPE section are necessary for calculating D values of all conceivable combinations of aqueous phase and TRUEX solvent.

During flowsheet calculations, distribution ratios for all components are transferred from SASPE to SASSE so that SASSE can calculate aqueous- and organic-phase compositions in the flowsheet. These calculated compositions are then transferred from SASSE to SASPE so that SASPE can calculate updated distribution ratios, which are then returned to SASSE. When organic-phase concentrations of metal salts are above tracer level,* the loading effect module, which accounts for solvent loading by metal salts (see Sec. V.A.1.c), is called to lower SASPE-calculated distribution ratios accordingly. This interaction between SASSE and SASPE continues until steady state is achieved.

In the SPACE section, the resultant flowsheet from SASSE is combined with user-specified plant information to calculate equipment size, plant space, and capital costs. The SPACE worksheet correlations assume that the hot (radioactive) processing area, which may be either a glovebox, a shielded cell, or a canyon, (1) is available and (2) has been cleaned out (that is, it does not contain any equipment and is nonradioactive enough that persons can work in the area).

The menu-driven INPUT/OUTPUT section (1) allows the user to choose which option (see Table V-1) will be run and to provide all the information needed by the GTM before calculations are begun and (2) generates reports (tabular and graphical) of results for the user. Several of the options in Table V-1 are new and were not available in GTM 1.1. The remaining options have been significantly improved from the earlier version of the model.

Version 2.1 is faster (nearly a factor of three for typical flowsheet calculations), easier to use, and more accurate than Version 1.1. To make the Macintosh and the IBM-compatible code nearly identical, we eliminated the use of HyperCard software for the Macintosh version; the user interface, as well as all the rest of the code, is now programmed in Microsoft Excel. As a result, the codes for both the Macintosh and IBM versions are 99% compatible. We will thus be able to make modifications to code for both computers in a more timely fashion.

Version 2.1 has the capability of calculating distribution ratios for the important components of acidic nitrate-based, TRU-containing waste and HLW streams independently of TRUEX-process flowsheets for either the TRUEX-TCE or the TRUEX-NPH solvents. All calculations except for solution density are based on an operating temperature of 25°C. This version will also calculate the concentration profile of feed components in flowsheets that are designed by the user and generated by the model for either centrifugal

---

*Tracer-level concentrations are generally in the range of $\leq 1 \times 10^{-4}$ M. When a species is at or below this concentration, its chemical behavior (and, therefore, its distribution ratio) is not influenced by its own concentration but by that of the other species in solution.

contactors, mixer settlers, or pulsed columns (see Sec. V.A.1.b). In Version 1.1 only centrifugal contactors could be modeled.

Table V-1. Options Available in GTM 2.1

Option No.	Description
1	Calculate the complete Generic TRUEX Model for a specific feed solution.
2	Calculate the charge balance, density, ionic strength, speciation, and activities (hydrogen, nitrate, and water) of an aqueous feed solution.
3	Calculate oxalic-acid additions to fission-product-containing waste.
4[a]	Calculate D values for a user-specified aqueous phase, where the organic phase is assumed to have been pre-equilibrated.
5[a]	Calculate D values for equilibration of user-specified aqueous and organic phases.
6	Complete flowsheet analysis with user-specified distribution ratios.
7	Generate a TRUEX flowsheet for a specific feed solution.
8	Estimate space and costs for user-specified flowsheet.
9[a]	Estimate solvent degradation for a specific TRUEX process.
10[a]	Generate reports from existing TRUEX flowsheets or space and cost calculations.

[a]Not included in Version 1.1.

Distribution ratio calculations, and therefore flowsheet calculations, with GTM 2.1 are more accurate because it (1) takes into account the unavailability of CMPO due to extraction of high concentrations of metal salts by the solvent and (2) calculates the complexation of cations by oxalate, fluoride, and sulfate for every stage of a flowsheet calculation. The latter calculation has allowed us to increase the number of possible components present in scrub and strip feeds from 3 to 13. Version 2.1 also now includes a 0.25 M Na_2CO_3 solvent wash, a 0.25 M HEDPA* /0.05 M HNO_3 solvent wash, and a 0.1 M nitric acid rinse in SASSE/SASPE flowsheet calculations; these additions may be treated as any other section in the TRUEX flowsheet (extraction, scrub, strip) where flow rates and number of stages per section are specified.

Another new feature in GTM 2.1 is the ability to estimate CMPO loss and increases in americium distribution ratios under stripping conditions due to hydrolytic and radiolytic degradation of the TRUEX-NPH solvent. Input required is number and type of

*HEDPA is 1-hydroxyethane-1,1-diphosphoric acid; this solvent wash can be used as typical for all the thermally unstable complexants.

TRUEX flowsheet sections (radiolysis is assumed to be only important in the extraction section), number of stages, type of contactor, feed flow rates, absorbed dose of the solvent (a default value is provided that is appropriate for treating high-level waste which is 20 years old), and the average composition of the aqueous phase in each section. The ability to generate and view reports from SASSE and SPACE spreadsheets generated earlier is also a new convenience for users.

Future enhancements of the GTM will allow the treatment of feed components specific to Idaho Chemical Processing Plant HLW (tetrafluoroborate, cadmium), speciation calculations for many more feed components (the number of species will increase from 43 to >110), and variation in the TRUEX solvent composition. In addition, the accuracy of our distribution-ratio models will be improved by adding both batch and continuous, countercurrent, verification-test data to the GTM data base.

b. Pulsed-Column Model

A new model has been developed for analyzing solvent extraction processes carried out in pulsed columns. Each column is treated as a series of well-defined equilibrium stages where the "backmixing" (i.e., other-phase carryover) between stages can be large. Mass transfer effects are modeled by choosing a stage height and degree of backmixing such that the same number of stages is appropriate for all extracted chemical components no matter what their distribution ratios. By having the same number of stages for all components, the same SASSE worksheet can be used for centrifugal contactors, mixer settlers, and pulsed columns. This greatly simplifies the calculations for multicomponent solvent extraction processes in columns and is more appropriate for the GTM than either the Height of an Equivalent Theoretical Stage (HETS) or the Height of a Transfer Unit (HTU).[1] Initial evaluation with literature data[2] showed that the new model works as well as the HTU method and better than the HETS method when calculated and actual data from pulsed columns are compared.

To use the pulsed-column model within the GTM, we revised SASSE so that it could handle any amount of backmixing at any stage. Further, SASSE now allows inclusion of feed and effluent streams at any stage (aqueous or organic), and steady-state values are calculated directly rather than iteratively. The result is a SASSE worksheet that can handle backmixing as well as any feed or effluent and yet is up to six times faster than the previous version. Applying the new model to pulsed columns is very easy if one uses it with the new SASSE worksheet. The column model can account for (1) backmixing, (2) either phase being the continuous phase, and (3) the number of columns used in a process.

Figure V-2 is the TRUEX flowsheet that we used to calculate the three sodium concentration profiles shown in Fig. V-3. As a base case, the sodium concentration profile for a

---

[1]R. E. Treybal, *Liquid Extraction*, 2nd ed., McGraw-Hill, New York (1963).

[2]H. R. Maxey, D. B. Chamberlain, G. J. McManus, E. L. Colton, and R. L. Nebeker, *Removal of Actinides from ICPP Fuel Reprocessing Wastes: Engineering Studies Terminal Report*, Exxon Nuclear Idaho Company, Idaho Falls, ID, ENICO-1057 (1980).

centrifugal contactor was calculated with 0.5% backmixing. The second case, a simple pulsed column model, has 35% backmixing of the aqueous phase with the organic phase, that is, aqueous-continuous operation. The backmixing of the dispersed organic phase is the same as that in the contactor, 0.5%. For this case, the sodium concentration in the last stage, stage 14, is many orders of magnitude higher than that for the base case. A full pulsed column model, the third case, has aqueous-continuous operation in the extraction (stages 1-5) and scrub (stages 6-7) sections, organic-continuous operation in the two strip sections (stages 8-14), a scrub column that is separate from the extraction column, and only 0.5% aqueous phase in the organic phase going from one column to the next. For this case, the sodium concentration profile is similar to that for the centrifugal contactor. Note that the number of stages (14) and the sodium distribution ratio (0.001) are the same in all three cases. Thus, the large changes in the concentration profile are a function of the backmixing, which varies with what equipment is used and how the equipment is assembled. The new SASSE worksheet, because it includes backmixing, can handle these differences easily.

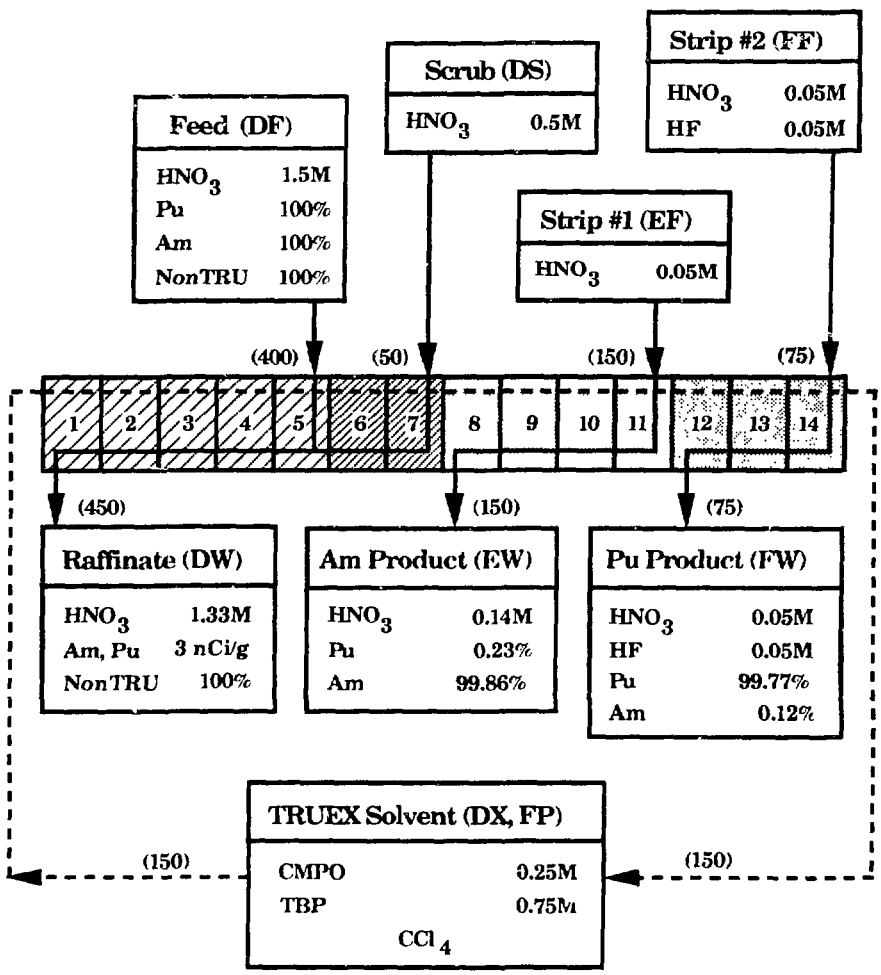

Fig. V-2. TRUEX Flowsheet for Comparison of Centrifugal Contactor and Pulsed Column Models

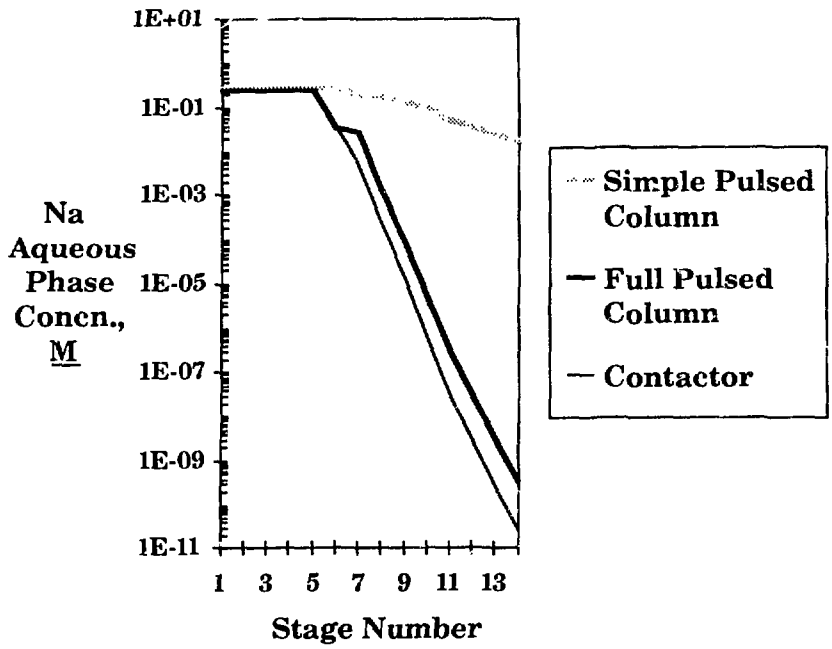

Fig. V-3. Effect of Backmixing on the Sodium Concentration Profile

c. Loading Effect Module

Version 1.1 of the GTM did not account for the effects of solvent loading by metal salts on species extraction. Because TRUEX is a waste treatment process, the effects of solvent loading will be small in most cases. However, when the concentrations of rare earth fission products are high, solvent loading by a combination of these species together with Fe, U, and TRU elements can lead to solvent loading effects. In these cases, the solvent is not loaded with only one species but with a combination of more than ten. Calculation of the solvent loading effect on the extraction of all components is straightforward but time consuming. We thus developed a mathematical algorithm for use in the GTM to reduce the computational time.

For every component given in Table V-2, the material balance for a single stage can be written equating the total amount of that component present initially in that stage, in the organic and aqueous phases, with the total amount distributed in both phases at steady state. From the material balance equations, we obtain N equations with 2N unknowns. Using the equilibrium constant for every component, we can relate the amount of that component present in the aqueous phase to that in the organic; this supplies another N equations. The ratio of organic-to-aqueous concentration (or distribution ratio) can be equated to the equilibrium constant multiplied by the concentration of free CMPO to the n'th power, where n depends on stoichiometry. Values for n are given in Table V-2. A material balance for CMPO provides one more unknown, the free CMPO concentration, and one more equation. Thus, we obtain 2N + 1 equations with 2N +1 unknowns from the material balance for each of the N components, the equilibrium constant for each of the N components, and the material balance for CMPO. The

Raphson algorithm. To reduce computational time, algebraic expressions were analytically derived for the Jacobian; also, all species that have the same exponential dependence on the extractant and similar distribution ratios were grouped as one "pseudocomponent" [Am, Pu(III), Cm, La, Ce, Pr, Nd, Pm, Sm, Eu, and Gd].

Table V-2. Exponential Dependence of the Extractant for Components Included in GTM Loading Effect Module

Component	Exponential Dependence
Americium	3
Plutonium III	3
Plutonium IV	2
Neptunium IV	2
Neptunium V	2
Uranium	2
Curium	3
Yttrium	3
Lanthanum	3
Cerium	3
Praseodymium	3
Neodymium	3
Promethium	3
Samarium	3
Europium	3
Gadolinium	3
Iron	3

We developed a new macro program to implement the numerical solution for the equations that we derived to account for solvent loading. The macro uses the aqueous and organic compositions for every component calculated by SASSE and the organic-to-aqueous flow rate to calculate the total initial amount present in a given stage. Also, distribution ratios for each component at the tracer level, in a given stage, are obtained from SASPE. This new macro calculates concentrations in each phase and new distribution ratios for every component based on loss of free CMPO. The new distribution ratios are then passed back to SASSE, which recalculates and passes concentrations of all components to SASPE. The SASPE recalculates new distribution ratios and passes them to the loading effect module. The loading effect module, in turn, calculates a new set of distribution ratio values. The iteration between SASSE, SASPE, and the loading effect module continues until the D values calculated by it in two consecutive iterations are constant to within 1%. The accuracy of this mathematical approach in calculating effects of solvent loading on distribution ratios is being tested in batch and centrifugal contactor experiments.

2. TRUEX Data-Base Generation

The objective of this effort is to collect extraction data, as well as aqueous solute and solvent thermodynamic activity data, to be used in GTM.

The data base, generated over the past four years from the literature and from our own laboratory measurements, contains information on the extraction behavior of all important feed components over a wide range of possible waste-stream and processing conditions, including solute composition, solvent composition, and temperature. Regarding solvent composition, some of our earlier work employed TCE as the diluent in the TRUEX solvent. Growing environmental, safety, and health concerns have militated against the use of chlorinated organic solvents; as a result, since 1989 our work has been directed exclusively to the use of either a normal paraffinic hydrocarbon C_{12}-C_{14} mixture (NPH) or n-dodecane (DD). Earlier work resulted in the collection of data on actinides (Am^{3+}, Cm^{3+}, Np^{4+}, Np^{5+}, Np^{6+}, Pu^{4+}, Th^{4+}, and U^{6+}); rare earth fission products (La, Ce, Pr, Nd, Pm, Sm, Eu, and Gd); other fission products (Y, Zr, Mo, Tc, Ru, Rh, and Pd); and important inert elements and species (Fe, Al, Mn, Ni, NO_3^-, F^-, HSO_4^-, $H_2PO_4^-$, and $C_2O_4^{2-}$). Over the past year, data have continued to be collected for a variety of the above-mentioned species by the TRUEX solvent under a expanded range of conditions of solute composition, solvent composition, and temperature (25 to 50°C). The need for this information results from our continuing efforts to test the model and increase its applicability to a wider range of process conditions and waste streams.

The composition of the TRUEX-NPH solvent has been optimized at 0.2 M CMPO and 1.4 M TBP diluted by either NPH or DD. (Dodecane is preferable to avoid third-phase formation at processing temperatures <30°C, while the NPH mixture has a higher flash point and is considerably less expensive.) Thus far, all the extraction-behavior models in the GTM are based on this composition; however, the next version of the GTM will allow the user to specify the concentrations of CMPO and TBP in the TRUEX-NPH solvent. Numerous data have, therefore, been collected to measure the effects of solvent composition on the extraction behavior of extractable species. Figures V-4 and V-5 exemplify these data. The effects of the aqueous HNO_3 concentration and the organic CMPO and TBP concentrations on the thorium distribution ratio are shown in Fig. V-4. The thorium distribution ratio is approximately proportional to $[HNO_3]^2$ and $[CMPO]^{2-3}$. The effect of TBP concentration at 1.4 and 2 M is experimentally indistinguishable. Figure V-5 shows the effect of the aqueous HNO_3 concentration and the organic TBP concentration on the extraction behavior of americium at constant (0.2 M) CMPO concentration. The data show that, at concentrations of TBP less than 1.4 M, D_{Am} is approximately proportional to $[TBP]^{-0.6}$.

In general, the distribution ratios for metal salts by CMPO and the TRUEX solvent are orders of magnitude higher than the ratio for TBP alone. However, for acidic compounds (e.g., HNO_3, $H_2C_2O_4$), extraction by TBP is an important factor in metal-salt extraction by the TRUEX solvent. Therefore, to model this extraction behavior, data must be collected for TBP alone. Figure V-6 is illustrative of the data collected. The figure shows the equilibrium concentrations of oxalic acid in the aqueous and organic phases for TBP dissolved in dodecane at two concentrations. The data in this figure fit curves based on the assumption that oxalic acid is extracted as the neutral molecule by CMPO and TBP, and its extraction by TBP alone can be modeled by the equilibrium

$$H_2C_2O_4 + 2\overline{TBP} \rightleftarrows \overline{H_2C_2O_4 \cdot (TBP)_2} \qquad (1)$$

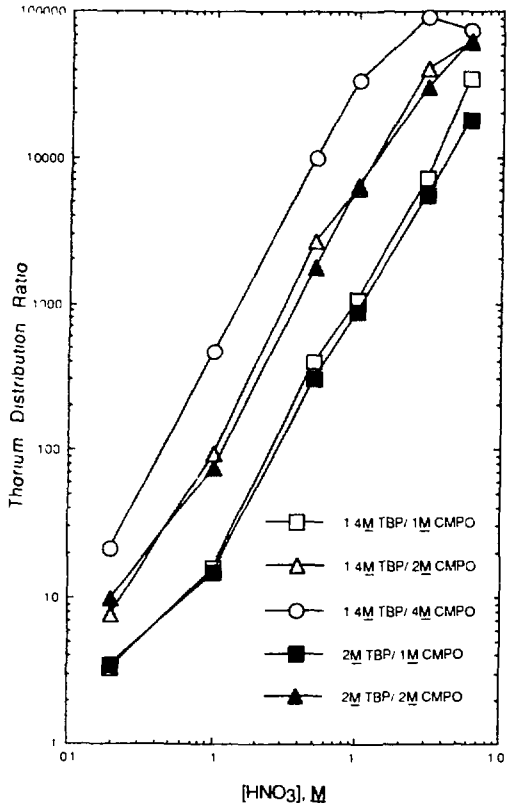

Fig. V-4.

Distribution Ratio of Th(IV) vs. Aqueous-Phase Nitric Acid Concentration and Organic-Phase Concentrations of CMPO and TBP. Dilvent is dodecane. All measurements at 25°C.

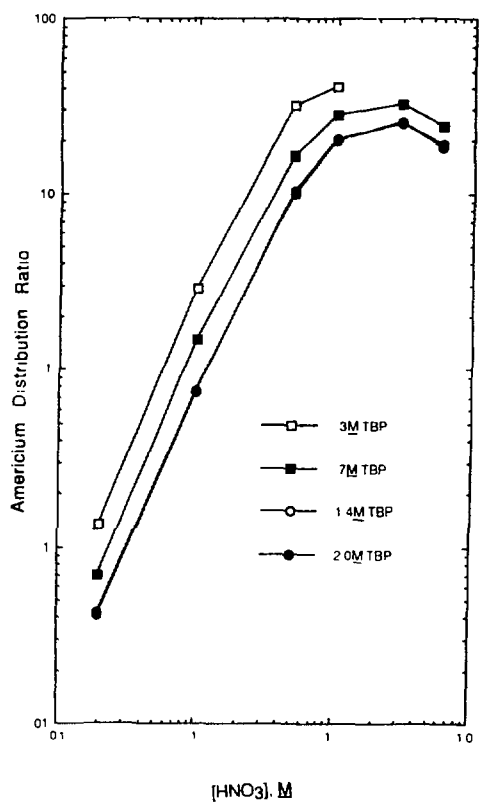

Fig. V-5.

Distribution Ratio of Am(III) vs. Aqueous-Phase Nitric Acid Concentration and Organic-Phase Concentration of TBP. Concentration of CMPO is 0.2M in dodecane. All measurements at 25°C.

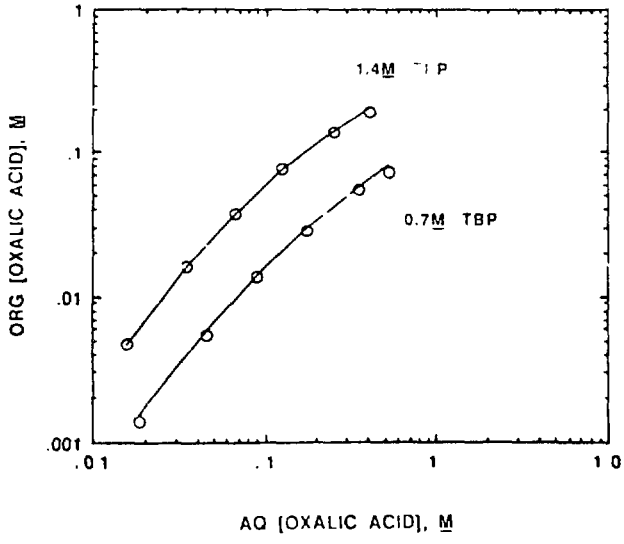

Fig. V-6.

Extraction Isotherms for Oxalic Acid between Water and TBP in Dodecane at 25°C

A more complete representation of this equilibrium would include activities for the aqueous species. In the GTM wherever possible, the various chemical equilibria underlying the extraction procedure have been cast in terms of thermodynamic activities of aqueous species. The literature has provided much information, but data on some species of great importance to GTM, for example Al^{3+} and $H_2C_2O_4$, are not available. We decided to obtain these data experimentally, and, after examining available experimental methods, chose the vapor phase osmometry technique. This technique measures the activity of the solvent in a solution, and so permits, after the appropriate thermodynamic calculations, the activity of the solute to be determined. Experimental work for $Al(NO_3)_3$ and $H_2C_2O_4$ in aqueous solution has been completed, and the results for $Al(NO_3)_3$ are depicted in Fig. V-7.

The collection of data for the GTM requires work beyond determining distribution ratio values or aqueous-phase thermodynamic activities. Typical of such work has been the development of an analytical method for determining rare earths with a commercially available spectrophotometer. The rare earth elements are a major component of many TRUEX feeds, and, since they are extracted by the TRUEX solvent, play a significant part in our modeling efforts. Accurate modeling requires accurate extraction data, and the present analysis method for determining rare earth elements, inductively coupled plasma/atomic absorption spectrometry (ICP/AES), is time consuming and associated with uncertainties that are undesirably large. The use of ultraviolet/visible/near infrared spectrophotometry is being investigated to address the need for a more expedient analysis method. A preliminary requirement is that accurate calibration standards must be prepared. However, meeting this requirement is complicated by the extensive hydrolysis of rare earth ions under all but the most acidic aqueous conditions. Painstaking preparative work has allowed us to surmount this problem. So far the spectrophotometric method shows promise to be more accurate than ICP/AES at neodymium concentrations comparable to those measured by ICP/AES.

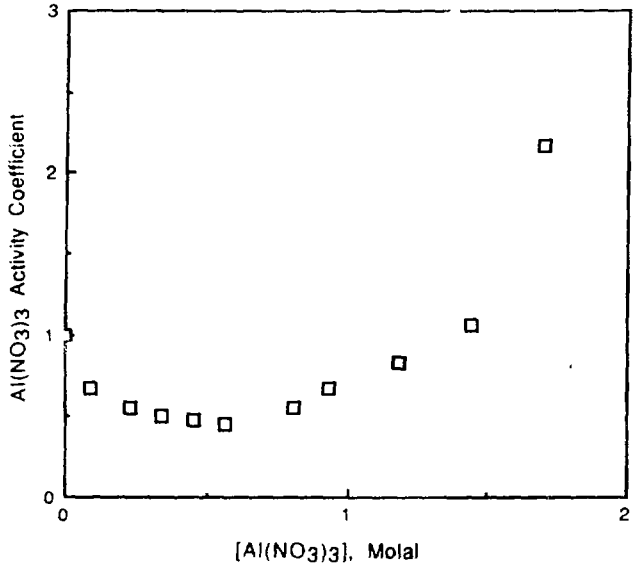

Fig. V-7.

Activity Coefficient of Aqueous Aluminum Nitrate as Function of Concentration

3. TRUEX Data-Base Development

The success of the GTM is dependent on underlying data that are sound, correct, and defensible. Further, the source of data must be easily traceable and auditable. Over the past several years, we have collected the data necessary to model the TRUEX process for high-level defense waste and other nitrate-based, TRU-containing waste (Sec. V.A.2). We have developed a computerized data base that collects all pertinent information in one location. The data base was designed using a Macintosh computer and the computer program Fourth Dimension (supplied by Acius, Inc., Cupertino, CA). The data base is intended to be useful to at least four customer types: program managers, individual experimenters who measure distribution ratios, modelers who develop the algorithms useful to the design of TRUEX flowsheets, and quality assurance auditors. The ability to rapidly identify categories of information in need of development is especially important to program managers and modelers. Fourth Dimension has a powerful hierarchical structure, extensive capabilities to provide a variety of report formats useful for the four customer types, and a variety of search capabilities. The ultimate utility of the data base is strongly dependent on its structural design. Incorporated into the structural design is the capability of producing text files of data sets that can be exported to external applications for graphical displays of the information.

The first version of the data base contains 337 data sets and 3511 individual measurements of distribution ratios for pertinent nuclides and major process reagents. Data entry is continuing. Future work includes the entry of distribution ratios obtained from the literature, followed by entry of activity coefficients.

4. Laboratory Verification Tests

Laboratory verification tests of the TRUEX process using centrifugal contactors are underway to investigate the extraction of actinides and other components from acidic waste

solutions. Objectives of these experiments are to (1) develop a better understanding of the TRUEX process chemistry, (2) test and verify process modifications, and (3) verify the species extraction behavior predictions and flowsheet calculations with the GTM. Four verification tests were completed this year, all with the TRUEX-NPH solvent.

Two of these verification tests were done to evaluate the use of interstage samplers. In previous verification tests, we have relied on samples collected from the centrifugal-contactor rotors at the end of the test (after shutdown) to measure the concentration profiles in the system. Results from the analysis of these samples have not always agreed with raffinate stream compositions. Therefore, we conducted a series of sampling tests using centrifugal contactors with 2-cm dia rotors. Two locations for sample collection during contactor operation were evaluated: (1) a 0.03-cm hole in the interstage lines on both the aqueous and organic side of the contactor and (2) the stage bottom drain valve. These tests verified that accurate profile samples can be generated by continuously collecting a low-flow sample (approximately 0.2 mL/min) from these locations. The disadvantage to collecting this type of sample is that it must be collected over a long period of time and the small hole in the interstage sampler is susceptible to plugging.

The other two verification tests were done in support of an effort to develop a TRUEX process that will convert analytical residue solutions generated from plutonium analysis at the New Brunswick Laboratory (NBL) into a nonTRU (i.e., low-level) waste. These wastes have been accumulating over the past year (approximately 150 L of solution containing 120 g plutonium) and contain varying concentrations of nitric, sulfuric, phosphoric, and hydrochloric acids, as well as U, Pu, Np, and Am. As a TRU waste, there does not appear to be a place to dispose of these solutions. If the TRU elements are reduced to less than 10 nCi/g, however, this waste can then be disposed of as low-level waste under existing regulations.

We developed the simplified flowsheet shown in Fig. V-8 for processing the plutonium-containing waste solutions. The TRUEX portion of the process will be demonstrated in a twenty-stage 4-cm centrifugal contactor installed in a glovebox. Two waste streams from the TRUEX process, the nonTRU waste stream and the solvent wash stream which contains the uranium, will not require further processing and will be sent for disposal to the Waste Management Operations of ANL's Plant Facilities and Services (PFS-WMO). The americium stream from the TRUEX process will be concentrated by evaporation, then reused in future laboratory experiments at CMT. The plutonium stream will be further processed by filtering the plutonium oxalate precipitate, then calcining the precipitate in an oven at 600°C. The filtrate will be evaporated to dryness and added to the plutonium oxalate for calcination. After calcination, the plutonium oxide will be converted to a metal and returned to the DOE complex.

The GTM is being used to design TRUEX process flowsheets of these waste solutions. The flowsheet developed to process the first batch of these waste solutions is shown in Fig. V-9. Two significant features of this flowsheet are worth special mention. First, the typical scrub feed stream is eliminated by combining the operation of the americium strip solution with the scrub solution. In stage 9, only a fraction of the aqueous phase is removed from the system (5%)--the rest carries down through the "scrub" section. This solution will act the same as a normal scrub solution, removing nitric acid from the organic phase. With this setup, the

americium concentration will build up in this section because >99% of the americium is stripped from the organic phase in stages 9 through 14, but only 5% of the americium is removed in stage 9. Concentrating americium in the effluent of this section will not be a radiation exposure problem because of the low americium concentrations in the feeds. Concentrating the americium stream by a factor of 100 keeps the americium product volume low.

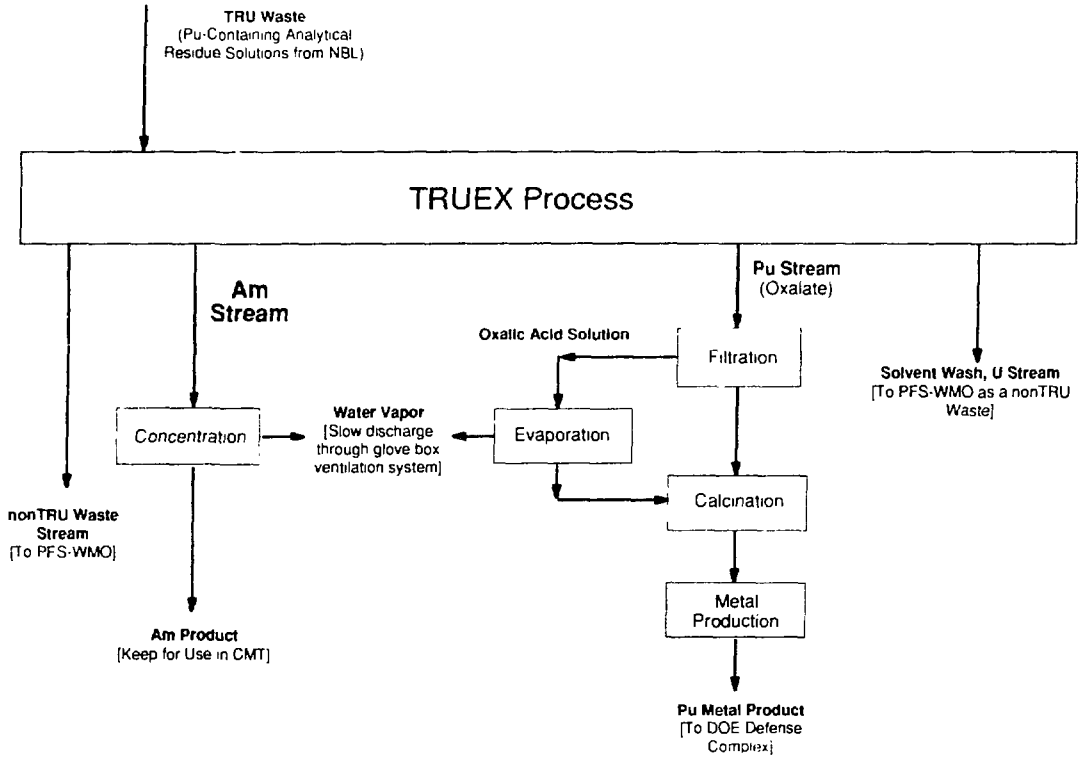

Fig. V-8. General Flowsheet for Processing Plutonium Waste Solutions of New Brunswick Laboratory

The second noteworthy feature of this flowsheet is the section with two separate plutonium strip solutions. Two feeds are necessary for this section because (1) the plutonium concentration is high enough in the solvent that plutonium oxalate will precipitate in the oxalate strip solution, and (2) distribution ratios of oxalic acid will be greater than one in stages where the plutonium concentration is low. If a single feed were used, most of the oxalate needed would be lost to the solvent leaving the section in stage 18, and very little would be available in the first plutonium-strip stage. This would essentially provide only one effective strip stage not four. Precipitation of $Pu(C_2O_4)_2$ would also likely occur completely in stage 18, causing the precipitate to pass through all four strip stages before exiting with the effluent at stage 15. This would increase the potential for the precipitate to not exit the contactor but collect in the rotors. With oxalic acid solution added directly into stage 15, all of the oxalic acid will be useful in stripping and precipitating plutonium from the organic phase. The amount of oxalic acid added directly to stage 15 will be adjusted to that needed for stoichiometrically complexing 100% of the plutonium. An excess of oxalic acid added here would strip uranium from the organic phase.

The feed to stage 18 has enough oxalic acid to keep D values for oxalate low and also has enough nitric acid to keep D values for uranium high.

During the past year, filtration, evaporation, and calcination equipment were tested with nonradioactive solution and were found to be satisfactory. Also, an 11-stage contactor was used to verify the operation of the scrub/strip section of the flowsheet. The processing of the first batch of plutonium-containing solutions was accomplished with the TRU content of the feed diminished by a factor of 22,000 in the raffinate. The TRU content of the waste was 1.8 nCi/mL, which compares favorably with the GTM-calculated volume of 1.0 nCi/mL. Our verification testing will demonstrate the applicability of this process to the much larger volumes of similar wastes being generated at Rocky Flats Plant, Los Alamos National Laboratory, and the Hanford site and will act as a basis for considering this process as a future waste treatment process at ANL and NBL.

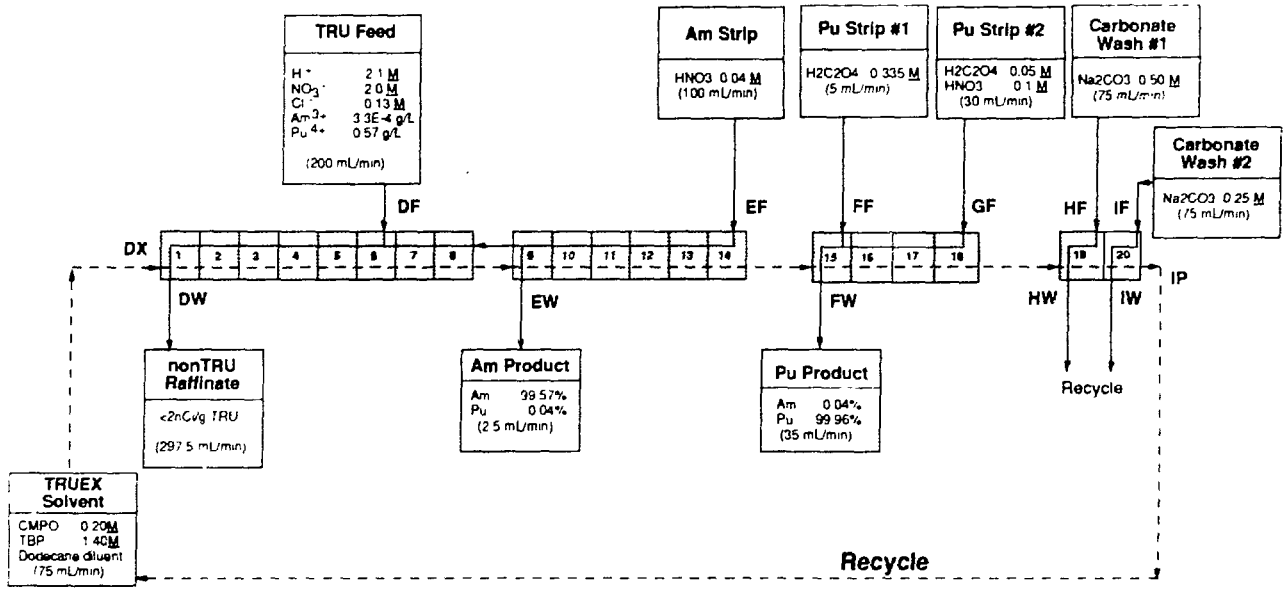

Fig. V-9. The TRUEX Flowsheet Developed for Processing Waste Solutions of New Brunswick Laboratory

5. TRUEX-NPH Solvent Degradation

The effects of hydrolysis and radiolysis on the extraction of TRUEX-NPH solvent were previously studied in laboratory experiments.[3,4] Our work in this period was concentrated on interpreting the results from these experiments.

---

[3]M. J. Steindler et al., *Chemical Technology Division Annual Technical Report, 1988*, Argonne National Laboratory Report ANL-89/15, pp. 71-74 (1989).

[4]M. J. Steindler et al., *Chemical Technology Division Annual Technical Report, 1989*, Argonne National Laboratory Report ANL-90/11, pp. 70-72 (1990).

In our earlier experiments, samples of hydrolyzed solvent were prepared by exposing solvent to aqueous solutions at 50, 70, and 95°C for times up to 800 h. The solution set included 0.25, 2.5, and 6.0 M HNO_3; the set also included two solutions simulating a Hanford waste stream containing a mixture of metal ions and nitric acid concentrations of 1.6 and 2.6 M. Radiolyzed solvent was prepared by exposing solvent samples to gamma radiation while in contact with aqueous solutions of the same composition but at a constant temperature of 50°C. Measurements of distribution of americium (D_{Am}) between degraded solvent and aqueous HNO_3 were used as an indicator of the extent of solvent degradation. Values of D_{Am} were measured at three nitric acid concentrations: 0.01, 0.05, and 2.0 M. At the highest acid concentration, distributions were apparently controlled by CMPO. Therefore, values of D_{Am} obtained with 2.0 M acid were used to follow CMPO concentration as a function of solvent degradation conditions.

The variation of D_{Am} for 2.0 M acid with absorbed dose was described in last year's report.[4] In the past year, we determined that D_{Am} (for 2 M acid) obtained with solvent degraded by hydrolysis is represented by the following relationship:

$$D_{Am} = D_{Am_o} e^{-nAe^{-E/RT}\{H\}t} \qquad (2)$$

where n is the power to which CMPO concentration depends on D_{Am}, E is the activation energy, A is a constant, R is the gas constant, T is the temperature, {H} is the hydrogen ion activity, and t is the irradiation time. In this equation, $A = 1/n\ e^{34.21}$ L mol^{-1} h^{-1}, $E = 27.3 \times 10^3$ cal mol^{-1} (114 kJ mol^{-1}), and $D_{Am_o} = 30.7$ for TRUEX-NPH solvent. Figure V-10 illustrates the fair agreement between experimental values of D_{Am} and values calculated by Eq. 2 (assuming n = 3) for TRUEX-NPH.

We also used the radiolysis and hydrolysis data to obtain expressions for (1) CMPO concentration in the degraded solvent and (2) the D_{Am} with the degraded solvent as a function of the number of process stages and other parameters used in describing radiolysis and hydrolysis. Under typical process parameters, our calculations with these expressions indicated that, in one cycle (extraction, scrubbing, stripping), the value of D_{Am} for 0.01 M acid increases about 30%, whereas the value of D_{Am} for 0.05 M acid increases about 6%. Thus, as expected, D_{Am} for 0.05 M acid is a less sensitive indicator of the acidic extractants formed in CMPO decomposition. Our calculated value for the fraction of CMPO decomposed during one year of processing (100 cycles) was quite low (8.6×10^{-4}).

The effectiveness of removing the products of CMPO degradation from TRUEX-NPH solvent by washing with aqueous sodium carbonate was tested on solvent that had been exposed to radiolysis or hydrolysis. When the solvent is equilibrated with 0.01 and 0.05 M HNO_3, D_{Am} generally increases with the extent of degradation, presumably because of the presence of acidic degradation products, which are powerful extractants. Washing the degraded solvent decreases the D_{Am} values. Values of D_{Am} for 0.01 M acid, being sensitive indicators of acidic extractants, are lowered by carbonate washing, but are still greater than the corresponding D_{Am} value for non-degraded solvent. This indicates that carbonate washing is generally not 100% effective.

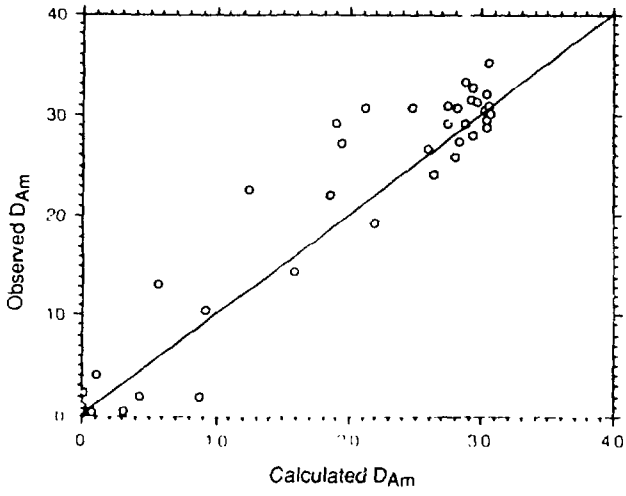

Fig. V-10.

Observed and Calculated Values for D_{Am} Obtained with Solvent Degraded by Hydrolysis at 50-95°C and 2.0 M HNO_3. The points are determined by the number pairs (D_{Am} observed, D_{Am} calculated). The line is determined by the condition (D_{Am} observed = D_{Am} calculated).

6. Monitoring and Control of TRUEX Processes

A TRUEX flowsheet designed for a specific application will be optimized for obtaining processing goals and "robustness." A robust flowsheet is one that will continue to meet processing goals (e.g., generate an extraction raffinate with a TRU concentration of less than 10 nCi/mL, loss of less than 1% plutonium to the americium-waste effluent, and ≤ 0.001% of the TRU in the solvent wash effluent) with wide variation in feed composition and rate. There are, however, limits to how robust a process can be, and beyond these limits, possessing the ability to monitor and control the process becomes very important. Examples of parameters to be monitored on-line include feed, effluent, and interstage compositions by use of pH, conductivity, spectrometry, density, and radioactivity measurements and influent flow rates. Control in the case of a detected problem would likely be limited to shutting down the process and feed flow. An important factor in selecting monitoring sensors for critical process variables and implementing control strategies is the inherent characteristics of multistage centrifugal contactors. The selection and placement of sensors will depend on both the static and dynamic behavior of the separation process with these contactors.

The purpose of our current efforts is to determine the instruments required for monitoring and controlling the TRUEX processes and to assess the interrelationship among the species concentrations, extraction behavior, and process variables. An eventual goal of these efforts is to develop a knowledge-based (expert) system which will be used to (1) analyze potential failure modes, (2) study propagation of failure modes and their consequences, (3) select instruments for detecting fault-initiating events and their optimum placement and required response times, and (4) control the operations of an optimized feed-specific TRUEX process.

We carried out a literature review and modeling efforts using GTM (Version 2.0) to determine the monitoring and control requirements for the TRUEX solvent extraction process. Our efforts indicated that conventional instruments are available to detect, monitor, and control basic process parameters (e.g., mass flow rate, liquid levels, fluid transport), but special analytical techniques will have to be developed for on-line monitoring and control of TRU

elements, especially at low concentrations. We also completed sensitivity analyses of the key process variables (e.g., the aqueous and organic flow rates, americium composition, feed composition, and the number of contactor stages) to assess their impact on TRUEX process operation. The results of these analyses are expected to provide a basis for selection of monitoring instruments and eventual implementation of control strategies. Since a number of choices for instruments are available for monitoring many of the physical parameters, we will select a set of instruments based on their basic operating principle, stability in a radiation and corrosive environment, physical size, accuracy, cost, signal output, and availability (off-the-shelf vs. special orders). The problems related to instrument maintainability and adaptability will be studied in the future.

Based on the SASSE model, we have derived the equations that govern the dynamic behavior of a TRUEX process. Once a flowsheet is specified, the equations can be used to describe the transient stagewise response of a perturbation in the process. With this dynamic model, important knowledge, such as how fast (process time delay) each stage of the system moves to a steady-state condition, can be obtained.

The next step in this effort will be selecting and purchasing an expert-system shell and fitting it with appropriate algorithms, selecting and purchasing monitoring and control equipment, and designing and demonstrating a pilot-plant operation at CMT.

B. *Centrifugal Contactor Development*

We have been modifying the basic design of the ANL centrifugal contactor as necessary to adapt it for specific solvent extraction processes. A key feature in these design efforts is the use of computational models for (1) the flow of the organic and aqueous phases through the contactor and (2) the vibrational parameters of the spinning motor/rotor combination. This year, these hydraulic and vibrational models were used to guide contactor development in several new areas, including (1) increased throughput for a given contactor diameter, (2) the use of new materials of construction (such as Kynar) for the contactor rotor, and (3) contactor operation at elevated temperatures. Other work focused on using the contactor as a concentrating device.

We have been working with Westinghouse Hanford Co. on a prototype 10-cm contactor for the proposed TRUEX facility at its Plutonium Finishing Plant. Using our vibrational and hydraulic models, we developed a new contactor design that should double process throughput without increasing the rotor diameter. Holding the rotor diameter at 10 cm makes the unit safe, owing to its geometry, with respect to nuclear criticality. Building on this design, we are now determining the highest possible throughput for a given contactor diameter. For this high-throughput contactor, we are combining our current models with new design concepts that will be evaluated experimentally. Our goal is to determine the vibrational and hydraulic parameters that limit contactor throughput for a given rotor diameter. The results will provide a basis for designing high-throughput contactors that have built-in safety with respect to nuclear criticality.

Work on a new contactor, a pyrocontactor that will operate at high temperatures (500 to 800°C), is continuing. The bulk of the work, the design of a high-temperature, controlled-atmosphere facility with the various feed and raffinate tanks, is now part of the pyroprocessing

work within the IFR program (Sec. VI.D.2). We are supporting this effort by providing hydraulic and vibrational analyses of the contactor design.

In a joint effort with Los Alamos National Laboratory (LANL), we are developing a contactor that will be used to remove Pu and U from chloride salt wastes and yet be resistant to concentrated HCl. The material of choice for this contactor is Kynar, a material that presents vibrational problems because it is not nearly as stiff as 304 stainless steel or Hastelloy C-22. Using our vibrational and hydraulic models, we have been evaluating contactors designed and fabricated by outside vendors. In addition, we are designing a new Argonne-type contactor that will be resistant to HCl and not have vibrational problems. The various designs will be tested at LANL.

Our final contactor activity was to explore the use of the centrifugal contactor as a concentrating device. This work builds on an impressive feature of centrifugal contactors when compared with other solvent-extraction equipment, that is, their ability to operate at very high and very low organic-to-aqueous (O/A) flow ratios. This work involved both theoretical and experimental efforts. In the theoretical part, we evaluated typical concentrator flowsheets, such as the one shown in Fig. V-11. In the experimental part, we demonstrated that, at extremely high (33) and low (0.01) O/A flow ratios, the normally high extraction efficiency (E) of centrifugal contactors is still fairly high (see Fig. V-12) and can be correlated with the organic-to-aqueous flow ratio (R) as follows:

$$E = 0.986(1 - 0.08 \mid \log R \mid) \tag{3}$$

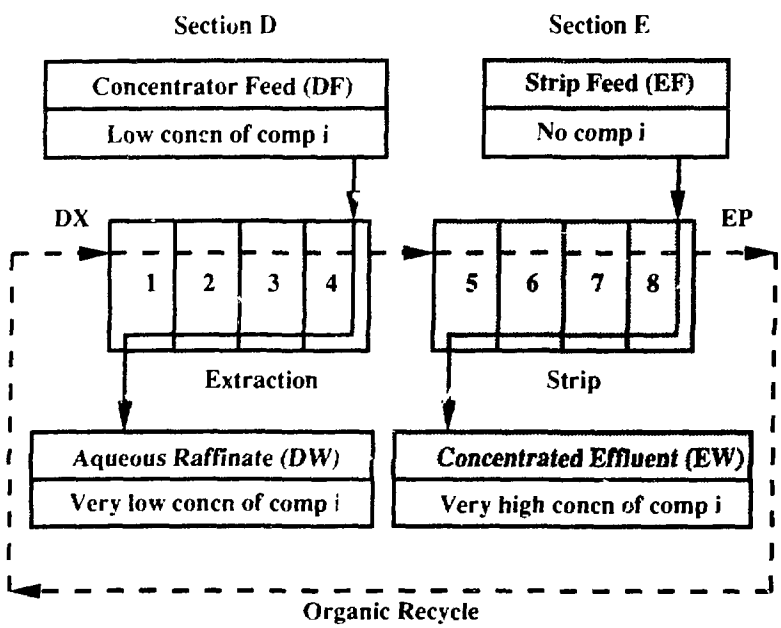

Fig. V-11. Typical Flowsheet for Concentrator Operation

Since this is the case, contactors can be used to concentrate (by factors of 10 to 1000 or more) those metal ions that have a high D value during extraction and a low D value during stripping. For such metal ions, one should be able to reduce, and in some cases eliminate, the need for downstream processing of one or more effluent streams.

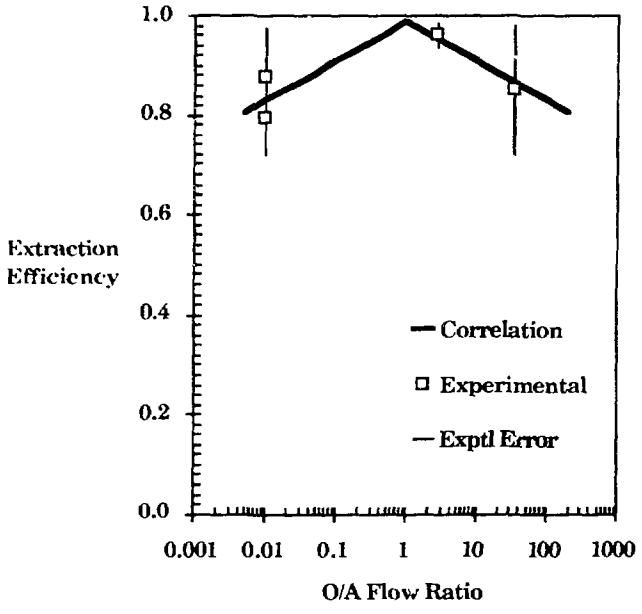

Fig. V-12.

Effect of O/A Flow Ratio on Extraction Efficiency in a Centrifugal Contactor

C. *Aqueous Biphase Process for Actinide Recovery from Solid Wastes*

The purpose of this project is to explore the possible application of aqueous biphase extraction to the treatment of solid radioactive wastes. Wet grinding of the solids to a particle size of 1 μm or less followed by aqueous biphase extraction will produce (1) a solid waste that would meet economic discard limits and (2) an actinide-bearing concentrate that would more effectively integrate with existing chemical recovery processes. The biphase extraction system will achieve high levels of separation and recovery in a completely aqueous system, utilizing reagents that are nontoxic and easily biodegradable.

In aqueous biphase extraction, colloid-size particles selectively partition between two immiscible aqueous phases. These aqueous/aqueous systems form spontaneously from mixtures of polymer and inorganic salt solutions. For example, combining equal volumes of a 15 wt % solution of sodium sulfate and a 15 wt % solution of polyethylene glycol (PEG) produces a turbid mixture which will separate after a few minutes, with the sodium sulfate concentrated in the bottom layer and the polymer concentrated in the top layer. Particles suspended in such a system will migrate to one aqueous phase or the other, depending on a complex balancing of particle interactions with the surrounding solvent through hydrogen bonding, hydrophobic bonding, etc. Process selectivity can be enhanced by system modification with surfactants containing the appropriate functional groups. Aqueous biphase extraction processes could be used in place of other techniques, such as oil flotation and conventional solvent extraction with an oil/water system. This would eliminate the need for costly petroleum-based diluents, which may generate concern as a source of pollution or a potential fire hazard. The water-soluble

polymers that can be used in biphase formation are inexpensive, nontoxic, and biodegradable. Another attractive feature of the aqueous/aqueous system is that extractions can be carried out using conventional contacting equipment, such as mixer/settlers, pulsed columns, and centrifugal contactors.

A number of DOE waste streams would be good candidates for treatment by aqueous biphase extraction processes. Some examples of specific waste streams involving particulates are pyrochemical wastes such as sands, slag, and crucible residues from the Savannah River Site, and incinerator ash, ceramic crucibles, and chloride salts from Rocky Flats Plant. These residues are heterogeneous materials in which the plutonium is distributed as discrete grains within a larger particle matrix (see Fig. V-13). Ultrafine grinding of these residues to an average particle size of about 1 μm can be used to liberate the plutonium from the particle matrix and thereby provide an opportunity to produce a plutonium concentrate in a significantly reduced volume.

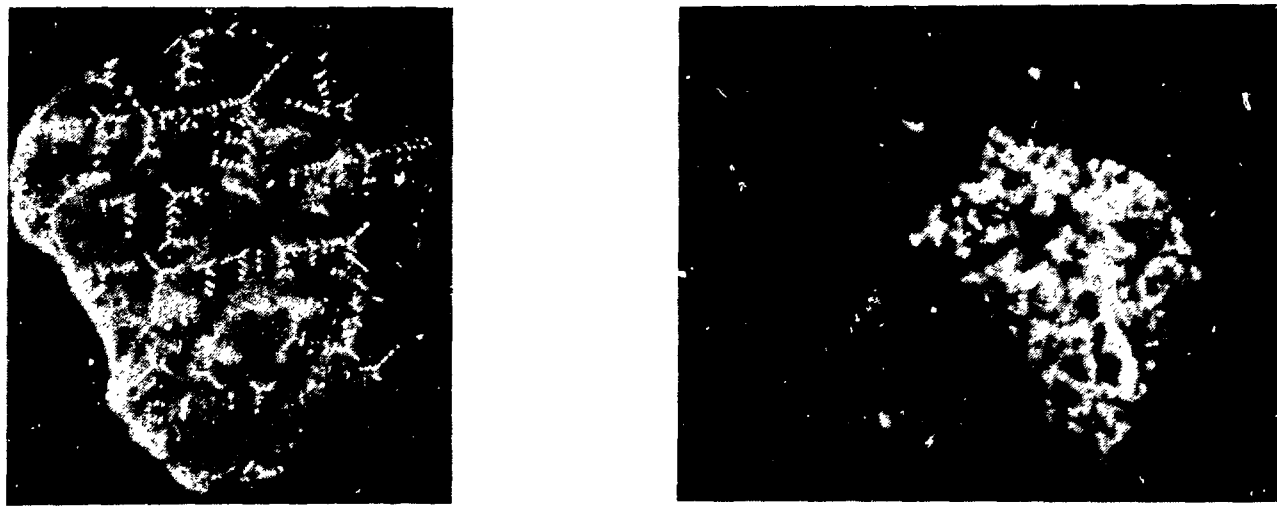

(a) (b)

Fig. V-13. Photomicrographs Showing Plutonium Grains (Bright Spots) in (a) Crushed Ceramic Crucible and (b) Ash Heel Particle in a Matrix of Metal Oxides and SiO_2

Preliminary work showed that metal oxides such as hematite (Fe_2O_3) and rutile (TiO_2) can be essentially completely separated from quartz (SiO_2) in a single stage by aqueous biphase extraction. The biphase system contained 15% PEG/ 7.5% Na_2SO_4. A feed particle size of about 1 μm was obtained by wet grinding in a planetary ball mill. During biphase extraction, >99.99% of the metal oxide particles reported to the bottom (Na_2SO_4) phase, and slightly greater than 99.99% of the quartz particles reported to the top (PEG) phase. This partitioning behavior was also achieved when both types of particles were added together to the aqueous biphase system, giving extremely large separation factors between the metal oxides and quartz.

Aqueous biphase separations depend upon differences in the surface properties of particles and not on bulk phase properties, like density. Consequently, those factors that influence surface properties can be used to control the partitioning of particles in an aqueous/aqueous system. Many of the same chemical reagents used in flotation to promote or suppress particle attachment at the air/water interface can be used in aqueous biphase systems for promoting separations between metal oxides, phosphates, carbonates, silicates, sulfides, etc.

We carried out partitioning studies of aged plutonium polymer in an effort to evaluate its applicability as a model system for predicting the partitioning behavior of plutonium-containing residues. If feasible, this would greatly simplify and speed the systematic study of partitioning behavior and reduce the amount of waste generated. The plutonium polymer studies might also lead to a better understanding of the behavior of hydrolyzed metal polymers in conventional oil/water solvent extraction systems. In addition, the potential application of aqueous biphasic extraction for separating plutonium polymer is of interest, since processing aqueous wastes containing this plutonium form is not currently possible by conventional solvent extraction or ion exchange.

Distribution ratios of plutonium polymer were measured for a number of PEG/Na_2SO_4 biphase systems containing various water soluble surfactants and metal complexants at concentrations of 0.01 and 0.1 wt %. Of the reagents examined, humic acid had the most pronounced influence on the partitioning behavior of the plutonium polymer. The distribution ratios of the plutonium polymer increased from 0.001, in the absence of humic acid, to 2.2 for a PEG/Na_2SO_4 system containing 0.01 wt % humic acid.

In almost every case, poor plutonium recoveries occurred when a phase transfer agent was added to the aqueous biphase system. With the addition of Aerosol OT, however, unaccounted plutonium was, on closer examination, found to be adsorbed at the liquid/liquid interface. This finding implies that the surfactant completely prevented the plutonium polymer from adsorbing onto the test tube walls. Aged plutonium polymer is notorious for adsorbing onto all kinds of surfaces (e.g., glass, metal, paper, cotton). This tendency makes it very difficult to process aqueous solutions containing polymerized plutonium.

Reports[5,6] in the literature suggest that this adsorption phenomenon is due to electrostatic interactions. Aqueous biphase partitioning in the PEG/Na_2SO_4 system, however, indicates that the adsorption mechanism is somewhat more complicated. For instance, during the extraction of aged plutonium polymer in the presence of colloidal SiO_2, >99.99% of the quartz reported to the top (PEG) phase, while the plutonium polymer remained in the bottom (Na_2SO_4) phase with a partition coefficient of 0.009. It is surprising that the plutonium polymer was not carried to the top phase by the colloidal SiO_2 because of its large surface area.

In future studies, we will correlate the partitioning behavior of the plutonium polymer with that of ultra-fine PuO_2 particles as a means of validating this model system.

---

[5]D. W. Ockenden and G. A. Welch, J. Chem. Soc., p. 3358 (1956).

[6]V. I. Grebenshchikova and Yu. P. Davydov, Radiochemistry (USSR) **3**, 167 (1961).

D. *Decontamination of Groundwaters*

We are evaluating a process that uses membrane-assisted solvent extraction (MASX) with membrane-assisted distillation stripping (MADS) for cleanup of contaminated groundwater and process streams. The contaminants of interest are volatile organic compounds (VOCs). We will compare this process with conventional remediation procedures, such as air stripping combined with activated carbon adsorption.

We developed the conceptual MASX/MADS process illustrated in Fig. V-14. In this process, contaminated groundwater enters the extraction unit and is contacted with a nontoxic, nonvolatile natural-oil solvent. The two liquid phases in the extraction unit are separated by microporous hollow fiber membranes. The membranes create a large surface area for mass transfer in the extraction unit. The contaminants are extracted from the groundwater into an oil phase. Groundwater exits the extraction unit with contaminants removed to levels as good as current drinking water standards. The oil phase is then heated and fed to a distillation stripping unit, which may be operated under vacuum. In the stripping unit, the VOCs are removed from the oil phase. The contaminants are then recovered in a cold trap condenser. The regenerated oil solvent is cooled and recycled back to the extraction module. Some type of energy recovery system will be used to recover the heat of the regenerated oil phase.

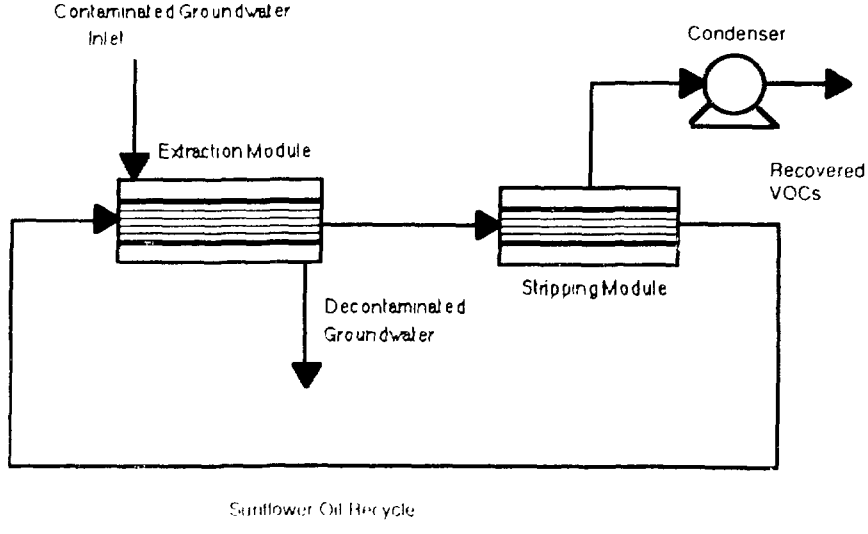

Fig. V-14. Flow Diagram of Conceptual MASX/MADS Process

Zander et al.[7] demonstrated, on a laboratory scale, the membrane-assisted solvent extraction of dilute VOCs from water using sunflower oil. The regeneration of the solvent and recovery of the VOCs by the MADS system have not yet been demonstrated. Work in this area of solvent regeneration is now in progress; parameters for operating this system have been determined from conceptual material and energy balances. The actual operating conditions of the stripping module will be determined after further thermodynamic data are obtained.

---

[7]A. K. Zander et al., J. Environ. Eng. **115**(4), 768 (1989).

VI. INTEGRAL FAST REACTOR PYROCHEMICAL PROCESS

The Integral Fast Reactor (IFR) is an advanced reactor concept proposed by, and under development at, ANL. Its distinguishing features are that it is a sodium-cooled, pool-type reactor (all major components of the primary system, reactor core, pumps, and heat exchangers are in a large sodium-filled pot); it employs a metallic fuel (an alloy of U, Pu, and Zr clad with a stainless steel-type alloy); and it has an integral fuel cycle (discharged core and blanket materials are processed and refabricated in an on-site facility). The advantages of this concept are (1) an exceptionally high degree of passive safety, resulting from use of a metallic fuel with a sodium coolant, (2) competitive economics, resulting from low costs for reactor construction and fuel recycle, and (3) low volume of radioactive waste relative to other fuel-cycle concepts.

The CMT Division has the responsibility for developing the on-site process for recovering plutonium and uranium from the core and blanket fuel, removing fission products from the recycled fuel, and incorporating them into suitable waste forms for disposal. To accomplish this, major efforts are directed toward flowsheet development for the electrorefining process, laboratory experiments on process chemistry, engineering-scale demonstration of the process, and studies of IFR waste treatment and management. The processes developed in this effort will be demonstrated in the Fuel Cycle Facility (FCF) for the Experimental Breeder Reactor-II (EBR-II) in Idaho. For this demonstration, reprocessed fuel will be used to refuel EBR-II for continued operation and to complete the fuel cycle.

A. *Process Flowsheet and Chemistry Studies*

The IFR pyrochemical process flowsheet has the necessary flexibility for providing the desired products (essentially pure uranium and a U-Pu mixture) from all IFR spent-fuel compositions while generating a minimum volume of waste that has very low transuranic (TRU) element content. The major focus of flowsheet refinement is examining the operational and safety issues associated with the FCF demonstration.

In the IFR pyrochemical process, spent fuel in its stainless-steel cladding is chopped into approximately quarter-inch lengths and placed in a basket that is introduced into molten salt at 500°C in an electrorefining vessel. The basket is connected to a dc power supply and made anodic; nearly pure uranium is removed from the spent fuel by electrotransport to solid cathodes, then the plutonium and any remaining uranium in the feedstock are electrotransported to liquid cadmium cathodes. More than 99.9% of the actinides are removed from the cladding hulls, and noble metal fission products either remain in the basket or fall as particulate to the bottom of the electrorefiner. The alkali and alkaline earth metals in the spent fuel are oxidized and remain in the electrorefiner salt, as do most of the rare-earth fission products.

As reported last year,[1] we have developed a computer code, PYRO, that accurately predicts the distribution of the elements in the electrorefiner during the individual operations that

---

[1]M. J. Steindler et al., *Chemical Technology Division, Annual Technical Report, 1989*, Argonne National Laboratory Report ANL-90/11, p. 99 (1990).

make up the pyrochemical process. We used the newest modifications of the PYRO code, along with various waste and feedstock compositions, to study fuel and waste processing strategies. The results indicated that fuel processing can be easily adapted to the various sorts of feedstocks that are expected, provided only that the results obtained in our earlier experiments hold up in the actual equipment with spent fuel as feed.

Where cadmium is used in the electrorefining process (cadmium cathodes), as well as salt extraction and stripping, the critical issue for product and waste composition is the distribution of rare earths and actinides between cadmium and the molten salt. We have acquired sufficient basic data and practical experience to assure that the product compositions will be satisfactory, and that adequate separations can be achieved in the lanthanide removal process. However, we are undertaking supporting chemistry studies to increase the precision with which we can calculate the distribution of the lanthanides and actinides between salt and cadmium and to test or eliminate the simplifications and assumptions used in our earlier quantitative flowsheet calculations.

As part of the supporting chemistry studies, we are measuring the separation factor for pairs of the rare earth elements up to atomic number 64 (gadolinium) and for neodymium vs. plutonium. These separation factors are being determined by measuring the distribution of these elements between salt (LiCl-KCl eutectic) and metal (cadmium) phases as a function of electrorefiner operating conditions at 500°C. We are also measuring activities and activity coefficients by electrochemical means for the most common rare earth elements. No major process changes have resulted from replacing our previous assumptions and approximations with experimental data (agreement with existing estimates was usually quite good). Detailed predictions of product compositions with respect to the behavior of the individual rare earth elements are expected to improve as more experimental data become available.

There were some unexpected findings, however. Yttrium was much more readily oxidized than expected; a provisional value for the separation factor between yttrium and lanthanum is approximately 30. Europium was so easily oxidized that it was closer in behavior to alkaline earths than rare earths. Also, it was expected to show a mixture of $EuCl_3$ and $EuCl_2$, at least under highly oxidizing conditions; we found only $EuCl_2$, even in the presence of excess $CdCl_2$.

We also found that interactions occurred among the rare-earth/cadmium intermetallic compounds. Usually, rare earth concentrations in saturated cadmium solution were half or less of the saturation level in binary rare-earth/cadmium systems. We believe that solid solutions among the intermetallic compounds are forming, and we are basing our current calculations on that assumption. Until a widely applicable description of the precipitating solid composition is available, element distributions based on unsaturated cadmium solutions should not be used where rare-earth-containing solids exist; order-of-magnitude errors are possible.

In support of safety analyses, we are investigating the affinity of the IFR electrolyte for water under hypothetical accident conditions. For these studies, water-salt samples having various compositions are equilibrated in conditions of constant temperature and humidity until they reach an unchanging composition. Samples having excess water evolve water, while salt-rich samples absorb water until all samples reach this constant composition. The boundary

between water-absorbing and water-evolving mixtures of salt and water is then determined as a function of temperature and humidity. This information is being used to evaluate accident scenarios for danger of criticality.

Figure VI-1 shows the unchanging composition derived as a function of sample temperature and humidity (indicated by humidifier temperatures). This figure shows the overall water composition that would be reached (from the salt-rich side) after a long time at various electrorefiner temperatures and absolute atmospheric humidities following a hypothetical accident. The conditions are conservative in that they correspond to low electrorefiner temperatures, unusually high humidities, and long times at those high humidities when compared to the expected electrorefiner conditions and the climate of the FCF site. Nonetheless, they show that accident-induced criticalities due to water absorption are unlikely. This work has been completed except for testing a few more conditions of temperature and humidity.

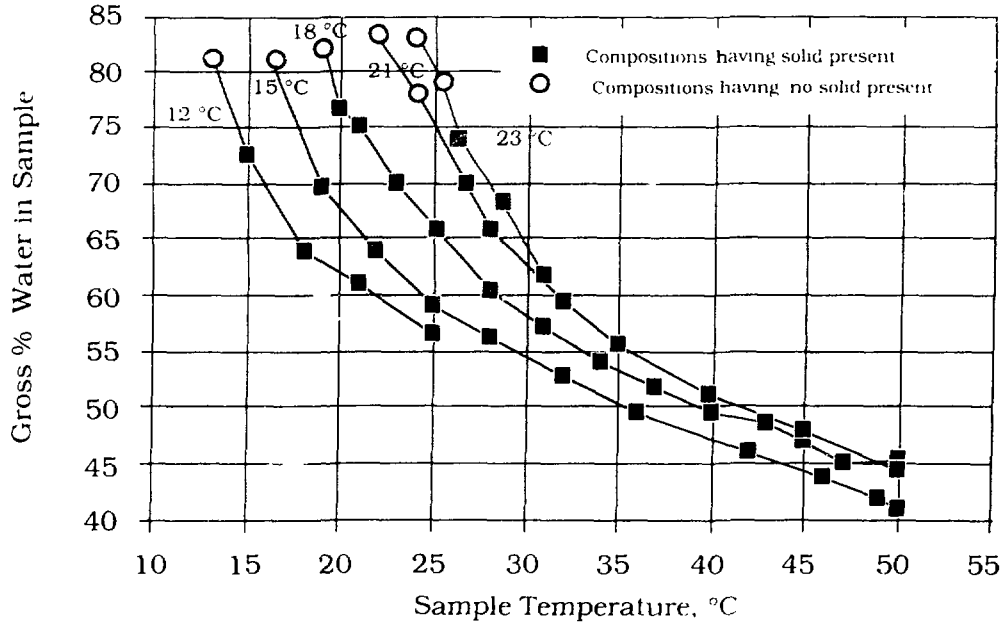

Fig. VI-1. Unchanging Salt-Water Compositions as Function of Sample Temperature and Humidifier Temperature (indicated at top of each curve)

B. *Process Development Studies*

The process development studies include experiments to determine the effect of impurities in the high-purity argon atmosphere on the plutonium behavior in the IFR electrorefiner, post-test examination of a laboratory-scale electrorefiner crucible to determine any life-limiting mechanisms, and experiments to study zirconium behavior in an electrorefiner.

1. Salt/Atmospheric Reactions

The IFR pyroprocess operations are normally carried out in a high-purity argon atmosphere (<10 ppm oxygen, <10 ppm water). It is of interest to know the plutonium behavior in the electrorefiner in the event that the argon gas purity were to be compromised in a hypothetical accident. We completed two tests in which salt, approximating that used in processing IFR fuel, was placed in an MgO crucible and exposed to varying levels of H_2O and O_2 at 500°C. The tests were conducted in a small tube furnace, utilizing once-through air (21°C dew point) that was exhausted through high-efficiency particulate air filters. The plutonium-containing salt for these experiments was obtained from our laboratory-scale electrorefiner.

In the first test, a diaphragm pump was used to introduce glovebox air into the furnace. The air exited the furnace through an outlet tube. The air flow rate was sufficient to replace the air volume every minute in the space over the molten salt. In the second test, a gas consisting of 100 ppm O_2 and 100 ppm H_2O in argon was fed to the furnace.

In both tests, the UCl_3 was rapidly oxidized from the salt. Since the crucible material was MgO, a thermodynamic potential for the reaction $(\text{uranium chloride})_{salt} + (MgO)_{solid} = (\text{magnesium chloride})_{salt} + (UO_2)_{solid}$ exists in this system. Therefore, a third test was run to determine if this reaction, rather than reaction with air in the cover gas, was responsible for the rapid loss of UCl_3 from the salt solution. In this test, the salt was added to two steel crucibles, one of which contained MgO crucible fragments.

Figure VI-2 shows the plutonium analytical data for tests I and II, and Fig. VI-3 the uranium data for test I (a similar plot was obtained with the uranium data for test II and is not included here). Figure VI-4 shows the uranium data for test III in the presence and absence of MgO. The data for the rare earth concentration in test II are given in Fig. VI-5.

The data in these figures show that the uranium concentration decreased much more rapidly than the Pu, Ce, Nd, Sm, and Y concentrations. As indicated by Fig. VI-4, the rapid decrease in uranium concentration in the first two tests was due to interaction of UCl_3 with the MgO crucible. Since the slopes for the curves in Fig. VI-2 are much less for test II than I, the oxidation rate for plutonium was reduced by decreasing the O_2 and H_2O content of the cover gas. The rate of decrease in Nd, Ce, Sm, and Y concentrations also depended on the O_2 and H_2O levels in the argon cover gas. As expected, the oxidation rate of plutonium was lower than that of uranium and greater than that of the rare earths.

The layer of material at the bottom of the MgO crucible from test I was analyzed by X-ray diffraction and was found to contain mostly salt, with two additional cubic phases. The first phase was UO_2, with a smaller amount of UO_2-PuO_2 solid solution or rare earth oxides. The second phase was PuO_2. This X-ray analysis indicated that the ratio of UO_2 to PuO_2 was 2:1. Thus, there was no preferential buildup of PuO_2.

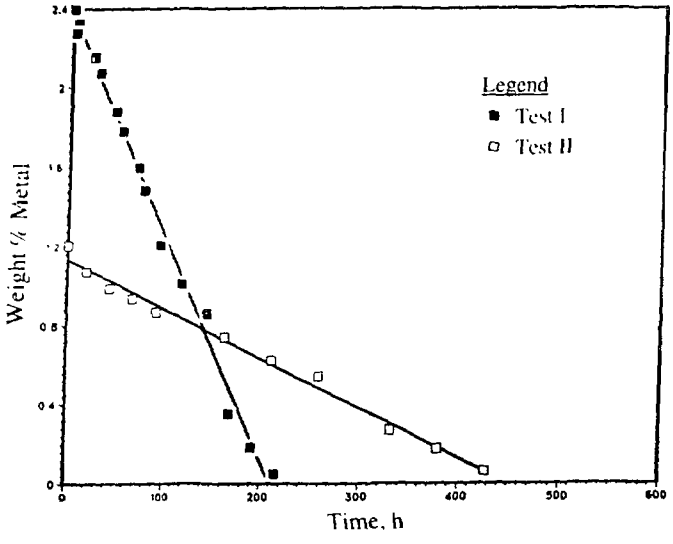

Fig. VI-2. Plutonium Analytical Results for Tests I and II

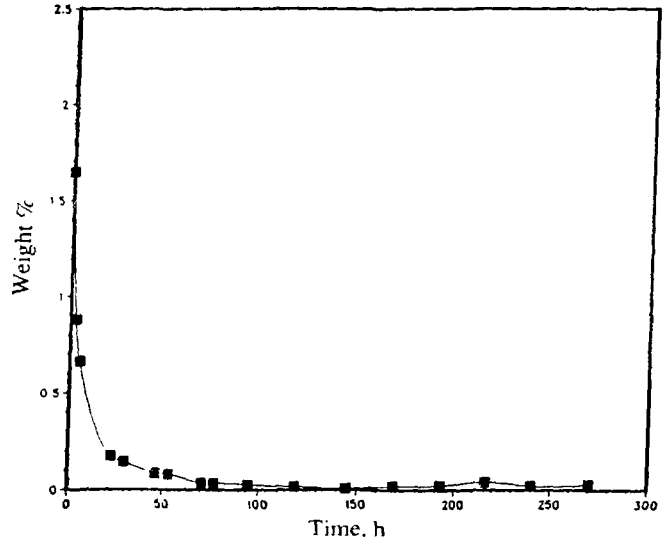

Fig. VI-3. Uranium Analytical Results for Test I

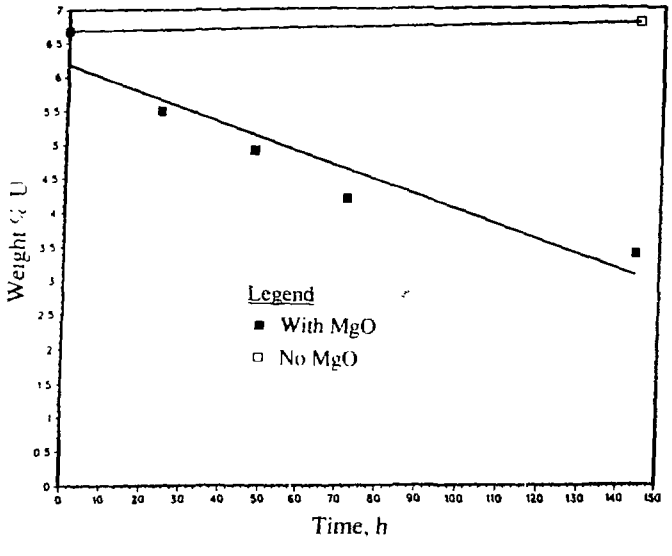

Fig. VI-4. Uranium Analytical Results for Oxidation of UCl_3 with and without MgO in Test III

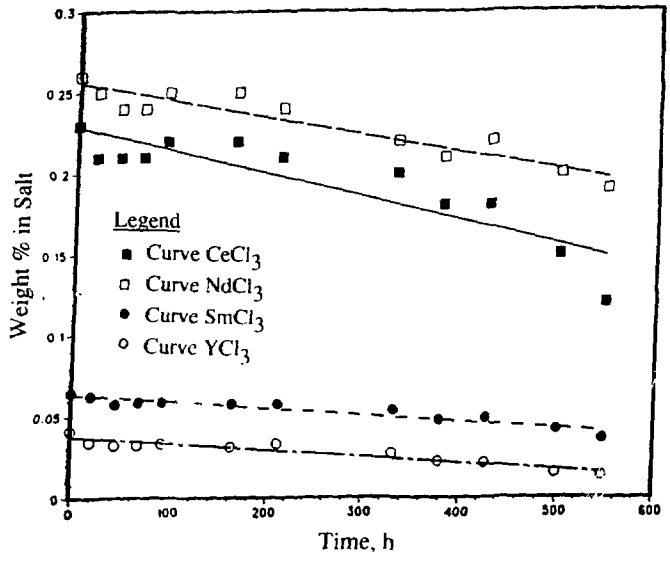

Fig. VI-5. Rare Earth Analytical Results for Test II

2. Examination of Laboratory-Scale Electrorefiner Crucible

Our laboratory-scale electrorefining cell was shut down after approximately four years of operation at ~500°C. This shutdown was caused by a water leak (in a copper cooling coil), which resulted in an air leak in the side arm of the furnace tube. Because the above tests revealed that $PuCl_3$ and UCl_3 in the salt are converted to oxides in the presence of oxygen, we decided not to reuse the 15-cm dia crucible for the electrorefiner cell and its contents. Further, we decided that destructive examination of the crucible would provide a good opportunity to obtain valuable information on the corrosion behavior of the crucible material (low-carbon steel) and on possible side reactions involving the electrorefiner contents (salt, Cd, U, Pu, Zr, and steel).

The crucible and its contents were visually inspected before sectioning the crucible to obtain a sample for metallographic examination. A pie-shaped section for this examination was obtained by sawing the crucible along its full length and then cutting this piece into a sample from the salt section, a sample from the salt/cadmium interface, and a sample that included a weld zone at the crucible bottom, which had contacted only liquid cadmium. The visual examination indicated no apparent breach of the crucible wall by either the salt or cadmium phases or any other corrosion effects.

The metallographic and scanning electron microscopy (SEM) analysis indicated that the crucible thickness in the salt region was slightly less than that in contact with cadmium. However, this difference was small and may have resulted from nonuniformity in the original material used to fabricate the crucible. A phase containing predominantly cadmium was found in contact with the crucible surface on all samples. The crucible interface in contact with cadmium metal, which had features common to all samples, was characterized by a thin layer (1-3 μm) of U-Fe adhering to the crucible surface. The ratio of U to Fe in the layer was close to the 67 mol % U-33 mol % Fe eutectic composition in the binary U-Fe system. Since the eutectic temperature is 723°C, the thin layer was likely formed by reaction of uranium dissolved in cadmium with the steel crucible. The thinness of the layer suggests that it is passivating and, thus, helps protect the steel from further attack.

The crucible corrosion appeared to occur evenly and at a low rate. This observation suggests that the crucible wall was subjected to slow, planar erosion. We found (1) no evidence for selective grain boundary attack on the steel and (2) very little salt in the samples, including that taken from the salt region. Thus, the steel crucible is stable in the chloride salt. We observed a light grey solid phase on the surfaces of the samples taken from the salt region and the salt/cadmium interface region. This phase essentially consisted of Cd and Zr, and elemental analysis of this phase indicated a composition of Cd_2Zr. This phase also contained small amounts of U and Pu (<5 wt %) and even lower amounts of Fe (<1 wt %).

Our examination also revealed incomplete penetration in the original weld joint (0.013-cm wide) where the crucible upper shell had been fusion welded to the crucible floor plate. Electrorefining material in the crucible had filled the entire length of this crevice, but no evidence was seen of substantial corrosion or erosion in the steel.

The results of these examinations provide experimental evidence that mild steel can safely be used as the material of construction for the IFR electrorefiner. We found no breach of the crucible wall or any life-limiting mechanism related to the use of mild steel as the crucible material. The amount of U and Pu found in an immobilized state, either by diffusion or precipitation processes, was not significant.

3. Zirconium Behavior Studies

Zirconium constitutes about 30 vol % of IFR fuel. This fuel will be anodically dissolved in the electrorefiner during fuel reprocessing. In the normal transport of uranium to a solid cathode and U-Pu to a liquid cadmium cathode, the bulk of the zirconium is not transported but is left in the electrorefiner. With repeated cycles, this zirconium accumulates. In the normal course of electrorefining, a small, fairly constant amount of uranium and plutonium metal heel is left in the electrorefiner. In the presence of this U/Pu heel, the zirconium remains in the metallic state and is not oxidized into the salt phase.

Zirconium behavior in the engineering-scale electrorefiner is reported in Sec. VI.C.4. One observation is that the zirconium solids do not disperse easily into the liquid phase. Instead, these solids seem to accumulate on solid surfaces in the electrorefiner. To more conveniently study the behavior of zirconium, we are undertaking a series of small-cell tests with a zirconium rod anode and cadmium pool anode. In 1990, a cell of the type Zr/LiCl-KCl-$ZrCl_x$/Cd(Zr) was operated at 500°C. No uranium was used and ~21 g zirconium was transferred from the zirconium rod anode to the cadmium pool cathode. Visual examination at the end of the test indicated that the zirconium had deposited on top of the cadmium pool. X-ray diffraction analysis of a deposit sample indicated that Cd_2Zr had formed. Metallographic and SEM examination of the cell is now in progress to determine the location and form of the zirconium. We plan to conduct additional tests to explore methods for removing zirconium from the electrorefiner.

C. *Engineering-Scale Process Development*

The key steps in the pyrochemical processing of spent fuel are dissolution and product recovery by electrodeposition using either solid or liquid cathodes or direct chemical reduction. Progress made in developing each step is discussed below. Also reported are results from tests of zirconium behavior and a device for harvesting the uranium deposit from a steel cathode. All tests were conducted in our engineering-scale electrorefiner (0.9-m dia crucible).

1. Dissolution of Spent Fuel

In earlier tests,[2] anodic dissolution of chopped, clad U-Zr alloy pins was demonstrated at the plant scale (~10 kg batch size). All of the alloy was removed from the cladding with a coulombic efficiency of about 50%; the anodic dissolution rate was 0.5 kg

---

[2]M. J. Steindler et al., *Chemical Technology Division, Annual Technical Report, 1989*, Argonne National Laboratory ANL-90/11, p. 101 (1990).

uranium per hour. After the anodic dissolution baskets were rotated at 250 rpm in the gas space above the salt in the electrorefiner to reduce the amount of salt on the hulls, only 2 g uranium, not associated with the residual salt, remained on the cladding hulls.

In this report period, anodic dissolution of U-Zr-fissium alloy pins was demonstrated at the plant scale. With a coulombic efficiency of about 50%, nearly all (~99.8%) of the uranium was removed from the cladding. Some of the cladding segments were empty, but some contained a residue. Chemical analysis of the residue in several segments showed that about 65 wt % salt and 20% of the initial zirconium remained in the pins. The zirconium was associated with Ru, Mo, and Rh. If anodic dissolution of irradiated fuel shows that a large portion of the cladding hulls is filled with a salt residue, a technique may be needed to remove this salt.

2. Electrotransport to Cathode

Improved performance has been achieved in the electrotransport of uranium from a cadmium pool anode to a single mandrel cathode. Previous tests[2] with multipin solid cathodes showed that the highest performance was attained with salt and cadmium mixing early in the run and no mixing during the later portion of the run. In tests done during the past year under these conditions, 9.5 kg (0.26 kg/h) and 9.3 kg (0.35 kg/h) of uranium were deposited on a single mandrel cathode in 37 h and 26.5 h, respectively. A uranium deposit collected on a single mandrel cathode is shown in Fig. VI-6. In the previous tests with single mandrel cathodes, salt mixing was continued during the entire run. Under this condition, the highest weight of uranium collected on the single mandrel cathode was 6.4 kg.

Fig. VI-6.

Photograph of Uranium Deposit (9.3 kg) on Single Mandrel Cathode

Tests were also conducted with the objective of electrodepositing 3 kg uranium in a liquid cadmium cathode (LCC) in 24 to 48 h. (Since the glovebox in which these tests were carried out is not a plutonium facility, uranium was used as a stand-in for plutonium.) Voltage-current measurements from several runs showed that the cell resistance decreased as the elevation of the LCC crucible above the cadmium anode was decreased. The apparent resistance was 49 mΩ at a crucible elevation of 13 cm (5-1/8 in.) and 22 mΩ at 10 cm (4 in.). Most of the resistance was due to the small cathode area of the crucible. Based on the weight of the product from one run, about 3 kg uranium was collected in 32.5 h with a collection efficiency of 49%. Figure VI-7 shows an autoradiograph of the sectioned product ingot. The dark areas (film exposed by β-radiation) show the location of uranium in the crucible. The radiograph indicates that the uranium distribution is good, i.e., under the cadmium surface and fairly uniform.

Tests with single mandrel cathodes and liquid cadmium cathodes will be continued to optimize process parameters and improve the electrotransport rate.

Fig. VI-7.

Autoradiograph of Sectioned Product Ingot from Test with Liquid Cadmium Cathode

3. Direct Chemical Reduction

Direct chemical reduction is being explored as an alternative to the LCC method for recovery of a mixed U-Pu product from the electrorefiner. In this process, cadmium chloride is added to the electrorefiner to oxidize the heavy metal, then a crucible containing cadmium and a lithium alloy is placed in the salt to reduce and collect the heavy metal. Based on the weight of product from one chemical reduction run with uranium (assuming that no cadmium was lost from the collection crucible), we determined that at least 2.5 kg uranium was collected in the crucible. However, most of the uranium was collected above the cadmium phase, near the top of the crucible. The concentration of the uranium-rich product was 65.3 wt % U, 29.1 wt % Cd, and 3.4 wt % salt. This concentration of cadmium would have been insufficient to form $PuCd_6$ (necessary for recovery of plutonium by this method), if plutonium had been present in this test.

Further work on direct chemical reduction has been deferred because of the difficulty in containing the reaction site to the ceramic crucible owing to the high mobility of the lithium reductant.

4. Zirconium Behavior

The zirconium behavior in the engineering-scale electrorefiner is being studied in conjunction with the other electrorefiner development work. In this study, unfiltered core samples (simple dip-tube sample through the liquid cadmium and electrolyte) and filtered samples of cadmium and electrolyte phases are being taken from the electrorefiner under various process conditions.

After numerous runs with the engineering-scale electrorefiner over the past 2 1/2 yr, the total zirconium charged to the electrorefiner is 11.0 kg. The amount of zirconium removed as part of the cathodes is 3.4 kg. Thus, 7.6 kg zirconium has accumulated in the electrorefiner. This quantity of zirconium is not reflected in our analyses of the core or filtered samples taken of the cadmium anode, which indicate a zirconium content of only 0.50 to 0.7 kg. Hence, approximately 7.0 kg zirconium is unaccounted for and is believed to be residing somewhere in the electrorefiner. The amount of unaccounted zirconium has increased as the runs have progressed.

The zirconium content of the cadmium anode, based on the core samples, is within a relatively narrow range of 0.4-0.8 kg. The values for the filtered anode samples are in a range of 0.3-0.7 kg for the same runs. The solubility limit of zirconium in cadmium is 0.22 wt %,[3] which corresponds to an overall zirconium content in the anode of about 0.55 kg if the material is completely mixed. The reasonable agreement between the averaged zirconium content in the core and filtered anode samples, as well as the fact that the values are close to the solubility limit of zirconium in cadmium, suggests that the cadmium anode is saturated and not full of suspended zirconium solids.

All of the core samples have shown a higher zirconium concentration at the bottom of the electrorefiner. The samples at the bottom exceed the saturation value, whereas the samples taken higher up in the cadmium are less than the saturation value. Core samples were also obtained at positions about 90° around the electrorefiner circumference. Some core samples were taken while mixing was being done, and others after mixing was stopped. The results indicated reasonable agreement in the zirconium values from each circumferential position and little effect of mixing.

It was suggested that zirconium loss from the electrorefiner may have occurred due to the formation of volatile $ZrCl_4$ (sublimation point 334°C). Samples were taken of material that had deposited on the upper positions of the heat shields (above crucible) and also material

---

[3]I. Johnson, K. E. Anderson, and R. Claypol, in *Chemical Engineering Division Summary Report--July, August and September 1960*, Argonne National Laboratory Report ANL-6231, p. 67 (1960).

condensed and deposited on one of the small ports on the electrorefiner cover during a period when the port was only partially covered. Since cadmium has a fairly high vapor pressure, most of the condensed material was expected to be cadmium. Analyses indeed indicated cadmium contents of 95% or greater, and the zirconium contents were only 0.02 wt % for the heat shield deposit and <0.001 wt % for the cover deposit.

Thus far, we have found no evidence of zirconium accumulation at the salt-cadmium interface, which might be expected if Zr-Cd intermetallics had formed. Another possibility is accumulation of zirconium on the vessel wall. The engineering-scale electrorefiner has a perforated metal crucible that fits inside the main vessel, leaving a 1/8-in. (0.3-cm) gap between the crucible and the main vessel wall and bottom. Since zirconium might have deposited in this annular space, we attempted to scrape the inside wall and sample for zirconium material. A ladle was used to scrape up one side wall, from the cadmium at the bottom through the salt layer. The analysis results for the main ladle sample are shown in Table VI-1. Also shown in Table VI-1 are analytical results for WS-1, a portion of the scraping that fell out of the top of the main ladle sample. The scraping presumably was collected higher on the electrorefiner wall, as reflected by its higher Li and K content. Interestingly, the zirconium content of this scraping is significantly higher than that of the average core sample, which is close to the saturation value of 0.22 wt %. This suggests that some zirconium-rich material may be adhering to the walls.

These studies will be continued to determine the options available for removing zirconium from the electrorefiner and further processing this material either as a waste to be discarded or as a material to be returned to the fuel cycle.

Table VI-1. Content of Sample from Wall Scraping

	Content, wt %	
	WS-1	Ladle
U	3.16	3.88
Zr	0.35	0.59
Cd	74.9	91.4
Li	1.61	0.16
K	6.10	0.60

5. Equipment Testing

We have fabricated and tested a device to harvest the uranium deposit collected on a steel mandrel cathode in the engineering-scale electrorefiner. The main elements of this device are a machined die mounted on backing plates, which are attached to a unistrut framework. This device is secured by bolting it to two sections of unistrut channel, which are welded to the floor of the electrorefiner glovebox. A bolted collar is attached to the cathode assembly and the die positioned around a clean portion of the cathode mandrel above the deposit. A glovebox crane is then attached to the cathode assembly. To harvest the uranium deposit, the mandrel is pulled slowly through the die by lifting the cathode assembly with the crane.

We tested the device with the 12 kg (9.3 kg uranium) deposit on the single steel mandrel cathode shown in Fig. VI-6. The purpose of the test was to determine the effectiveness of the device in removing the uranium deposit from the steel mandrel.

The uranium deposit was completely removed from the solid cathode mandrel, except for a thin layer of uranium. After uranium harvesting, this thin layer (less than 0.16 cm) can be removed by electrotransport of the uranium to the cadmium pool, and the mandrel can be reused in uranium electrodeposition runs. Information obtained during this test will be used to design the electrorefiner harvester equipment that will be used in the FCF. Further tests are planned in which devices, other than the glovebox crane, will be used to pull the mandrel out of the uranium deposit.

D. *Waste Treatment Processes*

Processes are being developed to recover TRU elements from the metal and salt wastes in the electrorefiner and to convert the treated materials into disposable high-level waste forms. The metal waste consists of cladding hulls, zirconium, and cadmium, which contains the noble metal fission products. Except for the cladding hulls, these wastes are expected to contain only small amounts of actinides. The salt contains the alkali metal, alkaline earth, rare earth, and halide fission products. It will also contain from 0.5 to 1.0% of the actinides fed to the electrorefiner. Efforts have been concentrated on developing processes for treating and immobilizing the waste salt.

1. Waste Treatment Flowsheet

We have updated the flowsheet for treating the salt and metal wastes discharged from the electrorefiner and proposed new steps which may have advantages for the overall fuel cycle. Among the more important changes is the removal of the bond sodium and alkali metal fission products from the chopped fuel by distillation. These metals are converted to chlorides in the salt stripper as described in Sec. VI.D.3. Separating the alkali metals from the fuel (1) minimizes the sodium content of the salt in the electrorefiner and thereby avoids raising its melting point; (2) reduces the use of $CdCl_2$ to oxidize electropositive elements in the fuel and thereby decreases the amount of cadmium in the waste; and (3) removes cesium from the electrorefiner and thereby reduces the heat load by about 30%.

To remove waste salt and metal from the electrorefiner after several electrorefining cycles, the following operations are used:

1. After the last cathode product has been removed, the traces of actinides and a fraction (~10%) of the zirconium in the cadmium pool are transferred to the salt by adding $CdCl_2$ to the salt.

2. Most of the zirconium remaining in the pool is electrotransported to solid cathodes. A small fraction of the collected zirconium becomes waste, and the rest is used in the recycled fuel alloy.

3. A pump-filter assembly is inserted in the electrorefiner to circulate first salt and then metal through a sintered metal filter to remove particles of insoluble impurities, such as UO_2, and undissolved noble metal fission products (Nb, Mo, Tc, Ru, and Rh). Some cadmium is retained in the filter to remove the cadmium-soluble fission products (Pd, Ag, In, Sn, Sb, and Te). The filters are sent to waste processing.

4. An amount of lithium sufficient to reduce most (~90%) of the actinide chlorides is added to the electrorefiner. This leaves about 75% of the rare earths in the salt phase. Then, all of the salt is removed from the electrorefiner and sent to the treatment steps described below.

The process steps used to treat the salt and metal discharged from the electrorefiner are shown in Fig. VI-8. To recover the TRU elements in the salt and separate them from rare earths, the salt is first contacted with a Cd-U solution at 500°C in a multistage, countercurrent extraction train. The uranium in the metal phase exchanges to a greater extent with TRU elements in the salt phase than with rare earths. Figure VI-9 illustrates the recovery of TRU elements and their separation from rare earths in extraction trains with four to seven equilibrium stages and metal/salt mass flow ratios from three to seven. These curves suggest that four to six actual stages in a countercurrent extraction train will suffice to obtain the desired separation of actinides from lanthanides and recover more than 99% of the TRU elements from the salt.

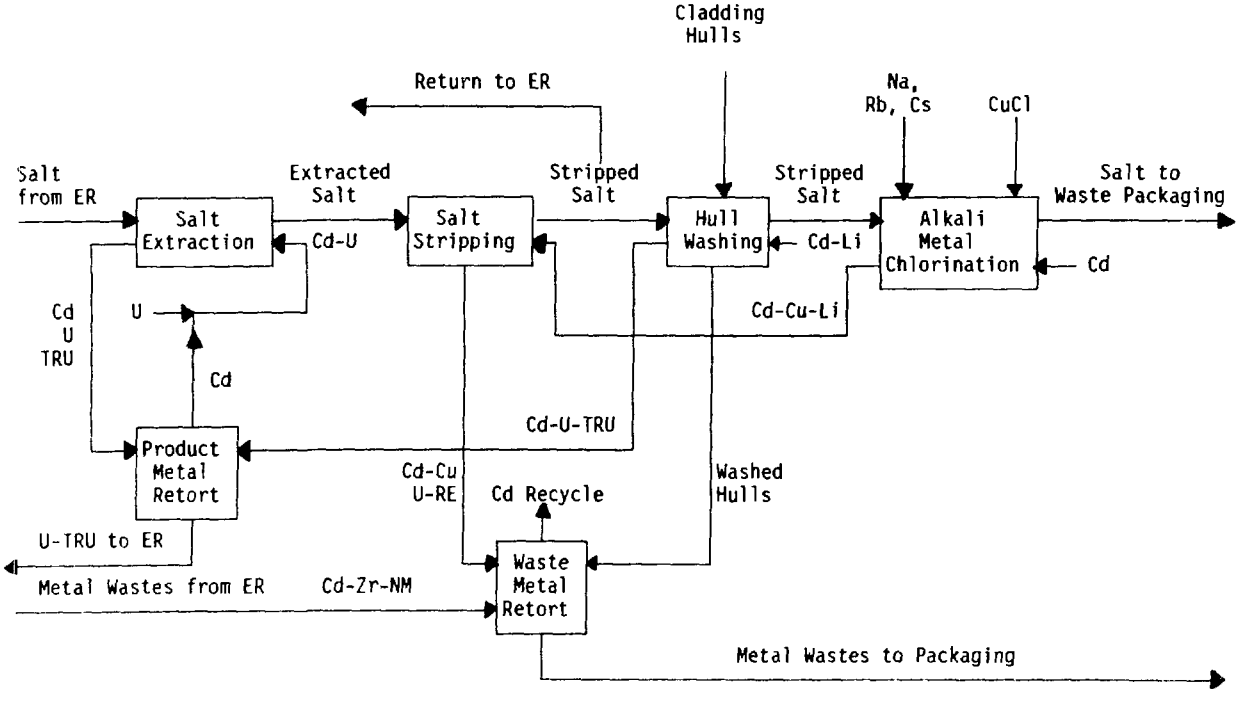

Fig. VI-8. Waste Treatment Flowsheet (ER = electrorefiner, RE = rare earths, NM = noble metals, TRU = transuranic elements)

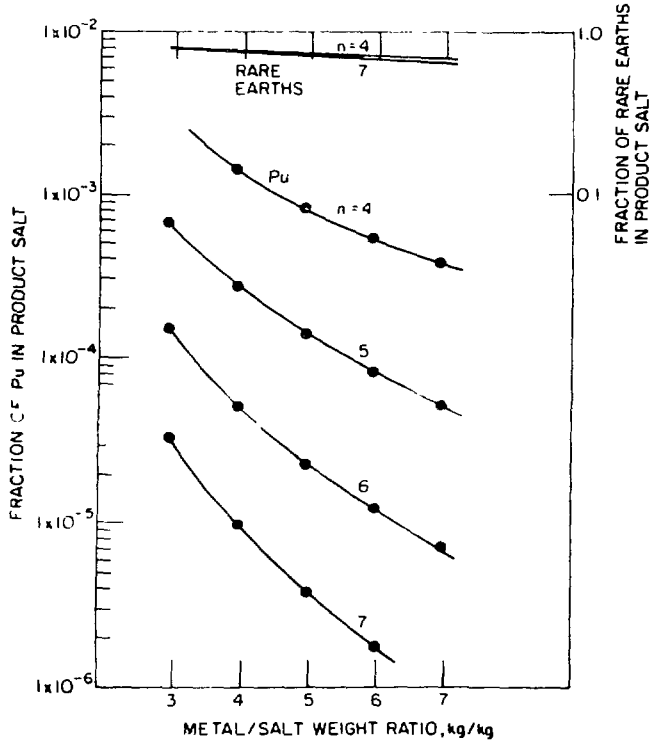

Fig. VI-9.
Extraction of Plutonium and Rare Earths from Salt by Multistage Contactors (n = number of stages)

After TRU elements are separated from rare earths in the extraction train, the entire batch of electrorefiner salt is fed to the stripper vessel, where three steps are performed: stripping, cladding hull washing, and alkali metal chlorination (see Fig. VI-8).

The treated salt is then absorbed into a zeolite, which strongly adsorbs the fission product Cs and Sr by ion exchange and contains the remaining salts in its "molecular cage." The initial investigations of this promising method for immobilizing waste salts are described in Sec. VI.D.4.

The filters from the electrorefiner are combined with zirconium, cladding hulls, and the stripping alloy, which contains the rare earth fission products and uranium. This mixture is fed to the waste metal retort, where it is mixed with copper, then most of the cadmium is distilled off and recycled. A small fraction is left with the metallic residue. The remainder is equivalent to the fission product cadmium and the $CdCl_2$ added to the electrorefiner to oxidize rare earth, alkali metal, and alkaline earth fission products in the fuel. It is expected that the cadmium, uranium, and most of the fission products will be dissolved in the copper. The metal waste mixture will be densified by pressing or melting, then encapsulated in a thick, corrosion-resistant container for disposal.

2. Salt Extraction

High-temperature centrifugal contactors (pyrocontactors) are being developed for separating TRU elements from rare earths in the IFR fuel cycle. A facility is being assembled for conducting experiments to determine the performance and extraction efficiency of the

pyrocontactor with molten cadmium and chloride salts at 500°C. The ultimate goal is to develop a liquid metal-salt extraction process that uses multistage, countercurrent pyrocontactors to recover the TRU elements from the waste salts produced in the FCF. The current effort is to design, fabricate, and assemble our test facility with a single-stage pyrocontactor.

The design of the pyrocontactor is patterned after centrifugal contactors for aqueous-organic systems. We have completed the preliminary design of the test facility and nearly completed the final design of the major test components. We also installed a glovebox to house the facility and nearly completed the design work needed for modifying and extending the glovebox for pyrocontactor testing.

3. Salt Stripping

The current concept of the stripper is a stirred vessel large enough to contain all of the salt from the electrorefiner. A prototype of the stripper vessel to be used in the FCF will be installed in a 0.46-m (18-in.) dia furnace well. We completed the design of the major components and nearly completed their fabrication. A pump-transfer line assembly will be used to transport about 60 L of salt containing rare earths and uranium from the electrorefiner into the stripper, which will contain about 20 L cadmium. The stripper will be equipped with an agitator capable of imparting mixing power densities up to 1.4 kW/m^3 (7 hp/1000 gal) in the salt and 5.9 kW/m^3 (30 hp/1000 gal) in the metal phase. Ports for sampling and charging materials, as well as fittings for instrumentation such as liquid level probes and reference electrodes, will be provided. Experiments will be conducted to determine stripping rates as functions of mixing intensity, effectiveness of filters, characteristics of insolubles, and performance of equipment and instruments.

4. Salt Immobilization

Although the treated salt will contain only trace amounts of actinides and very small amounts of rare earth fission products, it will contain Cs and Sr and is, therefore, a high level waste (HLW) according to the definition in the Code of Federal Regulations (Title 10, Part 60). As such, it must be disposed of in a geologic repository for HLW. Therefore, a waste form that will meet the acceptance criteria for the repository must be developed for the treated IFR waste salt. Definition of the exact acceptance criteria is still evolving, but in general terms, the waste form must be a solid monolith that is strong, leach resistant, and radiation resistant. It is also desirable that the salt immobilization process be relatively simple, amenable to remote operation, and compatible with the IFR pyroprocess.

With these general requirements in mind, we are developing a salt waste form that is fabricated in two steps: (1) immobilizing the waste salt in an inert, leach-resistant matrix, and (2) densifying the matrix to yield a mechanically strong, solid monolith. This matrix will then be sealed in a durable metal container. As the first step toward identifying a potential matrix for chloride salts, we considered the composition of various minerals. Naturally occurring minerals which occlude (or contain) chloride salts are known. ("Occlusion" is the incorporation of molecules into a zeolite cavity. "Hydration" can be thought of as the occlusion of water molecules.) Examples are sodalite, scapolite, and cancrinite. These minerals are zeolites, i.e.,

crystalline alkali metal and/or alkaline earth aluminosilicates that are characterized by an open framework with relatively large cavities and channels. The salt molecules are typically held in these cavities and are not readily released.

Efforts to identify zeolites that would occlude IFR waste salt and a process that would yield analogs of these naturally occurring minerals appear to have been successful. Promising results were obtained by contacting dehydrated A50, a synthetic zeolite having sodium as an exchangeable cation, with a molten salt (92.5 wt % LiCl-KCl eutectic salt, 5.0 wt % NaCl, 1.0 wt % CsCl, 1.0 wt % $BaCl_2$, and 0.5 wt % $SrCl_2$). The experiment consisted of pouring the molten salt at 450°C into a column of A50 supported on a quartz frit and allowing the salt to percolate through the column. The salt that flowed through the column and frit was collected and analyzed. The zeolite was washed with water to remove adhering salt, dried to constant weight, and analyzed.

Two types of reactions, ion exchange and salt occlusion, occurred between the molten salt and the zeolite. Most of the sodium ions in the zeolite were exchanged for ions in the salt, and the zeolite occluded about 40% of its weight in salt. Evidence for these statements is provided by the results given in Table VI-2. The moles of contained cations are shown in Table VI-2 for the same amount of zeolite: about 70.7 g of the initial zeolite (sodium form) and 100 g of the final zeolite-occluded salt compound. The original zeolite contained about 0.5 mol of exchangeable sodium ions. The cations in the final zeolite-salt in excess of this value were those in the occluded salt. From a charge balance, we calculated that the chloride content of the zeolite-salt compound should be 17 wt %; the results of two chloride analyses were 17.1 and 17.3%.

Table VI-2. Concentrations of Univalent and Divalent Metals in Zeolites

	Concentration[a]						
Sample	Ba	Cs	K	Li	Na	Sr	Total
FR-8[b]	0.010	0.015	0.190	0.703	0.032	0.007	0.957
Anhydrous A50[c]	0	0	0	0	0.498	0	0.498

[a]Concentration units are moles per 100 g of salt-equilibrated zeolite for FR-8, and moles per equivalent amount of anhydrous A50 zeolite (about 70.7 g A50).
[b]Final salt-equilibrated zeolite.
[c]Starting zeolite.

From the chemical analyses, we could not determine which cation is in the zeolite structure and which is in the occluded salt. However, it is clear that sodium in the original zeolite has exchanged almost completely with other cations. In addition, the cations in the zeolite-salt compound were enriched in Li, Ba, Sr, and Cs compared to their concentrations in the original salt. This was also shown by the analyses of the salt that passed through the zeolite column. The amounts of Ba, Cs, and Sr in this salt were at or below their detection limits; the estimated decontamination factors were 640, >700, and >250, respectively.

The above results are encouraging. They demonstrate that zeolites can sorb the cations of interest. However, the matrix must also contain these cations when the waste form is

eventually exposed to groundwater in the repository. Some short-term leach tests have been completed, and these results are also promising. The leach resistance of the washed and dried zeolites was measured for a 24-h leach period in terms of the percent released. The amounts of Ba, Cs, Li, K, and Sr released were <0.01, 0.06, 0.1, 0.01, and 0.01%, respectively. Thus, the zeolite matrix acts as a leach-resistant matrix under the conditions of the test.

The zeolite materials discussed above are in the form of powders, which would not be suitable for a HLW. Laboratory work to identify a method for solidifying the zeolite-salt compounds is at a very preliminary stage. We have conducted experiments to test the feasibility of densifying a matrix consisting of zeolite and copper powders. Hot isostatic pressing of various mixtures at 375°C and 69 MPa (10,000 psi) yielded solid monoliths that were relatively strong. Further experiments are planned in which zeolites with sorbed salt are hot isostatically pressed with copper powder.

Studies to determine the radiation resistance of zeolites with sorbed IFR waste salt are still in the planning stage. However, the radiation resistance of sodalite was studied by Thompson.[4] The results showed that exposure of sodalite to 1×10^{10} rad did not affect the sample volume or its leachability.

5. Compliance with Regulations for High-Level Waste Disposal

Two waste streams from the reprocessing of IFR fuels, salt and metal, might be classified as high-level wastes. In accordance with current waste-disposal philosophy, these wastes would be disposed of in a deep geologic repository. Thus, the producer of IFR reprocessing wastes must plan to comply with the requirements for HLW acceptance at a repository. To support such planning, we reviewed and analyzed information on the current status of HLW acceptance requirements to evaluate their applicability to IFR wastes. The results of reviewing and analyzing this information will be expressed in a document summarizing (1) the general background of standards, regulations, and current activities of waste producers and federal agencies, relative to preparations for disposal of HLW, and (2) our conclusions about the regulatory requirements that might be demanded of the IFR waste producer and the IFR waste package.

---

[4]G. H. Thompson, *Evaluation of Mineralization Processes for SRP Wastes*, Savannah River Laboratory Report DP-1389 (1975).

VII. ACTINIDE RECOVERY

Spent fuel from commercial water-cooled nuclear reactors (LWRs) contains a considerable quantity of unreacted fissile uranium as well as transuranic (TRU) elements (mainly Np, Pu, Am, and Cm). These actinide elements constitute a valuable energy resource, and the purpose of the current work is to develop processes for their recovery for use as nuclear fuel in Integral Fast Reactors (IFRs) (Sec. VI). We expect these processes to be simple and efficient and to provide a cost-effective method for recovery of actinides from LWR spent fuel. Removal of actinides from the spent fuel could considerably shorten the time required for assured confinement in the geologic repository. After that reduced time, the remaining radioactive elements are estimated to be no more toxic than the original ore from which the nuclear fuel was extracted.

High-temperature separation processes were developed in the 1960s at ANL[1] and in recent years as part of the IFR program (Sec. VI). They now appear to have potential as relatively uncomplicated, effective means for recovering uranium and TRU elements. The current work is aimed at extending these processes, combined with pyrometallurgical technology developed in past years, to determine whether or not they can be used to extract actinides from LWR spent fuel. Two processes are being examined. In both processes, the LWR spent oxide fuel is reduced to an alloy by reaction with calcium metal, and the actinide elements are then separated from the fission products. In one process, molten salt is used to selectively recover the TRU elements, while the other process uses liquid magnesium. Calcium metal is recovered from the CaO in the reduction salt by electrochemical methods and recycled along with the salt to minimize process wastes.

A. *Program Perspective*

The LWR spent fuel consists of both radioactive fission products and the fuel components (actinides). Fission products comprise hundreds of isotopes, which, along with energy, are the products of nuclear fission. The TRU elements are produced from neutron capture, as opposed to fission, in the fuel. The relative toxicities of the TRU elements and fission products contained in the LWR spent fuel are compared in Fig. VII-1, normalized to the toxicity of natural uranium ore, for times up to ten million years. Most of the fission products have relatively short half-lives, and their toxicity drops below that of the original uranium ore in a time span of the order of 200 years. The TRU elements, on the other hand, have long half-lives and their radiological toxicity remains higher than the original uranium ore for nearly a million years. In this difference lies an important incentive for separating the TRU elements from the spent fuel and recycling them back into a reactor, leaving a waste low in long-term toxicity. If 99.9% of the TRU elements is removed from the spent fuel, its toxicity level will be below that of an equivalent amount of natural uranium after a few hundred years. As the TRU elements are

---

[1] R. K. Steunenberg et al., "Pyrometallurgical and Pyrochemical Fuel Processing Methods," in *Progress in Nuclear Energy,* Series III, *Process Chemistry,* Vol. 4, pp. 461-504, Pergamon Press, Oxford (1969).

"burned up" (fissioned) in a reactor such as the IFR, they not only transmute to less toxic elements, but also produce electrical energy in the process.

Although actinide recovery does not eliminate the need for a geologic repository for nuclear waste disposal, it could simplify long-term waste management strategy. After about 50 yr from the time that spent fuel is removed from the reactor, decay heat from the TRU elements becomes significant compared to that from the fission products. Removal and recycle of the actinides, combined with aboveground storage of heat-producing fission products until most of their heat is dissipated, could allow closer spacing of waste packages in the repository. This closer spacing would use expensive repository space more efficiently. The reduced heat burden could also simplify analysis of repository performance, particularly in the short term (~300 yr), and thus increase confidence in repository performance predictions.

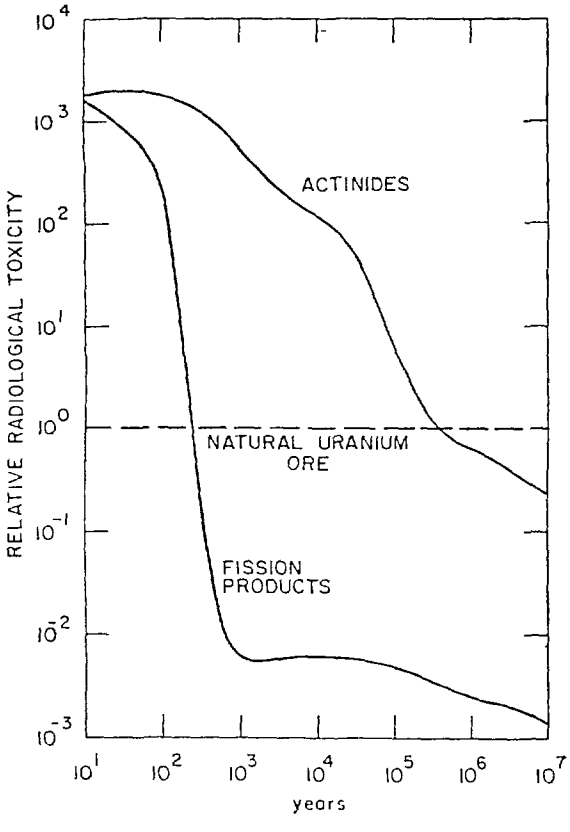

Fig. VII-1.

Relative Radiological Toxicity of Fission Products and Actinides Contained in the LWR Spent Fuel, Normalized to the Original Uranium Ore. (Based on data in Ref. 2.)

B. *Pyrochemical Process Development*

1. Salt Transport Process

In our salt transport process, oxide fuel is first reduced by calcium in a Mg-Cu/$CaCl_2$-CaF_2 system to produce a Cu-Mg alloy containing TRU elements and some fission products. The uranium, which also reduces, precipitates because of its low solubility in

[2]L. Koch, J. Less-Common Met. **122**, 371 (1986).

the alloy. Alkali, alkaline-earth, and halide fission products remain in the reduction salt, and the gaseous fission products are released.

A salt transport step follows the reduction and is used to extract the TRU elements from the uranium and less-reactive (more-noble) fission products. The rare earth elements remain with the TRU elements and are removed subsequently in the IFR process. The salt transport step is accomplished by equilibrating a $MgCl_2$-rich salt with both the Cu-Mg alloy (the donor) and a Zn-Mg alloy (the acceptor). Because of the relatively high activity coefficients of the actinides relative to magnesium in the donor alloy, these elements transfer to the salt phase, and then, because of the relatively low activity coefficients of the actinides relative to the magnesium in the acceptor alloy, they transfer to that alloy. This transport is accompanied by an equivalent transport of magnesium from the acceptor alloy to the donor alloy. The more-noble elements and most of the uranium remain with the Cu-Mg alloy.

The TRU elements and the rare earths are recovered as metals from the acceptor by evaporating the Zn and Mg, which are recycled. The recovered TRU elements are introduced into the IFR electrorefiner for use as IFR fuel.

The Cu-Mg alloy is separated from the uranium precipitate and recycled until the noble element fission products build up to a level suitable for disposal. Prior to disposal, the magnesium is distilled off from the Cu-Mg and recycled to the acceptor alloy. The resulting copper-noble element alloy is consolidated for disposal in a geologic repository.

The reduction salt contains CaO reaction product as well as some fission products. The fission products can be allowed to build up during several reduction cycles, but the CaO must be removed to recycle the salt. An electrolytic process is proposed to decompose the CaO selectively. The oxygen is discarded as CO_2, and the salt and calcium reductant are recycled. Eventually, the salt must be discarded when the heat generation from fission products becomes excessive. The methods under development for IFR salt waste processing will be used for disposal of the waste salt from this process.

We completed two series of runs at 790°C to evaluate the process chemistry for salt transport. Each series consisted of a reduction run followed by salt transport runs. A mixture of high-density UO_2, PuO_2, NpO_2, and representative fission products was used as synthetic LWR fuel. The salt transport involved equilibrating $MgCl_2$ transport salt sequentially with the Cu-Mg reduction alloy, a Zn-Mg acceptor alloy, then again with the Cu-Mg alloy, etc. Three transport cycles were used for each series. Three such cycles, with the volumes of materials used, were expected to recover >95% of the plutonium from the Cu-Mg.

The results of the two runs are in good agreement. Material balance information for the second run is presented in Table VII-1. The reductions were effective, and the transport was as expected; however, some of the plutonium in the acceptor was not in solution in the liquid zinc. This was unexpected, and we will determine the form of the precipitated plutonium. There appears to have been significant coprecipitation of neptunium with the uranium, but plutonium and americium coprecipitation was minimal. As can be deduced from Table VII-1, the percent extraction of americium by the acceptor alloy is less than that for plutonium and neptunium, but,

because the transport salt is recycled, this only results in an in-process inventory, which will reach a steady-state level.

Table VII-1. Analytical Results from Salt Transport Process Demonstration

Stream	Plutonium, mg	Americium, μg	Neptunium, mg
Oxide Feed	190	~2500	16
Reduction Salt	<0.5	2.5	0.02
Cu-Mg Alloy (donor)	8	33	0.7
Transport Salt	<0.8	1240	0.4
Uranium Precipitate	<2	30	3.6
Zn-Mg alloy (acceptor)	188	1530	11

In the next year, we will conduct experiments to optimize process variables and will build a retort for laboratory-scale demonstration of the recovery of a metallic TRU product.

2. Magnesium Extraction Process

The magnesium extraction process separates the TRU elements from uranium by extracting them into a liquid magnesium phase, which is immiscible with uranium. First the uranium-TRU element alloy is formed in a reduction step in which the oxide fuel is reduced with calcium in the presence of $CaCl_2$-CaF_2 salt. To obtain a liquid phase at 800°C, the uranium is alloyed with iron. The U-Fe alloy, with dissolved TRU elements and noble-metal and rare-earth fission products, is contacted with liquid magnesium. The TRU elements and some of the rare-earth fission products are extracted into the magnesium, leaving the U-Fe, noble metals, and the rest of the rare earths behind. The magnesium is retorted from the TRU product and recycled in the process. The TRU product becomes a feed stock for the IFR fuel cycle.

We completed two series of runs at 790°C to study the magnesium extraction process chemistry. Synthetic LWR fuel containing UO_2, PuO_2, NpO_2, and representative fission product elements was used. The reduction step involved mixing fuel, $CaCl_2$-CaF_2, U-Fe, and Ca at 790°C. In this step the alkali, alkaline-earth, and halide fission products remain in the salt, and gaseous fission products are released. The rare-earth and more-noble fission products are reduced into the U-Fe alloy along with the uranium and TRU elements. Following the reduction run, the liquid U-Fe alloy is contacted with molten magnesium at 790°C for a series of extractions. The rare earths are expected to accompany the TRU elements as they are extracted by the magnesium. The extraction process includes distilling magnesium from the TRU material to obtain a feed for an IFR electrorefiner. The rare earths will be removed from the TRU fuel in the electrorefiner.

The results of the two series of runs are in good agreement, but the material balances for the runs are poor. Analytical problems have been significant. The material balance for the second series, based on current analytical results, is presented as Table VII-2. The reductions were effective, but the extraction results are uncertain. In the coming year, we will analyze these

results further and will complete additional runs to better assess the process. A retort now being designed will be used to recover TRU elements from the magnesium extracts.

Table VII-2. Analytical Results from Magnesium Extraction Process Demonstration[a]

Stream	Plutonium, mg	Americium, μg	Neptunium, mg
Oxide Feed	210	~2800	11
Reduction Salt	<0.5	26	0.031
U-Fe Ingot	<5	?	?
1st Mg Extract	82	440	<0.8
2nd Mg Extract	<20	54	2.2
3rd Mg Extract	<20	15	1.2

[a]Analytical work is continuing.

3. Calcium/Salt Recovery

We completed several runs at 800°C to evaluate electrowinning of calcium from the CaO in reduction salts. A carbon anode was used to remove the oxygen as CO and CO_2. There was a sufficient margin between the decomposition potentials for $CaCl_2$ and CaO to make selective decomposition of CaO a possibility. The solubility of calcium in the salt can lead to parasitic reactions, but successful runs were made when a liquid cathode was provided to collect the calcium. The reduction salt had been contaminated by carbon dust from the anode in most of the runs; however, a special anode design is showing considerable promise for solving that problem. It has also been shown that the carbon is easily filtered from the salt.

In the next year we will continue anode design development and will conduct experiments to determine optimum operating parameters.

VIII. APPLIED PHYSICAL CHEMISTRY

The program in applied physical chemistry involves studies of the thermochemical, thermophysical, and transport behavior of selected materials in environments simulating those of fission and fusion energy systems.

A. *Liquidus-Solidus Temperatures for Core-Concrete Mixtures*

The objective of this research program is to provide experimental data on the onset of melting (solidus temperature) and the onset of solidification (liquidus temperature) for mixtures of urania, zirconia, and one of the following concretes: limestone, limestone-sand, basalt, or siliceous concrete. Such mixtures are expected to occur during the molten core-concrete interaction (MCCI) phase of hypothetical severe reactor accidents in light-water and pressurized-water reactors. A knowledge of the thermophysical properties of the solids, liquids, and gases that exist during the MCCI phase is crucial for understanding and modeling the consequences of an accident.

The results of this research are to be incorporated in the CORCON[1] thermal-hydraulic code, which is an integral part of the Source-Term Code Package for the Nuclear Regulatory Commission (NRC).[2] At present, CORCON employs an ideal-solution model to compute liquidus and solidus temperatures for mixtures of concrete with UO_2 and ZrO_2. For this model, the heats of melting of the concretes are estimated from heats of melting of individual components, and initial melting-temperature ranges[3] of the highly inhomogeneous concretes are assumed to be equivalent to their equilibrium solidus-liquidus temperature ranges. Solidus temperatures have been reported[4] for two concretes of unspecified composition, labeled as "basaltic concrete" and "limestone concrete," and for certain mixtures of these concretes with UO_2-ZrO_2. These data (and an assumption of ideal solid and liquid solutions) were later employed in the WECHSL code[5,6] to approximate solidus and liquidus temperatures for mixtures of UO_2-ZrO_2 and concrete.

---

[1]R. K. Cole, Jr., D. P. Kelly, and M. A. Ellis, *CORCON-Mod2: A Computer Program for Analysis of Molten Core-Concrete Interactions*, U. S. Nuclear Regulatory Commission Report NUREG/CR-3920 (1984).

[2]J. A. Gieseke, P. Cybulskis, H. Jordan, K. W. Lee, P. M. Schumacher, L. A. Curtis, R. O. Wooton, S. F. Quale, and V. Kogan, *Source Term Code Package*, U. S. Nuclear Regulatory Commission Report NUREG/CR-4587 (1986).

[3]D. A. Powers and F. E. Arellano, *Large-Scale Transient Tests of Interaction of Molten Steel with Concrete*, U. S. Nuclear Regulatory Commission Report NUREG/CR-2282 (1982).

[4]A. Skokan, H. Hollek, and M. Peehs, Nucl. Technol. **46**, 255 (1979).

[5]M. Reimann and S. Steifel, *The WECHSL-Mod2 Code: A Computer Program for the Interaction of a Core Melt with Concrete Including the Long Term Behavior*, Kernforschungszentrum Karlsruhe Report KfK-4477 (1989).

[6]G. Cenerino, "Application of the Core-Concrete Interaction Code WECHSL to Reactor Case," in *Proc. of the Committee on Safety of Nuclear Installations (CSNI) Specialist's Mtg. on Core-Debris Concrete Interactions*, Electric Power Research Institute Report EPRI NP-5054-SR, p. 6-3 (1987).

During an earlier study,[7] we found that the ideal-solution assumption was a poor approximation. If the ideal-solution assumption were valid, only one phase (the ideal solid solution) would form on cooling molten mixtures of these concretes with urania and zirconia. However, two solid phases crystallized from the melt on cooling mixtures of UO_2-ZrO_2 with limestone-sand or siliceous concrete from a temperature of 2125°C. One phase was rich in urania and zirconia, and the other was rich in silica, calcia, and magnesia. A mixture of the limestone concrete with UO_2-ZrO_2, when cooled from a temperature of 1875°C, yielded not only these two solid phases (with the UO_2-ZrO_2 phase also containing a significant concentration of CaO) but also MgO and $CaZrO_3$. We concluded that only two oxide phases existed in this mixture at 1875°C: (1) a solid oxide phase containing mainly urania, zirconia, and calcia and (2) a liquid oxide phase containing mainly calcia, zirconia, silica, and magnesia. The very small concentrations of magnesia and silica in the solid and of urania in the liquid indicated non-ideal behavior.

In this report period, we performed differential thermal analysis (DTA) measurements on limestone, limestone-sand, and siliceous concrete, as well as mixtures of these three, with UO_2-ZrO_2. The experiments were designed to aid researchers in ANL's Reactor Engineering Division in analyzing results from their large-scale MCCI experiments now in progress.[8] The samples (5 to 6 g for the calcined concretes alone or about 20 g for the mixtures of concrete, UO_2, and ZrO_2) were held in covered molybdenum crucibles (9 cm^3) that rested on a thermocouple within a high-temperature furnace cavity. A gas of Ar-3% H_2 (at a pressure of about 0.03 MPa) was added to the furnace cavity to minimize vaporization losses to less than 2% of the sample mass.

The DTA experiments were first performed with the calcined concretes alone (limestone, limestone-sand, and siliceous). These concretes were subjected to thermal cycling over a wide temperature range. The programmed temperature-cycling sequence consisted of cooling at 20°C/min, heating at 20°C/min, cooling at 10°C/min, and, finally, heating at 10°C/min. Next, 72.5 wt % UO_2-ZrO_2 (1.625:1 mole ratio of UO_2 to ZrO_2) was added to the concrete samples. The weight fractions of urania, zirconia, and concrete in these mixtures were chosen to be identical to those in the large-scale MCCI experiment employing siliceous concrete as a basemat.[8] The DTA experiments were then performed on each of the three UO_2-ZrO_2-concrete mixtures with the same cycling sequence as described above.

The UO_2-ZrO_2 mixtures added to the three concretes were individually prepared for each experiment from $UO_{2.25}$ and ZrO_2. The appropriate weights of $UO_{2.25}$ and ZrO_2 powders were mixed together in a molybdenum crucible and treated for 8 h or more in flowing He-6% H_2 at 1550°C, while the water concentration in the outlet gas stream was monitored with a thin-film alumina hygrometer to ensure that the reduction process was essentially complete (<100 ppm H_2O). Weight-loss measurements indicated that the $UO_{2.25}$ in each mixture was reduced to $UO_{2.00}$. The above process sintered the grey mixture of finely divided powders into a reddish-

---

[7]M. F. Roche, J. L. Settle, L. Leibowitz, and C. E. Johnson, *Vaporization of Strontium, Barium, Lanthanum, and Uranium from Mixtures of Urania, Zirconia, Steel, and Concretes at 2150 K and 2400 K*, Electric Power Research Institute Report EPRI NP-6613 (1990).

[8]D. H. Thompson and J. K. Fink, *ACE MCCI Test L2, Test Data Report, Volume I - Thermal Hydraulics*, Ace Consortium Report ACE-TR-C10 (1989).

brown cylindrical pellet of UO_2-ZrO_2, which could be conveniently added to each concrete sample.

The DTA curves for the calcined limestone-concrete sample (5.0 g) indicated solidus and liquidus temperatures of 1222 and 2304°C, respectively. The limestone-concrete composition, after calcining to remove CO_2 and H_2O, may be approximated as 71 wt % CaO, 12 wt % SiO_2, 12 wt % MgO, and 5 wt % other ingredients (mainly Al_2O_3). Ternary sections of the CaO-SiO_2-MgO-Al_2O_3 phase diagram for 10 wt % MgO[9] and 5 wt % Al_2O_3[10] indicate a solidus-liquidus temperature range of 1235°C to ~2250°C for a mixture containing 71 wt % CaO, 12 wt % SiO_2, 12 wt % MgO, and 5 wt % Al_2O_3. This range is in reasonable agreement with our solidus-liquidus temperature range of 1222 to 2304°C for the more complex limestone concrete.

To the limestone-concrete sample (5.0 g) were then added 10.4 g UO_2 and 2.9 g ZrO_2. The DTA curves for this sample showed a solidus temperature of 1247°C. From phase diagrams for the UO_2-CaO[9] and ZrO_2-CaO[11] systems and the DTA curves, we estimated a liquidus temperature of greater than 2450°C for the UO_2-ZrO_2 mixture with limestone concrete. However, the DTA measurements could not be extended to that temperature because the thermocouples (beryllia-insulated, molybdenum-sheathed W-Re alloys) failed when we attempted to do so.

The DTA curves for the limestone-sand concrete sample (4.9 g) yielded solidus and liquidus temperatures of 1120 and 1295°C, respectively. The composition of the calcined limestone-sand concrete may be approximated as 37 wt % CaO, 40 wt % SiO_2, 13 wt % MgO, 7 wt % Al_2O_3 (combining Al_2O_3 and Fe_2O_3), and 3 wt % other ingredients (mainly Na_2O). The Na_2O-CaO-MgO-Al_2O_3-SiO_2 phase diagram[10] has been studied in some detail; it contains compositions similar to that of the limestone-sand concrete. Ternary sections of this phase diagram show that a solidus-liquidus temperature range of 1120 to 1295°C is reasonable for the limestone-sand concrete. The DTA curves for the mixture of limestone-sand concrete (4.9 g), urania (10.2 g), and zirconia (2.9 g) indicated a solidus temperature of 1087°C and a liquidus temperature greater than 2365°C.

For the siliceous concrete sample (6.2 g), no crystallization peaks were detected in the DTA curves; instead, the sample exhibited a glass transition extending from 1130 to 1250°C. These temperatures are not equilibrium solidus and liquidus temperatures. Skokan et al.[4] reported the "softening temperature" of this concrete to be ~1140°C, and also noted that this softening temperature is more relevant than the thermodynamic crystallization temperature because the silicate-type melt solidifies to a glass. Our 1130°C value for the onset of the glass transition is in good agreement with the previously reported value of 1140°C.

---

[9]E. M. Levin, C. R. Robbins, and H. F. McMurdie, *Phase Diagrams for Ceramists*, American Ceramic Society, Columbus, OH (1964).

[10]E. M. Levin, C. R. Robbins, and H. F. McMurdie, *Phase Diagrams for Ceramists, 1969 Supplement*, American Ceramic Society, Columbus, OH (1969).

[11]E. M. Levin and H. F. McMurdie, *Phase Diagrams for Ceramists, 1975 Supplement*, American Ceramic Society, Columbus, OH (1975).

To the siliceous-concrete sample (6.2 g) were then added 12.7 g UO_2 and 3.6 g ZrO_2. The DTA curves for this mixture over the range 900 to 2300°C indicated a solidus temperature of 1134°C, very close to that for the siliceous concrete, and a liquidus temperature of 2276°C. Our earlier studies[7] indicated that a UO_2-ZrO_2 phase and a silicate phase were present on cooling mixtures of UO_2, ZrO_2, and siliceous concrete. Phase diagrams[10] are available for the SiO_2-UO_2 and SiO_2-ZrO_2 systems, but not for the UO_2-ZrO_2-SiO_2 system. Our measured liquidus temperature of 2276°C for the mixture of UO_2-ZrO_2 with siliceous concrete appears to be reasonable when compared with the liquidus temperatures in the SiO_2-UO_2 and SiO_2-ZrO_2 systems.

The liquidus-solidus temperatures from our DTA measurements are plotted in Fig. VIII-1; the values for UO_2-ZrO_2 (at 0 wt % concrete) were taken from the published phase diagram.[11] Also shown in Fig. VIII-1 are hypothetical liquidus-solidus curves obtained by assuming limited solubilities between the urania-zirconia-calcia phase and the concretes; these curves are not calculated from any theoretical model. The limited-solubility assumption, which is supported by our earlier phase studies,[7] is more reasonable than the solid-solution assumption currently employed in the CORCON code. The solidus-liquidus temperature intervals shown in Fig. VIII-1 are hundreds of degrees greater than the ideal-solution values currently employed in CORCON. At 27.5 wt % concrete and 72.5 wt % UO_2-ZrO_2, our measured values for the liquidus and solidus temperature differ by over 1200°C, while the differences in CORCON range from 500 to 750°C.

Additional data (at approximately 10, 60, and 85 wt % concrete) are needed to refine the hypothetical liquidus-solidus curves shown in Fig. VIII-1 and to establish the curves over the entire range of core-concrete mixtures that may be encountered in a hypothetical severe reactor accident. It is possible, for instance, that eutectic-type liquidus curves will be found for mixtures of either limestone concrete or limestone-sand concrete with UO_2-ZrO_2 since CaO forms eutectics with both UO_2[9] and ZrO_2.[11] Mixtures of siliceous concrete with UO_2-ZrO_2 (see phase diagrams for SiO_2-UO_2 and SiO_2-ZrO_2 systems[10]) are also likely to have complex liquidus-solidus curves.

B. *Support Studies for New Production Reactor*

A variety of nuclear materials are used in U.S. nuclear weapons. One of these, tritium, is rare in nature and must be produced in a nuclear reaction to obtain the quality necessary for manufacturing and maintaining nuclear weapons. Since tritium radioactively decays, weapons production requires a constant and reliable source of tritium. The only practical method for producing large quantities of tritium is to irradiate lithium targets with neutrons in a reactor designed for that purpose. The DOE initiated the New Production Reactor (NPR) Program to plan, design, and construct safe and environmentally acceptable new reactor capacity for an assured supply of tritium. The CMT Division is supporting this program by performing the following studies on an NPR that is a heavy water reactor (HWR-NPR): design studies for seals that meet stringent requirements on tritium control, calculational studies of detritiation requirements in the event of accidental releases of tritiated species into containment, and calculational and experimental studies of fission product release in a severe accident.

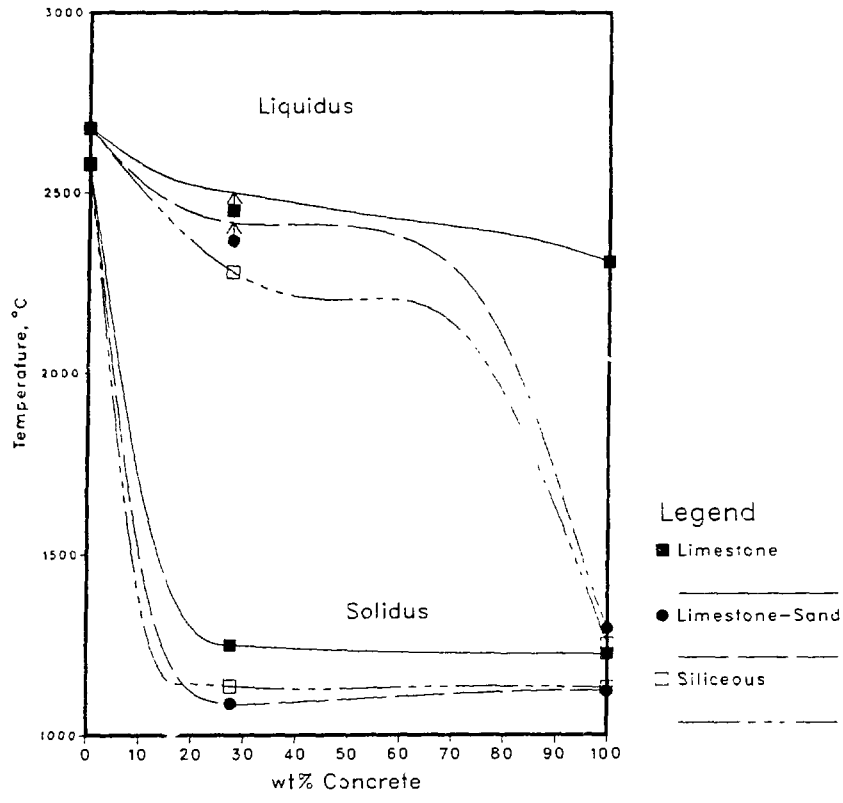

Fig. VIII-1. Liquidus-Solidus Data and Hypothetical Curves for Urania-Zirconia (1.625:1 Mole Ratio) and Concrete Mixtures. Arrow on top of symbols indicates "greater than." Data at 0 wt % concrete are for UO_2-ZrO_2 alone.

1. Seal Design

The objective of this effort was to determine guidelines for designing effective seals to be used for the tritiated water systems in the HWR-NPR. Seal design practices that are acceptable in pressurized-water and boiling-water reactors will not be acceptable for the HWR-NPR because of the stringent requirements on tritium control. Currently, the commercial nuclear power industry allows water leak rates to containment of 0.0065 L/s from unknown sources and up to 0.065 L/s from known sources. With a leak rate of 0.065 L/s being acceptable, the relative humidity within the containment buildings of commercial reactors is often 100%. At a water leak rate of 0.0065 L/s for the HWR-NPR (i.e., ten times lower than the commercial specification), the atmospheric tritium concentration within containment (volume of 10^5 m^3) would rise to 40 $\mu Ci/m^3$ in 10 min at a heavy-water tritium concentration of 1 Ci/L. An unprotected worker would receive a dose of 0.5 rem in only 100 h (~5 rem is the annual goal for each worker in the HWR-NPR). The development of seal systems which have cumulative leak rates $\leq$0.00026 L/s (30 times lower than any commercial specification) would be highly desirable for the HWR-NPR.

Regulatory and/or maintenance requirements have driven the development of new seal materials and/or concepts for nuclear reactors within the United States. Currently, asbestos valve packings and gaskets are being replaced to meet Environmental Protection Agency requirements and to reduce chloride leaching to the coolant from asbestos. Manufacturers have used graphite materials, including several types of expanded graphite, to replace asbestos in gaskets and valve packings. The expanded graphite forms are the most useful; however, each has a different leak rate for different seal designs, and leak rates for retrofits with graphite packing are not optimized. Thus, guidelines for seal designs with graphite in the HWR-NPR are needed to achieve lower leak rates.

In this report period, we determined the state of the art in seal development by reviewing the relevant literature for the design of flanges, elastometers, valves, and pumps. Organizations that have sponsored or generated sustained programs in seal design are Electric Power Research Institute, Atomic Energy of Canada, Ltd., and British Hydromechanical Research Association. Guidelines for the design of seals for the coolant system in the HWR-NPR were derived from their research as well as operating experience with commercial reactors in the United States, Canada, and Europe. Detailed discussion of the guidelines is given in an ANL report.[12] These guidelines should be especially important in designing the flange seal on the reactor head; the dynamic seals for the feed tubes, control rods, and safety rods; isolation valves; and reactor pumps. Additional capital costs may be incurred by following these guidelines, but they will probably be offset by the lower operating costs and other benefits derived from long-term reactor operation with seals having minimal leak rates.

2. Containment Habitability

The principal objective of this effort in the HWR-NPR Program is to provide an analytic tool for meeting the detritiation requirements in the event of accidental releases of tritiated species into the HWR-NPR containment environment given a particular release and subsequent removal scenario. A critical parameter is the time required to reduce the activity within the containment structure to a level that is acceptable for human entry (for the purpose of repair, maintenance, etc.) without elaborate protective measures. The reactor containment is composed of different compartments. We are developing a detailed model for detritiation in an individual compartment. This single-compartment model will be integrated into a multi-compartment effort for the total containment environment, which is being coordinated by Westinghouse Savannah River Laboratory.

Because of the oxidizing containment environment, the tritiated species in the event of leakage is expected to be dominated by DTO. This result is in contrast to the fusion reactor environment where both HT and HTO species are expected.[13,14] Furthermore, in the present

---

[12]P. A. Finn, *Guidelines to Achieve Seals with Minimal Leak Rates for HWR-NPR Coolant System Components*, Argonne National Laboratory Report ANL-90/29, in press.

[13]S. Tanaka, F. Ono, T. Masegi, and Y. Takahashi, Fusion Eng. Design 7, 353 (1989).

[14]R. G. Clemmer, R. H. Land, V. A. Maroni, and J. M. Mintz, *Simulation of Large Scale Air Detritiation Operations by Computer Modeling and Bench Scale Experimentation*, Argonne National Laboratory Report ANL/FPP/77-3 (1977).

detritiation model for fusion reactors, detailed consideration is given to the temporal and spatial evolution of the penetration profile of leaked species (e.g., DTO and D_2O) into structural components, which are assumed to consist of concrete walls with a barrier/coating on their inner surface (i.e., the surface facing the containment chamber). For the results that follow, the barrier/coating is considered to be epoxy paint. However, the model could easily be used for barriers of other materials, e.g., steel, provided the appropriate materials characteristics such as diffusion coefficient and adsorption rate constant are employed.

We developed a Dynamic Tritium Release and Analysis Model (DTRAM), which simulates the detritiation processes in the event of either chronic or burst releases of tritiated species into the containment structure of the HWR-NPR. The model incorporates the interaction between vapor-phase species and species on the surfaces and the bulk interior of structural components. The interactions include exchange, desorption, adsorption, dissolution, and bulk diffusion. The boundary conditions were chosen to be consistent with the physics and chemistry of the system. For example, a condition that is consistent with the dynamics of the adsorption/desorption processes on the surface of the barrier has been adopted. At the same time, the outer boundary condition for the concrete wall is chosen to be consistent with the expectation that the transport of tritiated species through the concrete is diffusion limited. The materials characteristics were obtained from an extensive literature search supplemented by available information from literature on fusion-technology-related activities.[13,14]

We carried out a series of calculations using DTRAM for both chronic and burst release scenarios. Figure VIII-2 shows the case for a burst release of tritiated species with a duration of 3×10^5 h into a chamber with a volume of 1.6×10^5 m^3. The concentrations of DTO in the vapor phase as well as in various components of the structural materials are shown as a function of time. The vapor-phase concentration is the highest up to approximately 10^3 s. Then, it reaches a steady state from which it abruptly declines after the leakage is stopped at ~ 3×10^5 s. However, the concentrations in the paint and the concrete continue to rise long after the vapor concentration has reached a steady state. For the paint surface, the concentrations actually surpass those of the vapor phase by well over an order of magnitude before they decline. For the concrete surface, they reach a lower but still significant level at about 10^8 s. This behavior indicates the relative difficulty of removing tritiated species from structural materials compared with the vapor species. This difficulty is primarily due to the lower transport rate in a heterogeneous structure such as concrete. The time necessary to reduce activity level to an acceptable regime is dominated by the retention capability of tritiated species of the structural materials. Thus, the present analysis indicates that one of the primary objectives in detritiation is to select the right combination of barrier/concrete materials and configuration such that tritium permeation is minimized in the first place.

It is important to realize that despite the "open" nature of the barrier/concrete structural components (in the sense that tritiated species can, in principle, diffuse through these structural units to be released to the external environment), the present calculational study indicates that virtually no such escape occurs. Even after 10^8 s, the concentration level 1 m into the concrete was calculated to be only of the order of 10^{-10} $\mu Ci/m^3$, a truly infinitesimal amount. Most of the DTO that penetrates into the concrete remains close to the paint/concrete interface even after such a long period of time. The important operating parameters here are the low value

of the effective diffusion coefficient of water in paint and concrete and the thickness of the concrete barrier used (~ 2 m). These factors give rise to the result of the virtual absence of tritiated-species escape from the concrete to the external environment.

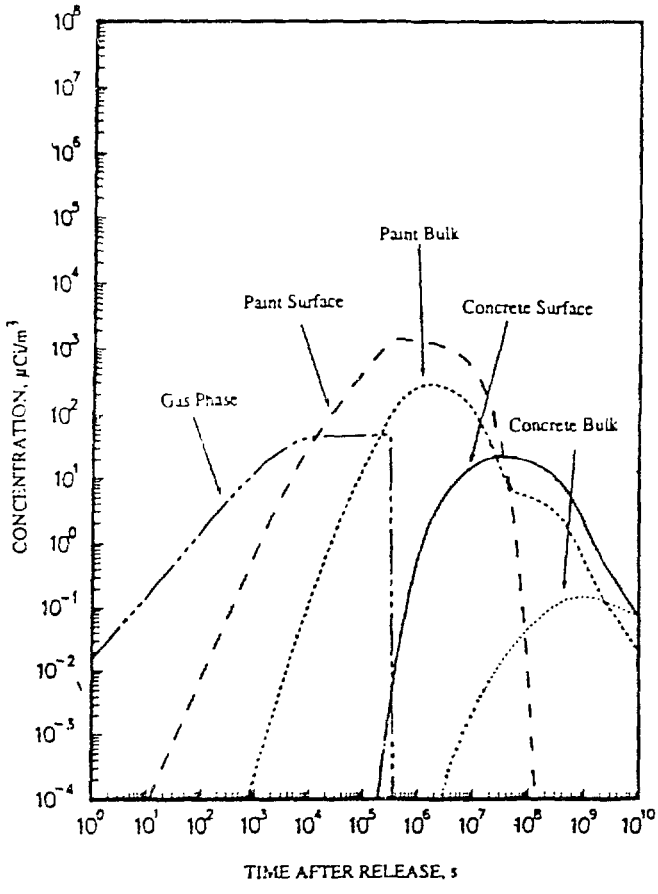

Fig. VIII-2.

Calculated Concentrations of DTO in Vapor Phase, Concrete, and Paint after Burst Release of Tritiated Species into Single Chamber

The effective diffusion coefficient of tritiated water through concrete is represented by the molecular diffusion of tritiated water through the capillary pathways that extend throughout the porous concrete medium. This molecular diffusional process is significantly affected by the convoluted nature of the capillary network and the (reversible) trapping of tritium on the surfaces of those capillaries by exchange and/or adsorption processes. These factors render the effective diffusion coefficient dependent on the composition and microstructure of the concrete, which, in turn, are affected by the method in which the concrete is processed. For the purpose of the present study, we circumvented accounting for these factors, in part, by using experimentally determined effective diffusion coefficients available in the literature. These transport properties are valid for the class of concrete used in those experiments The same approach was used for the molecular diffusion of tritiated species such as DTO through paint. Correlating quantitatively the general dependence of transport properties of tritiated species in concrete and paint on their microstructure is an important issue that needs to be investigated in future work.

3. Fission Product Release from Fuels and Target in Severe Accident

The objective of this effort is to develop models that will predict release of fission products and tritium from Al-U fuel and Al-Li targets in a severe accident with the HWR-NPR. The fission product and tritium release will be established under various conditions: initial release from fuel during melting, release from targets during melting, long-term release from melts as a function of temperature, and release from molten aluminum during high-temperature oxidation or burning. The work will include thermodynamic analyses using the SOLGASMIX computer code[15,16] to establish vapor species and their pressures for fuel only, target only, and fuel/target mixtures. Experiments will also be performed using transpiration and mass spectrometry to establish vapor pressures of species in fuel, targets, and other components.

We are using the transpiration technique for this work because it is uniquely suited for investigating all aspects of the release and transport process. The transpiration technique involves passing a gas at a high temperature and known flow rate over the material to be studied and then measuring the amount of material volatilized. Transpiration experiments will be performed as functions of flow rate, temperature, and condensed-phase composition. A high-temperature quadrupole mass spectrometer will be used to identify and measure species pressures where the transpiration method fails to identify low partial pressure gases. In the experiments to be performed, mixtures of Al-U and Al-Li with selected fission products (Cs, I, Te, Ba, Sr, Ru, La, and Mo) will be tested in flowing steam-hydrogen-helium mixtures at temperatures up to 1400°C.

a. Preparations for Experimental Work

Preliminary calculations showed that, because both fission-product I and Cs have such hign partial pressures, difficulty may be experienced in dissolving them in aluminum. In experiments involving the melting of fuel and target, mixtures of Al and U in the fuel and Al and Li in the target will be reacted with simulated fission products (I, Cs, Te, Sr, Ba, La, Ru, and Mo). Both elemental Cs and I will vaporize before aluminum melts as the temperature is raised from room temperature. The pressure of cesium is almost an atmosphere at the melting point of aluminum (660°C). Iodine pressure is much higher, boiling at 185°C. Since the vapor pressures of Cs and I are too high, these two elements should be added to the fuel and target as compounds with lower vapor pressures. If cesium is added as CsI and Cs_2Te, tying up the I and Te, 60% of the cesium will be left as atomic cesium. Cesium is immiscible with U and Li and almost completely immiscible with Al (about 0.05 wt % Cs). We have not found any thermodynamic data for other cesium compounds with Sr, Ba, Ru, or Mo. Measurements will be carried out with these substitutions to ensure that I and Cs will not be lost during the melting of the aluminum.

We attempted to find container materials compatible with Al-U fuel, Al-Li target, and simulated fission products at temperatures as high as 1400°C. These materials will be

---

[15]G. Eriksson, Chemical Scripta **8**, 100 (1975).

[16]T. M. Besmann, *SOLGASMIX-PV, A Computer Program to Calculate Equilibrium Relationships in Complex Chemical Systems*, Oak Ridge National Laboratory Report ORNL/TM-5775 (1977).

used in experiments to determine the extent of fission product release expected in a severe accident. We considered the enthalpies of formation for oxides, carbides, borides, and nitrides. Since aluminum oxide is compatible with the fuel, target, and fission products, and since aluminum oxide crucibles and tubes are readily available, aluminum oxide was chosen as the containment material. One disadvantage of aluminum oxide as a containment material is the problem of distinguishing between condensed aluminum and the aluminum in the oxide tube. In cases where this is necessary, we will use another material.

b. Preliminary Calculations for Fuel-Target-Fission Product Mixtures

The initial SOLGASMIX calculations were performed for U-Al fuel, Li-Al target, and selected fission products (Cs, I, Te, and Ba) at 727 and 1427°C. The temperature of 727°C was selected because it is slightly above the melting point of the intermetallic compound, LiAl; the temperature of 1427°C is a little higher than the 1400°C considered to be the upper temperature of interest. For the calculations, we used thermodynamic properties for species from the JANAF tables[17] and Barin and Knacke.[18] The following conclusions were reached: the species LiI is important in both gaseous and condensed phases; tellurium is bound by uranium as UTe in the condensed phase, especially at the lower temperature; iodine is not bound as UI_3 or AlI_3 either in the gas or condensed phases; and AlTe is significant in the gas phase.

In the available time, no inquiry into the ternary system, U-Al-Li, was made. It will be important to determine how immiscible the U-Al and U-Li systems are so that the most realistic calculations of distributions of fission products may be made. Experimental exploration of the overall features of the U-Al-Li phase diagram could be pursued by thermal analysis or quench-and-analyze techniques. A further question to be examined is whether it is more realistic to group the salt-like species (e.g., LiI, CsI, BaI_2, Li_2Te) as a separate phase rather than as solute in the metallic phases.

In the calculations, UTe was included as a species in the condensed phases, although no thermodynamic data for it were in the consulted literature sources. Instead, data for USe were used. The importance of UTe that emerged suggests that more detailed search for information or experimental efforts to derive its thermodynamic properties would be useful future work.

C. *Thermophysical Properties Studies*

Measurements and analyses are being performed to provide needed information on the thermodynamic and transport properties of Integral Fast Reactor (IFR) fuels. In 1990, our effort was focused on gaining a more thorough understanding of the phase relations involved in the

---

[17]M. W. Chase, Jr., C. A. Davies, J. R. Downey, Jr., D. J. Frurip, R. A. McDonald, and A. N. Syverud, *JANAF Thermochemical Tables*, 3rd ed., National Bureau of Standards, Washington, DC (1986).

[18]I. Barin and O. Knacke, *Thermochemical Properties of Inorganic Substances*, Springer-Verlag, Berlin (1977).

U-Pu-Zr fuel and in fuel-cladding systems. Also investigated were metallic fuel systems containing minor actinides, particularly, Np, Am, or Cm.

1. Plutonium-Uranium System

Calculation of the U-Pu-Zr phase diagram requires thermodynamic functions for all phases existing in the three binary subsystems; the ternary phase diagrams can be calculated from these functions. We have already completed an analysis of the U-Zr[19] system and have begun a similar analysis of the Pu-U system. The general methods used in our analyses[20,21] involve the critical evaluation and analysis of all relevant thermodynamic and phase equilibrium data for the system to obtain mathematical expressions for the thermodynamic properties of all phases as functions of composition and temperature. In this report period, we derived expressions for the thermodynamic properties of all eleven phases in the Pu-U system. The calculations were performed with programs of the F*A*C*T* (Facility for the Analysis of Chemical Thermodynamics) computer system based in Montreal.[20]

Aside from the phase diagram itself,[22] relatively little thermodynamic data exist for the Pu-U system. Chiotti et al.[23] have summarized the available data, which appear to be imprecise. In assessing the Pu-U system, we found that the melting transition for uranium presented a problem.[19,24] Briefly, the generally accepted value for the enthalpy of fusion (ΔH_f°) of uranium at the melting point, 2185 cal/mol (9146 J/mol),[25] appears to be inconsistent with the solidus-liquidus reported for the Pu-U system by Ellinger et al.[26] Another value for ΔH_f° was obtained by Savage and Seibel, 2900 cal/mol (12,100 J/mol), [27] which agrees better with the Pu-U phase diagram. We resolved this discrepancy in favor of ΔH_f° of uranium recommended by the International Atomic Energy Agency.[25] The result is that, while this ΔH_f° agrees reasonably well with the Pu-U liquidus, it results in a somewhat higher solidus. Ellinger et al.,[26] however, reported difficulties in measuring the solidus.

Figure VIII-3 shows the Pu-U phase diagram of Peterson and Foltyn.[22] The intermediate η and ξ phases presented the greatest difficulties in performing our assessment. We

---

[19]L. Leibowitz, R. A. Blomquist, and A. D. Pelton, J. Nucl. Mater. **167**, 76 (1989).

[20]C. W. Bale, A. D. Pelton, and W. T. Thompson, *F*A*C*T* Guide to Operations*, McGill University/Ecole Polytechnique, Montreal (1985).

[21]A. D. Pelton, in *Physical Metallurgy*, 3rd ed., R. W. Cahn and P. Haasen, eds., Chapter 7, North-Holland Publishing, New York (1984).

[22]D. E. Peterson and E. M. Foltyn, Bull. Alloy Phase Diagrams **10**, 160 (1989).

[23]P. Chiotti, V. V. Akhachinskij, I. Ansara, and M. H. Rand, *The Chemical Thermodynamics of Actinide Elements and Compounds - Part 5, The Actinide Binary Alloys*, International Atomic Energy Agency, Vienna (1981).

[24]L. Leibowitz, E. Veleckis, R. A. Blomquist, and A. D. Pelton, J. Nucl. Mater. **154**, 145 (1988).

[25]F. L. Oetting, M. H. Rand, and R. J. Ackermann, *The Chemical Thermodynamics of Actinide Elements and Compounds - Part I, The Actinide Elements*, International Atomic Energy Agency, Vienna (1976).

[26]F. H. Ellinger, R. O. Elliott, and E. M. Cramer, J. Nucl. Mater. **3**, 233 (1959).

[27]H. Savage and R. D. Seibel, *Heat Capacity Studies of Uranium and Uranium - Fissium Alloys*, Argonne National Laboratory Report ANL-6702 (1963).

expected that extrapolation of the appropriate phase boundaries to pure U and pure Pu would provide some guidance for estimating hypothetical transition temperatures. However, there is no reasonable way to extrapolate the two-phase $\eta + \xi$ field to the plutonium edge in the phase diagram. We took this to indicate some internal inconsistency in that portion of the diagram. Other regions of the diagram were also used to help determine parameters for these two fields. For example, the wide two-phase ξ + U($\propto$) field seems to be well supported experimentally. Because the boundaries are essentially parallel, the entropies of the $\xi \rightarrow$U($\propto$) transitions for pure U and pure Pu were taken to be zero.

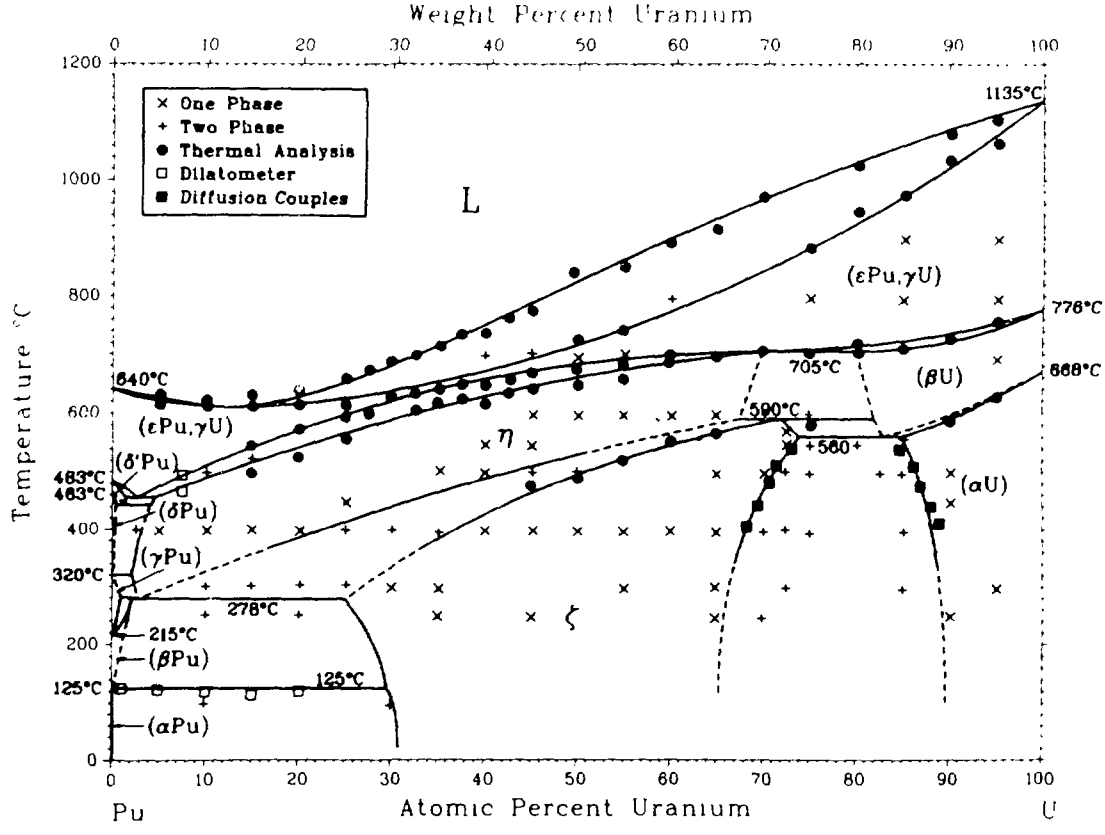

Fig. VIII-3. Published Plutonium-Uranium Phase Diagram from Peterson and Foltyn.[22] (Reproduced with permission.)

Our calculated Pu-U phase diagram is shown in Fig. VIII-4 and, in general, is similar to the diagram of Peterson and Foltyn[22] shown in Fig. VIII-3. As we discussed above, our solidus is higher than that in the literature because of the value chosen for ΔH_f° of uranium. The $\varepsilon + \eta$ boundaries are consequently shifted as well. The minimum in the calculated solidus-liquidus appears at 626°C and about 10 at. % U, compared with the Ellinger et al.[26] values of 610°C and 12 at. % U.

The region shown in Fig. VIII-3 between 560 and 705°C contains three invariants. Our calculated invariant at 702°C agrees well with Fig. VIII-3. Our calculated two-phase η + U(β) field differs from that shown in Fig. VIII-3, but there are essentially no experimental data

for that area. At 590°C we could not maintain the broad two-phase ξ + U(α) field and also produce a peritectoid. We chose to maintain the ξ + U(α) region because it appeared to be well supported experimentally and to modify the transition at 590°C to produce a eutectoid. However, the calculated ξ-η-U(β) eutectoid, which appears at 586°C, is not in serious disagreement with the experimental data.[22] Also, the calculated ξ-U(β)-U(α) eutectoid at 557°C is in good agreement with Fig. VIII-3. In general, only a small number of experimental points need be rejected in our calculated diagram. Recent information obtained from diffusion studies,[28] however, indicates that the two-phase U(β) + ε field may be wider than is shown in the calculated diagram. Because of the requirements imposed by the enthalpy and temperature of the U(β)→U(γ) transition, some modification of that region may be required.

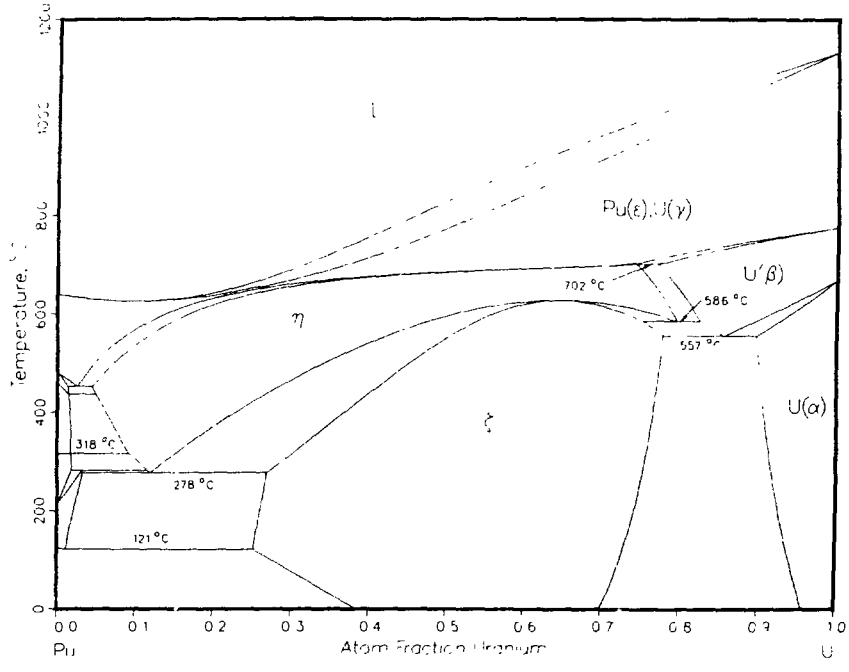

Fig. VIII-4. Calculated Plutonium-Uranium Phase Diagram

2. Iron-Uranium System

Some regions of the Fe-U phase diagram have been carefully studied, but there are significant regions which have received little attention. In a preliminary calculation of the Fe-U system, we were unable to generate a model that would reproduce the liquidus curve in the published Fe-U phase diagram.[29] Because of the importance of this system in analysis of fuel-cladding compatibility, we conducted some measurements using DTA in the composition region in question. A refined phase-diagram calculation was then performed.

---

[28]M. C. Petri and M. A. Dayananda, Purdue University, private communication (September 6, 1990).

[29]T. B. Massalski, ed., *Binary Alloy Phase Diagrams*, American Society for Metals, Metals Park, OH (1986).

The DTA measurements were performed using a thermal analysis instrument which had been installed in a helium-atmosphere glovebox for related work on plutonium-containing alloys. Calibrations were performed by measuring the melting points of a number of high-purity metals, including Standard Reference Materials obtained from the National Institute of Standards and Technology.

Our experimental data are shown in Fig. VIII-5 superimposed on the phase diagram of Massalski,[29] along with some data of Michaud.[30] We confirmed the 725 °C eutectic, with our mean value being 721 °C. Our experimental liquidus in this region differs somewhat from that in the published diagram. Also, Massalski[29] showed the iron-rich eutectic at 1055 °C; we found it at 1071 °C, very close to the temperature of 1080 °C reported by Gordon and Kaufmann.[31] Our experimental liquidus in this region is different from the published diagram but is consistent with Michaud's data.[30] Scanning electron microscopy of residues from our DTA tests confirmed the general expectations for the composition of the phases in this system.

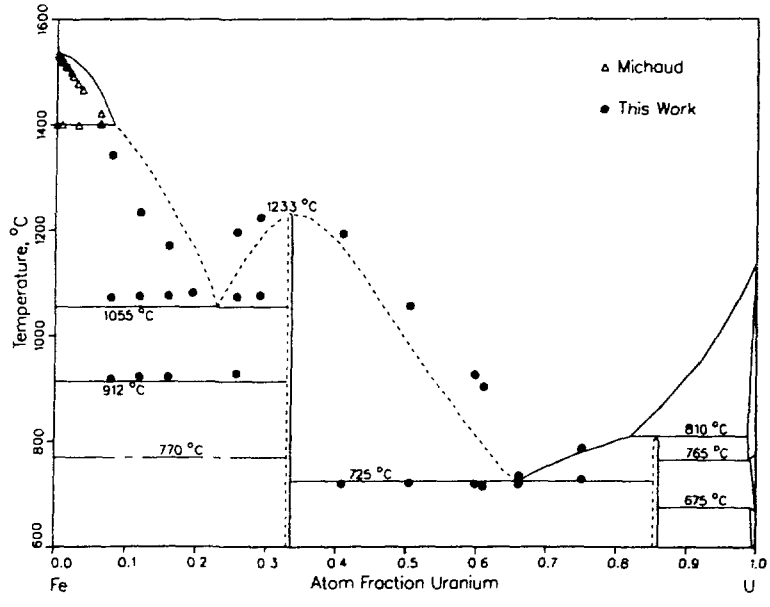

Fig. VIII-5. Uranium-Iron Phase Diagram of Massaliski[29] along with Data from this Work and Michaud[30]

We calculated the Fe-U phase diagram by the same methods as used for the U-Pu system. Figure VIII-6 shows our calculated Fe-U phase diagram (solid curve) along with our experimental data and the data from Michaud.[30] Our calculated Fe-U phase diagram, in general, is similar to the diagram of Massalski shown in Fig. VIII-5 but agrees better with our measurements. The major differences are in the liquidus curve, which had not been previously well defined, and in the temperature of the iron-rich eutectic. Our liquidus curve near pure iron

[30]G. G. Michaud, Can. Metall. Q. **5**, 355 (1966).
[31]P. Gordon and A. R. Kaufmann, Trans. AIME **188**, 182 (1950).

agrees well with the data of Michaud[30] and shows the correct theoretical limiting slope. Overall, we believe the current Fe-U diagram to be a reasonable representation of the system. Future work will include phase diagram calculations of some ternary iron-containing systems.

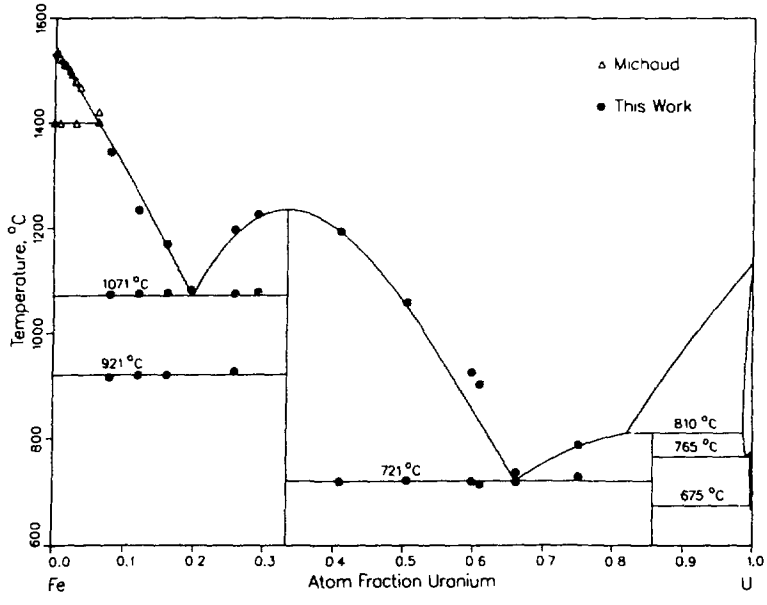

Fig. VIII-6. Calculated Uranium-Iron Phase Diagram[29] along with Data from this Work and Michaud[30]

3. Minor Actinide Systems

In several IFR fuel cycle concepts under consideration, the recycled fuel could contain concentrations of the so-called minor actinides, which would have an effect on the fuel properties and behavior. We conducted a preliminary analysis of metallic fuel systems containing the minor actinides.

In considering the addition of so-called minor actinides to IFR fuel, one must recognize that the actinides are not simple analogs of the rare earth elements, the lanthanides. In the lanthanides, the 4f electrons are highly localized and interact little with electrons in the 5d shell. In contrast, in the "light" actinides, through plutonium, the 5f electrons interact strongly with 6d and 7s states, thus forming a series more akin to the 3d transition metals than to the lanthanides. With the "heavy" actinides beginning with americium, the 5f electrons are more localized, and this group behaves somewhat more as a lanthanide-like series. As a result, a great many properties of the actinide elements change markedly between Pu and Am.

Crystal structure and phase relations also change notably as one traverses the actinide series. The crystal structure that exists at the melting point is body-centered cubic (bcc) in the lighter actinides but changes after plutonium to face-centered cubic (fcc). A bcc phase

expected to exist for americium has evidently not been found.[32] The heavier actinides, beginning with americium, also show a double hexagonal close-packed structure, which is not seen in the lighter elements of the series. These differences are also shown in phase behavior, as illustrated by the Np-Pu and Am-Pu phase diagrams.[29] A broad solution field below melting is bcc for Np-Pu and fcc for Am-Pu. These effects could be elaborated upon but the main point is clear: properties of actinide-containing alloys can change markedly in going from Pu to Am. Thus, if IFR fuel alloys are to contain significant amounts of minor actinides, particularly Am or Cm, careful study will be needed on the behavior and properties of this fuel since essential data (including density, thermal conductivity, and phase relations) are not available.

D. *Fusion-Related Research*

A critical element in development of a fusion reactor is the blanket for breeding tritium fuel. We are conducting experimental and calculational studies with the objective of determining the feasibility of using lithium-containing ceramics (e.g., Li_2O, $LiAlO_2$, Li_4SiO_4, Li_2ZrO_3) as breeder material. We also completed conceptual design of the tritium processing systems for the International Thermonuclear Experimental Reactor (ITER)--a tokamak fusion reactor that will be used to test plasma operations and reactor components for prototype fusion power reactors.

1. Desorption Measurements for $LiAlO_2$-H_2-H_2O(g) System

The objective of this effort is to provide experimental data that describe the kinetics of desorption of H_2O(g) and H_2(g) from ceramic tritium breeders and enable designers and modelers to predict the retention and release of tritium, especially in regard to the effectiveness of H_2 as a promoter of tritium release. Temperature programmed desorption (TPD), an established technique for measuring activation energies and other kinetic parameters relating to desorption, is the experimental tool for this project. Our earlier work dealt with desorption from $LiAlO_2$ on which H_2O(g) had been adsorbed.[33] The present report concentrates on desorption of H_2O(g) from $LiAlO_2$ treated with H_2 in helium gas at high temperature.

a. Blank (Empty Tube) Experiments

As in the earlier work, measurements were made first on an empty sample tube to determine the tube effects. Simulated TPD runs [spikes of H_2(g) introduced manually to an H_2O(g)-containing helium gas at intervals during a temperature ramp] showed that the relationships between the peaks for H_2 and H_2O evolution as a function of time could be distorted if the tube was not stabilized. However, treatment for several days at 670°C (943 K) with 990 ppm H_2 in helium gas resulted in uniform H_2 and H_2O peaks throughout a 200-750°C (473-1023 K) temperature ramp. The tube was then considered stabilized.

---

[32] J. J. Katz, G. T. Seaborg, and L. R. Morss, *The Chemistry of the Actinide Elements*, 2nd ed., Chapman and Hall, New York (1986).

[33] M. J. Steindler et al., *Chemical Technology Division Annual Technical Report, 1989*, Argonne National Laboratory ANL-90/11, pp. 123-125 (1990).

In the blank experiments, N_2 appeared in the gas phase upon the introduction of H_2 and was comparable to the level of evolved H_2O. The evidence indicated that the N_2 was not an impurity in the gases and did not come from a leak. Instead, the stainless steel tubing appeared to be the source. Nitrogen is commonly found dissolved in steel and the ability of H_2 to "denitride" steel is a known process.[34] The significance of nitrogen for the desorption of H_2 and H_2O from a ceramic breeder is not yet clear and needs further study. For the present, we assume that nitrogen is inert in the H_2 and H_2O desorption processes.

b. Desorption from $LiAlO_2$ Treated with H_2

Earlier work had shown that multiple processes are involved in $H_2O(g)$ adsorption on, and desorption from, ceramic oxides that are candidates for tritium breeders in fusion reactors.[35,36] It is of particular interest to determine the adsorptive-desorptive processes when the gas phase contains H_2. Our TPD measurements were made on $LiAlO_2$ that was treated with 990 ppm H_2 in helium gas in a stabilized tube at 400°C (673 K). The pretreatment lasted for 20-264 h. Surface OH^- formed in this process later led to desorption of $H_2O(g)$. The temperature ramps were from 200 to 750°C (473 to 1023 K), typically at about 5.5°C/min. We studied desorption of $H_2O(g)$ from the $LiAlO_2$ into pure helium and into helium with 990 ppm H_2.

For desorption into pure helium, the plot of H_2 evolution remained at essentially the baseline level until a temperature of approximately 600°C (873 K) was reached. This result suggests that the amount of H_2 adsorbed at 400°C (673 K) in the period before the run is small or negligible, or incapable of being desorbed. The rise in evolved H_2 into pure helium seen at 600°C (873 K) is possibly the result of interaction of the evolved H_2O with the stainless steel tube wall and/or the evolution of H_2 dissolved in the steel during the pretreatment with H_2. Further study of apparently evolved H_2 remains to be done.

It is significant that H_2O evolution occurred in all tests (even when desorptions were into helium with 990 ppm H_2), and the kinetic parameters for its desorption were derived from the data. The plots of H_2O evolution were shown, by deconvolution, to be the sums of either two or three sub-peaks. An example of each case is shown in Figs. VIII-7 and VIII-8. The peaks are taken to correspond to first-order desorption processes involving different types of sites on the surface of the $LiAlO_2$, designated as types A, B, and C. The activation energies for desorption in both pure helium and He-H_2 mixtures were calculated to be ~18 kcal/mol (75 kJ/mol) for the A type and 23 kcal/mol (96 kJ/mol) for the B type. No C-type peak was observed with pure helium, and the activation energy for desorption was calculated to be 28 kcal/mol (117 kJ/mol) for the C type with the He-H_2 mixture.

---

[34]J. D. Fast, *Interaction of Metals and Gases*, Vol. 2, Macmillan, London (1971).

[35]J. P. Kopasz, A. K. Fischer, and C. E. Johnson, Proc. of the Second Int. Symp. on Fabrication and Properties of Lithium Ceramics, in press.

[36]A. K. Fischer and C. E. Johnson, Fusion Tech. **15**, 1212 (1989).

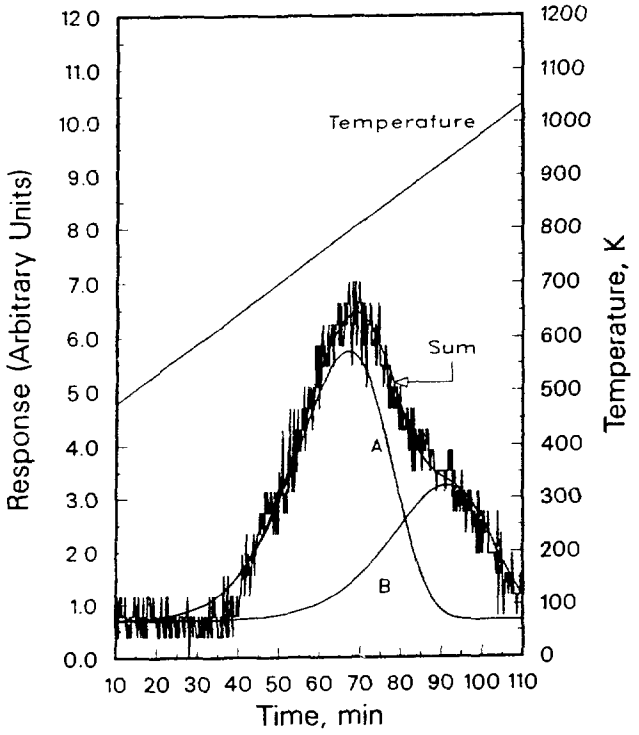

Fig. VIII-7.

Desorption of H_2O into Pure Helium after 120 h Pretreatment with 990 ppm H_2 in Helium at 400°C (673 K). Ramp rate is 5.6°C/min.

Fig. VIII-8.

Desorption of H_2O into Helium Containing 990 ppm H_2 after 20 h Pretreatment with 990 ppm H_2 in Helium at 400°C (673 K). Ramp rate is 5.6°C/min.

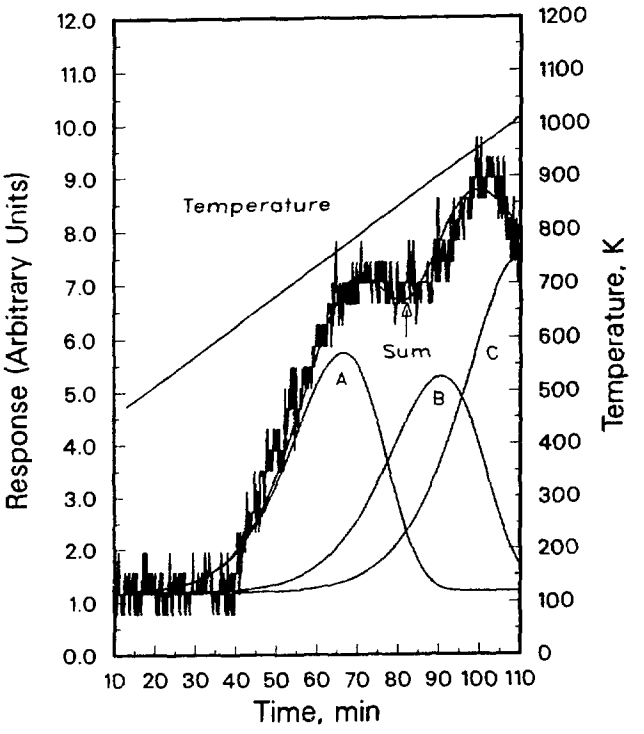

The peak magnitudes indicate that the frequently reported enhancement of tritium release attending the use of H_2 in the sweep gas might be related to increased population of B sites and to the emerging participation of C sites. Possibly, the soaking temperature of 400°C (673 K) was only marginally adequate to activate chemisorption of H_2 to populate the C sites. The conditioning of the $LiAlO_2$ at 400°C (673 K) with H_2 was at a relatively low temperature in the context of operation of solid breeders. The small effect of the H_2 addition observed here is consistent with the results from tritium residence-time measurements in at least two release experiments.[37,38]

A monotonic increase in the amplitudes of the A and B peaks was correlated with increased duration of pretreatment with H_2. This suggests that the buildup of surface OH^- was aided by the H_2 but was slow because the pretreatment periods were of the order of days. Thus, at higher pretreatment temperature, the buildup processes should be faster. Future work should inquire into whether the peaks increase in amplitude or if the relative peak populations shift for higher pretreatment temperatures.

The observation of first-order kinetics deserves consideration because of the generally accepted view that desorption of H_2O derived from chemisorbed OH^- on oxide surfaces is a bimolecular process involving recombination of OH^-.[39] The observation of first-order kinetics for a bimolecular process can be understood in terms of a theory originated by Lindeman,[40] which suggests that the overall process consists of bimolecular combination of OH^- to H_2O on the surface followed by unimolecular desorption of H_2O. The resulting rate equation predicts first-order kinetics if the rate constant for the reversal of the bimolecular step is greater than the rate constant in the forward direction of the unimolecular step. Different temperatures could alter the relationships among the rate constants so that the observed kinetics could become second order even though the same bimolecular-unimolecular mechanism operates.

Our value for the activation energy for desorption from the C peaks is close to the value reported by Kudo[41] for the activation energy of decomposition of LiOH (29.5 kcal/mol, 124 kJ/mol). Both are processes of $H_2O(g)$ evolution except that decomposing LiOH produces a Li_2O surface with scattered OH^- groups. The similarity in activation energies suggests that C-type OH^- sites on $LiAlO_2$ resemble OH^- sites on Li_2O in their H_2O-evolving behavior.

We are still uncertain whether released $H_2O(g)$ associated with the C peaks reflects only desorption from the surface, whether diffusion at high temperature from the bulk is

---

[37]M. Briec, J. Kopasz, S. Casadio, and H. Werle, "In-Pile Tritium Release from Lithium Ceramics and Influence of Surface Processes," Proc. of 1990 Symp. on Fusion Technology, in press.

[38]S. Tanaka, A. Kawamoto, M. Yamawaki, T. Terai, Y. Takahashi, H. Kawamura, and M. Saito, Fusion Eng. Design **8**, 155 (1989).

[39]A. K. Fischer and C. E. Johnson, in *Advances in Ceramics*, Vol. 25, American Ceramic Society, pp.29-39 (1989).

[40]W. J. Moore, *Physical Chemistry*, 3rd ed., Prentice-Hall, Englewood Cliffs, NJ (1962)

[41]H. Kudo, J. Nucl. Mater. **87**, 185 (1979).

increasingly augmenting the surface OH^- concentration, or if interactions are occurring between H_2 and the steel surface. These questions require further study.

2. Tritium Release Studies

a. Introduction

Tritium inventory is one of the key safety and economic issues for a fusion reactor design. It is desirable to minimize the tritium inventory during normal operation and during any transients which may occur to minimize the hazards related to any accidental release. Because of the high cost of tritium, it is desirable to minimize the amount of tritium needed to start up the reactor and operate to the point of tritium self-sufficiency. To accomplish these goals, one must have a thorough understanding of tritium transport in, and release from, the tritium breeding material. Current breeder blanket designs have focused on lithium ceramics as breeding materials; however, the mechanism of tritium release from these ceramics is not fully understood. We are investigating tritium release from these materials by performing laboratory (out-of-pile) experiments and analyzing results from in-pile experiments.

Our earlier developed model, which has been widely used to interpret experimental data on tritium release from lithium ceramics, considers diffusion in the grain and desorption from the surface as the rate-controlling mechanisms.[42] The model assumes a desorption mechanism which is pseudo first order in tritium, with desorption occurring with one constant activation energy. Other work has suggested that the desorption is second order in tritium, or that the desorption may be occurring with different activation energies.[36] We thus examined the validity of our diffusion-desorption model by comparing model predictions with tritium release data from in-pile and laboratory experiments.

b. Analysis of Results from In-pile Experiments

Tritium inventory in a ceramic breeder is dependent upon several key factors, including the tritium generation rate, the ceramic sample microstructure, and the purge gas composition. We analyzed in-pile experimental data on the effect of these parameters.

In the recent LILA-LISA experiment,[37] tests were performed to study the effect of the neutron flux, and consequently the tritium generation rate, on tritium release from Li_4SiO_4 and Li_2ZrO_3 samples. For a desorption mechanism which is first order or pseudo first order in tritium, the tritium residence time (defined as the inventory divided by the generation rate) will be independent of the generation rate, while for a desorption which is second order in tritium, the residence time will be inversely proportional to the square of the generation rate. We analyzed experimental data from Li_4SiO_4 samples tested at 450 and 500°C with He + 0.1% H_2 as the purge gas and two thermal neutron fluxes, 0.93×10^{17} and 0.40×10^{17} n/(m^2•s). The tritium residence times were independent of the neutron flux, indicating that the rate-controlling

[42]J. P. Kopasz, S. W. Tam, and C. E. Johnson, J. Nucl. Mater. **155-157**, 500 (1988).

mechanism is not second order in tritium. Since other factors indicate that desorption is the rate-controlling step for these samples, desorption is first order in tritium under these conditions.

Sample microstructure is a crucial factor affecting tritium release kinetics. Tritium inventory increases with increasing sample grain size; however, the dependence of the inventory on the grain size is also affected by the rate-controlling mechanism. We investigated the effect of the sample microstructure on tritium inventory in the TEQUILA experiment,[38] which included tests at 510-670°C on $LiAlO_2$ samples with different microstructures (grain radius of 0.15 to 6 μm). Results for experiments with He + 0.1% H_2 as the purge gas showed tritium residence times decreasing with decreasing grain size. This was also found to be the case in the LILA-3 experiment.[37] Further analysis of these data indicated that the tritium release is not controlled by diffusion processes. If diffusion was rate controlling, the ratio of the residence time for the large grain sample to that for the small grain sample would be 1600. The observed values (ranging from 10.8 to 26.6) are of the same order as that expected for desorption-controlled release (13.3). This finding suggests that desorption plays a major part in determining the tritium release under these conditions. Moreover, the slight deviations from the ratio expected from a pure desorption model suggest that other processes may play a minor role in determining tritium inventory.

In the TEQUILA experiment,[38] three purge gas compositions were investigated: He + 1.0% H_2, He + 0.1% H_2, and He + 50 ppm H_2 + 100 ppm H_2O. The tritium residence times derived from this experiment indicate that, for samples with small grain sizes, tritium release is better for a purge gas containing 1.0% H_2 than for one with 0.1% H_2. No differences were observed between the activation energies for desorption between these two purge gases. However, for the He-H_2-H_2O purge gas, the activation energy was lower than that for the other two gases. This leads to improved tritium release at low temperatures (460°C) for the He-H_2-H_2O purge gas, but poorer release at high temperatures (>500°C). The difference in the activation energies for these purge gases is consistent with earlier work in which the heat of adsorption was observed to vary strongly with the sample surface coverage.[36] These studies suggest that the tritium desorption activation energy is dependent on the hydroxide surface concentration.

c. Laboratory Experiments

In a joint project with Commissariat á l' Energie Atomique, Centre de Saclay, we performed several laboratory experiments on tritium release for $LiAlO_2$, one of the leading candidates for the breeder material. In these experiments, temperature anneals were performed on sintered $LiAlO_2$ pellet samples similar to those used in the TEQUILA experiment. Tritium release curves obtained from these experiments were in relative agreement with those of the in-pile experiments. The release curves were found to follow first-order kinetics, and the desorption rate constants were in good agreement with those determined from the TEQUILA data, considering that the purge gases were different (Ar-0.1% H_2 vs. He-0.1% H_2).

The laboratory experiments also revealed something that is not easily observed in the in-pile experiments, i.e., tritium is retained in the solid at low temperature, even after extended annealing times. For example, a sample of a preirradiated sintered pellet

composed of grains of 84-μm dia was annealed at 538°C for 1 week. A small tritium release peak was observed and decayed to the background level within 40 h. The anneal continued for an additional 120 h, with no further tritium release. The temperature was then increased to 850°C, which resulted in a large tritium release. These results indicate that the majority of the tritium is unable to leave the sample at 538°C, but is released at 850°C. Analysis of the kinetics of release at 538°C from in-pile experiments gives no evidence for the retained tritium at this temperature. This retained tritium suggests tritium exists in at least two distinct forms, one which is loosely held to the solid and a second which is more tightly bound to the solid. These two forms may be two different surface sites, with one site having a strong bonding energy, or may be different states in the bulk material, such as free tritium and tritium bound as a complex, such as a lithium-vacancy/tritium complex.

d. Conclusion

The results of our studies indicate that tritium release from lithium ceramics is controlled by diffusion and first-order desorption, with desorption playing the dominant role. The desorption activation energy is dependent on the purge gas composition and also appears to be a function of the surface hydrogen concentration. In addition, at low breeder blanket temperatures, tritium is retained in the solid. The retained tritium may be due to either surface or bulk effects. Laboratory annealing tests on pure and doped single-crystal materials are planned to identify the different states of tritium observed in the annealing experiments and to determine if tritium release characteristics can be improved by doping.

3. Tritium Inventory for ARIES Reactor Design

Using the diffusion-desorption model,[42] we estimated the tritium inventory for the breeder material in the ARIES fusion reactor design. The ARIES design represents an advanced concept whose blanket component uses Li_2ZrO_3 in sphere-pac form as the solid breeder, beryllium spheres as neutron multiplier, and SiC as the material of choice for the structural components. Input parameters to the model were derived from ARIES system design results that have been provided to us and include component dimensions, wall loading, tritium generation rates, volume fractions of breeder and multiplier, and maximum and minimum temperatures. A parabolic temperature profile was used to generate the temperature across the breeder bed. The diffusivity of Li_2ZrO_3 was taken from the literature.[43] Because there are no reported values for the desorption rate constant for this material, we used the corresponding quantity for Li_2O as recommended for design studies on ITER. The grain size was assumed to be 10 μm.

The results indicate that the total tritium inventory (per system surface area) at steady state is low, i.e., on the order of 8×10^{-12} mol/cm^2 (Fig. VIII-9). The steady state is reached in about 3000 s, a time that is fairly rapid. These results are a direct consequence of the relatively high-temperature operation for the design (600-700°C). One would expect that use of the "proper" desorption rate constant for Li_2ZrO_3, if and when it becomes available, would quantitatively alter the estimated inventory. However, due to the high temperature involved, the

[43]K. Okuno and H. Kudo, Fusion Eng. Design **8**, 355 (1989).

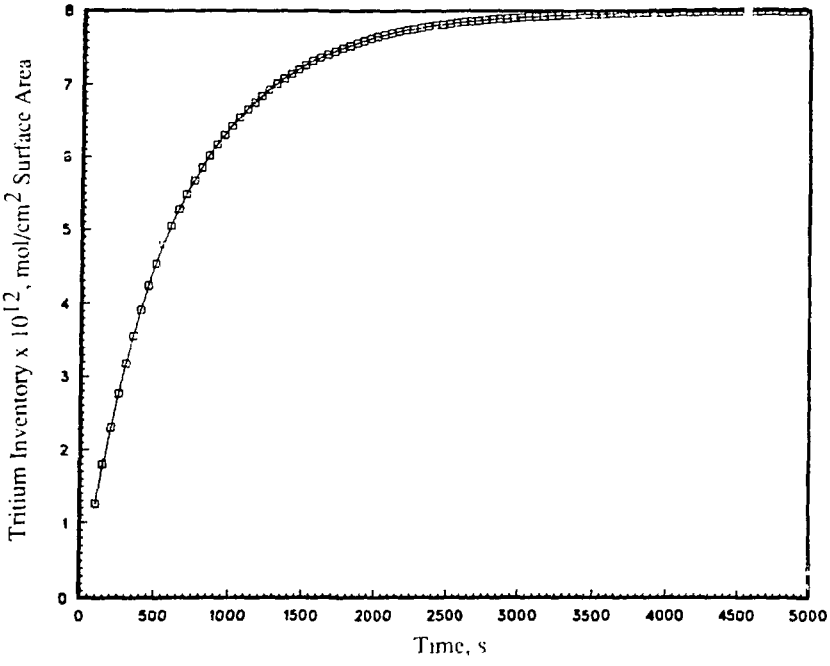

Fig. VIII-9. Total Tritium Inventory in Li_2ZrO_3 Breeder Calculated for ARIES Fusion Reactor Design

qualitative conclusion that the breeder tritium inventory would be low is expected to remain valid.

The above discussion pertains to the breeder inventory, which is not necessarily the same as total reactor-blanket inventory. This is particularly true for the ARIES design because of the intimate mixing of the breeder/multiplier components in sphere-pac configuration and the relative proximity of the SiC-composite structural materials. Because of the self-shielding effect and the small sizes of the breeder particles, a significant fraction of tritium generated within the breeder could end up in the beryllium multiplier and the structural materials via a recoil mechanism, where the tritium may become trapped owing to the potentially low transport coefficient for those materials. The limited and partly conflicting data in the literature indicate that tritium diffusion is extremely low in beryllium. In addition, under actual operating condition, the beryllium particles are likely to be coated with a BeO layer, which is not expected to enhance tritium escape from the multiplier. The diffusion coefficient of tritium in SiC is unknown and needs to be determined. Much further work is necessary to determine the tritium inventory in the multiplier/structural components.

4. Lithium Vaporization

Tritium may be found as LiOT within the ceramic breeder blanket. Depending on blanket temperature and the local tritium concentration, lithium (as LiOT) may be transported to cooler regions of the blanket. Such transport may cause loss of lithium from the blanket,

blocking of purge flow paths, and increase in tritium inventory. The objective of this effort is to investigate the transport of LiOT from the blanket material and corrosion of stainless steel structural material.

a. Measurements of LiOH(g) Transport

Preliminary experiments were carried out to determine if structural stainless steel could be corroded by LiOT(g) and/or LiOH(g) from the Li_2O blanket material. In this study, a silver boat was used to hold Li_2O with a 303 stainless steel sheet (1 x 3 cm) placed at desired distances (~0.5 or 0.1 cm) above the Li_2O. Neither the stainless steel sheet nor the sintered lithium oxide surfaces were flat enough to establish the very narrow separation distances exactly. The boat and plate were placed inside a silver-lined quartz tube, and the silver tube assembly was heated in a clam-shell furnace. Helium carrier gas containing a measured water concentration flowed through the silver tube at 750°C. Most of the LiOH gas, produced from water vapor and Li_2O, reacted with the stainless steel sheet. The remaining LiOH(g) condensed in cooler regions of the silver tube downstream from the Li_2O in the furnace. Three runs were completed at 10 cm^3/min (one without stainless steel sheet), and three at 100 cm^3/min.

After heating the boat to 750°C and cooling to room temperature, the boat was removed, and the silver tube was soaked in water to remove the LiOH (condensed in the silver tubing) for chemical analysis. The corrosion product formed by reaction of LiOH(g) with stainless steel was dissolved in nitric acid for lithium chemical analysis. The LiOH(g) pressure was calculated from the lithium analysis of the condensed LiOH in the silver tube and the ideal gas law.

The LiOH(g) pressure was determined by assuming that all the lithium condensed in the silver tube was entrained as LiOH(g) in the flowing helium. This, however, was not the case. At the low flow rate (10 cm^3/min), the apparent LiOH(g) pressures were an average of nine times higher than the equilibrium pressures calculated from Tetenbaum and Johnson.[44] Most of the LiOH (80-92%) thermally diffused to cooler regions of the silver tube. This was verified when the flow rate was increased to 100 cm^3/min, and the apparent LiOH pressures decreased to less than twice the equilibrium pressures calculated from Tetenbaum and Johnson's work.[44] At the higher flow rate, thermal diffusion was reduced to 39-53%, and the balance was entrained in flowing helium.

Table VIII-1 shows the lithium corrosion results for the six runs. There was reasonable agreement for calculated and measured lithium corrosion (i. e., within a factor of two) for runs 22, 23, and 26, but very poor agreement for runs 24 and 25. The separation distances for runs 24-26 may have been inaccurate because of a lack of plane surfaces and the relatively short distance between the Li_2O and stainless steel. The agreement between measured and predicted lithium corrosion for run 26 may have been fortuitous.

---

[44]M. Tetenbaum and C. E. Johnson, J. Nucl. Mater. **120**, 213 (1984).

Analysis of our attempts to measure corrosion of stainless steel and equilibrium pressure of LiOH(g) in a transpiration system led us to conclude that three processes occur simultaneously: (1) entrainment of LiOH(g) by the helium carrier gas, from its production in the hot zone, to condense in cooler regions outside the hot zone; (2) thermal diffusion of LiOH(g) to condense in cooler regions outside the hot zone; and (3) steady-state diffusion of LiOH(g) to the stainless steel, where LiOH(g) reaction corrodes the steel. Although we were able to measure the pressure of LiOH(g) for runs 23-25 within a factor of two of the accepted equilibrium value in the presence of stainless steel, we do not recommend this procedure. We believe a more reliable value can be obtained in the absence of any other material which will react with LiOH(g).

Table VIII-1. Lithium-Transport Results from Diffusion-Driven LiOH(g) Reaction with Stainless Steel

Run No.	He Flow, cm^3/min	Time, min	Distance,[a] cm	Weight Lithium, μg		
				Meas. for Ag Tube[b]	Meas. for SS Sheet[c]	Calc. for SS Sheet[c,d]
21	10	164	----	50	---	---
22	10	172	0.492	80	295	301
23	100	351	0.416	84	164	292
24	100	195	0.15	36	80	426
25	100	131	0.1	28	102	535
26	10	162	0.1	32	2800	1896

[a]Separation between Li_2O and stainless steel.
[b]Weight of lithium condensed on silver tube outside hot zone.
[c]Weight of lithium reacted with stainless steel sheet in hot zone.
[d]Calculated from equation of Treybal.[45]

b. Calculation of Stainless Steel Corrosion by LiOT

We used the above experimental results to calculate possible corrosion of structural steel in the ITER blanket driven by steady-state diffusion of LiOT(g) from the Li_2O blanket to the structural steel (303 stainless steel). For the calculations, we used ITER parameters furnished by the ANL Materials and Components Technology Division. For the reaction $Li_2O(s) + T_2O(g) = 2\ LiOT(g)$, we used Tetenbaum and Johnson's equilibrium constant[44] to calculate the pressure of LiOT at 450-750°C. The T_2O pressure, which is limited by the tritium breeding rate, was also calculated. The calculations apply to steady-state conditions where tritium is released at the design breeding rate (9.52×10^{-6}g tritium per day per gram of Li_2O).

The results of our calculations can be summarized as follows. The pressure of LiOH, in equilibrium with Li_2O, is proportional to the square root of the $T_2O(g)$ pressure and increases exponentially with temperature. The difference in LiOH and T_2O pressures varies by factors of 10^5 to 10^7. The T_2O pressure is relatively constant since it is fixed by the tritium

[45]R. E. Treybal, *Mass-Transfer Operations*, McGraw-Hill, New York, p. 22 (1968).

breeding rate. The transport of LiOH to the stainless steel is driven by the LiOH concentration gradient from that at the Li_2O surface and that at the steel surface. At the stainless steel surface, the pressure of LiOH is in equilibrium with that of $LiCrO_2$, $LiFeO_2$, $LiNiO_2$, or other mixed oxides of Cr, Fe, and Ni. The weight of Li_2O reacted per year per unit area of stainless steel at 450°C (5.33×10^{-3} g/cm^2 per year) is equivalent to 14% of the chromium in 303 stainless steel, which contains 18% chromium. The initial corrosion is controlled by diffusion of LiOT(g) in the pressure gradient. After a long period, the rate may be controlled by the diffusion of reactants in the corrosion layer or in the remaining steel alloy.

More experimental work is needed to verify and extend our calculations. Since the separation distance is so crucial, better methods for measuring it are needed, and longer runs are necessary to establish whether the corrosion rate is linear or decreasing with time.

5. Conceptual Design of Tritium Processing Systems for Breeder Blanket

The ITER will be fueled by tritium, which is bred in a blanket system that surrounds the plasma chamber. The mechanical design of the blanket is a series of semi-rectangular zones which contain water coolant, beryllium neutron multiplier, and Li_2O breeder material, with each zone isolated from the next by thin welded sections of stainless steel. Two separate helium purge streams are used to remove tritium from the Li_2O and the beryllium zones. Hydrogen (0.1%) is added to the helium stream used for the Li_2O zone.

We completed a detailed conceptual design for the tritium processing system needed for the Li_2O/Be blanket and reported it to the ITER design team.[46] Some highlights are reported here.

The processing system has three functions: (1) recover and purify tritium from the two purge streams, (2) remove waste products from the streams and recover the tritium in the waste products, and (3) recirculate the purge streams to the blanket zones. Components were selected to minimize the tritium inventory of the processing system, minimize waste products, and have the capability to withstand either an increase in the tritium release rate or leakage of water in the purge system. (The total tritium process inventory is < 20 g.)

The processing system has the following individual components. Filters placed at the purge stream exit from the blanket remove particulates, vapor species, and other impurities. Regenerative heat exchangers reduce the helium purge gas temperature from 400°C to -100°C. A set of cold traps separates water (0.47 kg/d) and 10% of the CO_2 from the helium. Two compressors and a storage system circulate the helium gas. A solid oxide electrolysis unit reduces water. A set of 5A molecular sieves at -196°C removes hydrogen isotopes, 1% of the helium, and all remaining impurities from the helium. A set of 5A molecular sieves at 25°C recovers H_2O, CO_2, and other impurities when the sieves at -196°C are regenerated and also

---

[46]P. A. Finn, D. K. Sze, and R. G. Clemmer, *Conceptual Design Considerations for the U. S. ITER Li_2O/Be Water Cooled Blanket, Revision 1.0*, Argonne National Laboratory Report ANL/FPP/TM-249 (1990).

removes water from the hydrogen stream from the electrolysis unit. A palladium/silver diffuser separates inert species from the hydrogen isotopes before the hydrogen is passed to a cryogenic distillation unit. An SAES getter held at 350°C prevents active impurities from entering the cryogenic distillation unit, if the diffuser fails. Waste products are sent to a waste recovery unit. Components are designed as modular units to minimize downtime if replacement of units is required.

To recover tritium from waste products, the waste recovery unit includes a set of 5A molecular sieves held at 25°C, a set of copper oxide beds held at 500°C, and a set of cold traps held at -100°C. If necessary, a set of zeolite beds at -196°C would trap radioactive Ar, Kr, and Xe, and a calcine solution would trap CO_2 (^{14}C) as calcium carbonate. The tritium is converted to tritiated water and recovered, while the nontritiated waste is passed to a stack system.

The three components unique to this processing system are the 5A molecular sieves, the solid oxide electrolysis unit, and the palladium/silver diffuser. Heating the sieves, held at -196°C, to -100°C will occur every two hours to minimize the in-process tritium inventory, most of which is in these sieves. The total residual tritium inventory trapped in these 5A molecular sieves after several years of operation can reach 134 g. To release this residual tritium requires prolonged heating of the bed at 250°C while hydrogen is circulated. Since this procedure is used to periodically remove H_2O, CO_2, and other impurities from these beds, the residual tritium inventory should be < 134 g.

The solid oxide electrolysis units have a minimum tritiated water inventory and have a high efficiency due to their high-temperature operation. A low capacity unit is used for the Li_2O purge stream since this zone is isolated from the water coolant. A high capacity unit is used for the beryllium purge stream since the water coolant is adjacent to this zone.

The palladium/silver diffuser prevents non-hydrogen species from entering the cryogenic distillation unit. Its use minimizes the tritium inventory and allows continuous processing. Because the gas stream which reaches the diffuser is > 95% hydrogen, the diffuser can operate at high efficiency. The recycle stream from the diffuser is cycled back to the -196°C sieves for reprocessing, thus minimizing tritium losses and the total helium content in the recycle stream.

IX. BASIC CHEMISTRY RESEARCH

Basic chemistry research is being pursued in four different areas: catalytic chemistry associated with molecular energy resources; materials chemistry of superconducting oxides as well as ordered and associated solutions at high temperature; interfacial processes of importance to corrosion science, catalysis, and high-temperature superconductivity; and the geochemical processes involved in water/rock interactions occurring in active hydrothermal systems.

A. *Fluid Catalysis*

An array of *in situ* kinetic and spectroscopic techniques at high pressure is being employed to determine reaction mechanisms and to explore new catalytic chemistry associated with small gaseous molecules derived from coal, natural gas, and petroleum. Our current research exploits the unique properties of supercritical fluids to uncover effects of high-reactive-gas diffusivities on the catalytic reactions of gases with liquid or solid substrates. The supercritical fluids have the potential to alleviate gas-liquid mixing and catalyst-recovery problems typical of many homogeneous catalytic processes. Using a high-pressure nuclear magnetic resonance (NMR) probe, we are determining steady-state concentrations of the species present in the cobalt carbonyl catalyzed hydroformylation of propylene (oxo catalysis) in supercritical carbon dioxide. In other research, the organometallic chemistry of metallophthalocyanines is being investigated in attempts to activate methane and other hydrocarbons in homogeneous solution by using catalysts derived from these extremely robust macrocycles.

1. Catalytic Chemistry in Supercritical Media

Because of their gas-like transport properties, complete miscibilities with gases, and sharp changes in dissolving power with fluid density, supercritical fluids[1] have the potential for both accelerating diffusion-controlled reactions of gases with liquid or solid substrates and separating catalysts or catalytic products by energy-efficient pressure (and thereby, fluid density) alterations. These features would seem to be particularly beneficial in homogeneous catalysis, where diffusion across the gas-liquid interface and catalyst separations are typical problems.

In this report period, we conducted *in situ* NMR experiments relevant to the oxo process. Judged from the gas-liquid mixing problems complicating some earlier research,[2] we expected this process to benefit from the use of supercritical media. The experiments were designed to determine the effect of supercritical CO_2 on the linear-to-branched aldehyde product ratio (which is of considerable industrial significance and is known to depend on concentration and stirring rate for reactions in liquid media) and to compare other rate and equilibrium processes involved in the catalytic cycle with measured values from conventional solvents.

---

[1]M. McHugh and U. Krukonis, *Supercritical Fluid Extraction*, Butterworths, Stoneham, MA (1986).

[2]R. L. Pruett, *Advances in Organometallic Chemistry*, eds., F. G. A. Stone and R. West, Vol. 17, Academic Press, New York, pp. 1-60 (1979).

Our NMR spectral measurements were conducted with a high-pressure probe that uses a toroid detector, shown schematically in Fig. IX-1. With use of the hybrid probe circuit in the figure, the torus was double tuned to allow computer switching between ^{1}H (f_H = 300.5 MHz) and ^{59}Co or ^{13}C (f_x = 71.1 or 75.6 MHz, respectively). The SP-1 clamp in the rf feedthrough ensured that the system was gas-tight up to 172 MPa (25,000 psi) at 298 K and allowed experiments with $Co_2(CO)_8$ at 34 MPa (5000 psi) and 523 K with no apparent ill effects on the pressure probe. Toroids are intrinsically more efficient than other detector types, i.e., those based on solenoid and Helmholtz coils,[3,4] and are especially useful in metal pressure probes since sensitivity losses due to magnetic coupling with the pressure vessel are minimized by confinement of the magnetic flux within the torus.[3] This confinement is particularly beneficial for measurements in supercritical media since it allows selective measurements of gaseous (i.e., dissolved) species in the detector coil yet minimizes interference from undissolved solids or liquids exterior to it. We determined the solubility of $Co_2(CO)_8$ in supercritical CO_2 at 333-453 K (with CO and H_2 also present, and a total gas density near 0.5 g/mL) by measuring NMR signals in the gas phase above an excess of the solid or liquid metal carbonyl. The solubility data are plotted in Fig. IX-2. From the plot, we derived the enthalpy and entropy of dissolution in CO_2: 20 ± 1.7 kJ/mol and 30 ± 4 J/mol•K, respectively.

From the beginning of our efforts with the oxo catalyst system, it was apparent that the properties of supercritical fluids, aside from the anticipated benefits for catalysis, are also of great value in high-pressure NMR experiments. Since only one phase (having a very high diffusivity) is present, there is no need for a separate stirring mechanism in the pressure probe or

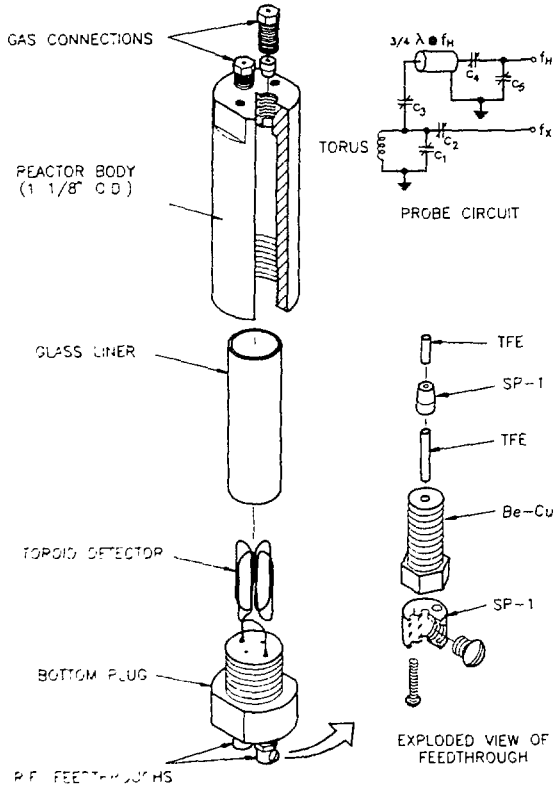

Fig. IX-1.

Design of Compact Pressure Probe Using Toroid NMR Detector (TFE = Teflon; f = frequency, c = capacitor)

[3]J. W. Rathke, J. Magn. Reson. **85**, 150 (1989).

[4]R. J. Klingler and J. W. Rathke, Prog. Inorg. Chem., in press.

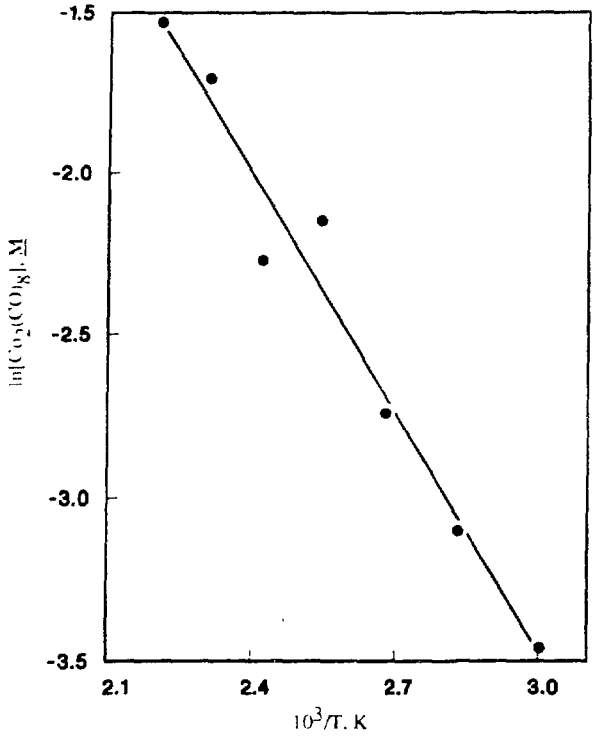

Fig. IX-2.

Solubility of $Co_2(CO)_8$ in Supercritical CO_2 (gas density of 0.5 g/mL) as Function of Temperature

the normally requisite measurements of gas-liquid partition coefficients. Furthermore, because of the low viscosity of the medium, rotational correlation times (and, therefore, line widths for quadrupolar nuclei in the NMR spectra, such as ^{59}Co) are significantly decreased. This latter effect greatly enhances the utility of NMR spectra for determining many of the metal nuclides present in organometallic catalysts.[4] For the hydroformylation reaction, the increased resolution allows direct observation of the relevant cobalt species, i.e., $RC(O)Co(CO)_4$, $HCo(CO)_4$, $Co_2(CO)_8$, and $Co_4(CO)_{12}$ (had it been present), without complications stemming from the frequent overlaps that occur with use of infrared spectroscopic techniques.

Figure IX-3 shows formation of butyraldehydes for the catalytic hydroformylation of propylene in supercritical CO_2 at T = 353 K, $P_{H2} = P_{CO}$ = 4.2 MPa (42 atm), $[Co_2(CO)_8]$ = 0.017 M, $[C_3H_6]$ = 0.14 M. Propylene hydroformylation proceeds cleanly in supercritical CO_2 (total gas density of 0.5 g/mL), yielding only the expected normal- and iso-butyraldehyde products, which were measured by integration of their characteristic proton signals near δ = 9.6 and 9.8 ppm, respectively, in an NMR spectrum. At the relatively low temperature used, reduction of the olefin to produce alkane or further reduction of the aldehydes to produce alcohols, even after prolonged reaction (~6 half-life periods), is insignificant, and *in situ* ^1H and $^{13}C\{^1H\}$ spectra did not indicate other products. Cobalt-containing catalytic intermediates were easily monitored by means of ^{59}Co NMR spectra collected alternately with the ^1H NMR data. A typical ^{59}Co NMR spectrum at T = 353 K and P = 22 MPa (219 atm) is shown in Fig. IX-4. The small peak near -2030 ppm corresponds closely with the chemical shift value obtained for a tetrahydrofuran solution of an authentic sample of $n\text{-}C_3H_7C(O)\text{-}Co(CO)_4$, prepared by reaction of $n\text{-}C_3H_7C(O)Cl$ with $NaCo(CO)_4$.[5] As judged from the asymmetry of the small peak in

[5]R. F. Heck and D. S. Breslow, J. Am. Chem. Soc. **84**, 2499 (1962).

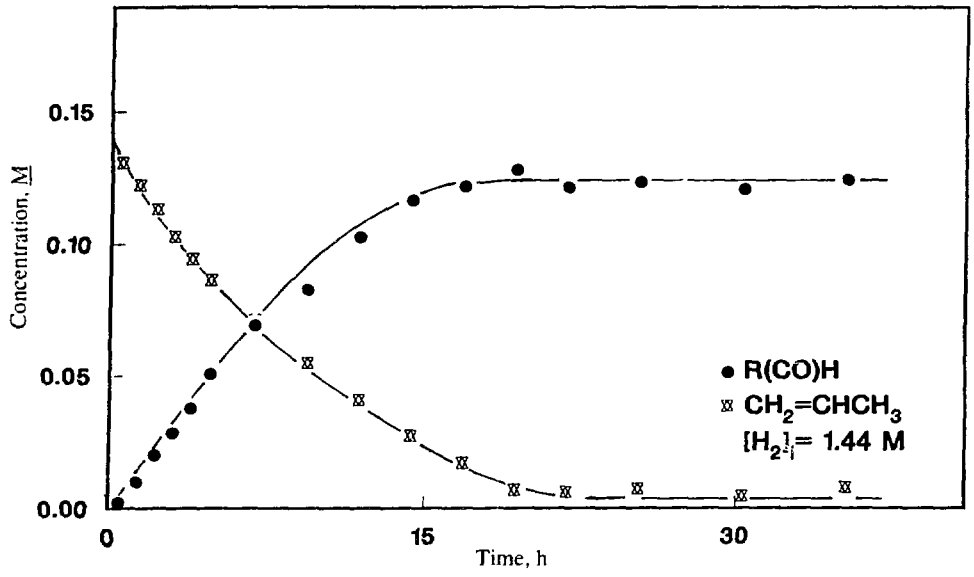

Fig. IX-3. Formation of Butyraldehydes (RC(O)H = [n-butyraldehyde] + [i-butyraldehyde]) for Catalytic Hydroformylation of Propylene in Supercritical CO_2 at 353 K

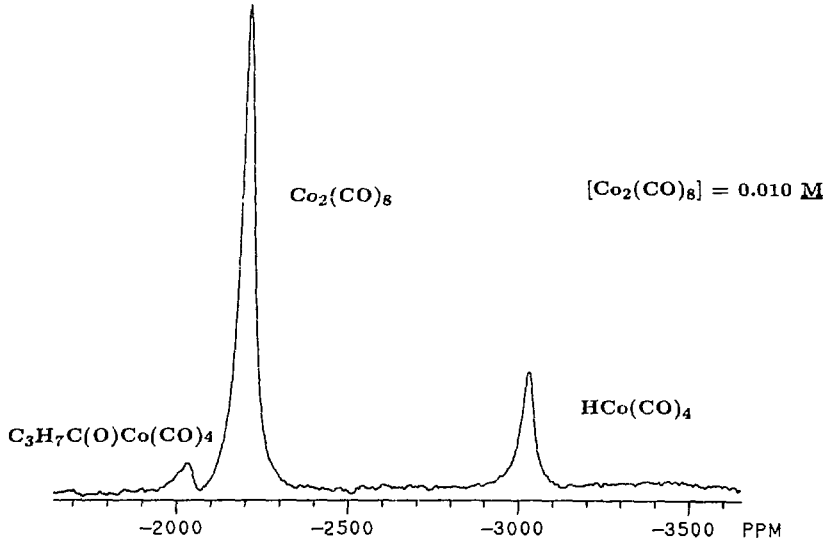

Fig. IX-4. ^{59}Co NMR Spectrum of Catalytic Intermediates, near the Steady State, during Hydroformylation of Propylene at 353 K in Supercritical CO_2

Fig. IX-4, the resonance might stem from both the normal and iso derivatives. Measurable quantities of $Co_4(CO)_{12}$ were not detected. The only species observed were $RC(O)Co(CO)_4$, $Co_2(CO)_8$, and $HCo(CO)_4$, as is consistent with Mirbach's infrared study of the reaction in liquid methylcyclohexane solution.[6]

[6]M. F. Mirbach and F. Marlis, J. Organomet. Chem. **265**, 205 (1984).

As shown in Fig. IX-5, the cobalt complexes reach a nearly steady-state condition early in the hydroformylation, which persists during the 15-h period that significant olefin is still present (see Fig. IX-3). During this period, $HCo(CO)_4$ is held below its equilibrium value for the reaction

$$Co_2(CO)_8 + H_2 \underset{k_{-1}}{\overset{k_1}{\rightleftharpoons}} 2HCo(CO)_4 \qquad (1)$$

which is only achieved after the olefin is fully consumed.

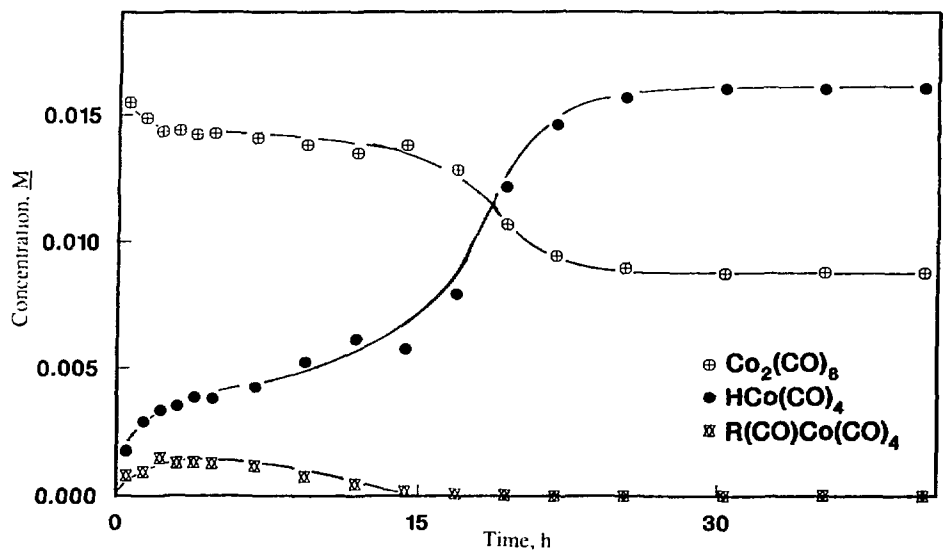

Fig. IX-5. *Concentrations of Catalytic Intermediates during* Propylene Hydroformylation in Supercritical CO_2 at 353 K

We have compared[7] our results for propylene hydroformylation in supercritical CO_2 with those of Mirbach[6] for the reaction of 1-octene in methylcyclohexane solution. Under comparable conditions, steady-state concentrations of the intermediates for the two cases do not differ greatly (i.e., by little more than a factor of three), and the overall hydroformylation rates are quite similar, d[aldehyde]/dt = 1.2 x 10^{-5} $\underline{M}^{-1}$ s^{-1} and 0.77 x 10^{-5} $\underline{M}^{-1}$ s^{-1}, for the methylcyclohexane and CO_2 systems, respectively. The forward and reverse rate constants for the equilibrium in Eq. 1 measured in CO_2 (k_1 = 0.16 Pa^{-1} s^{-1}, k_{-1} = 1.8 x 10^{-3} $\underline{M}^{-1}$ s^{-1}) also agree closely with the methylcyclohexane results (k_1 = 0.15 $Pa^{-1}s^{-1}$, k_{-1} = 1.7 x 10^{-3} M^{-1} s^{-1}). Although different olefins were used in the two studies, the comparisons are believed to be meaningful since Wender[8] has shown that hydroformylation rates for a wide range of straight-chain terminal olefins vary only slightly with chain length.

---

[7] J. W. Rathke, R. J. Klingler, and T. R. Krause, Organomet., in press.

[8] I. Wender, S. Metlin, S. Ergun, W. Sternberg, and H. Greenfield, J. Am. Chem. Soc. **78**, 5401 (1956).

The comparisons just cited indicate that, under conditions where reaction chemistry controls the rates (namely, at temperatures near 353 K), supercritical CO_2 does not alter the measured parameters much from those obtained for a typical hydroformylation-type medium. Thus, we anticipate that at higher temperatures, where mass transport across the liquid-gas interface normally controls the rates, the supercritical medium would achieve higher rates than expected for a liquid solvent. The rate enhancement might exceed the one or two orders of magnitude increase in diffusivities for small molecules in supercritical fluids compared with those in typical liquids.[1]

Although we have not yet experimented with hydroformylations in supercritical CO_2 at >353 K, other experiments indicate that CO_2 does not adversely affect the cobalt carbonyl catalyst up to at least 453 K. Thus, equilibration of $Co_2(CO)_8$ with H_2 to produce $HCo(CO)_4$ (Eq. 1) at high temperatures is achieved without complicating side reactions in supercritical CO_2. As shown in Fig. IX-6, equilibrium constants measured with use of ^{59}Co and ^{1}H NMR at temperatures spanning the range 333-453 K exhibit normal Van't Hoff behavior. Enthalpy and entropy changes determined from Fig. IX-6 (20 ± 0.8 kJ/mol and 18 ± 2 J/mol•K, respectively) are close to values measured for n-heptane solutions.[9,10]

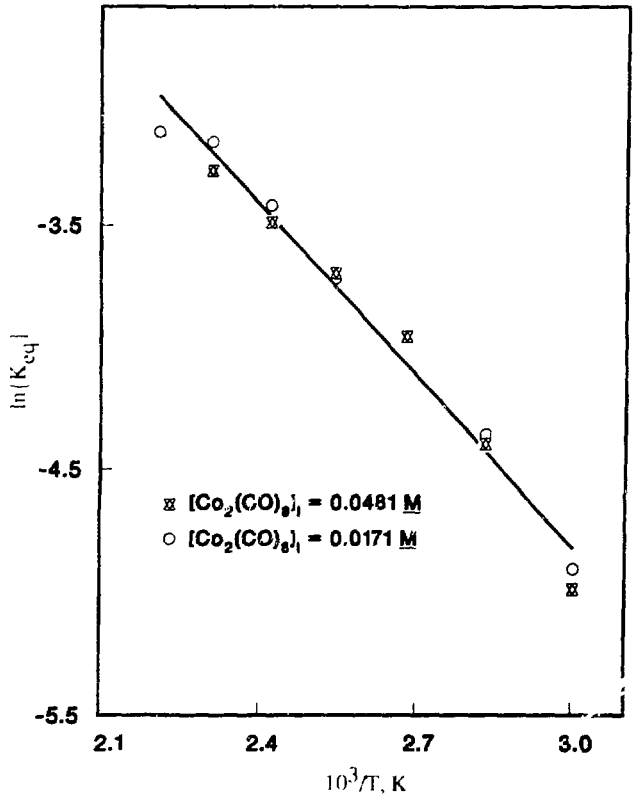

Fig. IX-6.

Van't Hoff Plot for Hydrogenation of Dicobaltoctacarbonyl in Supercritical CO_2 as Function of Temperature

[9]N. H. Alemdarogler, J. M. L. Penninger, and E. Oltay, Monatsh. Chem. **107**, 1043 (1976).
[10]F. Ungvary, J. Organomet. Chem. **36**, 363 (1972).

Perhaps of greater importance than reaction rate in hydroformylation catalysis is the selectivity to linear vs. branched aldehyde products. The ratio of n-butyraldehyde to i-butyraldehyde products in supercritical CO_2 solution, obtained by integration of the aforementioned proton signals, is 7.2. This value is appreciably higher than has previously been achieved with conventional solvents; measured values for these vary from 3.8 to 4.6.[11]

In future research, we intend to explore the role of the cobalt tetracarbonyl radical, $\bullet Co(CO)_4$, in the hydroformylation reaction. During the course of the research just discussed, we have obtained ample evidence for the existence of the radical at temperatures used in oxo chemistry. For example, line broadening of the ^{59}Co resonance of $Co_2(CO)_8$, attributable to exchange with the radical, and rapid hydrogen atom transfer from $HCo(CO)_4$ to the radical are new processes easily observed with the pressure probe. Although the generally accepted Heck and Breslow mechanism for hydroformylation[12] does not assign a role to the radical, it is difficult to believe that such a reactive species, when present, does not participate.

2. Hydrocarbon Activation Chemistry

The objective of this project is to study the activation of hydrocarbons when soluble metallophthalocyanines (MPc) are used as the catalysts. Metallophthalocyanines are well known for their catalytic activities on the autoxidation of hydrocarbons.[13,14] However, the mechanisms for these reactions are not well understood, since most of these reactions are operated in heterogeneous systems due to low MPc solubilities. Presumably, in these systems, the MPc activates O_2, which then oxidizes the hydrocarbons. Direct activation of hydrocarbons to form hydrido- and alkyl-MPc is another way of hydrocarbon activation. In the absence of oxygen, this seems to be the only viable path.

In this period, we explored the direct activation of hydrocarbons. A Rh-Rh bonded dimer, $((R_8Pc)Rh)_2$, where R_8Pc^{2-} is the dianion of 1,4,8,11,15,18,22,25-octapentylphthalocyanine, has been synthesized and shown to react with H_2 and CH_4 according to the reactions[15,16]

$$\left[(R_8Pc)Rh\right]_2 + H_2 \underset{N_2}{\overset{0.1\ MPa,\ 368\ K}{\rightleftharpoons}} 2(R_8Pc)RhH \qquad (2)$$

---

[11]P. Pino, F. Piacenti, and M. Bianchi, *Organic Syntheses via Metal Carbonyls*, eds., I. Wender and P. Pino, Vol. 2, Chapter 2, John Wiley, New York (1977).

[12]R. F. Heck and D. S. Breslow, J. Am. Chem. Soc. **83**, 4024 (1961).

[13]F. H. Moser and A. L. Thomas, *The Phthalocyanines*, Vols. 1 and 2, CRC Press, Boca Raton, LA (1983).

[14]P. E. Willis, Jr., and J. E. Lyons, Catal. Lett. **3**, 389 (1989).

[15]M. J. Chen, J. W. Rathke, S. Sinclair, and D. W. Slocum, J. Macromol. Sci. A, in press.

[16]M. J. Chen and J. W. Rathke, "Hydrogen and Methane Activation Studies Using Soluble Rhodium Phthalocyanine Dimers," Abstracts of XIVth Int. Conf. on Organometallic Chemistry, Detroit, MI, August 19-24, 1990, p. 177 (1990).

$$\left[(R_8Pc)Rh\right] + CH_4 \underset{N_2}{\overset{1.2\ MPa,\ 473\ K}{\rightleftharpoons}} (R_8Pc)RhH + (R_8Pc)RhCH_3 \qquad (3)$$

Reaction 2 is reversible, and the dimer is regenerated if the product solution is heated with N_2. Reaction 3 is also reversible but may be complicated by side reactions.

Based on the chemistry of structurally related Rh-porphyrin systems,[17] we assumed that reaction 3 proceeds with the initial reversible homolysis of the dimer:

$$(R_8Pc)Rh \rightleftharpoons 2\ (R_8Pc)Rh\bullet \qquad (4)$$

Therefore, the lower the Rh-Rh bond energy, the more active the dimer is for activating CH_4 and other hydrocarbons. The results for reaction 2 allow us to set 88 kJ/mol as the maximum Rh-Rh bond energy in $((R_8Pc)Rh)_2$. It is likely that the value is considerably lower.

Further work will be directed toward synthesis of Rh-Pc dimers with different substituents so that the Rh-Rh bond energy may be varied. The study will also be extended to MPc-catalyzed autoxidation of hydrocarbons. For this purpose, Fe-Pc and Co-Pc will be used, since they have been shown to be most active in heterogeneous systems.

B. *Materials Chemistry*

Our goal in this effort is to perform experimental and theoretical studies that lead to a basic understanding of materials chemistry. Our major focus is on high-critical-temperature (T_c) superconducting oxides, associated and ordered solutions at high temperatures, and compounds containing first-, second-, and third-row elements.

1. Studies of High-T_c Superconductors

We are investigating the properties of high-T_c superconducting oxides by use of emf measurements and molecular orbital calculations.

a. Structural Transitions and Thermodynamic Behavior

The objective of these studies is to investigate the structural transformations and nonstoichiometric and thermodynamic behavior of high-T_c superconductor oxide systems as a function of oxygen partial pressure, oxygen stoichiometry, and temperature by means of a coulometric titration technique where the oxygen content is varied by well-defined small amounts. Our previous electromotive force (emf) measurements on the high-T_c $YBa_2Cu_3O_x$

---

[17] A. E. Sherry and B. B. Wayland, J. Am. Chem. Soc. **112**, 1259 (1990).

system[18-20] indicated a miscibility gap centered at x = 6.65 with a consolute temperature of 473 K (200 ± 50°C). The objective of our current measurements is to investigate the effect of ionic size of Ln^{3+} (where Ln = Y, Gd, Nd) on the structural transitions and thermodynamic and nonstoichiometric behavior in the $LnBa_2Cu_3O_x$ system. The results of limited measurements on the n-type (electron-doped) superconducting $Nd_{1.81}Ce_{0.19}CuO_x$ system are also discussed.

Figure IX-7 shows the equilibrium oxygen pressures calculated from our emf measurements for isotherms in the temperature range 673-873 K (400-600°C) as a function of x in $NdBa_2Cu_3O_x$. At any given stoichiometry, these partial pressures of oxygen are higher than those reported earlier for the $YBa_2Cu_3O_x$ system.[18-20] Because of apparent hysteresis effects, we could not confirm the presence of an S-shaped isotherm at 673 K, as was found in the $YBa_2Cu_3O_x$ system. If present for the $NdBa_2Cu_3O_x$, the inflection in the isotherm would be at a higher value of x and much lower temperature than for the $YBa_2Cu_3O_x$. These results are consistent with the change in the observed composition dependence of T_c with ionic radii for Y and Nd in $YBa_2Cu_3O_x$ and $NdBa_2Cu_3O_x$.[21] The results of Veal et al.[21] show that there are two plateaus of T_c, at ~90 and ~60 K, and that T_c decreases with a decrease in x. In addition, T_c decreases more rapidly as a function of x with increasing ionic radius in the sequence Y, Gd, Nd. The results of Veal et al. also show that the lower plateau is nearly absent for the case of $NdBa_2Cu_3O_x$. One possible mechanism for producing these two plateaus is phase separation in a miscibility gap which would operate for the yttrium phase and not the neodymium phase.

We completed preliminary emf measurements as a function of oxygen stoichiometry on the n-type (electron-doped) tetragonal superconductor, $Nd_{1.81}Ce_{0.19}CuO_x$ (T_c = 24 K, x = 4).[22-23] Coulometric titration at 1023 K resulted in an irreversible oxygen partial pressure plateau, $p(O_2)$ = 32 Pa (3.2 x 10^{-4} atm), over a narrow composition range, $x = 3.97_5$ to 3.96_6, indicating a diphasic region. X-ray analyses indicated that the residue was apparently identical to the starting material, and therefore, the new phase differs subtly from the original. The transition temperature was found to be 13 K, compared with the original value of 24 K. The oxygen nonstoichiometry obtained by Suzuki et al.,[24] via thermogravimetric analysis measurements with $Nd_{1.85}Ce_{0.15}CuO_{4-\delta}$ at 1023 K (δ = 0.002), is much smaller than ours

---

[18]M. Tetenbaum, A. P. Brown, and M. Blander, "Phase Transformations and Thermodynamic Behavior of the $YBa_2Cu_3O_x$ System via EMF Measurements," Proc. of Ceramic Superconductivity Symp., American Ceramic Society, Vol. II, pp. 51-58 (1988).

[19]M. Tetenbaum, B. Tani, B. Czech, and M. Blander, Physica C **158**, 377 (1989).

[20]M. Tetenbaum, L. A. Curtiss, B. Czech, B. Tani, and M. Blander, "Oxygen Stoichiometry, Structural Transitions, and Thermodynamic Behavior of the $YBa_2Cu_3O_x$ System," *Physics and Material Science of High Temperature Superconductors*, eds., R. Kossowsky, S. Methfessel, and D. Wohlleben, NATO ASI Series E, Vol. 181, Kluwer Academic Publishers, Netherlands, pp. 279-296 (1990).

[21]B. W. Veal, A. P. Paulikas, J. W. Downey, H. Claus, K. Vandervoort, G. Tomlins, H. Shi, M. Jensen, and L. Morss, Physica C **162-164**, 97 (1989).

[22]D. G. Hinks, Material Science Division, Argonne National Laboratory, private communication (1990).

[23]J. D. Jorgensen, D. G. Hinks, P. Lightfoot, D. R. Richards, B. Dabrowski, S. Pei, D. T. Marx, A. W. Mitchell, and Y. Zheng, "Multiphase Behavior and the Superconducting Composition in $Nd_{2-x}Ce_xCuO_4$," submitted to Physica B.

[24]K. Suzuki, K. Kishio, T. Hasegawa, and K. Kitazawa, Physica C **166**, 357 (1990).

(δ = 0.025-0.034). Clearly, further processing and structural studies are required to characterize this intriguing n-type class of superconducting materials.

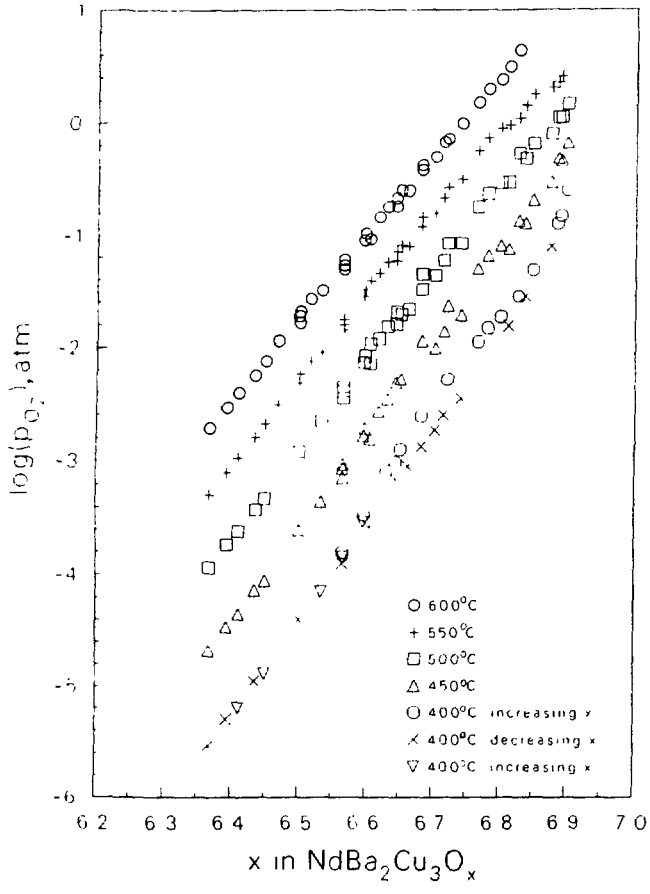

Fig. IX-7.

Partial Pressure of Oxygen as Function of Temperature and Oxygen Stoichiometry in $NdBa_2Cu_3O_x$

b. Molecular Orbital Calculations

The assignments of peaks in the optical absorption spectra of $YBa_2Cu_3O_x$ in the region <5 eV are important in the elucidation of the mechanism for superconductivity in these new materials.[25] Previously, we carried out *ab initio* molecular orbital calculations on the intra-atomic d → s excitation of divalent copper.[26] During the past year, we extended this work to calculating the intra-atomic d → s excitation of monovalent copper. In this work, we used CuO clusters representing the chains in $YBa_2Cu_3O_6$ which contain monovalent copper coordinated by two oxygen atoms.[27] The results of our study indicate that the intra-atomic d → s excitation lies in the region 4.0-4.5 eV for monovalent copper. This result suggests that the sharp peak at 4.1 eV observed in the optical absorption spectra of $YBa_2Cu_3O_x$ as x approaches 6 is due to d → s excitation.

---

[25]S. Uchida, S. Tajima, H. Takagi, and Y. Tokura, *Mechanisms of High Temperature Superconductivity*, eds., H. Kamimura and A. Oshiyama, Springer-Verlag, Berlin, p. 197 (1989).

[26]L. A. Curtiss and S. W. Tam, Phys. Rev. B **41**, 1824 (1990).

[27]M. K. Kelly, P. Barboux, J. Tarascon, and D. E. Aspnes, Phys. Rev. **40**, 6797 (1989).

2. Ordering and Association in Liquids

a. Solubilities of NiO in Molten Carbonates

The dissolution of the NiO cathode and transport to the anode is the principal failure mode for the current generation of molten carbonate fuel cells with a 62 mol % Li_2CO_3-38 mol % K_2CO_3 electrolyte. We analyzed measurements of the NiO solubility in alkali carbonates as a function of CO_2 pressure to deduce a basic understanding of the chemistry which would aid in improving fuel cell performance. We focused on a particularly broad range of measurements for the solubilities of NiO in alkali carbonates (Li_2CO_3, Na_2CO_3, K_2CO_3, Rb_2CO_3, and some binary mixtures) at 1183 K.[28]

For a particular alkali carbonate, the following equilibrium is important:

$$M_2CO_3(soln.) \rightleftarrows M_2O(soln.) + CO_2 \qquad (5)$$

where the activity of the alkali oxide increases with a decrease in CO_2 pressure, and the oxide concentration at a given pressure of CO_2 is highest in Li_2CO_3 and lowest in Rb_2CO_3. Analyses of the data were consistent with the presence of the solution species Ni^{2+} (i.e., $NiCO_3$), NiO, and NiO_2^{2-} (M_2NiO_2). From measurements of NiO solid in Na_2CO_3, K_2CO_3, and Rb_2CO_3 melts, we deduced solubility products and formation constants for the NiO and NiO_2^{2-} solution species in the reactions

$$NiO(s) \rightleftarrows Ni^{2+}(soln.) + O^{2-}(soln.) \qquad (6)$$

$$Ni^{2+}(soln.) + O^{2-}(soln.) \rightleftarrows NiO(soln.) \qquad (7)$$

$$NiO(soln.) + O^{2-}(soln.) \rightleftarrows NiO_2^{2-}(soln.) \qquad (8)$$

From these constants and the dissociation constants for the molten carbonates, we deduced the concentrations of the different species. In addition, we set an upper limit on the concentrations of NiO_2^{2-} and Ni^{2+} in molten Li_2CO_3. Our calculations indicated that the concentrations of the NiO_2^{2-} species are similar in all the alkali carbonates, but the concentrations of Ni^{2+} and NiO increase in going from Li_2CO_3 to Rb_2CO_3.

Of all these results, the most revealing for improving the fuel cell electrolyte is the concentration of Ni^{2+} (i.e., $NiCO_3$), which is the major solution species in fuel cell electrolytes at 923 K and CO_2 pressures $\geq$0.1 MPa (1 atm). With solid NiO present at a constant

---

[28]M. L. Orfield and D.A. Shores, J. Electrochem. Soc. **135**, 1662 (1988).

CO_2 pressure, the activity of $NiCO_3$ is a constant. Therefore, the $NiCO_3$ concentrations and NiO solubilities in different fuel cell electrolytes are inversely proportional to the activity coefficient of $NiCO_3$, which is highest in Li_2CO_3 and lowest in Rb_2CO_3. This is consistent with what is known of the activity coefficients of nickel salts in alkali salts with the same anions.[29,30] We have used this relationship between solubilities and activity coefficients to deduce improved electrolyte compositions, which appear to be promising in preliminary experiments. Further measurements of new fuel cell electrolytes will be made to optimize performance.

b. Conformal Ionic Solution Theory for Aqueous Electrolytes

The conformal ionic solution (CIS) theory is a statistical mechanical perturbation theory first proposed by Reiss et al.[31] for binary molten salts and proved to be most useful for higher order systems,[32,33] where reliable predictions have been made for a variety of molten salts. The simplest aqueous reciprocal salt system consists of two cations (A^+ and B^+), two anions (X^- and Y^-), and the dielectric solvent, H_2O. The solution of four ions in water is a quaternary system, with the four components being H_2O and any three of the four constituent salts AX, AY, BX, and BY. In this work, we used the CIS theory to deduce an expression for the thermodynamic properties of the quaternary aqueous reciprocal salt system, $(A^+,B^+/X^-,Y^-)$ -H_2O, in terms of the thermodynamic properties of the four lower order ternary subsystems, i.e., $(A^+/X^-,Y^-)$-H_2O, $(B^+/X^-,Y^-)$-H_2O, $(A^+, B^+/X^-)$-H_2O, $(A^+, B^+/Y^-)$-H_2O, and the four binary subsystems, i.e., AX-H_2O, AY-H_2O, BX-H_2O, BY-H_2O. The results justify some of the terms semiempirically deduced by Pitzer and coworkers[34-36] and lead to a general new term which predicts deviations from the "cross-square rule" of Wu et al.[37]

For the case in which the AX-H_2O binary is not one of the binary solution components, the Helmholtz free energy of mixing of an aqueous reciprocal salt solution containing one mole of salt at a given concentration (ΔA_m) from binary solutions of each of three of the four possible salts, all at the same concentration, is given by the expression:

$$\Delta A_m - RT(X_A \ln X_A + X_B \ln X_B + X_X \ln X_X + X_Y \ln X_Y) =$$

$$X_A X_X \Delta A^\circ + X_A \Delta A_A^E + X_B \Delta A_B^E + X_X \Delta A_X^E + X_Y \Delta A_Y^E - X_A X_B X_X X_Y \frac{(\Delta A^\circ)^2}{2\,zRT} \qquad (9)$$

---

[29]M. L. Orfield and D. A. Shores, J. Electrochem. Soc. **136**, 2862 (1989).

[30]M. Blander, "Thermodynamic Properties of Molten Salt Solutions," *Molten Salt Chemistry*, ed., M. Blander, Interscience, New York, pp. 127-237 (1964).

[31]H. Reiss, J. Katz, and O. J. Kleppa, J. Chem. Phys. **36**, 144 (1962).

[32]M. Blander and S. J. Yosim, J. Chem. Phys. **39**, 2610 (1963).

[33]M.-L. Saboungi and M. Blander, J. Chem. Phys. **63**, 212 (1975).

[34]K. S. Pitzer, "A Thermodynamic Model for Aqueous Solutions of Liquid Like Density," *Reviews in Mineralogy*, eds., I. S. E. Carmichael and P. H. Eugster, Mineralogical Society of America, Vol. 17, pp. 97-142 (1987).

[35]R. T. Pabalon and K. S. Pitzer, Geochim. Cosmochim. Acta **51**, 2429 (1987).

[36]K. S. Pitzer and J. M. Simonson, J. Phys. Chem. **90**, 3005 (1986).

[37]Y. C. Wu, M. B. Smith, and T. F. Young, J. Phys. Chem. **69**, 1868 (1965).

where ΔA° is the standard Helmholtz free energy change for the metathetical reaction

$$AY(soln) + BX(soln) \rightleftarrows AX(soln) + BY(soln) \qquad (10)$$

The individual values of A_i° in ΔA° are equal to the negative of the integral excess free energy of dilution to infinite dilution of the solution containing one mole of the salt i. The concentrations in Eq. 9, X_i, are the ion fractions of the designated ions and are either cation fractions or anion fractions, e.g., $X_A = N_A/(N_A + N_B)$, $X_X = N_X/(N_X + N_Y)$. Also in Eq. 9, ΔA_j^E is the excess free energy of mixing, up to the quadratic term, of the two-salt mixture in which the two salts have the common ion j (i.e., $\Delta A_X^E = X_A X_B \lambda_X$, where λ_X is an interaction parameter), and z is a parameter related to a complex set of integrals. For molten salts, z has a value of 5-6. For aqueous solutions, we use a value of z = 12. The significance of Eq. 9 is that predictions for quaternary solutions can be made from measurable quantities on lower order systems.

To test the cross-square rule, Wu et al.[37] measured enthalpies of mixing of six salt pairs (AX-BY, AY-BX, AX-AY, BX-BY, AX-BX, and AY-BY) of 1 molal solutions, each containing 1/2 mol of the salts, in the four systems listed in Table IX-1. We compared their measurements[37] with values calculated from an equation for enthalpies of mixing (ΔH_m) deduced from Eq. 9:

$$\Delta H_m = X_A X_X \Delta H^\circ + \sum_{j=c,a} X_j \Delta H_j^E - X_A X_B X_X X_Y \frac{(\Delta H^\circ)^2}{zRT} \qquad (11)$$

where c and a represent cations and anions, respectively, and $\Delta H^\circ = \Delta H^\circ_{AX} + \Delta H^\circ_{BY} - \Delta H^\circ_{AY} - \Delta H^\circ_{BX}$. We deduced the values of 1/2 ΔH° for reaction 10 as well as values for the last term in Eq. 11 (labeled ε in Table IX-1). The quantities in Table IX-1 indicate that ε is negligibly small for very small values of ΔH° (within experimental uncertainties, results are zero for the first three systems listed) and, as predicted, is significant when ΔH° is large (fourth system listed). As can be seen, the value of ε for the $(Na^+,K^+/Cl^-,NO_3^-)$- H_2O system was predicted by theory for z = 12. Further studies are needed to test the applicability of this value of z.

Table IX-1. Values for ΔH° and ε Calculated from Measured Data and from the CIS Theory

$A^+,B^+/X^-,Y^-$	$1/2\Delta H^\circ$,[a] cal/mol salt	ε, cal/mol	
		Measd.	Calcd.[b]
$Li^+,Na^+/Cl^-,Br^-$	12.11 (50.69)	-0.06_5	-0.005
$Li^+,K^+/Cl^-,Br^-$	32.13 (134.5)	+0.03	-0.036
$Na^+,K^+/Cl^-,Br^-$	19.92 (83.38)	-0.04	-0.014
$Na^+,K^+/Cl^-,NO_3^-$	179.4 (751.0)[c]	-1.1	-1.132

[a]Values in parentheses have units of J/mol salt.
[b]Calculated from $(-X_A X_B X_X X_Y (\Delta H^\circ)^2/12RT)$.
[c]Calculated by Wu et al.[37] from four measured values of ΔH_i at 298 K to be 178 cal/mol (745 J/mol).

The CIS theory can be a useful tool for deducing equations for the prediction of the solution properties of multicomponent aqueous ionic solutions. For aqueous reciprocal salt systems, the theory has led to a fundamental justification of the semiempirical terms proposed by Pitzer and coworkers[34-36] and to a new term which can be important in concentrated solutions. By comparison with structural models, the theory can also provide insights into solvation and association of ions in solution and guidance in planning a program for our future structural investigations using anomalous scattering of synchrotron X-rays.

c. Structure of Molten Salts

We have continued our experimental investigation into the structure of trivalent metal ion halides to probe the various mechanisms of the melting process.[38,39] The Intense Pulsed Neutron Source (IPNS) at ANL is being used to study the structure of yttrium chloride. We have chosen to contrast YCl_3 with $AlCl_3$, since both salts have the same crystalline structure but differ strikingly in many macroscopic properties. For example, YCl_3 melts at 994 K, while $AlCl_3$ sublimes at 466 K; the entropy of melting is extremely large (75.7 J mol $^{-1}$) for $AlCl_3$, while it is within the normal range for YCl_3 (31.8 J mol^{-1}); the same remark applies for the electrical conductivities, σ, and the volume changes upon melting (for YCl_3: $\sigma = 0.39\ \Omega^{-1}$ and $\Delta V/V_s = 0.0045$; for $AlCl_3$: $\sigma = 5 \times 10^{-7}\ \Omega^{-1}cm^{-1}$ and $\Delta V/V_s = 0.88$).

It is well known that $AlCl_3$ melts into a totally different liquid structure from that of the crystal, consisting of molecular Al_2Cl_6 units (two tetrahedra sharing a Cl-Cl edge), with a coordination number for Al-Cl of 4. We have established from our neutron data that, in a YCl_3 melt, yttrium ions remain in octahedral-type coordination since the Y-Cl coordination number is 5.8, compared with 6 in the solid. However, the Cl-Cl coordination in the liquid is about 8.2, appreciably less than in the solid.[40] Thus, YCl_3 melts into a loose octahedral network conserving layer-like order at intermediate range, while $AlCl_3$ melts into a molecular liquid. The difference in the melting behavior is related to the relative stability of tetrahedral and octahedral coordination under an increase of temperature and, hence, to a subtle difference in balance between ionic and covalent components of the bonding. This difference is accounted for by the phenomenological chemical scale of the elements and the classification suggested by Pettifor.[41] In spite of the identity in crystal structure, this places YCl_3 in a region of relatively high ionicity and $AlCl_3$ in a region of stronger covalency, with Y lying closer to Sr and Al closer to Zn. This work is being done in collaboration with D. L. Price (ANL Materials Science Division) and M. Tosi (International Center of Theoretical Physics, Trieste, Italy).

3. Quantum Chemical Studies

During the past year, we developed a Gaussian-2 (G2) theoretical procedure for calculating molecular energies of compounds containing first-row (Li→F) and second-row

---

[38]M. -L. Saboungi, W. Geertsma, and D. L. Price, Annu. Rev. Phys. Chem. **41**, 207 (1990).

[39]M. -L. Saboungi, M. A. Howe, and D. L. Price, "Structure of Molten Salts," Proc. of Seventh Int. Symp. on Molten Salts, eds., C. L. Hussey et al., Electrochemical Society, Vol. 90-17, pp. 8-17 (1990).

[40]M. -L. Saboungi, D. L. Price, C. Scamehorn, and M. P. Tosi, Europhys. Lett., in press.

[41]D. G. Pettifor, J. Phys. C. **19**, 285 (1986).

(Na→Cl) atoms. This procedure is based on *ab initio* molecular orbital theory and is an improvement on the recently proposed Gaussian-1 (G1) procedure.[42,43] The G1 procedure is based on Hartree-Fock theory and incorporates high levels of correlation energy using quadratic configuration interaction and large basis sets. New features in the G2 procedure include a correction for nonadditivity of diffuse-sp and 2df basis set extensions used in G1 theory, a basis set extension containing a third d-function and a second p-function, and a modification of the higher level correction used to correct for remaining basis set deficiencies. Results of G2 procedure calculations showed an overall improvement with respect to the G1 procedure when calculated values from both procedures were compared with well-established experimental values for atomization energies, ionization potentials, electron affinities, and proton affinities of a large number of species. For example, for atomization energies of 125 molecules, the average absolute deviation for G2 was 1.21 kcal/mol (5.06 kJ/mol), compared with 1.53 kcal/mol (6.40 kJ/mol) for the G1. Significant improvements in the accuracy of calculations were found for atomization energies of ionic molecules (such as LiF) and hydrides (such as C_2H_6, NH_3, N_2H_4, H_2O_2, and CH_3SH) and electron affinities of second-row species. Finally, G2 atomization energies for another 79 molecules, many of which have uncertain experimental data, were used to assess experimental data. The results indicated that a number of experimental values are in error. This work is being done in collaboration with J. Pople (Carnegie Mellon University) and R. Krishnan (AT&T Bell Laboratories).

The development of accurate quantum chemical techniques is important in many areas of materials chemistry, including catalysis studies and chemical vapor deposition modeling. We are applying the G2 procedure to several problems in materials chemistry. One of these is the calculation of the binding energies of small silicon clusters, which are important in semiconductor research but have limited experimental information available in the literature. Figure IX-8 shows a plot of the increase in binding energy of a silicon cluster (Si_n) as a function of addition of the n'th atom. Good agreement is found with experiment for n = 2,3, where some experimental data are available. For n = 4,5 there are no experimental data, and the theoretical results provide reliable data for these species. An interesting feature is the peak at n = 4, which indicates that a Si_4 cluster has a special stability compared with the n = 3 and n = 5 clusters. This work is being done in collaboration with R. Krishnan (AT&T Bell Laboratories) and P. W. Deutsch (Pennsylvania State University).

We have also developed contracted basis sets for correlation-level calculations of third-row non-transition metals (Ga through Kr). The basis sets that were derived have been tested and found to satisfactorily reproduce experimental properties such as geometric configurations, dipole moments, and vibrational frequencies for a range of molecules.[44] These basis sets have been used in studies of the dissociation energies and ionization potentials of GeH_n (n = 1-4), AsH_n (n = 1-3), and SeH_n (n = 1-2). The results are in good agreement with experiment where reliable data are available and have provided valuable guidance to interpreting

---

[42]L. A. Curtiss, C. Jones, G. W. Trucks, K. Raghavachari, and J. A. Pople, J. Chem. Phys. **93**, 2537 (1990).

[43]J. A. Pople, M. Head-Gordon, D. Fox, K. Raghavachari, and L. A. Curtiss, J. Chem. Phys. **90**, 5622 (1989).

[44]R. C. Binning, Jr., and L. A. Curtiss, J. Comp. Chem. **11**, 1206 (1990).

new experimental data.[45] This work is being done in collaboration with R. Binning (Illinois Institute of Technology).

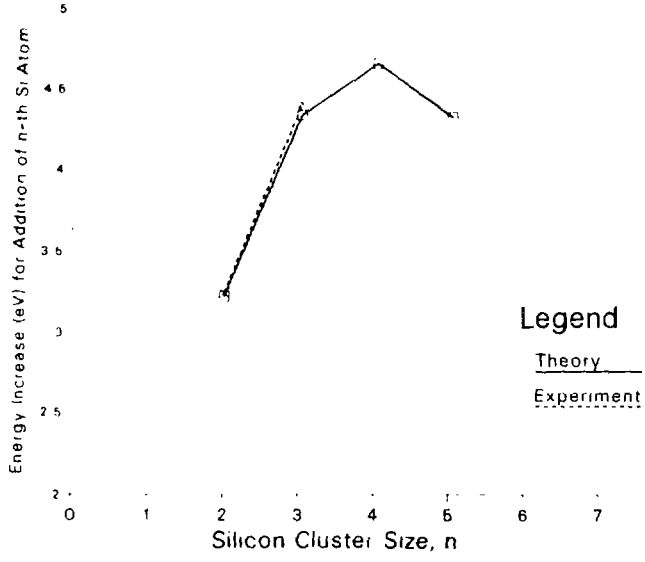

Fig. IX-8.

Increase in Binding Energy of Silicon Cluster (Si_n) with Addition of n'th Silicon Atom. (Calculations done at the equilibrium structures of the clusters.)

C. *Interfacial and Corrosion Science*

This research program consists of experimental and theoretical studies that focus on interfacial processes of importance to corrosion science, catalysis, and high-temperature superconductivity. The experimental work has three thrusts: (1) investigations of aqueous corrosion over a wide range of temperatures and pressures, using novel procedures based largely on the integration of spectroscopic, X-ray scattering, and electrochemical techniques, (2) studies of novel catalysis schemes employing molecular sieve materials, and (3) the preparation of high-T_c superconducting oxides in thin-film form. Paralleling semiempirical and *ab initio* theoretical research is carried out to support and extend all of the above experimental pursuits.

1. Aqueous Corrosion Research

The deleterious effects of aqueous corrosion in practical systems that operate between ambient temperature and the boiling point of water are widely recognized and can generally be avoided by appropriate choice of containment materials and/or application of a variety of corrosion inhibition practices. At higher temperatures, such as those existing in light water nuclear reactor (LWR) coolant systems, the corrosion reactions are much more rapid, passive surface layers become less stable, and localized corrosion processes, such as stress corrosion cracking (SCC), are exacerbated by even trace levels of some types of impurities. Under these conditions of high temperature and pressure, much less is understood concerning the mechanistic aspects of the corrosion processes or the synergistic effects of impurities, pH, etc. The overall goal of this research program is to provide experimental information against which

[45]B. Ruscic, M. Schwarz, and J. Berkowitz, J. Chem. Phys. **92**, 1865 (1990).

theoretical and empirical models of aqueous corrosion can be tested. Results during the past year are summarized below.

a. Spectroelectrochemical Studies of Aqueous Corrosion

The objective of this effort is to elucidate the relationship between the structural and electronic properties of metal/solution interfaces and the kinetics of metallic corrosion and passivation in aqueous environments. Laser Raman and UV-visible spectroscopies are employed to determine *in situ* the structure and composition of anodically formed corrosion films on metal surfaces. Photoelectrochemical and ac impedance techniques are used to characterize the electronic band structure of the films and to study their transport properties and conduction mechanism(s). Concurrently, dc and ac polarization, cyclic potentiodynamic sweeps, and other transient techniques are employed to further elucidate the interfacial processes involved in metal corrosion.

Using the technique of surface enhancement of Raman scattering (SERS) by electrodeposition of silver, we have successfully observed *in situ* the Raman spectra of the passive films on iron in the regions of Fe^{2+} formation (e.g., -0.8 to -0.4 V vs. standard calomel electrode) and Fe^{3+} formation (~0.1 V). At -0.6 V, we found that the films consist of a mixture of Fe_3O_4 and $Fe(OH)_2$; at 0.1 V, our results suggest that an inner layer of Fe_3O_4 still remains, together with an outer layer of αFe_2O_3 and FeOOH. This picture is consistent with thermodynamic requirements, and for the first time reconciles conflicting results in the literature regarding the surface phases present on iron in the various potential regions studied.

Small amounts of SCN^- are found to break down the passive films on iron with a concomitant increase in anodic corrosion current. Time-resolved Raman spectroscopy showed that during film breakdown, the iron oxide and hydroxide films are replaced by iron thiocyanate films that are non-passivating. The mechanism of breakdown appears to involve a complexation of Fe^{2+} and Fe^{3+} ions in the solid and in solution, with subsequent precipitation of iron thiocyanate phases. If the concentration of SCN^- is less than 0.001 M, the passive film appears to be capable of "healing" itself, thus preventing catastrophic breakdown.

We have developed a new method for the *in situ* analysis of monolayer amounts of materials on electrode surfaces based on a Raman difference technique that makes use of the two-dimensional imaging capability of a position-sensitive photomultiplier detector with a resistive anode. The principle of the method is to image two identical electrodes simultaneously using a single laser beam; one electrode is held at the potential for film formation (anodic) while the other is kept clean at a fairly cathodic potential. The spectra acquired simultaneously from each electrode are subtracted (anodic - cathodic) to obtain the spectral features of the corrosion film alone. The advantage of this technique is that the background scattering from the cell environment and the fluctuations in laser power during spectral acquisition cancel out. Thin films (~20 Å) of $Fe(H_2PO_4)_2$ produced during the open-circuit corrosion of iron in 0.1 M NaH_2PO_4 solution have been analyzed successfully in initial tests of system operation. Further refinement of the technique and extension to other systems are planned.

b. Electrode Kinetic Studies of Aqueous Corrosion

The research conducted under this task is concentrated on understanding the electrode kinetic aspects and atomistic mechanisms of metallic corrosion in aqueous solutions over a wide range of temperature and pressure. This is a completely novel area of investigation, since only minimal electrode kinetic research has ever been carried out above 333 K, and practically none above 373 K, in aqueous solutions. Our experimental measurements are closely coupled with the theoretical studies described in Sec. IX.C.1.c. Also, much of the experimentation is carried out under conditions directly relevant to corrosion in the LWR industry. These corrosion processes are almost exclusively electrochemical and involve the anodic dissolution of the metal together with the reduction of a component of the environment, such as dissolved oxygen. The essential elementary step in each of these reactions is the charge transfer between the solid surface and a solution species in the interfacial solution layer (the "interphase"). The kinetics of this step are strongly influenced by the molecular structure of the interphase and the potential gradients within it, both of which are completely different from related properties of the bulk solution. The electrode kinetic measurements are made by a combination of techniques that include use of galvanostatic, coulostatic, or potentiostatic pulse transients, ac capacitance measurements, and rotating disk-electrode techniques.

The coordinated theoretical/experimental studies have concentrated on the high-temperature/high-pressure (HTHP) charge transfer kinetics of the ferrous/ferric redox reaction. A number of workers[46] have reported an unexplained dependence on temperature of the transfer coefficient for complex electrode reactions. In earlier work, we attempted to determine whether a simple reaction would also behave anomalously.[47] Our results permitted us to draw the following important conclusion: a simple, outer-sphere charge transfer reaction does not behave anomalously at high temperatures (up to 548 K); hence, the discrepancies for complex reactions must be caused by an elementary step other than the charge transfer step.

It is well known that the ferrous/ferric reaction can be strongly catalyzed by trace levels of anionic impurities concentrated at the electrode/solution interface (which has led us to take every precaution in our HTHP work to avoid these effects). We did, however, suspect that earlier literature reports[48-50] of similar catalyzic effects by cations may be erroneous because the strong catalytic influence of trace amounts of anions may not have been scrupulously eliminated. Such effects of cations are difficult to justify on theoretical grounds because the reaction is expected to involve an outer-sphere path. This year, we investigated several under-potential deposited (UPD) systems in ultra-high purity solutions. For Cu on Au, Ag on Au, and Bi on Pt, a small but definite catalytic effect (less than one order of magnitude increase in the reaction rate) was observed in each case in the absence of any anion effects. A paralleling

---

[46]B. E. Conway, in *Modern Aspects of Electrochemistry*, Vol. 16, Plenum Press, New York, p. 103 (1985).

[47]M. J. Steindler et al., *Chemical Technology Division, Annual Technical Report, 1988*, Argonne National Laboratory Report ANL-89/15, p. 140 (1989)

[48]R. R. Adzic and A. R. Despic, J. Chem. Phys. **61**, 3482 (1974).

[49]I. T. E. Fonseca and A. C. Martin, Port. Electrochim. Acta **6**, 51 (1988).

[50]H. G. Bochmann and W. Vielstich, Electrochim. Acta **33**, 805 (1988).

theoretical study has offered a feasible explanation for this unexpected catalytic effect (see Sec. IX.C.1.c).

We are now extending our experimental/theoretical charge transfer studies to the Cu^{2+}/Cu electrode reaction, which consists of two consecutive electron transfers followed by the incorporation of the copper adatom into the metal lattice. While this reaction is much more complex than the Fe^{2+}/Fe^{3+} redox reaction, we expect that the first electron transfer step will be rate determining, and that we can modify our experimental/theoretical approaches for this case. In preparing for this study, we carried out a computer modeling analysis of the reliability of relaxation techniques for electrode kinetic measurements on multistep electrode reactions. The results indicate that we will be able to achieve the measurement conditions needed to obtain the rate of both the slow and the fast step of the Cu^{2+}/Cu reaction sequence.

c. Theoretical Studies of Aqueous Corrosion

The purpose of this research is to investigate the types of electron transfer reactions that control the rates of corrosion processes in LWRs. This theoretical study uses a combination of molecular dynamics and molecular orbital methods to study electron transfer at an electrolyte/electrode interface. The work is done in collaboration with J. W. Halley, a member of the Corrosion Institute at the University of Minnesota, who is carrying out the molecular dynamics simulations and developing algorithms for calculating electron transfer rates from the classical trajectories of the reactants. We are performing molecular orbital calculations to determine potentials for the molecular dynamics calculations and to provide insights into electronic effects.

Our theoretical study of the temperature dependence of the Fe^{2+}/Fe^{3+} electron transfer reaction has been completed. The results indicate that there is no anomalous temperature dependence (298 to 548 K) for the electron transfer rate, in agreement with the experimental findings reported in Sec. IX.C.1.b. In addition, the charge transfer coefficient and activation barrier calculated from the molecular dynamics simulations are in good agreement with those obtained from experiment. Another major finding of this study is that the Fe^{2+}/Fe^{3+} heterogeneous electron transfer reaction is nonadiabatic.

We began a theoretical investigation into the possible causes of the surprising catalytic effect on the Fe^{2+}/Fe^{3+} electron transfer rate observed (see Sec. IX.C.1.b) after a single layer of copper was deposited on the gold working electrode. (This type of metal-induced perturbation is not predicted by classical heterogeneous electron transfer theories.) We investigated two possibilities: (1) deposition of a copper layer increases the electronic coupling, and (2) the approach of the solvated ion is closer in the case of the copper-covered gold surface than for the clean gold surface, thus increasing the electronic coupling. Electronic structure calculations have ruled out the first possibility, and strongly pointed toward the second, providing additional evidence for the importance of the electronic factor in heterogeneous electron transfer.

During the past year, work continued on the development of the theoretical models of the Cu^{+} and Cu^{2+} ions in water necessary for studying the Cu^{2+}/Cu electron transfer process. We derived a pair potential for Cu^{+}/H_2O from *ab initio* molecular orbital calculations.

This potential, together with the pair potential for Cu^{2+}/H_2O derived last year,[51] has been successfully tested in molecular dynamics simulations of these ions in water at the University of Minnesota. We calculated two- and three-body interaction energies for tetrahedral, octahedral, and cubic arrangements of H_2O molecules around Cu^+ and Cu^{2+} ions in $[Cu(OH_2)_n]^{q+}$ clusters to assess the nonadditivity of interactions in these hydrated transition metal ion clusters. For Cu^{2+} there is a slow convergence of the interaction terms to the full many-body result, whereas for Cu^+ many-body effects are much less important.

A challenging problem in simulating the copper ions in water is to include the Jahn-Teller distortion of waters in the first solvation shell about Cu^{2+}. Information from X-ray diffraction indicates that this distortion is significant and needs to be included for accurate study of the electron transfer process.[52] There have been no previous molecular dynamics simulations of ions in water incorporating the Jahn-Teller effect. We plan to use *ab initio* calculations of the force field for a $[Cu(H_2O)_6]^{2+}$ cluster to provide the additional information needed to incorporate the Jahn-Teller effect in our simulation based on pair potentials. In addition, large cluster calculations will be carried out to study the effect of the second solvation shell on the Jahn-Teller distortion as a further aid in developing the molecular dynamics model for this ion in water.

d. Synchrotron Radiation Studies of Metal/Solution Interfaces

To complete the interpretation of the kinetic and molecular information derived from the above electrochemical, spectroscopic, and theoretical studies, complementary data are needed on elemental density profiles and ordering behavior within the interfacial corrosion layers that form on metal surfaces and in the double-layer region adjacent to the metal surface. In particular, it is important to understand the role played by dissolved solution species, pH, and the solvent (water) molecules during the formation of passive films and the restructuring of the double layer. Techniques based on synchrotron radiation offer many intriguing possibilities for such studies. These possibilities have been assessed, a research plan has evolved, and experiments are underway using the National Synchrotron Light Source (NSLS) at Brookhaven National Laboratory.

In this effort, an experimental technique that permits direct *in situ* X-ray investigations of metal/solution interfaces in an electrochemical cell under uniform potential control has been developed and successfully demonstrated. This success is due, in large part, to beneficial collaborations with Hoydoo You (ANL Materials Science Division) and Wenbing Yun (ANL Advanced Photon Source Division). During the past year, we began studies of metal film electrodes in aqueous media by using an X-ray/electrochemical cell (XEC) of special design. *In situ* X-ray reflectivity data were obtained for Cu, Ag, Au, and Ni/Cr films (200 to 500 Å thick) supported on single crystal silicon and sapphire substrates. In the case of copper, we collected data (see Fig. IX-9) over a range of potentials corresponding to fully reduced and heavily oxidized conditions. Variations in the reflectivity modulation could be correlated with the

---

[51] M. J. Steindler et al., *Chemical Technology Division Annual Technical Report, 1989*, Argonne National Laboratory Report ANL-90/11, p. 157 (1990).

[52] M. Magini et al., *X-Ray Diffraction of Ions in Aqueous Solutions: Hydration and Complex Formation*, CRC Press, Boca Raton, LA (1987).

formation and removal of oxide films at the copper/electrolyte interface. The model developed for analyzing the *in situ* X-ray reflectivity data (based on Fresnel's equations) allows the determination of interfacial corrugations (roughness) and has shown that the oxide layers grown on metal films have corrugations that are commensurate with the corrugation of the underlying metal film. In the case of the Ni/Cr bimetallic film, modulation from both metal layers was clearly seen in the reflectograms.

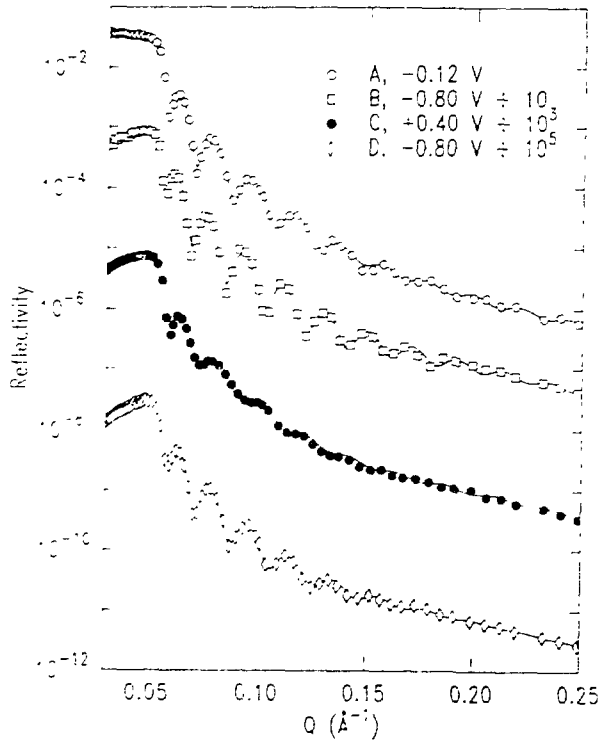

Fig. IX-9.

Reflectivity of Cu-on-Si Electrode at Various Potentials in Borate Buffer Solution (pH = 8.4). Curves were calculated, while symbols correspond to experimental data. Curves B and D represent oxide free metal; curves A and C show the presence of oxide layers on the metal surface.

Attempts to measure the width of the electrical double layer on a thin-film gold electrode using Cs^+ as a probe ion indicated that the film surface roughness and long-term systematic drifts were limiting our ability to make meaningful measurements. Two modifications were made to overcome this problem. One involved replacing the gold film electrode with a single-crystal platinum electrode that had been specially treated to achieve an ultra-smooth surface. The second involved linking the potentiostat computer control to the X-ray spectrometer computer system, so that the two potentials used in the double-layer measurement could be imposed sequentially (with dual channel data storage) at each reflection angle. This should reduce the long-term systematic noise that tended to distort the data when complete reflectograms were recorded first at one potential, then at a second.

The novel, narrow-pass, transmission-reflection geometry of the XEC has proven to be well suited for controlled potential studies with aqueous electrolytes. Many of the expected advantages of this approach have been realized in our recent work at the NSLS, and we hope to exploit these advantages in experiments planned for the next year. In one type of study, we will complete X-ray reflectivity measurements of anodic film formation, cathodic reduction of oxide surface layers, and metal dissolution for iron and nickel films. The second type of study will continue our efforts to measure anion and cation density gradients in the electrical double

layer by using single-crystal gold and platinum electrodes that are "atomically smooth" (i.e., distortion of a surface under study is flat to within atomic dimensions). In the longer range, new spectroscopic techniques, such as high-resolution X-ray Raman spectroscopy, that take advantage of the unique features of the Advanced Photon Source (APS) under construction at ANL will be developed, tested for concept viability at existing synchrotron facilities, and eventually used on the APS.

2. Research on Molecular Sieve Materials

Recent advances in the synthesis of novel molecular sieve materials have opened new vistas for product-selective catalysis of fuels and chemical feedstocks. This research is focused on studies of the mechanisms of sieve formation in gel media and the catalytic properties of the framework structures produced therefrom.

a. Theoretical Studies of Molecular Sieve Synthesis

Ab initio molecular orbital calculations and inelastic neutron scattering measurements are being used to examine the effects of the molecular sieve framework on the vibrational frequencies and rotational diffusion of occluded template molecules. The torsional frequencies of the tetraethylammonium (TEA) cation have been computed by molecular orbital methods to help assign low frequency torsional and bending peaks in the inelastic neutron scattering spectra of TEA^+ in various molecular sieve materials. The results indicate that a previous infrared study[53] incorrectly assigned peaks in the 60-110 cm^{-1} region to lattice vibrations when (according to the molecular orbital calculations) they are actually due to ethyl torsional vibrations. Investigation of the potential energy surface of TEA^+ for rotation about the C-C and C-N bonds revealed four distinct configurations that correspond to local minima of nearly equal energy.

Using *ab initio* molecular orbital theory, we have initiated an investigation of the Brönsted acid strengths of ZSM-5 zeolites. We are using Si_nO_m clusters (tied off with hydrogens) to study the dependence of proton affinity of the oxygen site on cluster size and the "level" of theory (i.e., basis set size and correlation effects). Clusters containing up to eight silicon atoms are being investigated. The G2 procedure discussed in Sec. IX.B.3 (accurate to ± 8 kJ/mol) has been used to calculate the proton affinity and gas phase acidity of silanol ($SiOH_4$) and to assess the reliability of lower level calculations currently being used on larger clusters, for which no experimental data are available. The results on $SiOH_4$ indicated that the extended 3-21G basis set[54] gives proton affinities and gas-phase acidities that are accurate to 5-10%. The G2 procedure will also be used to calculate the proton affinity of disiloxane, another species related to the larger clusters. We plan to use the Si_nO_m clusters to investigate the effect of substitution of metal atoms on the acid strength of the oxygen site. The characteristics (vibrational frequency, charge, and proton affinity) of the bridging OH group will be studied as a function of substitution of B, Al, Ga, Ti, and Fe on the Si site. The effect of geometry changes

---

[53]L. Aimone, J. P. Badiali, and H. Cachet, J. Chem. Soc. Faraday Trans. **73**, 2 (1977).

[54]M. S. Gordon, J. S. Binkley, J. A. Pople, W. J. Pietro, and W. J. Hehre, J. Am. Chem. Soc. **104**, 2797 (1982).

will be included, and the results will be correlated with infrared spectroscopic studies of the O-H stretching frequencies. This type of study will also be extended to determine the effect of similar substitutions in aluminophosphate molecular sieves.

Computer programs for the calculation of near-edge X-ray fine structure (NEXAFS) spectra of molecular sieve materials have been set up and tested on MgO. The programs employ local density approximation calculations on clusters of atoms to determine the photoabsorption cross section as a function of energy near the absorption edge for a particular core electron in the central atom of the cluster. The calculated spectra of MgO were in agreement with the measured spectra.[55] We plan to make theoretical calculations of NEXAFS spectra of Si_nO_m clusters designed to represent molecular sieve materials for comparison with experimental studies. The dependence of the theoretical spectra on cluster size will be calculated. A comparison between the theoretical absorption spectra (vs. increasing cluster size) and the experimental spectra can provide a check on the quality of theoretical cluster models because oxygen K-edge spectra can be directly correlated with long-range electronic effects in oxides.

b. Studies of Catalysis by Molecular Sieve Materials

In this research effort, we seek to gain new understanding of the catalytic activity and product selectivity demonstrated by molecular sieve cage networks of medium pore size (4 to 8 Å). Infrared spectroscopy is used in conjunction with gas chromatography to provide detailed information on structure-composition-reactivity relationships for a variety of light hydrocarbon reactions on selected aluminosilicate and aluminophosphate framework systems. In the past, we showed that when Co(II) is substituted for Al(III) in the framework of certain aluminophosphate ($AlPO_4$) molecular sieves and the resulting Co(II)-containing $AlPO_4$ (CoAPO) is calcined in oxygen, the Co(II) is oxidized to Co(III).[56] More recently, we reported that methane can reduce Co(III)APOs to HCo(II)APOs at 773 K with concomitant production of C_{2+} hydrocarbons.[57]

During the past year we continued our investigations of the redox properties of CoAPO and CoAPSO molecular sieves (where S indicates silicon substitution for some phosphorus atoms), with emphasis on catalyst stability and lifetime. Infrared (IR) spectroscopy and powder X-ray diffraction (XRD) were used to examine the framework structure and crystallinity of various metal-substituted aluminophosphate molecular sieves having the $AlPO_4$-34 and AlPO-5 structure. The IR and XRD data were recorded for as-synthesized molecular sieves (i.e., still containing the template cation), freshly calcined sieves, and sieve samples that had been repeatedly subjected to oxidative calcining followed by reduction with methane. In the case of CoAPO-34 and CoAPSO-34 (P:Co = 12 or 6), evidence was seen (in both IR and XRD) for deterioration of the framework structure after the initial calcining and after repeated calcination/methane reduction cycles. The CoAPO-5s (P:Co = 48 or 24) exhibited

---

[55]T. Linden, H. Sauer, W. Engel, and K. Kambe, Phys. Rev. **B33**, 22 (1986).

[56]L. E. Iton, I. Choi, J. Desjardins, and V. A. Maroni, Zeolites **9**, 535 (1989).

[57]M. J. Steindler et al., *Chemical Technology Division Annual Technical Report, 1989*, Argonne National Laboratory Report ANL-90/11, pp. 159-160 (1990).

considerably greater framework and crystallographic stability, but this is probably more a function of the P:Co ratio than framework structure type. We intend to determine the fate of the framework-bound cobalt sites during this deterioration using near edge X-ray absorption techniques.

3. Preparation of High-T_c Films by Alloy Oxidation

The objective of this research effort is to develop methods for preparing high-T_c superconducting ceramic films by oxidizing liquid alloy precursors. Previous studies[58] indicated that single-phase liquids with the composition MBa_2Cu_3 (M = Eu or Yb) and melting points <1173 K can be oxidized to produce textured films of $MBa_2Cu_3O_7$ (123) if the liquid metal is supported on a suitable single-crystal substrate, such as $SrTiO_3(100)$. The resulting high-T_c films show preferential orientation of the 123 phase a-b planes parallel to the substrate surface and carry critical currents (J_c) in the 10^4 to 10^5 A/cm^2 range. To improve the potential for practical application of this method, it is desirable to find lower cost substrates, adapt the liquid phase oxidation procedure for 123 materials to more abundant metals than Eu and Yb, and extend the technique to the bismuth- and thallium-based high-T_c phases.

We have initiated a collaborative research program with American Superconductor Corp. (Watertown, MA) to explore and exploit the potential of the liquid alloy oxidation process for producing high-T_c structures in thin-film and thick-film embodiments. A specially designed high-temperature/high-vacuum apparatus[59] was used in this work.

Thick $YbBa_2Cu_3O_{7-x}$ films, exhibiting preferential orientation of the a-b crystal planes parallel to the substrate surface ("texture") near the film/substrate interface, have been prepared by oxidation of the liquid alloy precursor $YbBa_2Cu_3$ (mp, ~1143 K) supported on single-crystal ceramic substrates (see Fig. IX-10). Parametric studies of processing variables (substrate dip temperature, oxidation temperature and time, and oxygen pressure during oxidation) were conducted to optimize film properties, such as T_c, J_c, high-T_c phase purity, and texturing. With $SrTiO_3(100)$ and MgO(100) substrates, evidence is seen for textured $YbBa_2Cu_3O_{7-x}$ films that show orientation of the c-axis perpendicular to the substrate surface within 5 μm of the alloy/substrate interface. Beyond 5 μm the c-axis growth direction begins to randomize and texturing is lost. Typical T_c values for these films have been around 80 K, indicating that the oxygenation of the $YbBa_2Cu_3O_{7-x}$ phase has not been completed to the point where $x \rightarrow 0$.

Future work will focus on (1) increasing T_c of the films through improvements in oxygenation procedures/conditions, (2) reducing alloy/substrate interaction, and (3) developing a method for "wiping" the alloy film to reduce overall film thickness. A desirable outcome of our effort in the coming year would be the preparation of textured $YbBa_2Cu_3O_7$ films with T_c near 90 K and J_c approaching 10^5 A/cm^2.

---

[58]H. S. Chen, A. R. Kortan, F. A. Thiel, and L. C. Kimberling, Appl. Phys. Lett. **55**, 191 (1989).

[59]M. J. Steindler et al., *Chemical Technology Division Annual Technical Report, 1989*, Argonne National Laboratory Report ANL-90/11, p. 161 (1990).

Fig. IX-10. Micrograph of Thick $YbBa_2Cu_3O_{7-x}$ Film on Single-Crystal Substrate

D. Geochemistry

The geochemistry research program includes efforts in two general areas: (1) geochemistry and evolution of hydrothermal systems associated with volcanic areas and (2) isotopic and organic geochemistry of carbon in sedimentary basins. The approach being taken is to investigate specific problems through detailed chemical and isotopic analyses of rock, mineral, water, and gas sampled from appropriate field areas. Potential applications of this work are in nuclear waste management; geothermal energy development; and exploration for minerals, oil, and natural gas.

1. Uranium-Series Disequilibrium Geochronology of Yellowstone Travertines

The extent of radioactive disequilibrium among members of the ^{238}U and ^{232}Th decay series can be exploited for many applications in the earth and environmental sciences. We have been applying actinide-series measurements for investigating the rates and mechanisms of element redistribution and the time scale of hydrothermal activity in several active hydrothermal systems. One of our recent applications has been to determine the ages of travertine deposits in the northern part of Yellowstone National Park. (Travertines are calcium carbonate deposits, consisting primarily of the minerals aragonite and/or calcite, that can be produced at the Earth's surface where groundwater emerges in a saturated or supersaturated state with respect to the

solubility of calcium carbonate.) The purpose of this work is to gain an improved understanding of the timing of the last glaciation and the influence of the glaciation on the underlying hydrothermal systems.

The alpha decay of ^{234}U (half-life = 245,000 yr) to ^{230}Th (half-life = 75,400 yr) is the "clock" by which we determine travertine age. Travertine generally contains a negligible amount of ^{230}Th relative to ^{234}U when it forms; therefore, the activity ratio of ^{230}Th to ^{234}U increases from near zero (when the travertine is deposited) to near unity (when ^{230}Th reaches radioactive equilibrium with ^{234}U). The time required for radioactive equilibrium to be approached in a closed system (from $^{230}Th/^{234}U = 0.000$ to 0.99, if $^{234}U/^{238}U = 1.00$) is about 500,000 yr. This represents a practical upper limit of age determination by the $^{230}Th/^{234}U$ method, because the accuracy and precision with which this ratio can be determined are limited by uncertainties in (1) the initial amount of ^{230}Th in the sample, (2) the absolute values of radioactive decay constants, and (3) the analytical determination of $^{230}Th/^{234}U$.

Our travertines samples are from a valley through which a 1000-m thick outlet glacier flowed during the last glaciation in the Rocky Mountains, known as the Pinedale Glaciation.[60] The stratigraphic relations of these travertines with respect to glacial till deposits constrain their relative ages. Some are clearly pre-Pinedale, and some are clearly post-Pinedale. Most are from the post-Bull Lake era (the Bull Lake occurred prior to the Pinedale glaciation, i.e., 130,000 to 170,000 yr ago). Variations in the elevation of travertines imply fluctuation of hydrologic conditions in the hot spring system from which they were deposited. The hydrologic fluctuations reflected in the distribution of travertines presumably are related to climatic variations associated with glaciation, and can be interpreted in terms of subsurface permeability distribution. Previous studies[61] based on obsidian hydration and radiocarbon dating showed that the full glacial conditions of the Pinedale Glaciation occurred 30,000 to 40,000 yr ago, deglaciation was complete by about 15,000 yr.

Our study of travertine ages is being done in collaboration with K. L. Pierce, a glacial geologist with the U. S. Geological Survey in Denver, and M. T. Murrell, a geochemist at Los Alamos National Laboratory (LANL). A preliminary survey of travertine ages was first performed at CMT, using alpha spectrometry techniques.[62] Because improved resolution of ages was desired, a subset of travertine samples was taken to LANL, where recently developed mass spectrometric techniques for uranium-series measurements have yielded data of significantly better precision than attainable by alpha spectrometry. At LANL, we chemically separated the U and Th in these samples and performed the mass spectrometric analysis. The results of the mass spectrometric measurements allowed us to calculate precise ages (e.g., 9,920 ± 74 yr; 19,570 ± 124 yr; 57,112 ± 585 yr for three separate travertine samples). The ages were determined to be analytically reproducible and consistent with all geologic constraints. We expect to augment the data set for travertines from several additional localities, and then to examine the implications of the data with respect to glacial chronology, paleoclimate, and

---

[60]K. L. Pierce, "History and Dynamics of Glaciation in the Northern Yellowstone National Park Area," U. S. Geological Survey Professional Paper 729-F (1979).

[61]K. L. Pierce, J. D. Obradovich, and I. Friedman, Geol. Soc. Am. Bull. **87**, 703 (1976).

[62]M. J. Steindler et al., *Chemical Technology Division Annual Technical Report, 1989*, Argonne National Laboratory Report ANL-90/11, pp. 162-164 (1990)

geothermal hydrology. Complementary data on the isotopic compositions of C, O, and Sr in the travertines are also being collected at CMT.

2. Isotope and Organic Geochemistry of Lacustrine Rift Basins

Geochemical studies are underway to elucidate organic matter evolution in lacustrine rift basins. The results of this work will improve understanding of factors controlling the quality and quantity of organic matter in lacustrine source rocks, and will help define the limiting conditions for petroleum formation and survival beyond the "oil window." Our field and analytical studies performed to date have focused on organic matter alteration around magmatic intrusions. We are also undertaking laboratory simulations of organic matter maturation.

The wide range of carbon and oxygen isotopic compositions determined by us last year[62] for the Animikie Basin (Minnesota) was demonstrated to be of primary origin and not caused by thermal alteration. Eighteen microbands from a 3-cm thick intermediate slate sample were analyzed; carbon and oxygen isotopic variations comparable to the regional variation noted last year were observed in this single sample. The observed isotopic variation appears to be consistent with widely believed bacterial mediation that may have occurred during iron carbonate precipitation in Proterozoic times.

Drill core and outcrop samples from the Culpeper Basin (Virginia) were prepared and analyzed for total organic carbon (TOC), total carbonate carbon (TCC), and isotopic compositions. Carbonate and organic carbon were significantly depleted in samples immediately adjacent to the Rapidan Sheet, indicating thermal decomposition effects. No anomalous enrichment in TOC, such as that observed in the Animikie Basin, was observed in the Culpeper Basin. Coupled ^{13}C and ^{18}O depletion in carbonates sampled close to the magmatic intrusion indicates the dominant influence of simple decarbonation reactions. Carbon isotopic fractionation in TOC is consistent with preferential loss of ^{12}C-enriched hydrocarbons of low molecular weight adjacent to the magmatic intrusion. Ongoing isotopic and molecular studies on extractable organics will help clarify the details of organic matter evolution in this system.

Increasingly complex organic materials (i.e., pentadecane→sucrose→lubricating oil →kerogen) were exposed to various temperatures (473-873 K) in the presence of excess oxygen so that the isotopic consequences of this thermal treatment could be determined. These stepped-combustion experiments were intended, in part, to be analogs of the thermal maturation process. More importantly, however, the objective was to evaluate whether stepped-combustion experiments can resolve isotopically distinct components in complex organic mixtures. The results strongly indicate that organic compounds undergo partial oxidation and molecular and isotopic restructuring when exposed to increasing temperature under oxidizing conditions. Early released ^{13}C-depleted carbon could not be unambiguously related to ^{13}C-depleted hydrocarbon components of complex mixtures (e.g., in kerogen), since this was also observed in the pentadecane experiments. Similarly, late released (i.e., high temperature) ^{13}C-enriched carbon in these experiments is unlikely to reflect ^{13}C-enriched molecular components in the starting organic materials.

3. New Facilities

A VG Prism II isotope ratio mass spectrometer having a gas chromatograph-combustion inlet system was installed this year. The mass spectrometer is now running to specifications, and establishment of secondary standards is virtually complete. Hundreds of carbon and oxygen isotope ratio measurements, including those reported above, have been performed with this new instrument. More work is in progress to rectify remaining problems with the gas chromatograph-combustion inlet system.

X. ANALYTICAL CHEMISTRY LABORATORY

The Analytical Chemistry Laboratory (ACL) is a full-cost-recovery service center, with the primary mission of providing a broad range of analytical chemistry support services to the scientific and engineering programs at ANL. In addition, the ACL conducts research in analytical chemistry, works on instrumental and methods development, and provides analytical services for governmental, educational, and industrial organizations. The ACL handles a wide range of analytical problems, from routine standard analyses to unique problems that require significant development of methods and techniques.

The ACL is administratively within CMT, the principal user, but provides support for all the technical divisions and programs at ANL. The ACL has four technical groups--Chemical Analysis, Instrumental Analysis, Organic Analysis, and Environmental Analysis--which together include about 50 technical staff members.

The Chemical Analysis Group uses wet-chemical and instrumental methods for elemental, compositional, and isotopic analyses of solid, liquid, and gaseous samples. The Instrumental Analysis Group uses nuclear counting techniques in radiochemical analyses for a range of samples (low-level to highly radioactive environmental samples). Other types of analyses done by this group are gas chromatography (GC), X-ray diffraction (XRD) and fluorescence of solids, inert gas fusion of metals, and neutron activation of either liquids or solids. The Organic Analysis Group uses a number of complementary techniques to separate and analyze complex organic mixtures and compounds at the trace level, including synthetic fuels, toxic substances, fossil-fuel residues and emissions, pollutants, biologically active compounds, pesticides, and drugs. The Environmental Analysis Group performs inorganic environmental and hazardous waste analyses and coal analysis.

The majority of the ACL technical accomplishments are contained in previous sections of this report and in similar reports of other ANL divisions. Selected accomplishments are also summarized here.

Engineering Studies of Pyrochemical Processes for Integral Fast Reactor (IFR) Fuels

In the electrorefining of U and Pu fuels for the IFR, metallic fuel pins (U, Pu, Zr) are dissolved in a molten cadmium anode, and the actinide elements are electrochemically transported through a halide-salt electrolyte to the cell cathode, where they are collected as a metallic deposit. Engineering-scale studies of this electrorefining process are being conducted in CMT (Sec. VI. C) to develop models that can predict the recovery of U and Pu, as well as the decontamination of these elements from fission-product elements and process materials. The ACL has contributed to this effort by determining elements of interest in samples from the cadmium anode, the halide-salt electrolyte, and the cathode product. Special dissolution procedures are followed for each type of sample matrix, and separation schemes based on solvent extraction and ion exchange are used to isolate the desired elements from matrix components and, subsequently, to separate these elements from each other. Uranium and plutonium concentrations in IFR samples are measured with a "hot" inductively coupled plasma/atomic

emission spectroscopy (ICP/AES) instrument. Whenever higher precision and accuracy than attainable with ICP/AES are required, the mass spectrometric isotope dilution (MSID) technique is used. Additional analyses by high resolution gamma-ray spectrometry with a high-purity germanium detector are performed on samples to determine ^{237}Np, ^{241}Am, and ^{244}Cm. The purpose is to better understand the behavior of these elements in the electrorefining process.

The waste electrorefining salts generated by IFR fuel reprocessing will be contacted with Cd-Li-K alloys to remove essentially all of the actinides. The treated salt will then be immobilized in a mortar for disposal as an intermediate-level waste. Workers in the IFR Program are developing formulations of ^{90}Sr- and ^{137}Cs-containing mortar, which possess high compressive strength and low leachability (Sec. VI. D). We have developed a procedure that employs Cerenkov counting for the determination of ^{90}Sr. Post-test samples of mortar formulations were analyzed for ^{90}Sr by Cerenkov counting, as well as for ^{137}Cs by gamma spectrometry and chloride ion by ion chromatography. The analytical data showed that ^{90}Sr leaches more slowly than ^{137}Cs, and that chloride ions leach more rapidly than either Sr or Cs. Leach rates of all the mentioned components were found to increase with curing temperature and decrease with curing time.

The ACL also provided chemical analyses as part of a large-scale electrorefining experiment to demonstrate the anodic dissolution of simulated IFR fuel. Chemical analyses by ICP/AES and XRD indicated successful dissolution of the uranium constituent.

During 1990, approximately 630 samples were analyzed for all the CMT engineering groups associated with this program, with almost 230 samples from electrorefining studies, 120 from fission-product distribution studies, and 280 from waste studies. Each of these samples required determination of up to ten elements.

Rare-Earth Characterization Studies

In one of the Chemical and Engineering Support Studies being conducted in CMT for the IFR (Sec. IV. A), the distribution of the more abundant rare earths between the salt phase (as the rare-earth chlorides) and the cadmium phase (as metals) is being determined as a function of electrorefiner operating conditions. In the experiments performed for this work, lanthanum and one other rare earth are dissolved in a pool of cadmium, which is covered with a layer of molten LiCl-KCl eutectic. Samples of the metal and salt phases are withdrawn from the system following step-wise changes in the redox potential (varied by addition of cadmium chloride) or temperature and are submitted to the ACL for chemical analysis.

In most cases, each salt-phase sample is analyzed to determine Li, K, Cd, and the pertinent rare earths by ICP/AES and chloride by silver-chloride gravimetry. Required ICP/AES detection limits for the rare earths are met by carefully selecting analysis wavelengths and generating profiles of individual emission lines. Each cadmium metal sample is similarly analyzed to determine Li, K, and the rare earths by ICP/AES. Cadmium in the metals is measured by titration with ethylenediaminetetraacetic acid (EDTA).

During this year, experiments were completed on three rare earth pairs (La-Nd, La-Sm, and La-Ce) and on a special study involving Nd and Pu. We developed special procedures to accommodate a need for additional information in the La-Sm study and in the studies that involved neodymium. In the case of samarium, the divalent state of the rare earth is relatively stable, and a method was required to determine the amount of samarium that was present as samarous ion. This measurement was made with a method developed previously for studying europous ion in similar situations. The method involves dissolving the salt sample in a nitrogen-sparged solution containing excess ferric [Fe(III)] ion, which is reduced to ferrous [Fe(II)] by the divalent rare earth. The resulting ferrous ion is accurately determined by titration with Ce(IV) using a Ferroin indicator. In contrast to europium where virtually all the rare earth was divalent, only about 20% of the samarium was found to exist in this oxidation state.

For the experiments involving the La-Nd pair, lower detection limits and higher precision than ICP/AES could provide were required for the neodymium determinations. Consequently, we established a method for MSID measurement of neodymium, in which weighed aliquots of the dissolved salt or metal samples are spiked with a known quantity of ^{150}Nd-separated isotope and the neodymium fraction of the spiked sample is isolated by column-extraction chromatography for mass spectrometric analysis. The column packing used for this separation contained octyl(phenyl)-N,N-diisobutylcarbamoylmethylphosphine oxide (CMPO) complexant coated on an XAD-7 resin support. Precision of better than 0.5%, relative, and detection limits on the order of 1 μg neodymium per gram of sample were achieved with this approach.

The MSID technique was also applied for measuring Nd and Pu in the study that involved these elements. The ABBEX (from Eichrom Associates, Evanston, IL) column material gave excellent separation of neodymium from plutonium, as well as from the other cations (e.g., K, Li, Cd) present. For the plutonium measurements, a portion of each dissolved sample was spiked with ^{244}Pu prior to extraction of the plutonium fraction from acid-deficient aluminum nitrate solution into hexone for mass spectrometric analysis. Precision and detection limits for the plutonium determinations were comparable to those for neodymium. Data from all these studies are being used by the CMT researchers to develop and validate computer models that predict rare-earth behavior during IFR electrorefining operations.

Zeolite Immobilization of IFR Waste Salt

The concept of immobilizing IFR waste salt in a zeolite matrix is being investigated by researchers in the CMT Division (Sec. VI. D). Experiments are being conducted to obtain baseline sorption data for single salt components and also to simulate a tentative salt-treatment process in which multicomponent salts are involved. Support from the ACL for these studies has involved developing procedures for complete dissolution of bare and salt-laden zeolites for chemical analysis to determine concentrations of specific components; in addition, conventional procedures such as ignition and pyrohydrolytic decomposition have been applied to determine halide content. More than 175 samples were analyzed for this effort during the past year. Data from these analyses are helping to guide selection of zeolite forms to achieve desired performance levels and to understand the mechanism (e.g., ion exchange vs. occlusion) by which a given zeolite immobilizes specific components of the waste-salt materials.

Studies of Alkali in Hot Off-Gas from Pressurized Fluid-Bed Combustors (PFBC)

Alkali metal compounds present in the hot off-gas from PFBC, such as chlorides and sulfates of sodium and potassium, can cause corrosion of the gas turbine used to recover energy released during combustion. Researchers in CMT are developing an analytical alkali sorber bed technique for reliable quantification of the level of vapor-phase alkali in PFBC off-gas on a time-averaged basis so that the effectiveness of different alkali control strategies might be evaluated (Sec. II). In this technique, analytical alkali sorber beds containing activated bauxite or diatomaceous earth are inserted in the primary sorber bed (activated bauxite) that is used to condition the PFBC process stream. After a given test, the analytical sorber beds are contacted with an appropriate leaching solution. We analyzed these leachates for alkali metals by atomic absorption spectrophotometry and for anions by ion chromatography. Other types of samples are analyzed by various techniques to provide additional data on sources of alkalis and their performance in this system. During the past year, we analyzed more than 350 samples of bauxite leachate and other samples (auxiliary absorber solutions, PFBC feed materials, fly ash, and gases) in support of this project.

Analysis of Environmental Samples

The ACL provided analytical services to a variety of environmental monitoring, characterization, and remediation projects administered by ANL programmatic divisions and programs at other DOE facilities. Samples processed this year included approximately 620 waters, 1000 soils/sediments, and 370 miscellaneous matrix samples (air, filters), which were analyzed according to protocols described in the Contract Laboratory Program (CLP) Statements of Work (SOW) from the U.S. Environmental Protection Agency (EPA), the methods described in EPA document SW-846,[1] or other appropriate procedures.

Environmental analyses provided by the ACL include determination of inorganic constituents (metals, anions, cyanide, sulfide, oil and grease, total dissolved and suspended solids), organic compounds (volatiles, semivolatiles, polychlorinated biphenyls/pesticides, phenolics), and radionuclides (gamma emitters, gross alpha/beta, actinides).

Geoscience Programs

Analytical measurements were performed in support of geoscience programs at ANL. These measurements include characterization of groundwater samples by analysis for cations with ICP/AES or atomic absorption techniques; measurement of anion concentrations (F^-, Cl^-, NO_3^-, NO_2^-, SO_4^{2-}, Br^-, I^-) by ion chromatography; determination of pH, alkalinity, or other properties by classical methods; and isotopic measurements by thermal-ionization mass spectrometry (TIMS). These techniques were applied to thermal waters from Yellowstone National Park and to thermal waters, gases, steam condensates, and gas-sampling absorber solutions from volcanoes in Colombia, Equador, and Papua New Guinea.

---

[1]U. S. Environmental Protection Agency, *Test Methods for Evaluating Solid Waste*, EPA Document SW-846, Office of Solid Waste and Emergency Response, Washington, DC (November 1986).

In support of the Yellowstone studies (Sec. IX. D), we were required to implement procedures to isolate and purify strontium from geological samples for isotopic analysis by TIMS. This requirement led us to investigate a new approach to isolating strontium from such samples (described below). This new approach reduced the time and effort for preparing strontium isotopic samples by a factor of four to five and permitted an increase in the number of samples processed for the Yellowstone Project. Isotopic characterization of Yellowstone hot springs was further expanded this year to include investigating the behavior of lithium isotopes in the samples.

We also improved our capabilities for determining anions in geological samples by acquiring specialized guard columns for our ion chromatograph. These columns permit analysis of waters containing substantial quantities of humic substances and organic acids, which had interfered with past measurements on samples from some locations.

Isolation of Strontium from Geological Samples for Isotopic Analysis

The isotopic geochemistry of strontium is a well-established tool for tracing the origins and migration of groundwater systems that existed in past geological times, as well as those that exist in the present. For isotopic analyses, strontium must be isolated from the sample matrix. The most difficult step in this isolation is separating the strontium from the relatively large amounts of calcium with which it is almost always associated. This separation has conventionally been accomplished by classical cation exchange in a procedure that requires large ($\geq$50 mL) ion-exchange columns and enormous volumes (approaching 1 L per sample) of high-purity acid solutions. We have investigated the application of a new column-extraction packing material to this separation. The packing (Tradename Sr•Spec) uses a crown ether of the 18-crown-6 type, which is coated on an inert resin substrate. It was developed for extracting and recovering radioactive ^{90}Sr from liquid nuclear waste and exhibits exceptional selectivity for strontium over most other elements.

Using synthetic mixtures and actual geological samples, we have shown that microgram quantities of strontium can be effectively isolated from milligram quantities of calcium and other metals with a column containing only 1 to 2 mL of the Sr•Spec packing. The strontium is selectively retained on the column from 3 N nitric acid with extremely high selectivity and is eluted with less than 20 mL of very dilute acid. Our studies with this separation procedure indicated that no measurable amount of extraneous strontium was picked up (negligible blanks), and no measurable fractionation of isotopes occurred. The new packing appears to be nearly ideal for this application.

Separation of ^{178m}Hf from Tantalum Target Materials

A long half-life (31 yr) and a very high spin (16^+) make ^{178m}Hf a unique candidate projectile for use in accelerator beams and targets for the study of high-spin phenomena in nuclear and atomic physics. Researchers in the Physics Division attempted to produce and isolate this nuclide by bombarding a stack of thin (0.8 mm) tantalum foils with protons in the Brookhaven Linac Isotope Production Facility; this technique produced ^{178m}Hf by proton-induced spallation. The ACL was requested to separate the hafnium-product isotopes from the

foils so that direct gamma spectroscopy might be done. We dissolved each tantalum foil in nitric/hydrofluoric acid and made the separation by anion ion exchange in a mixture of HCl and HF. Under the conditions of the separation, tantalum strongly adsorbed on the ion-exchange column, while hafnium was only slightly adsorbed. The strong ^{182}Ta activity was efficiently removed. However, other radioisotopes (e.g., ^{172}Hf, ^{175}Hf) in some of the foils still obscured the ^{178m}Hf peaks in the direct gamma-ray spectra. Nevertheless, cross-section data for two foils (at different proton energies) were obtained. The separations that we performed allowed determination of the cross-section data, which were presented at the First International Conference on Radioactive Nuclear Beams (October 16-18, 1989, Berkeley, CA).

Measurement of Volatiles in Sulfur Product from Microwave Decomposition of H_2S

Researchers from the Energy Systems Division studying the gas-phase decomposition of gaseous sulfur compounds by microwave heating required information about volatile species associated with the product from their process. In response to this need, we developed procedures whereby sulfur-containing samples could be outgassed under reduced pressure and/or at elevated temperature, and the evolved gases could be directly measured before, during, or after heating. For these measurements, the sulfur sample was placed in a vacuum-tight Pyrex vessel, which was placed in a tube furnace and attached to a CEC 21-620 mass spectrometer. Each of six samples of sulfur deposited from microwave-heated streams of H_2S, H_2S plus CH_4, or H_2S plus CO_2 was analyzed. For two samples, gases released at 25 (ambient), 50, 100, and 120°C (melted sulfur) were measured; for the other four, measurements were made only at 25 and 120°C.

Other than residual air, the only gas detected at 25 and 50°C was trace H_2S. At the higher temperatures, appreciable volumes (0.1 to 0.3 cm^3) of gas, principally H_2S, were released. Water was the next most abundant component from each sulfur sample, with lesser amounts of Ar, CS_2, and CO_2. Two samples gave detectable amounts of SO_2; one sample gave COS and trace hydrocarbons. These data will help to guide decisions on feasibility and methodology regarding recycling or disposal of the sulfur product from technologies that might be developed from the studies in progress.

Plutonium Residue Recovery Program

Several different chemical processes have been explored in CMT to determine which one is the most efficient for recovering plutonium from various types of scrap and residues. These processes utilize a number of different molten-salt mixtures along with varying reductant alloys containing two or more of the following: Al, Cu, Ca, Mg, Zn, U, and Fe. Also as part of this program, experiments have been performed to investigate molten-salt metal systems for use in actinide recycle of light water reactor fuel (Sec. VII).

In tests of these processes, material balances must be accurate, and reliable analyses of the feed material, salt, and reductants have to be performed. The primary analysis done by us was quantification of elements by ICP/AES and gamma spectrometry. In addition to the reductants and plutonium, elements of interest were Am, Np, B, Cd, Fe, K, Li, Mo, Na, Si, Ta, Ti, Pd, Ru, and W. Approximately 130 samples were analyzed in this year.

Decomposition Products from Thermally Unstable Complexants

Vinylidene 1,1-diphosphonic acid (VDPA) is a member of a new class of complexing agents under development in the Chemistry Division. These complexing agents, called Thermally Unstable Complexants (TUCS), were designed to be strong complexants for specific metals under very acidic conditions (≥8 M acid) and to decompose to innocuous products upon heating for a period of time. These properties make the TUCS particularly attractive in certain separation/recovery processes, where they may be used and destroyed without having to be dealt with in the waste stream. To support a study of the decomposition of VDPA in nitric acid, we used ion chromatography (IC) to determine the concentrations of intermediates and products (e.g., organophosphonic acids, phosphate ion) so that the decomposition kinetics could be followed. Interference from nitrate ion was found to limit the utility of IC for this purpose under "isocratic" elution conditions (i.e., constant eluant concentration). To resolve this problem, we developed a gradient-elution IC procedure that uses sodium hydroxide solution as eluant instead of the conventional carbonate/bicarbonate solution. Thus, the nitrate interference was overcome for nitrate-to-phosphate ratios up to about 100.

Molten Corium Concrete Interaction (MCCI) Studies

In MCCI experiments at the Reactor Engineering Division, mixtures of uranium oxide, zirconium, steel, fission product elements, and concrete are heated to temperatures simulating reactor meltdown conditions. The objective is to study the vaporization behavior of the elements present and to understand the release of refractory fission products during a degraded-core accident. Samples of solidified melt, aerosols collected by impaction or on filters, and gases are examined to study interaction and transport of the simulated reactor materials. Analytical support for these studies involves application of a wide variety of measurement techniques and requires considerable flexibility in approaching the analytical problems that arise from changes in the materials that are brought together in going from one test to the next. The concretes that have been used in particular experiments have ranged from common limestone-aggregate to highly siliceous concretes (common in Europe) to serpentine-aggregate concrete brought in from Russia. In some recent tests, volatile fission-product metals (e.g., In, Te) were added to the corium simulation and had to be accounted for in methods used to dissolve and analyze sample materials from each test.

Typically, the solidified melt and aerosol samples are analyzed for Ag, Al, Ba, Ca, Ce, Cr, Cu, Fe, K, La, Mg, Mn, Mo, Na, Ni, Si, Sn, Sr, U, W, Zn, Zr, and other metals by ICP/AES; for silicon by AAS or classical gravimetry; for soluble anions by ion chromatography; and for miscellaneous elements such as S, C, or N by appropriate methods. Often, XRD measurements are made to identify particularly interesting phases in selected samples. Gas samples are analyzed by mass spectrometry.

This year, we analyzed samples from two large-scale MCCI tests involving high-silica concretes and relatively volatile fission-product elements (In, Te, Ru). Materials from these tests were especially difficult to analyze because of the high-silica concrete that was involved and the tendency of some added fission-product elements to be lost by volatilization (Te, Ru, Sn, In) or by precipitation (Ag, Ce, La) under conditions required to dissolve the silica matrix. Ultimately,

we adopted a procedure which involved dissolving two separate portions of each sample. The first portion was dissolved in a closed Teflon or Teflon-lined vessel with a mixture of nitric and hydrofluoric acids. The solution from this step was used to determine (by ICP/AES) 23 of the 25 metals of interest and was found to give equivalent results whether we used microwave-heated digestion vessels or Teflon-lined pressure vessels (Parr decomposition vessels) heated overnight in a conventional oven. For determining the rare earth elements (Ce and La), which form insoluble fluorides in the HF dissolution, we treated a second portion of each sample as before, but then treated the solution and residue from the preparation with perchloric acid to expel HF and silicon (as SiF_4). The perchlorate residues were dissolved in dilute nitric acid, uranium was separated from the mixture by anion-exchange chromatography as needed, and the solutions were analyzed for Ce and La by ICP/AES. For all elements, good agreement (typically 5% or better) was obtained between duplicate preparations on individual samples, as well as duplicate portions of materials that were submitted as separate samples. Results of these analyses will be used to evaluate and improve computer codes that are designed to predict the melt and aerosol behavior under conditions of the MCCI tests.

Volatile Organic Compounds and Inorganic Gases in Storage Drum Headspace

One of the tasks for DOE's Waste Isolation Pilot Plant (WIPP) Program is to characterize volatile organic gases and inorganic gases present in drums containing mixed (radioactive plus hazardous) waste. These drums are to be placed in bins, which will go into DOE's long-term mixed waste storage facility in Carlsbad, NM.

The ACL has been designated as the backup laboratory for analysis of headspace gas samples for volatile organic compounds (VOC) and inorganic gases from the WIPP Program. The primary laboratories are located at Idaho National Engineering Laboratory and Rocky Flats Plant.

To determine the 29 target VOCs specified in the WIPP-Quality Assurance Project Plan, we assembled a cryogenic-based system for sample-inlet preconcentration. This system is interfaced to a GC that is coupled to a mass selective detector (MSD) and is designed to analyze samples from SUMMA canisters by using an analytical method adapted from the EPA (Compendium Method TO-14).[2] For initial work, a cryogenic trapping interface was selected rather than a solid adsorbent trapping interface, because it has better trapping efficiency than the solid adsorbent for polar VOCs, such as methanol. Using the cryogenic trapping interface in a direct injection mode, we have analyzed a test mixture of some VOCs at their limit of quantitation. Thus, we have demonstrated that our cryogenic system will meet WIPP needs.

We are also developing a sample-inlet concentration system based on solid adsorption, which is typically used to concentrate and analyze nonpolar and medium-polarity VOCs. The

---

[2]W. T. Winberry, Jr., N. T. Murphy, and R. M. Riggan, *Compendium of Methods for the Determination of Toxic Organic Compounds in Ambient Air*, U. S. Environmental Protection Agency, Research Triangle Park, NC (June 1988).

inlet systems based on solid adsorption and cryogenic trapping will be evaluated for trapping efficiency and cost-effectiveness. Based on this evaluation, the analytical method to be used for WIPP will be recommended. Inorganic gases will be determined by mass spectrometry (MS).

Protocol for determining gases from the headspace of waste drums in the WIPP requires the use of sample canisters free of trace organic contaminants. Argonne has been designated as the laboratory responsible for the cleaning and certification of sample canisters to be used by each laboratory participating in the program. We are in the process of setting up and testing equipment for cleaning the canisters on a relatively large scale, 100 or more per month. The equipment will allow a batch of, typically, eight canisters to be sequentially heated to 100°C, evacuated, backfilled with high-purity humidified air, and re-evacuated; the cycle will be repeated three times. One canister from each cleaned batch will be repressurized with clean humidified air and analyzed for volatile organic compounds by the same technique (sorbent trapping and GC/MS) used for field samples.

Preparation of Samples for the National Energy Agency Committee on Reactor Physics (NEACRP) Study

In March 1990, we prepared eight sets of three tritium solutions for the NEACRP International Tritium Comparison Study. Laboratories participating in this study are located in Canada, France, Italy, Japan, Switzerland, and the United States. Each set of three was prepared from National Institute of Standards and Technology (NIST) tritium standard SRM4926-D. All dilutions were done by weight, and all weighings were done in triplicate. Aliquots were heat sealed in engraved glass ampoules and distributed to the participants for analysis. Prior to shipping, each aliquot size was assayed by liquid scintillation counting to verify the quality of the solutions.

JANUS Water Analysis

The JANUS reactor at ANL is primarily used for investigating the biological effects of radiation. We periodically sample and analyze the primary coolant water for its radionuclides. The purpose of the analysis is safety related because the isotopes detected indicate the integrity of the fuel plates used to power the reactor. The isotopes that are present in normal operations are ^{24}Na (a neutron activation product) and minute amounts of short-lived fission products. The presence of isotopes such as ^{137}Cs, which have never been observed, would strongly suggest the breach of fuel plate(s) and trigger appropriate corrective actions.

Plutonium(VI) Speciation Study

The CMT Division is studying ^{242}Pu hydrolysis in a nuclear waste program (Sec. IV. C). In this effort, the speciation of Pu(VI) in near-neutral solutions and in perchlorate media is being investigated using laser photoacoustic spectroscopy and conventional absorption spectroscopy. Purification of the ^{242}Pu solutions and adjustment to desired concentrations and pH were done in the ACL plutonium laboratory.

To establish the nature of the plutonium complexes that exist under different conditions, we first purified the ^{242}Pu-containing solution using an ion exchange method. The desired plutonium concentrations (between 10^{-5} and 10^{-2} M) and oxidation state (VI, by fuming with $HClO_4$) were then obtained, and the pH was adjusted to various values between 3.0 and 6.0. The desired purity and concentrations of the plutonium were confirmed by α-spectrometry, as well as 2π proportional counting and liquid scintillation counting.

Analysis of Cotton and Waters

Tambrands, Inc., requested analysis of cotton and water samples for very low levels of radionuclides. Its interest was the identification and quantification of any radionuclides present in the cotton after being treated with a particular water. Submitted to the ACL were three types of cotton and three samples of water.

This request necessitated the coordinated use of various methodologies available for analyzing environmental-type samples containing α-, β-, and γ-emitting radionuclides. Water samples were reduced in volume and prepared first for analysis of γ-emitting radionuclides. The α-emitting thorium and plutonium isotopes were determined on one portion of the concentrated sample by using the standard α-spectrometric isotope dilution method. A second portion of the concentrated sample was used for determining ^{226}Ra by the radon emanation method. The cotton sample analyses were coordinated in a similar way, except that the initial step was the ashing of the sample. All measurements yielded levels of radioactivity comparable to background levels.

Radium in Water

Radium in water is still of great concern to municipalities and home owners where water is used for drinking and cooking. Radium in drinking water is regulated by the EPA, where the maximum allowable total radium is 5.0 pCi/L.

The Environmental Research Division is conducting a study where groundwater may be contaminated by rain water run off in the vicinity of uranium mill tailings and uranium ore storage piles. Numerous groundwater and lake water samples were collected for determining ^{226}Ra by the radon emanation method. This method can be performed on a small sample with the sensitivity as low as 0.02 pCi per sample.

Using this same method, we completed numerous ^{226}Ra determinations on geological brines, the salty waters that surface first when one drills for oil. In cases where large volumes of samples were available, the analysis was done by concentrating radium on a selective ion-exchange complexing resin, which was, in turn, gamma counted for radium. Analysis for ^{226}Ra and ^{228}Ra was performed on approximately 60 samples. Typical values measured were 1 pCi/L or less.

ANL-West Soils, Vegetations, and Waters

The soil, vegetation, and water samples collected at ANL-West as part of its environmental survey sampling plan are sent to the ACL and analyzed for various radionuclides. Industrial

waste ponds are sampled semiannually, and soils and vegetation surrounding the Laboratory are sampled annually.

The samples received from ANL-West are analyzed for gamma and alpha emitters, specifically thorium and plutonium isotopes. Approximately 40 samples were analyzed this year. Measured concentrations for thorium were comparable to levels expected for naturally occurring thorium; for plutonium, levels were typically 10^{-15}Ci per gram of soil, which is the level expected from fallout.

Radiation Damage Studies for Superconducting Super Collider (SSC) Detector Research

As part of the SSC detector research, the High Energy Physics Division is evaluating semiconductor fabrication processes with the aim of designing radiation-hardened electronics. For this project, we have characterized the neutron flux spectrum for two positions, H-2 and VT-3, at the ANL Intense Pulsed Neutron Source (IPNS) by irradiating various metals chosen to have neutron reaction products across the expected neutron spectrum. The activities of the resulting activation products are measured by gamma spectrometry and then used to calculate the time-corrected reaction rate, which is then input to STAYSL, a computer program that determines the neutron spectrum. With these reaction rates, neutron fluence values of subsequent irradiations in those positions can be determined by using Co and Ni dosimeters. To date, we have prepared 90 Co and Ni dosimeters, 49 of which have been used in irradiations at IPNS. The investigators have since moved their experiments to ANL's Fast Neutron Generator, which was found to have a more desirable neutron spectrum. We have completed analyses of 10 dosimeter sets from this facility, with analysis of another four dosimeter sets in progress.

Synchrotron Thrust Group Activities

The CMT/APS Synchrotron Thrust Group was founded in January 1989 to explore possible CMT use of the ANL Advanced Photon Source (APS) for current and future research programs. The APS, which is currently under construction at ANL, will be a national user facility for examining material structures from microscopic sizes down to atomic dimensions. The eventual goal of the group is to develop a plan for utilization of the APS by CMT. The major activity of the group in 1990 was preparing a Letter of Intent (LOI) to use the APS; this is the first action required from groups interested in performing research at APS.

The CMT Division is involved in many different research activities, and for this reason there is interest in a variety of APS capabilities rather than a specific one. The main areas of interest to CMT are the following: synchrotron radiation X-ray diffraction for structural determination of various types of materials; synchrotron radiation X-ray fluorescence, which offers the potential of lower limits of detection and light element determination; various synchrotron radiation X-ray absorption methods for determination of molecular species, *in situ* kinetic studies, and determination of amorphous material structures; and a variety of imaging techniques (e.g., tomography, microscopy, and lithography).

After much deliberation, the group decided to submit a proposal for CMT to develop a multipurpose facility based on the bending-magnet side of an APS sector and to seek a

collaborator from the other prospective users who would develop the insertion-device side of the sector. The CMT beam line would be operated independently of the insertion-device beam line, both as a research facility and as a service facility similar to ACL. This unique arrangement would allow easy access to state-of-the-art X-ray diagnostics for the scientific community both at ANL and off site.

The response to our LOI directed us to pursue collaboration with physical research divisions at ANL, which are proposing a similar facility, and we have initiated contacts with them.

Radiological Environmental Analyses for Rocky Flats Plant (RFP)

The 1980s brought a heightened awareness of environmental concerns to DOE. In response, many DOE sites have either initiated or strengthened programs designed to clean up the environment. As a result, the ACL has been requested to perform radiochemical analyses for the RFP Environmental Restoration Program.

In late May, the ACL received approximately 200 soil samples from RFP. Prior to analyses, these samples were dried, sieved, and milled to ensure homogeneity. The soils were then analyzed for gamma emitters, Pu, Am, and U, and the results reported to RFP. As work progresses, subsequent radiochemical analyses may be required on these samples. Measurements were made with a typical detection limit of 0.01 pCi per gram of sample.

Analysis of Cores from Pressure Vessel of Experimental Boiling Water Reactor (EBWR)

Seven samples of the EBWR pressure vessel, currently being dismantled at ANL, have been provided to ACL in the form of cores of 1-in. (2.5-cm) dia and 2.5-in. (6-cm) length. The vessel is made of mild steel with a thin layer of stainless steel on the inner surface. The ACL was asked to confirm that the inner layer of the vessel is 304 stainless steel and also to identify the radionuclides present in these cores, along with their associated activity levels, to allow for proper waste disposal. These data, from the various measured activation rates, will be used to estimate the neutron fluence over the lifetime of the reactor.

The cores were first cut into segments, and gamma spectrometry was used to determine the ^{60}Co content. Small pieces of each segment were taken for dissolution and determination of cobalt content by ICP/AES, which will also be used to determine the composition of the stainless steel. After ion-exchange separation of the nickel from the bulk of the iron, the solutions of the stainless and mild steel segments will be used to determine the activity level of ^{63}Ni.

Analytical Support Using X-Ray Diffraction (XRD) and Scanning Electron Microscopy (SEM)

This year, 312 XRD and SEM analyses were completed in support of ANL programs (e.g., IFR development, nuclear waste research, battery and fuel cell development, and basic studies on thin-film superconductive materials).

The mechanical Philips X-ray diffractometer of ACL was automated for data collection, reduction, and display using commercially available upgrade packages. For this automation, we purchased a commercial interface "Databox" for data collection and a commercial data reduction package. The original mode of mechanical operation can still be used as backup in case of automation disruption.

Fourier Transform Infrared (FTIR) Microscopic Analysis of Fluid Inclusions

We used FTIR microscopy to study the structure of organic material trapped in inclusions of halite rock as part of a research program in the Materials and Components Technology Division. The instrumentation consists of a Spectra-Tech IRPLAN-II and a Nicolet 60SX FTIR.

Most of the present methods used for the study of fluid inclusions require opening the fluid cavity and withdrawing the contents for analysis, whereas FTIR microscopy is a noninvasive technique with which one can characterize functional groups present in the fluid and identify the hydrocarbon constituents. At present, we are using *in situ* FTIR microscopy to analyze fluid inclusions in halite samples from southwestern New Mexico.

Studies in Organic Fluid Fouling in Heat Exchange Systems

In collaborative work with the Energy Systems Division, we studied the fouling of heat exchange systems with an organic fluid model. The goal was to elucidate the fouling mechanism by characterizing the soluble precursors in the organic fluid. Samples of 6% styrene in heptane were removed from a heat exchange system at varying time intervals and analyzed by several methods: GC with flame ionization detector, supercritical fluid chromatography (SFC), GC/MS, SEM, XRD, and FTIR microscopy. System temperatures ranged from 30 to 180°C (90 to 350°F).

Results indicated that the predominant mode of degradation of the organic working fluid is polymerization of the vinyl chain (chain-to-chain). The following mechanism was proposed:

monomer + monomer --> dimer
dimer + monomer --> trimer
trimer + dimer --> pentamer

Subsequent reactions increased the chain length by dimer units. In addition, other degradation products were formed. Cleavage of the styrene vinyl chain resulted in the formation of substituted benzenes. The phenyl radical produced from the cleavage process reacted to form quarterphenyl. Small quantities of chain-to-ring polymerization products were noted as well. Methodology has also been developed to evaluate the fouling deposit on the heat exchange system pipe by FTIR microscopy, SEM, and XRD.

FTIR Analysis of Semivolatiles in Soils

We are developing a new method to characterize, in the field, contaminated soil samples for explosives, pesticides, and selected volatile and semivolatile analytes. We initially

demonstrated that individual volatile and semivolatile analytes can be desorbed and analyzed in a cell at elevated temperatures (~180°C). Using the pure analytes as standards, we then attempted analysis of mixtures. To date, the qualitative and quantitative determination of up to four analytes in a mixture has been successfully completed. The program has now progressed to the analysis for explosives in soil samples by thermally desorbing them from soils and qualitatively and quantitatively identifying them by FTIR. Analysis of a preliminary set of spiked soil samples has shown excellent recoveries and quantitative accuracy within 15%. This technology is applicable for site characterization and site remediation and could play a significant role in the cleanup of the Joliet Army Ammunition Depot or other areas contaminated by explosives.

Remote Detection of Chemical Agents with FTIR

Our current studies in remote FTIR detection of chemical agents are being extended to include different mixtures, environmental backgrounds, and sampling pathlengths. All work has been done with an XM21 remote FTIR provided by the Chemical Research Development and Engineering Center (CRDEC).

In 1990, several substitutes for chemical agents (methanol, diethyl malonate, isopropanol, dimethyl methylphosphonate, chloroform, and carbon tetrachloride) were studied both in the laboratory and in the field. Data were collected at distances of 0.5 to 5 km from targets such as municipal incinerators, Grace Chemical Co., Baltimore-Washington International Airport, and Bethlehem Steel. Results to date, although mostly qualitative, are highly encouraging. Field tests were also performed at Aberdeen Proving Ground, where SF_6 releases were detected at 150-200 m concurrently with releases of known amounts of agent-related chemicals. Because of the situation in the Middle East, the XM21 remote FTIR had to be returned to CRDEC. We are building our own laboratory remote FTIR system to continue the program here.

Incinerator Monitoring for Organic Analytes

A collaborative study with the Energy Systems Division was undertaken to monitor incinerator effluent from different feeds and to correlate the feed content with stack effluent by qualitatively and quantitatively analyzing the effluent. A library of the FTIR spectra of chemicals of interest has been built, and the FTIR is now being coupled with an incinerator. The technology has the potential to provide the analytical requirements mandated by the Clean Air Act to monitor organic emissions.

Determination of Volatile Organic Compounds for Lake Michigan Study

In a collaborative study with the Environmental Research Division, we are determining air quality over various parts of Lake Michigan by analyzing ambient air samples for hydrocarbons. Volatile organic compounds play a major role in the formation of ozone. To study the air quality over Lake Michigan, we collected ambient air samples in 6-L SUMMA canisters at sites in Illinois, Indiana, and Wisconsin during periods of predicted high ozone concentrations. We then analyzed the samples for 54 target hydrocarbons by use of a modified EPA Method TO-14 and flame ionization detection (FID). Results of this study are being used to formulate a more

comprehensive sampling program. We will also confirm, by GC/MSD, the presence of hydrocarbons found in these samples by FID.

The EPA Method TO-14 required building a sample inlet manifold and using a cryogenic trap for preconcentration of the air samples. Thus, an automated cryotrap (Chemical Data Systems Model 330) was interfaced to a Hewlett-Packard GC/MSD system.

Walter Reed Army Institute of Research (WRAIR) Site Characterization

The WRAIR building was proposed to be constructed on an uncontrolled landfill site in Forest Glenn, MD. Before construction of the building, hydrological and chemical characterization of this site was required. The principal objectives of the site-characterization part of this study were as follows: (1) determine, precisely, the geometry of the landfill and lay out a sampling grid and (2) obtain and analyze representative samples of the soil fill materials, surface water, organic soil vapors, and groundwater to provide the basis for a credible qualitative human risk analysis.

We assisted the U.S. Army Corps of Engineers in preparation of the sampling, analysis, and quality assurance plans for the site. We also managed the total analytical work for this project and performed most of the analyses. Chemical analysis of surface water, groundwater, and landfill soils followed the analytical protocol promulgated under the EPA's Contract Laboratory Program for its Target Compound List and Target Analyte List. These protocols were used to determine the concentration of volatile organic compounds, semivolatile organic compounds, polychlorinated biphenyls/pesticides, radionuclides, and many of the metals analyzed. We also participated in preparing the final report of this study.[3]

Evaluation of Gas Chromatography/Matrix Isolation-Infrared (GC/MI-IR) Spectroscopy

In a project funded by the U.S. EPA, a commercially available GC/MI-IR spectrometer was evaluated as a means for quantitative analysis of standard mixtures. The reproducibility of response was 40 to 60%, which is poorer than expected. In subsequent studies, we found that the algorithm used by the quantitation software and the design of the open-split interface contributed to the poor reproducibility of this procedure.

Method Development and Testing

In collaboration with Region V of the U.S. EPA, we adapted EPA Method TO-14 tc use with an ion trap mass spectrometer. After method development in the laboratory was completed, a field test was undertaken. Samples were collected on a rooftop of a school building in Chicago and were analyzed. We determined the content of target compounds and identified non-target

---

[3]W. Harrison, A. S. Boparai, B. Nashold, S. A. Sandberg, S. A. Foster, J. J. Russell, M. J. Schweighauser, R. R. Heinrich, D. G. Graczyk, N. K. Meshkov, and C. Tome, *Site Characterization and Qualitative Human Risk Assessment for the Walter Reed Army Institute of Research Building Site, Forest Glen, Maryland*, Argonne National Laboratory Report ANL/ESD/TM-9 (July 1990).

compounds. The results of this study were presented at the EPA Air and Waste Management International Symposium, Raleigh, NC, in May 1990.

High Performance Liquid Chromatographic (HPLC) Separation of Explosive and Other High Molecular Weight Compounds

The Energy Systems Division is involved in a bioremediation project for high explosives in the soil at the Joliet Army Ammunition Depot. In a collaborative study with the Energy Systems Division, we developed an HPLC capability to determine high explosives such as TNT, RDX (cyclo-1,3,5-trimethylene-2,4,6-trinitramine), HMX (cyclotetramethylene tetranitramine), etc., in soil samples. This capability is now being applied to soil samples.

In another application of HPLC, we measured polymers of styrene-produced fluids that are used in heat exchangers. These will be useful to determine the polymer structure.

Supercritical Fluid Chromatography (SFC)/Matrix Isolation-Infrared (MI-IR) Spectroscopy

We studied the possibility of interfacing the SFC and MI-IR techniques. Initial studies used supercritical carbon dioxide as the mobile phase. The deposition of the mobile phase was performed under conditions where most of the carbon dioxide was removed. Infrared spectra of test compounds (a mixture of aromatic hydrocarbons) were then obtained of essentially the condensed phase. We thus demonstrated that the SFC/MI-IR interface works. These experiments have been expanded to study supercritical fluid extraction followed by GC/MI-IR.

New Capabilities within the ACL

New capabilities of the ACL established in 1990 include (1) a gas mass spectrometer system capable of determining inorganic and low-molecular-weight organic gases with high precision and sensitivity and (2) a system for determining toxic organic compounds in SUMMA canisters containing ambient air.

Because of the large number of analytical samples received by the ACL throughout the year, many requiring multiple analyses, much time is spent on sample notification, tracking, and records management. To make these operations more efficient, the ACL developed a computer-assisted bar code reading system to enhance our sample tracking capability. The bar code system is designed to permit quick, error-free logging, distribution, and tracking of analytical samples. Installation of a computer-assisted station for bar code reading is planned for each of the ACL laboratories.

XI. R&D PROGRAM COORDINATION OFFICE

The R&D Program Coordination Office in CMT is assisting DOE in establishing and maintaining a national program of applied R&D in the environmental restoration and waste management area. The objective of the applied R&D is to improve the efficiency, safety, and timeliness of environmental cleanup activities so that DOE can meet its 30-year environmental compliance and cleanup goals.

Currently available technology is not adequate to assess environmental contamination, take permanent remedial action, and eliminate or minimize the environmental impact of future operations. Technical resources to address these shortcomings exist within the DOE system and the private sector, but the involvement of the private sector in attaining permanent and cost-effective solutions has been limited. In April 1990, a request for proposals (RFP) was announced with the objective of acquiring private-sector contractors that will perform the R&D needed to help DOE meet its cleanup goals.

The RFP contained detailed instructions for submitting proposals in one of four general areas: groundwater remediation; soil remediation; characterization and sensing of buried objects, contamination, and/or geological/hydrological features; and containment of contamination. The objective is for the contractors to develop technologies that can be demonstrated at a DOE site within 18 months and implemented at selected DOE sites within 3 years at an affordable cost. Each area is briefly discussed below.

Soil Remediation. Soils, sludges, and sediments at DOE sites are contaminated with radionuclides, toxic metals, and hazardous organic compounds. Contamination has resulted from a variety of operations, including the use of soil columns, ponds, and liquid waste storage tanks, as well as the subsurface disposal of waste. The potential for migration of radionuclides and heavy metals from contaminated soils necessitates development of technologies to treat the contaminated volume in a manner that effectively protects public health, safety, and the environment.

Successful technologies in soil remediation must be able to satisfy one or more of the following requirements: isolation and containment of radioactive constituents or heavy metals, long-term immobilization without migration of radioactive constituents or heavy metals, removal of radioactive constituents or heavy metals for treatment, degradation of organics or organometallics to innocuous products such as carbon dioxide and water, elimination or reduction of contaminants to acceptable limits of chemical toxicity, and removal of chemical constituents for treatment.

Groundwater Remediation. Radionuclide, heavy metal, and/or inorganic ion contamination exists in groundwater at many DOE sites. This contamination has resulted from a variety of operations, including the use of liquid waste storage tanks and disposal of liquid wastes to cribs (engineered leach fields), trenches, and ponds. Many contaminants are dispersed in the soil column (unsaturated zone) and the groundwater. Because of the migration potential of these contaminants, technologies are needed to treat the contaminated groundwater in a manner that effectively protects the environment and human populations. In addition, contamination of

groundwater with organics is a problem at many DOE sites. The two most common contaminants are trichloroethylene and carbon tetrachloride. Other organics used at DOE sites that may contaminate the groundwater include nonvolatile organics that are soluble (extractants and complexing agents) and insoluble (polychlorinated biphenyls and pesticides).

Successful technologies in groundwater remediation must satisfy one or more of the following requirements: removal or destruction of organics in the presence of other wastes; isolation of heavy metal, radioactive, and/or inorganic constituents; removal of heavy metal, radioactive, and/or inorganic constituents; reduction of contaminant concentrations to acceptable limits; and elimination of contaminant impacts to the surrounding environment.

Characterization and Sensing of Buried Objects, Contamination, and/or Geological/Hydrological Features. Most DOE sites have some form of subsurface contamination, ranging from buried concentrated waste forms, such as tanks or trenches, to dispersed contaminants in soil or water. Specific needs are locating, characterizing, and mapping buried tanks and other concentrated waste forms; locating contamination in groundwater and vadose zones; tracking the migration of contaminants; and characterizing soils. Worker safety is of particular concern with buried wastes. Current subsurface sensing and characterization methods for dispersed contaminants primarily involve a time-consuming, expensive process for drilling wells, taking samples, sending samples to laboratories, and waiting for results. Drilling is very expensive and leads to possibilities for additional spread of contamination. Sampling often disturbs the environment to such an extent that results may be invalid. Particularly during remediation activities, lack of real-time analysis leads to costly delays in operations involving personnel and equipment. Groundwater monitoring may continue for many years. Accurate determination of the spatial distribution, movement, and concentrations of contaminants is essential to assessing remediation needs and designing remediation measures.

Successful technologies in characterization and sensing of buried objects, contamination, and/or geological/hydrological features must satisfy one or more of the following requirements: improve information content and level of confidence of site characterizations, reduce environmental or personnel risk of characterization activities, and substantially reduce the time or cost required for site characterization.

Containment of Contamination. Contamination by hazardous and radioactive materials in soils, sludges, and groundwaters exists at many DOE sites. Where concentrated sources of contamination exist but immediate restoration cannot be initiated, it is desirable to temporarily contain the source of contamination and prevent dilution or migration of contaminants. Sources of such contamination include ponds, liquid waste storage tanks, and soil from subsurface disposal of waste.

Successful technologies in containment of contamination must satisfy one or more of the following requirements: short-term isolation or containment of radioactive, inorganic, and organic constituents; immobilization of contaminants; and changes in subsurface migration patterns away from environmentally sensitive areas (e.g., drinking water aquifer) or toward remediation site.

In June 1990, 147 proposals to develop technologies in the above four areas were received from 108 organizations. These proposals were evaluated by 42 technical reviewers drawn from ANL, other national laboratories, other federal agencies, and academia. The results of these evaluations were presented to R&D Program Coordination Office staff, DOE staff, and an ANL Source Evaluation Board (SEB). The SEB approved the recommendations of the technical evaluators and authorized ANL to begin contract negotiations with 15 offerors (13 private firms, 1 university, and 1 government laboratory). Negotiations and preparation of contracts were completed over the next two months, and all contracts started by October 1, 1990. The R&D Program Coordination Office is providing technical and management oversight to assist the contractors in meeting their milestones within budget and on schedule.

Via a memorandum of understanding, the Department of Energy and Environmental Protection Agency are co-sponsoring five Hazardous Substance Research Centers (HSRCs), each of which is made up of universities from the same region. These centers are the Northeast Hazardous Substance Research Center, Great Lakes and Mid-Atlantic Substance Research Center, Waste Minimization and Management Center, Hazardous Substance Research Center for Federal Regions 7 & 8, and Western Region Hazardous Substance Research Center. Research at the centers includes several projects on biotechnology for waste remediation, pollutant transport mechanisms, chemical and thermal destruction of organics, and waste minimization during facility decontamination. The R&D Program Coordination Office serves as the technical and administrative interface between DOE and the centers. Activities have included attending Science Advisory Committee meetings, developing an accurate data base of HSRC-funded research for DOE planning purposes, and presenting an overview of DOE environmental and waste management activities at an HSRC-sponsored scientific symposium and introductory meetings at selected centers.

XII. COMPUTER APPLICATIONS

The Computer Applications Group provides assistance to CMT staff in many aspects of computer-related activities, including (1) information management systems and data-base development, (2) office automation, (3) laboratory data acquisition and control, (4) computer modeling and simulation studies, (5) small and large computer system networking, (6) post-analysis of experimental results, (7) graphics applications, (8) computer operating system maintenance, (9) procurement of automatic data processing equipment, and (10) advisory, educational, and consulting services.

The Computer Applications Group has the responsibility for software maintenance and development of (1) several major minicomputer data acquisition systems, (2) the Division's Local Area VAX cluster consisting of eleven VAX's, and (3) Macintosh and IBM-compatible personal computer (PC) networks. The Group also provides hardware maintenance of various small systems and peripherals, including the Division's extensive terminal communications system and local area networks.

Utilization of PC's both for data acquisition/control/analysis and modeling has continued to increase. Over one hundred such systems now exist. Group personnel continued work on the computer program portion of the Generic TRUEX Model for the CMT Separation Science and Technology Group (see Sec. V.A.1 for further discussion). The model, which runs on a Macintosh or IBM-compatible PC, calculates a TRUEX solvent extraction flowsheet based on input of a specific feed solution and a specific set of process goals and constraints, and it estimates the space and cost requirements to install a TRUEX process for a specific application.

Group staff also continue to support the Analysis and Diagnostic Laboratory (ADL), formerly the National Battery Test Laboratory. Operating for over a decade, the ADL evaluates a wide variety of battery systems (Sec. I.B), some of which require unusual charging or discharging regimes, or feature a local "intelligent controller" that requires unique interfacing to the ADL control system computer. It is an ongoing effort to develop software to support the testing of new battery systems as they arrive at the laboratory. Significant effort was given to improving the software (LSI-11) used to control simulated driving profile discharges in battery tests. This included adding a data collection mode that dramatically reduces computer system overhead and disk storage requirements; a "Dynamic Voltage Termination" capability based on the battery internal resistance and the current drawn; a re-designed memory configuration that allows expanded control over test operations; and a minimum power capability test that serves as a battery termination condition. The ADL control system capabilities were also enhanced so that (1) task names and software revision levels are verified before task execution is attempted, (2) battery tests can be started and terminated in any sub-cycle; and (3) the manual/automatic control mode switching for battery tests is faster and easier. Additionally, a data archiving system has been developed for a recently purchased VAXstation 3100 and an optical disk system, which uses DECnet/Ethernet for transparent transmission of data between the VAXstation and the PDP-11/44 data acquisition system in the ADL.

In the past year, the Division's VAX 6220 was upgraded to a Model 6320 (increasing capacity by 35%); it continues to provide the primary computing resources for CMT's diverse computing needs. Other members of CMT's VAX cluster are providing computing cycles for the High-Temperature Materials Group (Sec. IX.B), for scientific workstation applications and program development, and for laboratory automation as replacements for older 16-bit PDP-11 computer systems. Addition of an optical storage subsystem for archival backups has been completed. A 4-mm DAT cartridge tape has supplemented conventional magnetic tape for backup of on-line disk storage.

Computer networks continue to grow in importance in the Laboratory's computing environment. Connection of CMT's VAX to the Laboratory-wide Ethernet permits access to local resources, such as the Computing and Telecommunications Division's (CTD) Cray and VAX 8700 computer systems and to external networks such as HEPNET (high energy physics) and ESNET (DOE energy sciences). An NJE interface permits the file transfer capability to and from the CTD IBM 3084 batch and time-sharing systems and to the BITNET educational network; TCP/IP software permits direct access to the world-wide Internet. This software supports electronic mail, general file transfer capabilities, and interactive log-ins to other systems on the network, including all CTD computers. Plans to upgrade the Laboratory-wide Ethernet backbone to a fiber-optic based backbone are in progress. This would increase network throughput between buildings at ANL by 100-fold.

Personal computers connected to the Ethernet are able to use CMT's VAX as a disk, file, and/or print server via Personal Computing Systems Architecture (PCSA) network software from Digital Equipment Corporation (DEC). This is particularly useful for those systems that are now employed for administrative and graphics applications and for other PC systems which rely on the VAX for data analysis. The PCSA offers support for both Microsoft Windows and MIT's X-Windows standard, which enables a PC user to "window" into several applications running on one or more nodes on the network. Installation of DEC's PATHWORKS for Macintosh software on the VAX provides many of the same file, print, and windows services to the CMT Macintosh PC community.

Group staff provided computer support for CMT Environment, Safety, and Health activities. A VAX-based chemical inventory system was implemented. It provides CMT staff with the ability to enter, update, examine, and report information regarding chemicals used in their work. It also gives the CMT safety officer the ability to locate hazardous chemicals. The group also acquired a compact-disc read-only-memory (CDROM) system for handling the Division's Material Safety Data Sheet (MSDS) requirements, installed this system on a PC accessible to CMT staff, and developed software for printing the output data sheets on the Division's main printer via the PCSA network.

To help users become familiar with the many software products and utilities running on the VAX, the Computer Applications Group has continued its series of workshops which, together with handout materials, are intended to increase the computer skills of CMT personnel. These workshops are being expanded to cover PC and networking topics as well.

A block diagram of the Divisional computing configuration is shown in Fig. XII-1.

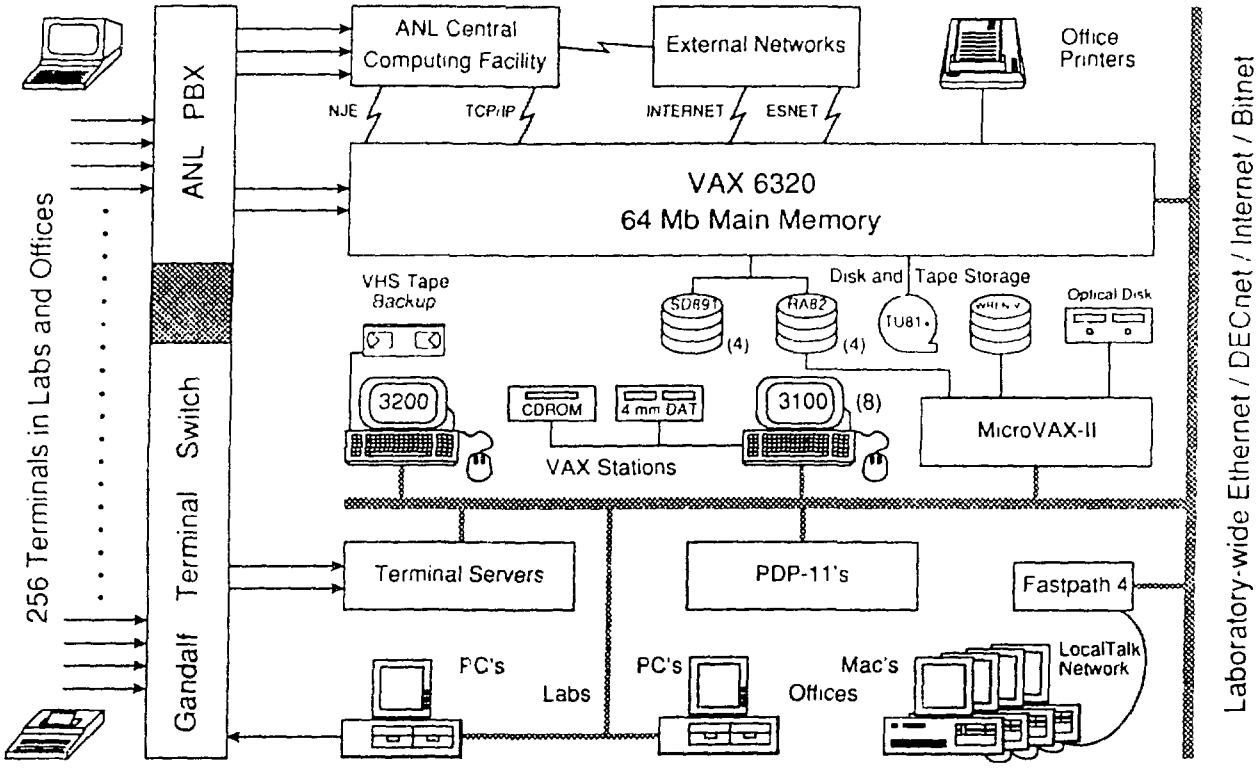

Fig. XII-1. Block Diagram of CMT Computing Facilities

XIII. ADDENDUM.

CHEMICAL TECHNOLOGY DIVISION PUBLICATIONS--1990

The Division's publications and oral presentations for 1990 were entered into a bibliographic data base. The pages that follow are a printout of this information sorted into six categories: (1) journal articles, books, and book chapters, (2) patents, (3) ANL progress and topical reports, as well as contributions to reports published by organizations other than ANL, (4) abstracts and papers published in proceedings of conferences, symposiums, workshops, etc., (5) oral presentations at scientific meetings and seminars not referenced in the fourth category, and (6) papers accepted for publication but not yet published.

Chemical Technology Division Publications — 1990

A. Journal Articles, Books, and Book Chapters

Secondary Phase Formation during Nuclear Waste-Glass Dissolution
T. A. Abrajano, J. K. Bates, A. B. Woodland, J. P. Bradley, and W. L. Bourcier
Clays and Clay Miner. **38**(5), 537–548 (1990)

Geochemistry of Reduced Gas Related to Serpentinization of the Zambales Ophiolite
T. A. Abrajano, N. C. Sturchio, B. M. Kennedy, G. L. Lyon, K. Muehlenbachs, and J. K. Bohlke
Appl. Geochem. **5**, 625–630 (1990)

Chemical Basis for Pyrochemical Reprocessing of Nuclear Fuel
J. P. Ackerman
Ind. Eng. Chem. Res. **30**(1), 141–145 (1990)

Isotope Shifts of Zn Neutral Atoms Measured by Two-Photon Doppler-Free Laser-Induced Fluorescence Spectroscopy
H. F. Arlinghaus, W. F. Calaway, C. E. Young, M. J. Pellin, and D. M. Gruen
Vacuum **41**, 204–206 (1990)

Getting in Tune
P. M. Aznavoorian, L. A. Raphaelian, and R. J. Wingender
Environ. Lab. **2**(4), 34–36 (1990)

High Sensitivity Photoacoustic Spectrometer for Variable Temperature Solution Studies
J. V. Beitz, M. M. Doxtader, V. A. Maroni, S. Okajima, and D. T. Reed
Rev. Sci. Instrum. **61**(5), 1395–1403 (1990)

Compact Contracted Basis Sets for Third-Row Atoms: Ga-Kr
R. C. Binning and L. A. Curtiss
J. Comput. Chem. **11**(10), 1206–1216 (1990)

Theoretical Study of GeH_n, AsH_n, and SeH_n: Bond Dissociation Energies
R. C. Binning and L. A. Curtiss
J. Chem. Phys. **92**, 1860 (1990)

Theoretical Study of GeH_n, AsH_n, and SeH_n: Ionization Energies
R. C. Binning and L. A. Curtiss
J. Chem. Phys. **92**(6), 3688–3692 (1990)

The Raman Spectra of Several Uranyl-Containing Minerals Using a Microprobe
B. M. Biwer, W. L. Ebert, and J. K. Bates
J. Nucl. Mater. **175**, 188–193 (1990)

Aqueous Reciprocal Salt Systems: Application of Conformal Ionic Solution Theory
M. Blander
J. Phys. Chem. **94**(20), 7872–7875 (1990)

High-MgO Composite Ceramics for Use in Sodium-Based Cells
I. Bloom and M. C. Hash
Mater. Lett. **10**(3), 105–108 (1990)

Resonance Ionization Mass Spectroscopy of Sputtered Osmium and Rhenium Atoms
J. D. Blum, M. J. Pellin, W. F. Calaway, C. E. Young, D. M. Gruen, I. D. Hutcheon, and G. J. Wasserburg
Anal. Chem. **63**, 209–214 (1990)

Trace Analysis of Osmium and Rhenium by Resonance Ionization Mass Spectrometry of Sputtered Atoms
J. D. Blum, M. J. Pellin, W. F. Calaway, C. E. Young, D. M. Gruen, I. D. Hutcheon, and G. J. Wasserburg
Secondary Ion Mass Spectrometry, SIMS VII, eds., A. Benninghoven, A. M. Huber, and H. W. Werner, Wiley Publ. Co., New York (1990)

In Situ Measurement of Osmium Concentrations in Iron Meteorites by Resonance Ionization of Sputtered Atoms
J. D. Blum, M. J. Pellin, W. F. Calaway, C. E. Young, D. M. Gruen, I. D. Hutcheon, and G. J. Wasserburg
Geochim. Cosmochim. Acta **54**, 875–861 (1990)

Modeling of Sulfide Capacities in Ternary Slags
B. Chen, R. G. Reddy, and M. Blander
J. Min. Met. Mater. **41**(11), 101 (1990)

Autoxidation of Trimethylamine in Aqueous Solutions
M. J. Chen, J. C. Linehan, and J. W. Rathke
J. Organ. Chem. **55**, 3233–3236 (1990)

Peripherally Substituted Phthalocyanines
M. J. Chen, J. W. Rathke, S. Sinclair, and D. W. Slocum
J. Macromol. Sci. Chem. **A27**(9-11), 1415–1431 (1990)

The Cr/Th Ratio in Precambrian Pelites from the Kaapvaal Craton as an Index of Craton Evolution
K. C. Condie and D. J. Wronkiewicz
Earth Planet. Sci. Lett. **97**, 256–267 (1990)

A New Look at the Archean—Proterozoic Boundary: Sediments and the Tectonic Setting Constraint
K. C. Condie and D. J. Wronkiewicz
Developments in Precambrian: The Precambrian Continental Crust, and Its Economic Resources, ed., B. P. Radhakrishna, Elsevier, Amsterdam (1990)

Gaussian-1 Theory of Molecular Energies for Second-Row Compounds
L. A. Curtiss, C. Jones, G. W. Trucks, K. Raghavachari, and J. A. Pople
J. Chem. Phys. **93**(4), 2537–2545 (1990)

Nonadditivity of Interaction in Hydrated Cu^{+} and Cu^{2+} Clusters
L. A. Curtiss and R. Jurgens
J. Phys. Chem. **94**, 5509–5513 (1990)

Theoretical Investigation of Intra-Atomic Electronic Excitation Energies of Divalent Cu in $YBa_2Cu_3O_7$
L. A. Curtiss and S. W. Tam
Phys. Rev. B **41**(4), 1824–1828 (1990)

The Potential of Continuous Emission Monitoring of Hazardous Waste Incinerators Using Fourier Transform Infrared Spectroscopy
J. C. Demirgian and M. D. Erickson
Waste Manage. **10**, 227–231 (1990)

Boron Dimer: Dissociation Energy and Ionization Potentials
P. W. Deutsch, L. A. Curtiss, and J. A. Pople
Chem. Phys. Lett. **174**(1), 33–36 (1990)

Electrolytic Separation and Recovery in Caustic of Steel and Zinc from Galvanized Steel Scrap
F. J. Dudek, E. J. Daniels, Z. Nagy, S. Zaromb, and R. M. Yonco
Sep. Sci. Technol. **25**(13/15), 2109–2132 (1990)

Palladium Deuteride Formation in the Cathode of an Electrochemical Cell: An *In Situ* Neutron Diffraction Study
G. P. Felcher, R. L. Hitterman, L. Redey, J. W. Richardson, and F. J. Rotella
Bull. Am. Phys. Soc. **35**, 370 (1990)

The Characterization of High-Critical-Temperature Ceramic Superconductors by Vibrational Spectroscopy
J. R. Ferraro and V. A. Maroni
Appl. Spectrosc. **44**(3), 351–366 (1990)

A Study of Nickel Passivation in Acidic Chloride Solution Using Optical Second Harmonic Generation
J. M. Frye, M. W. Schauer, M. J. Pellin, D. M. Gruen, and C. A. Melendres
Chem. Mater. **2**, 245–248 (1990)

Properties of LiOH and $LiNO_3$ Aqueous Solutions
P. J. Gierszewski, P. A. Finn, and D. W. Kirk
Fusion Eng. Des. **13**, 59–71 (1990)

Synthesis of Tl-Ca-Ba-Cu-O Superconductors
K. C. Goretta, J. G. Chen, N. Chen, M. C. Hash, and D. Shi
Mat. Res. Bull. **25**, 791–798 (1990)

Radiation Damage Calculations for Compound Materials
L. R. Greenwood
Stand. Tech. Publ. 1046 **II**, 633–641 (1990)

Spectroscopic and Diffraction Techniques in Interfacial Electrochemistry
C. Gutierrez and C. Melendres, editors
NATO-ASI Series, Kluwer Academic Publishers, Dordrecht, Netherlands (1990)

Thermodynamic Properties of the Zeolite Stilbite
D. A. Howell, G. K. Johnson, I. R. Tasker, P. A. G. O'Hare, and W. S. Wise
Zeolites **10**, 525–531 (1990)

ICP/AES Actinide Detection Limits
E. A. Huff and D. L. Bowers
Appl. Spectros. **44**(4), 728–729 (1990)

Synthesis of 85 K Bi-Sr-Ca-Cu-O Superconductor
F. A. Karbarz, O. D. Lacy, K. C. Goretta, U. Balachandran, D. Shi, J. G. Chen, M. Xu, and M. C. Hash
Mat. Res. Bull. **25**, 251–256 (1990)

Multiple Activation Energies for Tritium Release from Ceramic Breeders
J. P. Kopasz, A. K. Fischer, and C. E. Johnson
Adv. Ceram. **27**, 317–328 (1990)

Measurement of Sodium and Potassium Vapours in PFBC of Beulah Lignite
S. H. D. Lee and E. L. Carls
J. Inst. Energy **63**(457), 203–210 (1990)

A Study of the Thermodynamic and Reducing Properties of Lithium in Cadmium at 773°K
M. A. Lewis and T. R. Johnson
J. Electrochem. Soc. **137**(5), 1414–1418 (1990)

Methods for Measuring Radium Isotopes: Emanometry
H. F. Lucas, F. Markun, and R. Boulenger
Volume 1 in *The Environmental Behaviour of Radium*, Int. Atomic Energy Agency, Vienna, Chapt. 3-2, pp. 149–172 (1990)

The Use of Vibrational Spectroscopy in the Characterization of High-Critical-Temperature Ceramic Superconductors
V. A. Maroni and J. R. Ferraro
Practical Fourier Transform Infrared Spectroscopy, Industrial and Laboratory Chemical Analysis, eds., J. R. Ferraro and K. Krishnan, Academic Press, Orlando, FL, pp. 1–39 (1990)

Spectroscopic Characterization of Oxide Films on Type 304 SS Exposed to Water at 289°C: Correlation with the Fe-Cr-H_2O Pourbaix Diagram
V. A. Maroni, C. A. Melendres, T. F. Kassner, R. Kumar, and S. Siegel
J. Nucl. Mater. **172**, 13–18 (1990)

Mathematical Analysis of a Four-Point Conductivity Probe for Cylindrical Samples
S. L. Marshall and L. Redey
Rev. Sci. Instrum. **61**, 2659 (1990)

Difference Raman Spectroscopy for "In-situ" Analysis of Electrode Surfaces
C. A. Melendres
J. Electroanal. Chem. **286**, 273–277 (1990)

Laser Raman Spectroscopy in Studies of Corrosion and Electrocatalysis
C. A. Melendres
Spectroscopic and Diffraction Techniques in Interfacial Electrochemistry, eds., C. Gutierrez and C. Melendres, Kluwer Academic Publishers, Dordrecht, Netherlands, pp. 181–222 (1990)

Monolithic Solid Oxide Fuel Cell Development
K. M. Myles and C. C. McPheeters
J. Power Sources **29**, 311–319 (1990)

DC Relaxation Techniques for the Investigation of Fast Electrode Reactions
Z. Nagy
Modern Aspects of Electrochemistry, Vol. 21, Chapt. 6, eds., R. E. White, J. O'M. Bockris, and B. E. Conway, Plenum Publishing, New York, pp. 237–292 (1990)

Weld-Pool Pyrometallurgy
C. A. Natalie, D. L. Olson, and M. Blander
Chapter 5 in *Welding, Theory and Practice*, eds., D. L. Olson, R. Dixon, and A. L. Liby, Elsevier Science Publishers, Amsterdam, Netherlands, pp. 149–173 (1990)

Inelastic Neutron Scattering from Non-Framework Species within Zeolites
J. M. Newsam, T. O. Brun, F. Trouw, L. E. Iton, and L. A. Curtiss
Chapter 3 in *Novel Materials in Heterogeneous Catalysis*, Am. Chem. Soc. Symp. Ser. **437**, 25–37 (1990)

Boron Isotope Systematics of the Yellowstone (Wyoming) Hydrothermal System: A Reconnaissance
M. R. Palmer and N. C. Sturchio
Geochim. Cosmochim. **54**, 2811–2815 (1990)

Secondary Neutral Mass Spectroscopy Using Three-Colour Resonance Ionization: Osmium Detection at the p.p.b. Level and Iron Detection in Silicon at the <200 p.p.t. Level
M. J. Pellin, C. E. Young, W. F. Calaway, J. E. Whitten, D. M. Gruen, J. D. Blum, I. D. Hutcheon, and G. J. Wasserburg
Phil. Trans. R. Soc. Lond. A **333**, 133–146 (1990)

Electrochemically Generated Oxygen Contamination in Submerged Arc Welding
A. Polar, J. E. Indacochea, and M. Blander
Weld. J. (Suppl.) **69**(2), 68–74 (1990)

Calorimetric Measurements on Electrochemical Cells with Pd-D Cathodes
L. Redey, K. M. Myles, D. W. Dees, M. Krumpelt, and D. R. Vissers
J. Fusion Energy **9**(3), 249–256 (1990)

Structure of Liquid Equiatomic KSn and CsSn
H. T. J. Reijers, M.-L. Saboungi, D. L. Price, and W. van der Lugt
Phys. Rev. B **41**(9), 5661–5666 (1990)

Molecular-Dynamics Study of Liquid NaPb, KPb, RbPb, and CsPb Alloys
H. T. J. Reijers, W. van der Lugt, and M.-L. Saboungi
Phys. Rev. B **42**(6), 3395–3405 (1990)

Formation of Zintl-Ions in Alkali-Lead Alloys
H. T. J. Reijers, W. van der Lugt, M.-L. Saboungi, and D. L. Price
J. Non-Cryst. Solids **117/118**, 56–59 (1990)

ICP/AES: A Modern Analytical Tool
C. S. Sabau
American-Romanian Acad. Sci. Arts J. **13–14**, 251–263 (1990)

Ordering in Liquid Alloys
M.-L. Saboungi, W. Geertsma, and D. L. Price
Annu. Rev. Phys. Chem. **41**, 207–244 (1990)

Structural and Thermodynamic Evidence for the Survival of Zintl Ions Through the Melting Process: The Alkali-Lead Alloys
M.-L. Saboungi, G. K. Johnson, D. L. Price, and H. T. J. Reijers
High Temp. Sci. **26**, 335–344 (1990)

Comparisons of Emissions of Transit Buses Using Methanol and Diesel Fuel
D. J. Santini and J. B. Rajan
Transport. Res. Record, No. 1255, pp. 108–118 (1990)

Book Review: *Geology of High-Level Nuclear Waste Disposal: An Introduction*, by I. S. Roxburgh
N. C. Sturchio
J. Geol. **98**(1), 131 (1990)

Radium Isotopes, Alkaline Earth Diagenesis, and Age Determination of Travertine from Mammoth Hot Springs, Wyoming
N. C. Sturchio
Appl. Geochem. **5**, 631–640 (1990)

Oxygen and Carbon Isotope Ratios of Hydrothermal Minerals from Yellowstone Drill Cores
N. C. Sturchio, T. E. C. Keith, and K. Muehlenbachs
J. Volcan. Geotherm. Res. **40**, 23–37 (1990)

Variations in Chemistry of Acid-Sulfate-Chloride Springs at Nevado del Ruiz Volcano, Columbia, November 1985 through December 1988
N. C. Sturchio and S. N. Williams
J. Volcan. Geotherm. Res. **42**, 201–208 (1990)

SO_2-NO_x Control in a Staged Slagging Combustor with Hydrated Lime Injection
W. M. Swift and F. G. Teats
Processing and Utilization of High-Sulfur Coals III, eds., R. Markuszewski and T. D. Wheelock, Elsevier Science Publishers, Amsterdam, Netherlands, pp. 537–549 (1990)

Is There a Strange Attractor in a Fluidized Bed?
S. W. Tam and M. K. Devine
Measures of Complexity and Chaos, eds., N. B. Abraham et al., Plenum Press, New York, pp. 193–197 (1990)

Oxygen Stoichiometry, Structural Transitions, and Thermodynamic Behavior of the $YBa_2Cu_3O_x$ System
M. Tetenbaum, L. A. Curtiss, B. Czech, B. S. Tani, and M. Blander
Physics and Materials Science of High Temperature Superconductors, eds., R. Kossowsky et al., Kluwer Academic Publishers, Dordrecht, Netherlands, Vol. 181, pp. 279–296 (1990)

Atomic Motions in Liquid KPb—A Molecular Dynamics Investigation
K. Toukan, H. T. J. Reijers, C.-K. Loong, D. L. Price, and M.-L. Saboungi
Phys. Rev. B **41**(17), 11739–11742 (1990)

Thermodynamic Properties of Liquid Rb-Pb Alloys
P. J. Tumidajski, A. Petric, T. Takenaka, A. D. Pelton, and M.-L. Saboungi
J. Phys.: Condens. Matter **2**, 209–220 (1990)

Thermodynamic Properties of the Ternary Na-Bi-Te and K-Bi-Te Alloys by Electromotive Force Measurements with an Alumina Solid Electrolyte
P. J. Tumidajski and M.-L. Saboungi
CALPHAD **14**(1), 89–104 (1990)

Tunable Laser Flash Absorption: A New Technique for Measuring Rates and Yields of Chemical Reactions at High Temperatures
W. A. VonDrasek, S. Okajima, J. H. Kiefer, P. J. Ogren, and J. P. Hessler
Appl. Opt. **29**(38), 4899 (1990)

Solubility of $CoCl_2$ in Molten NaCl-$AlCl_3$
C. Wai, I. Bloom, D. Caveny, and M. Blander
J. Phys. Chem. **94**, 1666–1669 (1990)

Sulfur Dioxide from Nevado del Ruiz Volcano, Columbia: Total Flux and Isotopic Constraints on its Origin
S. N. Williams, N. C. Sturchio, M. Calvache, R. Mendez, A. Londono, and N. Garcia
J. Volcan. Geotherm. Res. **42**, 53–68 (1990)

Adsorption and Redox Thermodynamics of Strongly Adsorbed Cytochrome *c* on Tin Oxide Electrodes
J. L. Willit and E. F. Bowden
J. Phys. Chem. **94**, 8241–8246 (1990)

The Effects of Acid Demineralization on the Sulfur-Containing Compounds Found in an Illinois-Basin High-Sulfur Coal
R. E. Winans, R. L. McBeth, and J. E. Young
Processing and Utilization of High-Sulfur Coals III, eds., R. Markuszewski and T. D. Wheelock, Elsevier Science Publishers, Amsterdam, Netherlands, pp. 53–65 (1990)

Geochemistry and Mineralogy of Sediments from the Ventersdorp and Transvaal Supergroups, South Africa: Early-Proterozoic Evolution of the Kaapvaal Craton
D. J. Wronkiewicz and K. C. Condie
Geochim. Cosmochim. Acta. **54**, 343–354 (1990)

B. Patents

Removal of Copper from Ferrous Scrap
M. Blander and S. N. Sinha
Patent No. 4,925,488, issued May 15, 1990

Real Time Infrared Aerosol Analyzer
S. A. Johnson, G. T. Reedy, and R. Kumar
Patent No. 4,942,297, issued July 17, 1990

Cathode for Molten Carbonate Fuel Cell
T. D. Kaun and F. C. Mrazek
Patent No. 4,939,111, issued July 3, 1990

Cathode for Molten Carbonate Fuel Cell
T. D. Kaun and F. C. Mrazek
Patent No. 4,891,280, issued January 2, 1990

Electrolytic Cell with Reference Electrode
R. W. Kessie
Patent No. 4,888,102, issued December 19, 1989

Electromagnetic Confinement and Movement of Thin Sheets of Molten Metal
R. J. Lari, W. F. Praeg, and L. R. Turner
Patent No. 4,905,756, issued March 6, 1990

Sidewall Containment of Liquid Metal with Vertical Alternating Magnetic Fields
R. J. Lari, W. F. Praeg, L. R. Turner, J. E. Battles, J. R. Hull, and D. M. Rote
Patent No. 4,974,661, issued December 4, 1990

Process for Direct Conversion of Reactive Metals to Glass
J. B. Rajan, R. Kumar, and D. R. Vissers
Patent No. 4,898,692, issued February 6, 1990

Overdischarge Protection in High-Temperature Cells and Batteries
L. Redey
Patent No. 4,935,316, issued June 19, 1990

Microwave-Enhanced Chemical Processes
R. Varma
Patent No. 4,935,114, issued June 19, 1990

C. Reports

Strategy for Experimental Validation of Waste Package Performance Assessment
J. K. Bates, T. A. Abrajano, D. J. Wronkiewicz, T. J. Gerding, and C. A. Seils
ANL-90/21 (August 1990)

Application of the NNWSI Unsaturated Test Method to Actinide Doped SRL 165 Type Glass
J. K. Bates and T. J. Gerding
ANL-89/24 (August 1990)

NNWSI Waste Form Testing at Argonne National Laboratory, Semiannual Report, January–June 1987
J. K. Bates, T. J. Gerding, T. A. Abrajano, W. L. Ebert, and J. J. Mazer
Lawrence Livermore National Laboratory Report UCRL-21060-87-1 (1990)

NNWSI Waste Form Testing at Argonne National Laboratory, Semiannual Report, January–June 1988
J. K. Bates, T. J. Gerding, W. L. Ebert, J. J. Mazer, and B. M. Biwer
Lawrence Livermore National Laboratory Report UCRL-21060-88-1 (1990)

NNWSI Waste Form Testing at Argonne National Laboratory, Semiannual Report, July–December 1987
J. K. Bates, T. J. Gerding, W. L. Ebert, J. J. Mazer, and B. M. Biwer
Lawrence Livermore National Laboratory Report UCRL-21060-87-2 (1990)

TRUEX Hot Demonstration: Final Report
D. B. Chamberlain, R. A. Leonard, J. C. Hoh, E. C. Gay, D. G. Kalina, and G. F. Vandegrift
ANL-89/37 (April 1990)

Test Results for 36-V Li/FeS Battery
A. A. Chilenskas, R. F. Malecha, W. H. DeLuca, A. F. Tummillo, and R. L. Hogrefe
ANL-90/1 (January 1990)

Performance and Life Evaluation of Nickel/Iron Battery Technology for Dual Shaft Electric Propulsion Vehicle
C. C. Christianson, W. H. DeLuca, R. L. Hogrefe, C. E. Webster, and J. E. Kulaga
Electrochemical Technology Program Technical Report for the DSEP Technology Evaluation Period March 1986 to October 1988 (May 1990)

Evaluation of Cleaned Coal in FBC
W. F. Podolski and M. K. Clemens
Final Technical Report for September 1, 1989 through August 31, 1990, prepared for Illinois Center for Research on Sulfur in Coal (1990)

Isotope Geochemistry: A Critical Component of Energy Research
D. Cole, D. Curtis, D. Depaolo, T. Gerlach, J. Laul, H. Shaw, B. Smith, and N. C. Sturchio
Los Alamos National Laboratory Report LA-11849-MS (1990)

Electric Vehicle Battery Testing and Development at Argonne National Laboratory, 1989 Annual Report
W. H. DeLuca, J. A. Smaga, A. F. Tummillo, R. L. Hogrefe, C. E. Webster, and J. K. Kulaga
Electric Power Research Institute Report EPRI CU-6968 (September 1990)

Remote Detection of Chemical Agents by Infrared Spectroscopy Progress Report for FY 1989
J. C. Demirgian and S. M. Spurgash
ANL/ACL-90/1 (February 1990)

The Reaction of Glass during Gamma Irradiation in a Saturated Tuff Environment. Part 4: SRL 165, ATM-1c, and ATM-8 Glasses at 1E3 R/h and 0 R/h
W. L. Ebert, J. K. Bates, and T. J. Gerding
ANL-90/13 (May 1990)

Conceptual Design Description for the Tritium Recovery System for the U. S. ITER Li_2O/Be Water Cooled Blanket, Revision 1.0

P. A. Finn, D. K. Sze, and R. G. Clemmer

ANL/FPP/TM-249 (November 1990)

Desorption Characteristics of the $LiAlO_2$-H_2-H_2O(g) System

A. K. Fischer and C. E. Johnson

Fusion Reactor Materials Semiannual Progress Report for the Period Ending March 1990, DOE/ER-0313/8, pp. 286–289 (1990)

Analytical Chemistry Laboratory Progress Report for FY 1990

D. W. Green, R. R. Heinrich, D. G. Graczyk, P. C. Lindahl, A. S. Boparai (with contributions from ACL Staff)

ANL/ACL-90/2 (December 1990)

Nuclear Technology Programs Semiannual Progress Report, April–September 1988

C. E. Johnson, G. F. Vandegrift, J. K. Bates, K. A. Barnthouse, R. A. Benson, B. M. Biwer, P. E. Blackburn, N. R. Blake, R. A. Blomquist, D. L. Bowers, D. J. Chaiko, D. B. Chamberlain, L. S. Chow, R. G. Clemmer, J. M. Copple, A. Crabtree, W. L. Ebert, P. A. Finn, A. K. Fischer, D. R. Fredrickson, T. J. Gerding, L. R. Greenwood, J. C. Hoh, A. Intasorn, P. T. Kelsheimer, J. P. Kopasz, J. D. Kwok, L. Leibowitz, R. A. Leonard, P. MacLean, J. J. Mazer, D. T. Reed, L. Reichley-Yinger, M. F. Roche, W. B. Seefeldt, J. Sedlet, C. A. Seils, J. L. Settle, N. Simonzadeh, J. E. Stangel, D. V. Steidl, D.-K. Sze, I. R. Tasker, L. E. Trevorrow, P.-K. Tse, E. H. Van Deventer, E. Veleckis, A. B. Woodland, and D. J. Wronkiewicz

ANL-90/15 (October 1990)

Nuclear Technology Programs Semiannual Progress Report, October 1987–March 1988

C. E. Johnson, G. F. Vandegrift, J. K. Bates, K. A. Barnthouse, R. A. Benson, B. M. Biwer, P. E. Blackburn, R. A. Blomquist, D. J. Chaiko, D. B. Chamberlain, W. L. Ebert, P. A. Finn, A. K. Fischer, D. R. Fredrickson, T. J. Gerding, L. R. Greenwood, J. C. Hoh, A. Intasorn, I. Johnson, J. P. Kopasz, J. D. Kwok, A. B. La'O, J. M. Leddin, L. Leibowitz, R. A. Leonard, J. J. Mazer, D. T. Reed, L. Reichley-Yinger, M. F. Roche, W. B. Seefeldt, C. A. Seils, J. L. Settle, N. Simonzadeh, J. E. Stangel, D. V. Steidl, W. E. Streets, I. R. Tasker, L. E. Trevorrow, P.-K. Tse, E. H. Van Deventer, and E. Veleckis

ANL-89/29 (August 1990)

Alkali Vapor Removal Activities

S. H. D. Lee and E. L. Carls

Int. Gas Turbine and Aeroengine Technology Report for 1990, Int. Gas Turbine Institute, pp. 21–22 (1990)

Determination of Alkali-Vapor Emission from Pressurized Fluidized-Bed Combustion of Illinois Coal

S. H. D. Lee and F. G. Teats

Final Technical Report for December 1, 1989 through August 31, 1990, prepared for Illinois Center for Research on Sulfur in Coal (1990)

Practical Superconductor Development for Electrical Power Applications, Annual Report for FY 1990

R. B. Poeppel, K. C. Goretta, U. Balachandran, I. Bloom, S. E. Dorris, J. T. Dusek, J. E. Emerson, K. C. Goretta, K. E. Gray, M. Hash, S. A. Johnson, R. T. Kampwirth, M. Kulberg, D. S. Kupperman, M. T. Lanagan, V. A. Maroni, R. L. McDaniel, J. H. Meiser, J. J. Picciolo, J. P. Singh, C. A. Youngdahl

ANL-90/47 (October 1990)

Practical Superconductor Development for Electrical Power Applications, Semiannual Report, October 1989–June 1990

R. B. Poeppel, K. C. Goretta, U. Balachandran, I. Bloom, S. E. Dorris, J. T. Dusek, J. E. Emerson, K. C. Goretta, K. E. Gray, M. Hash, S. A. Johnson, R. T. Kampwirth, M. Kullberg, D. S. Kupperman, M. T. Lanagan, V. A. Maroni, R. L. McDaniel, J. H. Meiser, J. J. Picciolo, J. P. Singh, C. A. Youngdahl

ANL-90/25 (June 1990)

Vaporization of Strontium, Barium, Lanthanum, and Uranium from Mixtures of Urania, Zirconia, Steel, and Concretes at 2150 K and 2400 K

M. F. Roche, J. L. Settle, L. Leibowitz, and C. E. Johnson

Electric Power Research Institute Report EPRI-NP-6613 and Advanced Containment Experiments Report ACE-TR-C13 (January 1990)

Post-Test Analysis of CSPL Sodium/Sulfur Cells

J. A. Smaga and J. J. Marr

Exploratory Battery Technology Development and Testing Report for 1988, Sandia National Laboratories Report SAND89-3039, pp. 49–52 (October 1989)

Post-Test Analysis of CSPL Sodium/Sulfur Cells

J. A. Smaga and J. J. Marr

Exploratory Battery Technology Development and Testing Report for 1989, Sandia National Laboratories Report SAND90-1195, pp. 2-38 to 2-41 (December 1990)

Chemical Technology Division Annual Technical Report, 1989

M. J. Steindler et al.

ANL-90/11 (March 1990)

PFBC Evaluation of Illinois Limestones for Reducing SO_2 and HCl Emission

W. M. Swift and S. H. D. Lee

Final Technical Report for December 1, 1989 through August 31, 1990, prepared for Illinois Center for Research on Sulfur in Coal (1990)

D. Abstracts and Proceedings Papers

Analytical Electron Microscopy of Leached Nuclear Waste Glasses
T. A. Abrajano, J. K. Bates, and J. P. Bradley
Ceram. Trans. **9**, 211-228 (1990)

The Breeding Blanket Interface (BBI) and the Tritium System Test Assembly (TSTA)
J. Anderson, J. Barthit, R. Sherman, D.-K. Sze, P. A. Finn, R. G. Clemmer, Y. Naruse, H. Yoshida, K. Okuno, and M. Enoeda
Proc. of the 13th IEEE Symp. on Fusion Engineering, Knoxville, TN, October 2–6, 1989, pp. 804–807 (1990)

Vapor Hydration and Subsequent Leaching of Transuranic-Containing SRL and WV Glasses
J. K. Bates, W. L. Ebert, and T. J. Gerding
Proc. of the Int. High-Level Radioactive Waste Management Conf., Am. Nucl. Soc., Las Vegas, NV, April 8–12, 1990, p. 1095 (1990)

Parametric Effects of Glass Reaction under Unsaturated Conditions
J. K. Bates, T. J. Gerding, and A. B. Woodland
Mater. Res. Soc. Symp. Proc. **176**, 347–354 (1990)

Identification of Secondary Phases Formed during Unsaturated Reaction of UO_2 with EJ-13 Water
J. K. Bates, B. S. Tani, E. Veleckis, and D. Wronkiewicz
Mater. Res. Soc. Symp. Proc. **176**, 499–506 (1990)

Product Consistency Leach Tests of Savannah River Site Radioactive Waste Glass
N. E. Bibler and J. K. Bates
Mater. Res. Soc. Symp. Proc. **176**, 327-338 (1990)

Comparison of the Layer Structure of Vapor Phase and Leached SRL Glass by Use of AEM
B. M. Biwer, J. K. Bates, T. A. Abrajano, and J. P. Bradley
Mater. Res. Soc. Symp. Proc. **176**, 255–263 (1990)

Calculations of the Thermodynamic Properties of Metallurgical Solutions
M. Blander
Proc. of the Int. Symp. on Computer Software in Chemical and Extractive Metallurgy, Montreal, Canada, August 28–31, 1990, pp. 3–14 (1990)

Predictions of Entropies and Free Energy Functions of Vapor Molecules and Liquids
M. Blander
Program and Abstracts, Thermodynamic Data Systematics Symp., Uppsala, Sweden, June 10–14, 1990, p. 8 (1990)

Calculation of the Solubilities of Oxides in Carbonate and Sulfate Mixtures
M. Blander and A. Pelton
Extended Abstracts, 177th Electrochem. Soc. Meeting, Montreal, Canada, May 6–11, 1990, Vol. 90–1, p. 1181 (1990)

Ordered Ionic Liquids: Chloroaluminates and Silicates
M. Blander, P. Tumidajski, I. Bloom, and D. Newman
Extended Abstracts, 177th Electrochem. Soc. Meeting, Montreal, Canada, May 6–11, 1990, Vol. 90–1, pp. 1182–1183 (1990)

Novel, Sodium-Ion Conducting Composite Electrolytes
I. Bloom and M. C. Hash
Extended Abstracts, 178th Electrochem. Soc. Meeting on Physical Electrochemistry/High Temperature Materials, Seattle, WA, October 14-19, 1990, Vol. 90-2, p. 1086 (1990)

Design Considerations for the Development of Advanced Sodium/Metal-Chloride Cells
I. Bloom, P. A. Nelson, L. Redey, S. K. Orth, C. L. Hammer, R. S. Skocypec, D. W. Dees, M. C. Hash, and D. R. Vissers
Proc. of the 25th Intersoc. Energy Conversion Eng. Conf., Reno, NV, August 12–17, 1990, Vol. 3, pp. 341–347 (1990)

Leached Nuclear Waste Glasses: Ultramicrotomy and Analytical Electron Microscopic Characterization
J. P. Bradley and J. K. Bates
Proc. of the 12th Int. Congress for Electron Microscopy, Seattle, WA, August 13–17, 1990, pp. 444–445 (1990)

Development of a Process for Treating Red Water by Organic/Inorganic Separation and Biodegradation
D. J. Chaiko, L. Reichley-Yinger, E. R. Orth, E. H. Van Deventer, G. F. Vandegrift, M. Krumpole, J. E. Helt, R. D. Coleman, S. N. Kakar, T. S. Tsai, K. Horken, W. Killian, and N. F. Sather
Proc. of the 14th Annual Army Environmental R&D Symp., Williamsburg, VA, November 14–16, 1989, pp. 303–314 (1990)

Sulfide Capacities of CaO-FeO-SiO_2 Slags
B. Chen, R. G. Reddy, and M. Blander
Proc. of the Third Int. Conf. on Molten Slags and Fluxes, University of Strathclyde, Glasgow, Scotland, June 27–29, 1990, pp. 270–272 (1990)

The Breeding Blanket Interface (BBI): Recent Results for the Solid Breeder and the Aqueous Salt Solution Blanket Concepts
R. G. Clemmer, P. A. Finn, L. R. Greenwood, D. K. Sze, J. R. Bartlit, R. Sherman, J. L. Anderson, H. Yoshida, Y. Naruse, K. Okuno, and M. Enoeda
Proc. of the 13th IEEE Symp. on Fusion Engineering, Knoxville, TN, October 2–6, 1989, pp. 78–84 (1990)

Optical, Electrochemical, and Modeling Studies of the Metal/Water Interface: Applications to Aqueous Corrosion
L. A. Curtiss, D. M. Gruen, V. A. Maroni, C. A. Melendres, Z. Nagy, and M. J. Pellin
Extended Abstracts, Corrosion Research in Progress Symp., Las Vegas, NV, April 23–27, 1990, pp. 41–44 (1990)

Status of Solid Oxide Fuel Cells for Transportation
D. W. Dees and R. Kumar
Proc. of the 1990 Fuel Cell Seminar Program and Abstracts, Phoenix, AZ, November 25–28, 1990, pp. 71–75 (1990)

Status of Argonne Life Evaluation of Valve Regulated Lead-Acid Batteries
W. H. DeLuca, R. L. Hogrefe, C. E. Webster, and A. F. Tummillo
Proc. of the Fourth Int. ILZRO Lead-Acid Battery Seminar, San Francisco, CA, April 25–27, 1990, pp. 217–228 (1990)

Performance Evaluation of Advanced Battery Technologies for Electric Vehicle Applications
W. H. DeLuca, A. F. Tummillo, J. E. Kulaga, C. E. Webster, K. R. Gillie, and R. L. Hogrefe
Proc. of the 25th Intersoc. Energy Conversion Eng. Conf., Reno, NV, August 12–17, 1990, Vol. 3, pp. 314–319 (1990)

Life Evaluation of Valve Regulated Lead-Acid Batteries for Cycling Applications
W. H. DeLuca, A. F. Tummillo, C. E. Webster, R. L. Hogrefe, and J. F. Miller
Proc. of the 25th Intersoc. Energy Conversion Eng. Conf., Reno, NV, August 12–17, 1990, Vol. 3, pp. 320–325 (1990)

The Influence of Penetrating Gamma Radiation on the Reaction of Simulated Nuclear Waste Glass in Tuff Groundwater

W. L. Ebert, J. K. Bates, T. A. Abrajano, and T. J. Gerding

Ceram. Trans. **9**, 155–164 (1990)

Solid Breeder Blanket Option for the ITER Conceptual Design

Y. Gohar, H. Attaya, M. C. Billone, P. A. Finn, S. Majumdar, L. R. Turner, C. C. Baker, B. E. Nelson, and R. Raffray

Proc. of the 13th IEEE Symp. on Fusion Engineering, Knoxville, TN, October 2–6, 1989, pp. 53–57 (1990)

Hyper- and Hypobaric Processing of Tl-Ca-Ba-Cu-O Superconductors

K. C. Goretta, J. L. Routbort, D. Shi, J. G. Chen, M. Xu, and M. C. Hash

Mat. Res. Soc. Symp. Proc. **169**, 365–368 (1990)

Self-Discharge Study of Li-Alloy/FeS_2 Thermal Cells

R. A. Guidotti, F. W. Reinhardt, and J. A. Smaga

Proc. of the 34th Int. Power Sources Symp., Cherry Hill, NJ, June 25–28, 1990, pp. 132–135 (1990)

Structure of Some Trivalent Molten Salts by Neutron Diffraction

M. A. Howe, D. L. Price, and M.-L. Saboungi

Extended Abstracts, 177th Electrochem. Soc. Meeting, Montreal, Canada, May 6–11, 1990, Vol. 90–1, pp. 1176–1177 (1990)

Electrochemical Reactions in Submerged Arc Welding with SiO_2-CaO-CaF_2 Fluxes with High and Low Silica Contents

J. E. Indacochea, A. Polar, and M. Blander

Proc. of the Second Int. Conf. on Trends in Welding Research, ASM Int., Gatlinburg, TN, May 14–18, 1989, pp. 563–567 (1990)

Electrochemical Transport of Manganese between the Flux and the Weld Metal in Submerged Arc Welding

J. E. Indacochea, A. Polar, and M. Blander

Proc. of the Second Int. Conf. on Trends in Welding Research, ASM Int., Gatlinburg, TN, May 14–18, 1989, pp. 581–586 (1990)

Lithium Transport Molten-Salt Electrolyte Battery Cells Leading to Overcharge Tolerance

T. D. Kaun

Extended Abstracts, Heat and Mass Transport in Batteries and Fuel Cells Symp., AIChE Meeting, Chicago, IL, November 11–16, 1990, p. 221 (1990)

Rechargeable Molten-Electrolyte Lithium Batteries—A Status Report

T. D. Kaun

Proc. of the Symp. on Rechargeable Lithium Batteries, Electrochem. Soc., ed., S. Subbaro, Hollywood, FL, October 15–20, 1989, Vol. 90–5, p. 294 (1990)

Testing of a Sealed Bipolar Li/FeS_2 Stack

T. D. Kaun and M.J. Duoba

Extended Abstracts, 178th Electrochem. Soc. Meeting on Fuel Cells and Battery Power Sources for Transportation, Seattle, WA, October 14–19, 1990, Vol. 90–2, p. 189 (1990)

Development of a Sealed Bipolar Li-Alloy/FeS_2 Battery for Electric Vehicles

T. D. Kaun, M. J. Duoba, K. R. Gillie, M. C. Hash, D. R. Simon, and D. R. Vissers

Proc. of the 25th Intersoc. Energy Conversion Eng. Conf., Reno, NV, August 12–17, 1990, Vol. 3, pp. 335–340 (1990)

Li Alloy/FeS_2 as a Sealed Bipolar Battery
T. D. Kaun, M. J. Duoba, K. R. Gillie, D. R. Simon, and D. R. Vissers
Proc. of the 34th Int. Power Sources Symp., Cherry Hill, NJ, June 25–28, 1990, p. 29 (1990)

Sealing Li-Alloy/FeS_2 Cells for a Bipolar Battery
T. D. Kaun, M. J. Duoba, K. R. Gillie, and J. A. Smaga
Proc. of the Symp. on Rechargeable Lithium Batteries, Electrochem. Soc., ed., S. Subbaro, Hollywood, FL, October 15–20, 1989, Vol. 90–5, p. 315 (1990)

Methanol Reformers for Fuel Cell Powered Vehicles—Some Design Considerations
R. Kumar, S. Ahmed, M. Krumpelt, and K. M. Myles
Proc. of the 1990 Fuel Cell Seminar Program and Abstracts, Phoenix, AZ, November 25–28, 1990, pp. 76–79 (1990)

Measurement of Alkali Vapors in PFBC Exhaust
S. H. D. Lee and W. M. Swift
Proc. of the DOE Seventh Annual Coal-Fueled Heat Engines and Gas Stream Cleanup Systems Contractors' Review Meeting, Morgantown, WV, March 26–28, 1990, pp. 384–390 (1990)

Gas Generation from the Irradiation of Mortar
M. A. Lewis and D. W. Warren
Ceram. Trans. **9**, 97 (1990)

The Use of Additives for Reducing Hydrogen Yield in Mortar Containing Slag and Chloride Salts
M. A. Lewis and D. W. Warren
Mat. Res. Soc. Symp. Proc. **176**, 53–54 (1990)

Laser Raman Spectroscopy for "In-Situ" Analysis of Corrosion Films on Metals
C. A. Melendres
Extended Abstracts, 178th Electrochem. Soc. Meeting, Seattle, WA, October 14–19, 1990, Vol. 90–2, pp. 365–366 (1990)

Laser Raman Spectroscopy and Photoelectrochemical Studies of the Corrosion-Passivation Behavior of Copper and Iron in Thiocyanate Solutions
C. A. Melendres, T. J. O'Leary, J. Acho, and J. Solis
Proc. of the 30th Australasian Corrosion Association Conf., Auckland, NZ, November 19–23, 1990, pp. 50–58 (1990)

Effect of Thiocyanate on the Corrosion and Passivation of Copper and Iron: Raman Spectroscopy and Photoelectrochemical Studies
C. A. Melendres, T. J. O'Leary, and R. J. Boegart
Extended Abstracts, 177th Electrochem. Soc. Meeting, Montreal, Canada, May 6–11, 1990, Vol. 90–1, pp. 28–29 (1990)

Effect of Double Layer Structure on the Determination of Corrosion Rates from Electrochemical Measurements
Z. Nagy and R. E. Hawkins
Extended Abstracts, 177th Electrochem. Soc. Meeting, Montreal, Canada, May 6–11, 1990, Vol. 90–1, pp. 56–57 (1990)

Catalytic Effect of UPD Layers on the Ferrous/Ferric Redox Reaction
Z. Nagy, N. C. Hung, D. J. Zurawski, and R. M. Yonco
Extended Abstracts, 178th Electrochem. Soc. Meeting, Seattle, WA, October 14–19, 1990, Vol. 90–2, pp. 1028–1029 (1990)

Proceedings of the 25th Intersociety Energy Conversion Engineering Conference, Volumes 1-6
P. A. Nelson, W. W. Schertz, and R. H. Till, editors
American Institute of Chemical Engineers, New York (1990)

Correlations between Structure, Spectra and Thermodynamics: Solutions of Cobalt, Silver, Cadmium and Nickel in Molten Sodium Tetrachloroaluminate
D. S. Newman, P. J. Tumadajski, and M. Blander
Extended Abstracts, 177th Electrochem. Soc. Meeting, Montreal, Canada, May 6–11, 1990, Vol. 90-1, p. 1212 (1990)

Speciation of Pu(VI) in Near-Neutral to Basic Solutions Via Laser Photoacoustic Spectroscopy
S. Okajima, D. T. Reed, J. J. Mazer, and C. S. Sabau
Materials Research Soc. Symp. Proc. **176**, 583 (1990)

U. S. Research and Development Program on Fuel Cells for Transportation Applications
P. G. Patil, R. A. Kost, and J. F. Miller
Proc. of the Tenth Int. Electric Vehicle Symp., Hong Kong, China, December 3–6, 1990, pp. 657–669 (1990)

Quasichemical Model for Thermodynamic Properties of Multicomponent Slags
A. D. Pelton, G. Eriksson, and M. Blander
Proc. of the Third Int. Conf. on Molten Slags and Fluxes, University of Strathclyde, Glasgow, Scotland, June 27–29, 1990, pp. 66–69 (1990)

Helium Isotopes and Gas Geochemistry at Rabaul Celdera, Papua New Guinea
N. M. Perez, S. N. Williams, Y. Sano, N. C. Sturchio, and C. H. McKee
Program and Abstracts, Geol. Soc. of America, Dallas, TX, October 29–November 1, 1990, Vol. 22, p. A-351 (1990)

Lithium Batteries for Pulse Power
L. Redey
Extended Abstracts, 178th Electrochem. Soc. Meeting, Seattle, WA, October 14–19, 1990, Vol. 90–2, p. 17 (1990)

Self-Discharge and Related Phenomena in Li-Alloy/Metal Sulfide Cells
L. Redey and S. L. Marshall
Extended Abstracts, 175th Electrochem. Soc. Meeting, Los Angeles, CA, May 7–12, 1989, Vol. 89–1, p. 27 (1990)

Resistivity Measurements of Halide-Salt/MgO Thermal-Cell Separators
L. Redey, M. McParland, and R. Guidotti
Proc. of the 34th Int. Power Sources Symp. on Thermal/Reserve Batteries, Cherry Hill, NJ, June 25–28, 1990, p. 128 (1990)

Investigation of $Ni/NiCl_2$ Electrodes in Basic Chloroaluminate Melt
L. Redey and D. R. Vissers
Extended Abstracts, 176th Electrochem. Soc. Meeting, Hollywood, FL, October 15–20, 1989, Vol. 89–2, p. 143 (1990)

Corrosion Product Identification and Relative Rates of Corrosion of Candidate Metals in an Irradiated Air-Steam Environment
D. T. Reed, V. Swayambunathan, B. S. Tani, and R. A. Van Konynenburg
Materials Research Soc. Symp. Proc. **176**, 517 (1990)

Palladium Deuteride Formation in the Cathode of an Electrochemical Cell: An *In Situ* Neutron Diffraction Study
F. J. Rotella, J. W. Richardson, L. Redey, G. P. Felcher, and R. L. Hitterman
Abstracts, Am. Crystall. Assoc. Annual Meeting, New Orleans, LA, Am. Inst. Phys. Series 2, ISSN 0569, Vol. 18, p. 64 (1990)

Structure of Molten Salts
M.-L. Saboungi, M. A. Howe, and D. L. Price
Proc. of the Seventh Int. Symp. on Molten Salts, 177th Electrochem. Soc. Meeting, Montreal, Canada, May 6–11, 1990, Vol. 90-17, pp. 8–17 (1990)

A New Calculational Method for Deducing the Complex Chemistry of Coal Ash Deposits
S. Sinha, K. Natesan, and M. Blander
Proc. of the Conf. on Mineral Matter & Ash Deposition from Coal, Santa Barbara, CA, February 22–26, 1988, pp. 117–126 (1990)

Cathode Materials and Structures Development
J. L. Smith, G. H. Kucera, and A. P. Brown
Proc. of the Second Symp. on Molten Carbonate Fuel Cell Technology, Seattle, WA, October 14–19, 1990, Vol. 90-16, pp. 226–246 (1990)

Geothermal Systems within the Mammoth Corridor in Yellowstone National Park and the Adjacent Corwin Springs KGRA
M. L. Sorey, E. M. Colvard, and N. C. Sturchio
Trans. of Geotherm. Resources Council **14**, 729–733 (1990)

Uranium-Series Disequilibrium Ages of North Yellowstone Area Travertines: Chronology of Pinedale Glaciation and the Quaternary Hydrothermal System
N. C. Sturchio, M. T. Murrell, K. L. Pierce, and M. L. Sorey
EOS, Trans. of Am. Geophys. Union **71**, 1683 (1990)

Hydrothermal Fluids of Purace Volcano, Colombia
N. C. Sturchio, S. N. Williams, and Y. Sano
Program and Abstracts, Geol. Soc. of America, Dallas, TX, October 29–November 1, 1990, Vol. 22, p. A-57 (1990)

Heat and Seed Recovery Technology Project
W. M. Swift
Proc. of the MHD Contractor's Review Meeting, Pittsburgh, PA, January 22–24, 1990, pp. 195–221 (1990)

Measurements of Thermodynamic Properties and Phase Equilibria in 1-2-3 Superconducting Oxides
M. Tetenbaum and M. Blander
Program and Abstracts, Thermodynamic Data Systematics Symp., Uppsala, Sweden, June 10–14, 1990, p. 9 (1990)

Oxygen Stoichiometry and Thermodynamic Behavior of the $YBa_2Cu_3O_x$ System
M. Tetenbaum, L. A. Curtiss, B. S. Tani, B. Czech, and M. Blander
Extended Abstracts, CALPHAD XIX Conf., Noordwijkerhout, Netherlands, June 17–22, 1990, p. 38 (1990)

Evaluation of Nickel/Metal Hydride Batteries for Electric Vehicle Applications
A. F. Tummillo, W. H. DeLuca, and J. E. Miller
Extended Abstracts, 178th Electrochem. Soc. Meeting, Seattle, WA, October 14–19, 1990, Vol. 90-2, pp. 161–162 (1990)

Development of Fiber-Based Nickel Hydroxide Electrodes for Nickel/Iron Batteries
M. J. Vanderpool, G. G. Paul, and J. F. Miller
Proc. of the Electrochem. Soc. Meeting on Nickel Hydroxide Electrodes, eds., D. A. Corrigan and A. Zimmerman, Hollywood, FL, October 16–18, 1990, Vol. 90-4, pp. 397–402 (1990)

Premonitory Geochemical Evidence of Magmatic Reactivation of Galeras Volcano, Colombia
S. N. Williams, M. L. Calvache, N. C. Sturchio, J. A. Zapata, R. A. Mendez, B. Calvache, A. Londono, F. Gil Cruz, and Y. Sano
EOS, Trans. Am. Geophys. Union **71**, 647 (1990)

E. Papers Presented at Scientific Meetings

New Decade of Geoscience Research in East Asia: Hydrocarbon Research
I. A. Abrajano
Presented at the Workshop on the New Decade of Geoscience Research in East Asia, Honolulu, HI, July, 27–30, 1990

Thermal-Hydraulic Model of a Solid-Oxide Fuel Cell
S. Ahmed and R. Kumar
Presented at the AIChE Annual Meeting, Chicago, IL, November 11–16, 1990

Analysis of Canister Air Samples Involving Cryogenic Trapping Prior to GC/MS
D. V. Applegate
Presented at the Thirteenth Analytical Chemistry Laboratory Technical Meeting, Argonne National Laboratory, December 6, 1990

The Need for Innovative Energy Research and Development
D. L. Barney
Presented at the 1990 Kansas State University Chemistry Alumni Lecture, Manhattan, Kansas, October 18, 1990

Integrated Testing of Glass
J. K. Bates
Presented at the National Academy of Sciences Conf., Washington, DC, December 20, 1990

Site-Specific Glass Degradation Tests Under Repository Conditions
J. K. Bates
Presented at the Nuclear Waste Technical Review Board Meeting, Pleasanton, CA, August 28, 1990

Radionuclide Content of Secondary Mineral Phases that Form during Glass Reaction
J. K. Bates and W. L. Ebert
Presented at the 92nd Annual Meeting and Exposition of the Am. Ceram. Soc., Dallas, TX, April 22–26, 1990

The Role of Surface Layers in Glass Leaching Performance
J. K. Bates, W. L. Ebert, J. J. Mazer, J. P. Bradley, C. R. Bradley, and N. L. Dietz
Presented at the Fall Meeting of the Materials Research Soc., Boston, MA, November 26–29, 1990

Experimental Validation of Near-Field Performance Assessment
J. K. Bates and A. B. Woodland
Presented at the 92nd Annual Meeting and Exposition of the Am. Ceram. Soc., Dallas, TX, April 22–26, 1990

Lithium Mass Transport in Ceramic Breeder Materials
P. E. Blackburn and C. E. Johnson
Presented at the Ninth Topical Meeting on the Technology of Fusion Energy, Oak Brook, IL, October 7–11, 1990

Ordered Ionic Liquids
M. Blander
Presented at the Materials Science Division Seminar, Argonne National Laboratory, January 11, 1990

Evaluation of Novel Solid Electrolyte Materials
I. Bloom, D. W. Dees, M. C. Hash, and M. Krumpelt
Presented at the Morgantown Energy Technology Center Contractors' Review Meeting, Morgantown, WV, May 2–3, 1990

Evaluation of Alternative Solid Electrolyte Materials
I. Bloom, D. W. Dees, J. D. Pullockaran, M. C. Hash, and M. Krumpelt
Presented at the Second SOFC Electrochemistry Workshop, EPRI, Palo Alto, CA, June 11, 1990

Analysis of Kerogens by Pyrolysis/Gas Chromatography/Matrix Isolation—Infrared Spectrometry/Mass Spectrometry
A. S. Boparai, E. L. Delemeester, J. F. Schneider, and T. A. Abrajano
Presented at the 41st Pittsburgh Conf. and Exposition on Analytical Chemistry and Applied Spectrometry, New York, March 5–9, 1990

Theoretical Studies on the Vibrational Frequencies and Barriers for Internal Rotation in Tetraethylammonium Cation
H. V. Brand, L. A. Curtiss, and L. E. Iton
Presented at the 23rd Midwest Theoretical Chemistry Conf., Madison, WI, May 17–19, 1990

Preliminary Results of Laboratory Studies of Repository Chemistry for the Waste Isolation Pilot Plant
L. H. Brush, D. Grbic-Galic, D. T. Reed, S. Tong, R. H. Vreeland, and R. E. Westerman
Presented at the Fall Meeting of the Materials Research Soc., Boston, MA, November 26–29, 1990

Modeling of Sulfide Capacities in Ternary Slags
B. Chen, R. G. Reddy, and M. Blander
Presented at the Annual Meeting of Metallurgical Soc., Anaheim, CA, February 19–22, 1990

Hydrogen and Methane Activation Studies Using Soluble Rhodium Phthalocyanine Dimers
M. J. Chen and J. W. Rathke
Presented at the 14th Int. Conf. on Organometallic Chemistry, Detroit, MI, August 19–24, 1990

Electric Vehicle Battery and Fuel Cell Program at ANL
C. C. Christianson, G. Henriksen, D. Vissers, J. Smaga, W. DeLuca, J. Miller, M. Krumpelt, and R. Kumar
Presented at the DOE/Laboratory Project Review and Coordination Meeting, Argonne, IL, September 6–7, 1990

Flibe Chemistry Studies
R. G. Clemmer, D. K. Sze, P. E. Blackburn, E. VanDeventer, and V. A. Maroni
Presented at the Ninth Topical Meeting on the Technology of Fusion Energy, Oak Brook, IL, October 7–11, 1990

The Role of Laboratory Analog Experiments in Assessing the Performance of Waste Package Materials
J. C. Cunnare and J. K. Bates
Presented at the Fall Meeting of the Materials Research Soc., Boston, MA, November 26–29, 1990

Accurate Thermochemical Data from Quantum Chemical Calculations
L. A. Curtiss
Presented at the Midwest Thermodynamics Symp., Huron, OH, May 20–22, 1990

Development of Contracted Basis Sets for Third-Row Main Group Elements
L. A. Curtiss
Presented at the Workshop on Methodology of the Evaluation of Integrals in LCAO Calculations, Argonne National Laboratory, August 23–25, 1990

Many-Body Interactions in Transition Metal Ion/Water Systems: *Ab Initio* Molecular Orbital and Molecular Dynamics Studies

L. A. Curtiss

Presented at the Int. Conf. on Intermolecular Interactions in Chemistry and Biology, Podebrady: Experiment and Theory, Czechoslovakia, September 17–22, 1990

Quantum Chemical Studies of Haloaluminates

L. A. Curtiss

Presented at the Molten Salts Miniworkshop, Argonne National Laboratory, May 14, 1990

Theoretical Investigation of Intra-Atomic Electronic Excitation Energies in Monovalent and Divalent Cu in $YBa_2Cu_3O_{7-x}$

L. A. Curtiss, S. W. Tam, and P. W. Deutsch

Presented at the Am. Chem. Soc. Southeast-Southwest Regional Meeting, New Orleans, LA, December 5–7, 1990

Status and Results of EPRI Battery Test and Development Project at Argonne National Laboratory

W. H. DeLuca and J. A. Smaga

Presented at the EPRI Electric Vehicle Battery Testing Project Review, Argonne National Laboratory, August 21, 1990

Qualitative and Quantitative Analysis of Target Analyses Using Remote Detection FTIR

J. Demirgian and S. M. Spurgash

Presented at the 41st Pittsburgh Conf. and Exposition on Analytical Chemistry and Applied Spectroscopy, New York, March 5–9, 1990

Qualitative and Quantitative Analysis of Target Analyses Using Remote Detection FTIR

J. C. Demirgian

Presented at the 12th Analytical Chemistry Laboratory Technical Meeting, Argonne National Laboratory, March 22, 1990

Monitoring Incinerator Emissions from Remote Sites Using Fourier Transform Infrared Spectroscopy

J. C. Demirgian, S. Spurgash, and C. T. Snyder

Presented at the Second Annual Pacific Northwest Int. Section/Air and Waste Management Assoc. Conf., Portland, OR, November 14–16, 1990

Remote Monitoring of Incinerator Emissions Using FTIR

J. C. Demirgian and S. M. Spurgash

Presented at the Ninth Annual Int. Symp. on Incineration of Hazardous, Infectious, Radioactive, and Mixed Wastes, San Diego, CA, May 14–18, 1990

Thermochemical Data for Some Hydrogen-Silicon Compounds Using Quantum Chemical Calculations

P. W. Deutsch

Presented at the Midwest Thermodynamics Symp., Huron, OH, May 20–22, 1990

The Importance of Secondary Phases in Glass Corrosion

W. L. Ebert and J. K. Bates

Presented at the Fall Meeting of the Materials Research Soc., Boston, MA, November 26–29, 1990

PCBs: A Societal, Environmental and Analytical Problem

M. Erickson

Presented at the Center for Disease Control, San Antonio, TX, April 16, 1990

PCB Analysis: Status and Challenges
M. D. Erickson
Presented at the Int. Conf. on Organohalogen (DIOXIN 90) Compounds, Bayreuth, Federal Republic of Germany, September 10–14, 1990

New Method for Isolating Strontium for Isotopic Analysis
A. M. Essling
Presented at the 13th Analytical Chemistry Laboratory Technical Meeting, Argonne National Laboratory, December 6, 1990

Conceptual Design Description for the Tritium Recovery System for the U.S. ITER Li_2O/Be Water Cooled Blanket
P. A. Finn, D. K. Sze, and R. G. Clemmer
Presented at the Ninth Topical Meeting on the Technology of Fusion Energy, Oak Brook, IL, October 7–11, 1990

Processes for Desorption from $LiAlO_2$ Treated with H_2 as Studied by Temperature Programmed Description
A. K. Fischer
Presented at the Ninth Topical Meeting on the Technology of Fusion Energy, Oak Brook, IL, October 7–11, 1990

Design Optimization of Bulk Shield Options for ITER
Y. Gohar, H. Attaya, and P. A. Finn
Presented at the Ninth Topical Meeting on the Technology of Fusion Energy, Oak Brook, IL, October 7–11, 1990

Processing Thallium-Based Superconductors
K. C. Goretta, M. T. Lanagan, J. R. Hull, J. L. Routbort, D. Shi, N. Chen, and M. C. Hash
Presented at the 92nd Annual Meeting and Exposition of the Am. Ceram. Soc., Dallas, TX, April 22–26, 1990

Characterization and Calibration of a Daly Scintillation Detector for Thermal Ionization Mass Spectrometry of Uranium
D. G. Graczyk
Presented at the 12th Analytical Chemistry Laboratory Technical Meeting, Argonne National Laboratory, March 22, 1990

Environmental Analysis/Management Challenges of Getting Started
D. W. Green
Presented at the 14th Annual Quality Awareness Day, Argonne, IL, April 5, 1990

Radiation Damage Calculations for Fusion Insulators, Tritium Breeders, Alloys, and Superconducting Materials
L. R. Greenwood
Presented at the Seventh ASTM-EURATOM Symp. on Reactor Dosimetry, Strasbourg, France, August 27–31, 1990

Measurements of Activation Cross Sections for Fusion Reactor Applications
L. R. Greenwood and D. L. Bowers
Presented at the Seventh ASTM-EURATOM Symp. on Reactor Dosimetry, Strasbourg, France, August 27–31, 1990

Waste Management Programs at Argonne
J. E. Helt
Presented at the Conf. on the Initial Five-Year RDDT&E Plan, Phoenix, AZ, April 17–20, 1990

Application of ICP/AES to the TRUEX Process
E. A. Huff and D. B. Chamberlain
Presented at the Winter Conf. on Plasma Spectrochemistry, St. Petersburg, FL, January 8–13, 1990

Temperature Effects in Electrode Kinetics: The Ferrous/Ferric Redox Reaction
N. C. Hung, Z. Nagy, and R. M. Yonco
Presented at the 23rd Great Lakes Regional Meeting of the Am. Chem. Soc., DeKalb, IL, May 30–June 2, 1990

Ceramic Breeder Materials
C. E. Johnson
Presented at the Seventh CIMTEC-World Ceramic Congress and Satellite Symposia Main Congress, Montecatini Terme, Italy, June 24–30, 1990

Bipolar Electric Vehicle Battery
T. D. Kaun
Presented at the State of Illinois Challenge Grant Review, Illinois Dept. of Commerce and Community Affairs, Argonne, IL, August 28, 1990

Sealed Bipolar Li/FeS_2 Battery Development
T. D. Kaun
Presented at the Workshop on Batteries for the Electric Battlefield, U. S. Army Electronics R&D Command, Cherry Hill, NJ, June 25, 1990

Hydrogen Activation by Soluble Metal Oxide Complexes
R. J. Klingler, T. R. Krause, and J. W. Rathke
Presented at the Am. Chem. Soc. Meeting, Boston, MA, April 22–27, 1990

Molten Carbonate Fuel Cell Research
G. H. Kucera, J. L. Smith, and A. P. Brown
Presented at the Morgantown Energy Technology Center Contractors' Review Meeting, Morgantown, WV, May 2–3, 1990

Requirements for a Fuel Cell for Transportation Application
R. Kumar
Presented at the Direct Methanol/Air Fuel Cell Workshop, Washington, DC, May 14–16, 1990

Determination of Alkali-Vapor Emission from Pressurized Fluidized-Bed Combustion of Illinois Coal
S. H. D. Lee and F. G. Teats
Presented at the Eighth Annual Illinois Coal Development Board Contractors' Technical Meeting, Urbana, IL, July 31–August 2, 1990

Backmixing Effects in Solvent Extraction Processes
R. A. Leonard, M. C. Regalbuto, and G. F. Vandegrift
Presented at the AIChE Annual Meeting, Chicago, IL, November 11–16, 1990

Component Concentration Using the Centrifugal Contactor in Solvent Extraction Processes
R. A. Leonard, D. G. Wygmans, M. O. Wasserman, and G. F. Vandegrift
Presented at the 14th Actinide Separations Conf., Gatlinburg, TN, May 14–17, 1990

PYRO-New Capability for Isotopic Mass Tracking in Pyroprocess Simulation
J. R. Liaw and J. P. Ackerman
Presented at the Physor '90 Int. Conf. on the Physics of Reactors: Operation, Design, and Computation, Marseille, France, April 23–27, 1990

USDOE Applied Research and Development Private Sector Initiatives
S. Lien, S. S. Borys, and M. D. Erickson
Presented at the Hazardous Waste Research Conf., Manhattan, KS, May 21–22, 1990

Oxidative Coupling of Methane by Transition Metal-Substituted Aluminophosphate Molecular Sieves
V. A. Maroni, S. A. Johnson, J. H. Meiser, L. E. Iton, K. E. Creasy, and B. R. Shaw
Presented at the Fall Meeting of the Materials Research Soc., Boston, MA, November 26–29, 1990

Activation of Methane by Transition Metal-Substituted Aluminophosphate Molecular Sieves
V. A. Maroni, K. A. Willms, H. Nguyen, and L. Iton
Presented at the Am. Chem. Soc. Meeting on Liquid Fuels from C-1 Precursors, Boston, MA, April 22–27, 1990

Current Distribution in Cylindrical Porous Electrodes
S. L. Marshall
Presented at the Seventh Int. Symp. on Molten Salts, 177th Electrochem. Soc. Meeting, Montreal, Canada, May 6–11, 1990

Sintering of Four-Material Structures by Control of Powder Properties
C. C. McPheeters, U. Balachandran, S. E. Dorris, and J. J. Picciolo
Presented at the Third Int. Conf. on Ceramic Powder Processing Science, San Diego, CA, February 4–7, 1990

Bonding Normal-Conducting Metals to High-T_c Superconducting Ceramics
J. H. Meiser, C. A. Blue, D. C. Hague, H. M. Saito, and V. A. Maroni
Presented at the Seventh Int. Symp. on Molten Salts, 177th Electrochem. Soc. Meeting, Montreal, Canada, May 6–11, 1990

A Method for Forming Electrical Contacts between High-T_c Superconducting Ceramics and Normal-Conducting Metals
J. H. Meiser, D. C. Hague, H. H. Saito, C. A. Blue, and V. A. Maroni
Presented at the Spring Meeting of the Materials Research Soc., San Francisco, CA, April 16–21, 1990

Difference Raman Spectroscopy for the "In-Situ" Analysis of Electrode Surfaces
C. A. Melendres
Presented at the DOE Corrosion Contractors' Meeting, University of Minnesota, September 13–14, 1990

Laser Raman Spectroscopy for "In-Situ" Analysis of Electrode Surfaces
C. A. Melendres, J. Acho, and R. Knight
Presented at the Gordon Research Conf. on Physical Electrochemistry, New London, NH, July 30–August 3, 1990

Recent Advances in Electrochemical Corrosion Rate Measurements
Z. Nagy
Presented at the Gordon Research Conf. on Electrochemistry, Ventura, CA, January 15–19, 1990

Catalytic Effect of UPD Layers on Outer-Sphere Electron Transfer Reactions
Z. Nagy, L. A. Curtiss, N. C. Hung, D. J. Zurawski, and R. M. Yonco
Presented at the Gordon Research Conf. on Physical Electrochemistry, New London, NH, July 30–August 3, 1990

Impedance Modeling of Sodium-Nickel Chloride Cells
P. A. Nelson and I. D. Bloom
Presented at the AIChE Annual Meeting, Chicago, IL, November 11–16, 1990

Shipping, Use, and Disposal/Recycle Considerations for Sodium/Beta Batteries in EV Applications
P. G. Patil, G. L. Henriksen, D. R. Vissers, and C. C. Christianson
Presented at the DOE/EPRI Beta Battery Workshop, Chester, England, June 12–14, 1990

Evaluation of the Combustion of Cleaned Coal in FBCs
W. F. Podolski and M. K. Clemens
Presented at the Eighth Annual Illinois Coal Development Board Contractors' Technical Meeting, Urbana, IL, July 31–August 2, 1990

Catalytic Chemistry in Supercritical Media
J. W. Rathke, R. J. Klingler, and M. J. Chen
Presented at the Basic Energy Sciences Catalysis and Surface Chemistry Research Meeting, Gaithersburg, MD, March 26–28, 1990

Cold Fusion
L. Redey
Presented at the Cold Fusion Seminar, Argonne National Laboratory, February 1990

Lithium-Alloy/Metal-Disulfide Battery for Ultra-High Power Density Application
L. Redey and A. F. Tummillo
Presented at the 25th Intersoc. Energy Conversion Eng. Conf., Reno, NV, August 12–17, 1990

Corrosion of Copper-Based Materials in Irradiated Moist Air Systems
D. T. Reed and R. A. Van Konynenburg
Presented at the Fall Meeting of the Materials Research Soc., Boston, MA, November 26–29, 1990

Migration of Radionuclides in Geologic Media: Fundamental Research Needs
D. T. Reed, J. M. Zachara, R. E. Wildung, and F. J. Wobber
Presented at the Fall Meeting of the Materials Research Soc., Boston, MA, November 26–29, 1990

Electron Transfer Rates at Metal Electrodes
Y. J. Rhee, J. W. Halley, J. Hautman, A. Rahman, L. A. Curtiss, and Z. Nagy
Presented at the Gordon Research Conf. on Electrochemistry, Ventura, CA, January 15–19, 1990

Comparison of Instrumental Methods Used in the Determination of Uranium, Plutonium, and Americium
C. Sabau
Presented at the 15th Int. ARA Congress, Ecole Polytechnique, Montreal, Canada, June 14–18, 1990

Order in Disordered Liquids
M.-L. Saboungi
Presented at the Interfaculty Reactor Institute at Delft University of Technology, Delft, Netherlands, April 26, 1990

Polyanionic Species in Liquid Alkali-Lead Alloys
M.-L. Saboungi
Presented at the Centre de Thermodynamique et de Calorimètrie, CNRS, Marseille, France, June 5, 1990

Order and Disorder in Liquid Alloys
M. L. Saboungi, G. K. Johnson, and D. L. Price
Presented at the Int. Bodrum School of Physics Conf. on Highlights of Condensed Matter Theory, Turkish Phys. Soc., Bodrum, Turkey, September 26–October 5, 1990

Structure of Trivalent Halides
M.-L. Saboungi and D. L. Price
Presented at the Molten Salts Discussion Group, London, England, December 17, 1990

Liquid Alloys with Strong Interactions
M.-L. Saboungi, D. L. Price, G. K. Johnson, and H. T. J. Reijers
Presented at the Thermodynamics of Alloys Conf., Barcelona, Spain, May 23–26, 1990

Matrix Isolation as an Interface for GC/IR: How Does It Fit in With the Other GC/IR Interfaces?
J. F. Schneider
Presented at the 17th Annual Meeting of the Federation of Analytical Chemistry and Spectroscopy Societies, Cleveland, OH, October 7–12, 1990

Analysis of Semivolatile Pollutants by Gas Chromatography/Matrix Isolation—Infrared Spectrometry/Mass Spectrometry
J. F. Schneider, P. M. Aznavoorian, and L. F. Sytsma
Presented at the 41st Pittsburgh Conf. and Exposition on Analytical Chemistry and Applied Spectrometry, New York, March 5–9, 1990

Methane Coupling by Metal Oxides: The Case for a Redox System Involving the Metal
D. W. Slocum and V. A. Maroni
Presented at the 14th Int. Conf. on Organometallic Chemistry, Detroit, MI, August 19–24, 1990

Obsidian Hydration Dating as a Function of Temperature, Composition, and Relative Humidity
C. M. Stevenson, J. J. Mazer, and J. K. Bates
Presented at the Annual Meeting of the Soc. for California Archaeology, San Francisco, CA, April 6, 1990

X-Ray Fluorescence Spectrometry: An Analytical Tool
W. E. Streets
Presented at the Science Careers in Search of Women Conf., Second Annual Conf. Focused on High School Women in Pursuit of a Career in Science, Argonne, IL, May 18, 1990

Computerized Calculation of Environmental Levels of Radioactivity Determined by Gamma Spectrometry
W. E. Streets, B. S. Tani, and L. R. Greenwood
Presented at the 36th Annual Conf. on Bioassay, Analytical, and Environmental Radiochemistry, Oak Ridge, TN, October 22–26, 1990

Computerized Calculation of Environmental Levels of Radioactivity Determined by Gamma Spectrometry
W. E. Streets, B. S. Tani, and L. R. Greenwood
Presented at the 13th Analytical Chemistry Laboratory Technical Meeting, Argonne National Laboratory, December 6, 1990

PCDDs and PCDFs in Humans
S. Swanson and M. D. Erickson
Presented at the EPRI Dioxin Conf., Palo Alto, CA, June 11–13, 1990

PFBC Evaluation of Illinois Limestones for Reducing SO_2 and HCl Emissions
W. M. Swift and S. H. D. Lee
Presented at the Eighth Annual Illinois Coal Development Board Contractors' Technical Meeting, Urbana, IL, July 31–August 2, 1990

Possible Design Modification of ITER Fuel Cycle
D. K. Sze, P. A. Finn, J. Anderson, J. Barthl, and R. Sherman
Presented at the Ninth Topical Meeting on the Technology of Fusion Energy, Oak Brook, IL, October 7–11, 1990

A Study of Fluidized-Bed Dynamical Behavior—A Chaos Perspective
S. W. Tam and M. K. Devine
Presented at the EPRI Workshop on Application of Chaos, San Francisco, CA, December 4–7, 1990

Thermodynamic Activities of Aqueous Species for the Generic TRUEX Model
I. Tasker
Presented at the National Institute for Standards in Technology, June 13, 1990

Thermodynamic Activities of Aqueous Species for the Generic TRUEX Model
I. R. Tasker, A. A. DiFilippo, S. Smidt, and G. F. Vandegrift
Presented at the National Institute for Petroleum and Energy Research Conf., Bartlesville, OK, June 1, 1990

Thermodynamic Behavior of High-T$_c$ Oxide Systems Via EMF and Related Measurements
M. Tetenbaum, P. Tumidajaski, I. D.Bloom, D. L. Brown, and M. Blander
Presented at the Sixth Int. School on Condensed Matter Physics on New Physical Problems in Electronic Materials, Varna, Bulgaria, September 21–29, 1990

Some Recent Observations on the Nonstoichiometric Behavior of the $NdBa_2Cu_3O_x$ System Via EMF Measurements
M. Tetenbaum, P. Tumidajski, I. Bloom, D. Brown, and M. Blander
Presented at the Gordon Research Conf. on Superconductivity, Poster Session I, Ventura, CA, March 19-23, 1990

Nonstoichiometric and Thermodynamic Behavior of the $NdBa_2Cu_3O_x$ System via EMF Measurements
M. Tetenbaum, P. Tumidajski, D. L. Brown, I. Bloom, and M. Blander
Presented at the Fall Meeting of the Materials Research Soc., Boston, MA, November 26–29, 1990

Oxidation of IFR Salt
Z. Tomczuk, J. J. Heiberger, and W. E. Miller
Presented at the 14th Annual Actinide Separations Conf., Gatlinburg, TN, May 14–17, 1990

Atomic Motions in Liquid KPb—A Molecular Dynamics Investigation
K. Toukan, H. T. J. Reijers, D. L. Price, and M.-L. Saboungi
Presented at the 40th Meeting of the Am. Crystallographic Assoc., New Orleans, LA, April 8–13, 1990

Groundwater Decontamination of Volatile Organic Compounds by MASX/MADS
G. F. Vandegrift
Presented at the Technology Transfer Conf., Atlanta, GA, February 6–8, 1990

Development of High Performance Sodium/Metal Chloride Cells
D. R. Vissers, I. D. Bloom, M. C. Hash, L. Redey, C. L. Hammer, D. W. Dees, and P. A. Nelson
Presented at the DOE/EPRI Beta Battery Workshop, Chester, England, June 12–14, 1990

Determination of Protactinium-231 for the Lansdowne Project
L. L. Wetter
Presented at the 12th Analytical Chemistry Laboratory Technical Meeting, Argonne National Laboratory, March 22, 1990

Voltammetric Determination of Intrinsic Activation Parameters for Protein Electron Transfer: The Cytochrome c/Tin Oxide System

J. L. Willit and E. F. Bowden

Presented at the Gordon Research Conf. on Physical Electrochemistry, New London, NH, July 30–August 3, 1990

Effects of Alpha and Gamma Radiation on Glass Reaction in an Unsaturated Environment

D. J. Wronkiewicz, J. E. Young and J. K. Bates

Presented at the Fall Meeting of the Materials Research Soc., Boston, MA, November 26–29, 1990

Specular X-ray Reflection for the "In-Situ" Study of Electrode Surface:

H. You, C. A. Melendres, Z. Nagy, W. Yun, and V. A. Maroni

Presented at the DOE Corrosion Contractors' Meeting, University of Minnesota, September 13–14, 1990

F. Papers Accepted for Publication

Stable Isotope Geochemistry of Organic Matter Alteration in Animikie Basin Sediments Within the Thermal Aureole of the Duluth Complex
T. A. Abrajano, B. D. Holt, and G. R. Dyrkacz
To be published in Organ. Geochem.

Proceedings of the 14th Symposium on the Scientific Basis for Nuclear Waste Management
T. A. Abrajano and L. H. Johnson, editors
To be published by the Mater. Res. Soc.

Partition of Lanthanum and Neodymium Metals and Chloride Salts Between Molten Cadmium and Molten LiCl-KCl Eutectic
J. P. Ackerman and J. L. Settle
To be published in J. Less-Common Met.

Mechanism of Tritium Release from Lithium Ceramics Irradiated with Neutrons
F. Botter, J. Mongin, B. Rasneur, S. Tistchenko, and J. P. Kopasz
To be published in Fusion Technol.

Leached Nuclear Waste Glasses: Ultramicrotomy and Electron Microscopic Characterization
J. P. Bradley and J. K. Bates
To be published in Microbeam Anal. 1990

In-Pile Tritium Release from Lithium Ceramics and the Influence of Surface Processes
M. Briec, J. P. Kopasz, S. Casadio, and H. Werle
To be published in Fusion Technol.

Bonding of a Water Molecule to Copper Atom
L. A. Curtiss and E. Bierwagen
To be published in Chem. Phys. Lett.

A Contracted Bromine Basis Set for Use in Calculation of Molecular Energies
L. A. Curtiss and R. C. Binning
To be published in Int. J. Quat. Chem.

Temperature Dependence of the Heterogeneous Ferrous-Ferric Electron Transfer Reaction Rate: Comparison of Experiment and Theory
L. A. Curtiss, J. W. Halley, J. Hautman, N. C. Hung, Z. Nagy, Y.-J. Rhee, and R. M. Yonco
To be published in J. Electrochem. Soc.

GAUSSIAN-2 Theory for Molecular Energies of First- and Second Row Compounds
L. A. Curtiss, K. Raghavachari, G. W. Trucks, and J. A. Pople
To be published in J. Chem. Phys.

The Sorption of Water on Obsidian and a Nuclear Waste Glass
W. L. Ebert, R. F. Hoburg, and J. K. Bates
To be published in Phys. Chem. Glasses

Desorption of H_2O and H_2 from Steel and $LiAlO_2$ by Temperature Programmed Desorption
A. K. Fischer and C. E. Johnson
To be published in J. Nucl. Mater.

Ceramic Breeder Materials
C. E. Johnson
To be published in Ceram. Int.

Research and Development Status of Ceramic Breeder Materials
C. E. Johnson
To be published in J. Nucl. Mater.

Thermodynamic Studies of Zeolites: Clinoptilolite
G. K. Johnson, I. R. Tasker, R. Jergens, and P. A. G. O'Hare
To be published in J. Chem. Thermodyn.

Composition and Spectral Characteristics of Ambient Aerosol at Mauna Loa Observatory
S. A. Johnson and R. Kumar
To be published in J. Geophys. Res.

Treatment of Wastes from Fuel Cycle of Integral Fast Reactors
T. R. Johnson, M. A. Lewis, and D. F. Fischer
To be published in Abstracts, Waste Management Research, Int. Atomic Energy Agency, Issue No. 20

Homogeneous Catalytic Hydrogenation of Carbon Monoxide
R. J. Klingler and J. W. Rathke
To be published in Prog. Inorg. Chem.

Enhanced Tritium Transport and Release by Solids Modification
J. P. Kopasz, S. W. Tam, and C. E. Johnson
To be published in J. Nucl. Mater.

A New Model for Solvent Extraction in Columns
R. A. Leonard, M. C. Regalbuto, D. B. Chamberlain, and G. F. Vandegrift
To be published in Sep. Sci. Technol.

The Experimental Hydration of Obsidian as a Function of Relative Humidity and Temperature
J. J. Mazer, C. M. Stevenson, W. L. Ebert, and J. K. Bates
To be published in Am. Antiq.

Effect of Thiocyanate on the Corrosion and Passivation Behavior of Copper and Iron: Laser Raman Spectroscopy and Photoelectrochemical Studies
C. A. Melendres, T. J. O'Leary, and J. Solis
To be published in Electrochim. Acta

Specular X-ray Reflection for the "In-Situ" Study of Electrode Surfaces
C. A. Melendres, H. You, V. A. Maroni, Z. Nagy, and W. Yun
To be published in J. Electroanal. Chem.

Effect of Double Layer Structure on the Determination of Corrosion Rates from Electrochemical Measurements
Z. Nagy and R. E. Hawkins
To be published in J. Electrochem. Soc.

Cell Design for *In-Situ* X-ray Scattering Study of Electrodes in Transmission Geometry
Z. Nagy, H. You, R. M. Yonco, C. A. Melendres, W. Yun, and R. M. Yonco
To be published in Electrochim. Acta

Battery Construction, Testing, and Materials
P. A. Nelson and T. D. Kaun
To be published in *Molten Salt Techniques, Vol. 4*, eds., R. J. Gale and D. G. Lovering, Plenum Publishing Co. Ltd., London, England

Speciation of Pu(VI) in Near-Neutral Solutions via Laser Photoacoustic Spectroscopy
S. Okajima, D. T. Reed, J. V. Beitz, C. S. Sabau, and D. L. Bowers
To be published in Radiochim. Acta.

Fundamentals of the Chemical Behavior of Select Welding Fluxes
A. Polar, J. E. Indacochea, and M. Blander
To be published in Welding J.

Two-Stage Melting in Cesium-Lead
D. L. Price, M.-L. Saboungi, R. Reijers, D. Kearly, and R. White
To be published in Phys. Rev. Lett.

Propylene Hydroformylation in Supercritical Carbon Dioxide
J. W. Rathke, R. J. Klingler, and T. R. Krause
To be published in Organomet.

Alpha Particle-Induced Formation of Nitrate in the Cm-Sulfate Aqueous System
D. T. Reed and D. L. Bowers
To be published in Radiochim. Acta

Radiolytic Formation of Ammonia in Oxygen-Containing Systems
D. T. Reed, V. Swayambunathan, and R. A. Van Konynenburg
To be published in *Radiation Physics and Chemistry*

Vaporization of Strontium, Barium, Lanthanum, and Uranium from Mixtures of Urania, Zirconia, Steel, and Concretes at 2150 K and 2400 K
M. F. Roche, L. Leibowitz, J. L. Settle, C. E. Johnson, R. C. Vogel, and R. L. Ritzman
To be published in Nucl. Technol.

Melting in Trivalent Metal Chlorides
M.-L. Saboungi, D. L. Price, C. Scamehorn, and M. P. Tosi
To be published in Europhys. Lett.

Evaluation of Gas Chromatography/Matrix Isolation-Infrared Spectroscopy for the Quantitative Analysis of Environmental Samples
J. F. Schneider, K. R. Schneider, S. E. Spiro, D. R. Bierma, and L. F. Sytsma
To be published in Appl. Spectrosc.

New Evidence on the Long Valley Hydrothermal System from Wells, Fluid Sampling, Electrical Geophysics, and Age Determinations of Hot Spring Deposits
M. L. Sorey, G. Suemnicht, N. C. Sturchio, and R. Sundquist
To be published in J. Volcan. Geotherm. Res.

Thermodynamic Properties and Phase Diagram of Liquid Potassium-Indium Alloys by Electromotive Force Measurements
T. Takenaka, A. Petric, and M.-L. Saboungi
To be published in J. Phys.: Cond. Matt.

Investigations of Hydrogen/Li_2O Surface Interactions via Quantum Chemical Cluster Methods
S. W. Tam, J. Wright, L. A. Curtiss, and C. E. Johnson
To be published in J. Nucl. Mater.

Thermodynamic Behavior of High-Tc Oxide Systems Via EMF and Related Measurements
M. Tetenbaum, P. Tumidajski, J. Bloom, D. Brown, and M. Blander
To be published in the Proc. of the Int. School of Condensed Matter Physics, World Scientific Publishing Corp.